

DESIGN, SYNTHESIS, AND PRECLINICAL EVALUATION OF LIGAND-TARGETED CONJUGATES FOR CANCER RADIOTHERANOSTICS

by

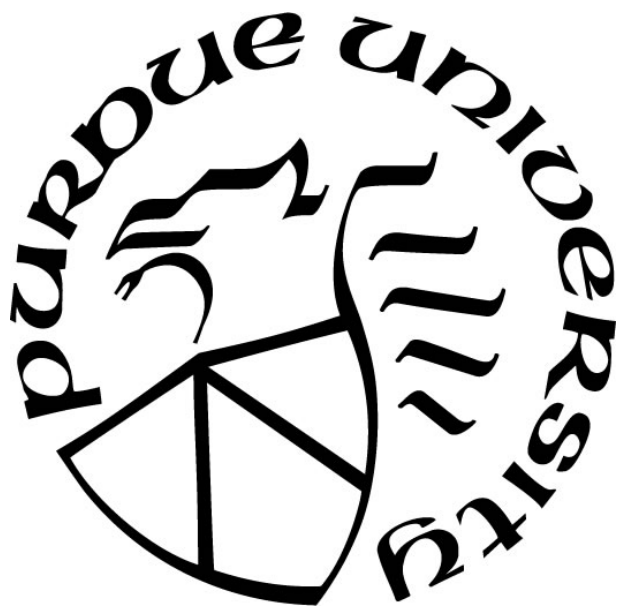
Spencer Dirk Lindeman

A Dissertation

Submitted to the Faculty of Purdue University

In Partial Fulfillment of the Requirements for the degree of

Doctor of Philosophy



Department of Chemistry

West Lafayette, Indiana

August 2021

THE PURDUE UNIVERSITY GRADUATE SCHOOL
STATEMENT OF COMMITTEE APPROVAL

Dr. Philip S. Low, Chair

Department of Chemistry

Dr. Chittaranjan Das, Co-Chair

Department of Chemistry

Dr. Mingji Dai, Co-Chair

Department of Chemistry

Dr. David H. Thompson

Department of Chemistry

Approved by:

Dr. Christine Hrycyna

Dedicated to my beloved wife, Leslie, whose immeasurable sacrifices and unwavering belief in me made this work possible.

Also dedicated to my wonderful parents, Dirk and Jennifer, who taught me to strive for new educational heights in the pursuit of the betterment of mankind.

ACKNOWLEDGMENTS

I would like to acknowledge my advisor Dr. Philip S. Low for his inspiring scientific ingenuity, and his patient guidance throughout my doctoral journey. My lab manager Dr. Madduri Srinivasarao for his additional tutelage, guidance, and kindness. My colleague Dr. Ramesh Mukkamala for his vital, numerous contributions our collective FAP research, specifically his synthesis of the majority of the FAP conjugates used in this work, as well as his close tutoring during my own synthesis. My fellow graduate student Imrul Shahriar for his expert contributions in computational docking. Also, my former colleague Dr. Xiaofei Yang for synthesizing several additional FAP conjugates for testing. My fellow graduate student Losha Jung for her essential contributions to our folate brush border membrane research together. My associate Dr. Spencer Gardeen for his astute counsel during our scientific discussions. My mentor Dr. Daniel Sheik for taking me under his wing at the beginning of my graduate student journey. My team members Dr. Fenghua Zhang, Dr. Suraj Hettiarachchi, Dr. Estela Puchulu-Campanella, and Dr. Yen-Hsing Li during our IPF research for their examples of productivity and efficiency. Former lab members Dr. Xin Liu, Dr. Isaac Marks, Dr. Weichuan Lou, Dr. Boning Zhang, Dr. Stewart Low, and Dr. Jeffery Nielsen for all teaching me various experimental procedures at various points in my graduate studies.

I would also like to acknowledge my team of undergraduates: Roxanne Huff, Autumn Horner, Pooja Tudi, Joshua Hinsey, Anders Hovstadius, Peter Martone, Taylor Schleinkofer, Lexi Lautenschlaeger, and Owen Booth for not only their crucial contributions directly to this research, but for going the extra mile with their willing sacrifices and personal support. Also, to my former undergraduates who entrusted a portion of their scientific training and education to me: Kylie Middleton, Maya McCants, Helena Kuang, and Kasia Ashwill.

I would like to acknowledge Dr. Andy Schaber of the Purdue Imaging Facility at the Bindley Science Center for his assistance with the animal imaging instruments and overall collaboration. Dr. Abigail Cox of the Purdue University College of Veterinary Medicine for her toxicology analysis contributions to the FAP project. Kristina Grayson of the Bindley Bioscience Center for her assistance in flow cytometry cell sorting. Dr. Cheryl Nutter of HuLow Medical and Dr. Ivan Rosas of Brigham and Women's Hospital of Harvard Medical School for their scientific instruction.

TABLE OF CONTENTS

LIST OF TABLES.....	9
LIST OF SCHEMES	10
LIST OF FIGURES	12
LIST OF ABBREVIATIONS.....	15
ABSTRACT.....	16
CHAPTER 1. LIGAND-TARGETED RADIOTHERANOSTICS: A REVIEW	17
1.1 Abstract.....	17
1.2 Introduction	17
1.3 Oncological Targets & Respective Ligands.....	18
1.4 Radioactive Payloads.....	22
1.5 Linker Design to Enhance Pharmacokinetics.....	24
1.6 Combination Therapies	26
1.7 Conclusion.....	27
1.8 References	28
CHAPTER 2. ALBUMIN-BINDING MOTIF ENHANCES THERANOSTIC TARGETING OF FIBROBLAST ACTIVATION PROTEIN RADIOLIGAND: PRECLINICAL EVALUATION IN MULTIPLE TUMORS.....	54
2.1 Abstract.....	54
2.2 Introduction	54
2.3 Materials and Methods	55
2.3.1 Materials.....	55
2.3.2 Synthesis of FAP5 intermediates	57
Synthesis of Fragment 1.....	57
Synthesis of Fragment 2.....	57
2.3.3 Synthesis of FAP5-DOTA conjugates	58
Synthesis of FAP5-DOTA.....	58
Synthesis of FAP5-IP-DOTA.....	60
2.3.4 Enzyme Inhibition Assays.....	61
2.3.5 Cell Culture	61

2.3.6	Transfection and Cell Sorting	62
2.3.7	Chelation and Radiolabeling	63
2.3.8	Computational Docking	63
2.3.9	Cell Binding Studies.....	63
2.3.10	Animal Husbandry	64
2.3.11	Tumor Models	64
2.3.12	SPECT/CT scans	64
2.3.13	Radioactive Biodistribution.....	65
2.3.14	Radiotherapy	65
2.3.15	Toxicology	66
2.3.16	Statistical Analysis	66
2.4	Results	66
2.4.1	Synthesis of FAP-Targeted Drug Conjugates	66
2.4.2	<i>In vitro</i> assays of FAP5-DOTA Conjugates.....	70
2.4.3	<i>In vivo</i> evaluation of the tumor retention, biodistribution, and pharmacokinetics of FAP5-DOTA conjugates	72
2.4.4	Radiotherapy of ¹⁷⁷ Lu-FAP5-IP-DOTA in 4T1 tumor-bearing mice	76
2.4.5	Radiotherapy of ¹⁷⁷ Lu-FAP5-DOTA Conjugates in Human Tumor Xenografts	78
2.5	Discussion.....	81
2.6	Conclusion	84
2.7	References	84
2.8	Appendix A. Supplemental Information	92
CHAPTER 3. PRECLINICAL INVESTIGATION OF THERANOSTIC FIBROBLAST ACTIVATION PROTEIN RADIOLIGANDS: FURTHER OPTIMIZATIONS.....		101
3.1	Abstract.....	101
3.2	Introduction	101
3.3	Materials and Methods	102
3.3.1	Materials.....	102
3.3.2	Chelation	102
3.3.3	Formulation	103
3.3.4	Amino Acid Solution Administration	103

3.3.5	Radiotherapy	103
3.3.6	NIR Imaging.....	103
3.3.7	Murine pulmonary fibrosis model.....	104
3.4	Results	104
3.4.1	<i>In vitro</i> Evaluation of Binding of FAP5 Ligand Analogs	104
3.4.2	<i>In vitro</i> Evaluation of FAP5 Ligand Binding with Modified Linkers.....	105
3.4.3	<i>In vitro</i> Evaluation of FAP5-DOTA Conjugates with Different Spacer Lengths .	107
3.4.4	Synthesis and Evaluation of FAP5-NOTA Conjugates with Alternative Phenyl-based Albumin Binders.....	107
3.4.5	Reducing Renal Uptake of FAP5-IP-DOTA with Co-Administration of Amino Acid Solution	109
3.4.6	Improved Radiotherapy with High Dosing Regimen of ¹⁷⁷ Lu-FAP5-IP-DOTA ..	110
3.5	Discussion.....	112
3.6	Conclusion.....	115
3.7	References	115
3.8	Appendix B. Supplemental Information.....	121
CHAPTER 4. FACILITATING RENAL CLEARANCE OF FOLATE CONJUGATES VIA BRUSH BORDER MEMBRANE ENZYME-MEDIATED DEGRADATION: PRECLINICAL EVALUATION FOR CANCER THERANOSTICS		126
4.1	Abstract.....	126
4.2	Introduction	126
4.3	Materials & Methods.....	128
4.3.1	Materials.....	128
4.3.2	Synthesis of Folate Conjugates with Brush Border Membrane Cleavable Linker	129
	Solid Phase Synthesis of Folate with Brush Border Membrane Cleavable Linker.....	129
	Synthesis of S0456 maleimide.	130
	Synthesis of Evans Blue maleimide.	130
	Synthesis of Iodophenyl maleimide.	131
	Synthesis of final Folate conjugates.....	131
4.3.3	Cell Culture	131
4.3.4	Chelation and Radiolabeling	131

4.3.5	Cell Binding Studies.....	132
4.3.6	Animal Husbandry	132
4.3.7	Tumor Models	133
4.3.8	NIR Imaging.....	133
4.3.9	SPECT/CT scans	133
4.3.10	Radiotherapy	134
4.3.11	Statistical Analysis	134
4.4	Results	134
4.4.1	Synthesis of Folate-Targeted NIR Conjugate with BBM-Cleavable Linkers.....	134
4.4.2	<i>In vitro</i> validation of FR targeting by S0456-MVK(Folate)-OH	136
4.4.3	<i>In vivo</i> evaluation of S0456-MVK(Folate)-OH Renal Clearance and Tumor Targeting.....	138
4.4.4	Synthesis of DOTA-MVK(AB-Folate) Conjugates with Several Albumin-Binders..	142
4.4.5	<i>In vitro</i> validation of FR targeting by DOTA-MVK(AB-Folate)-OH conjugates	145
4.4.6	<i>In vivo</i> evaluation of Renal Clearance and Tumor Targeting of DOTA-MVK(AB-Folate)-OH conjugates.....	147
4.4.7	Radiotherapy of ¹⁷⁷ Lu-DOTA-MVK(AB-Folate)-OH conjugates in KB tumor-bearing mice.....	149
4.5	Discussion.....	152
4.6	Conclusion.....	154
4.7	References	154
4.8	Appendix C. Supplemental Information.....	159
	CURRICULUM VITA	166
	PUBLICATIONS.....	169

LIST OF TABLES

Table 1.1. Common nuclides currently used in nuclear medicine, and their respective applications, fundamental properties, and common chelators.	22
Table 2.1. Summary of histopathology of necropsy tissues from ¹⁷⁷ Lu-FAP5-IP-DOTA radiotherapy studies. # Examined refers to total number of sections examined from multiple mice. DL = Diagnostic Lesions.	83

LIST OF SCHEMES

- Scheme 2.1. Synthesis of FAP5 Final Intermediate 1. Reagents and conditions for Fragment 1: (a) Boc₂O, TEA, DCM, rt, overnight; (b) NaBH₄, MeOH, THF, 55°C, 5h; (c) NBS, PPh₃, DMF, rt, 6h; (d) NaN₃, DMF, 65°C, overnight..... 67
- Scheme 2.2. Synthesis of FAP5 Final Intermediate 2. Reagents and conditions for Fragment 2: (a) i. LiHMDS, THF, -78°C, 1h; ii. tert-butyl-bromoacetate, 2h; (b) DBU, DCM, 0°C-rt, 24h; (c) H₂/Pd-C, MeOH, rt, overnight; (d) 4,4-difluoro-L-prolinamide, HATU, DIPEA, DMF, rt, 3h; (e) imidazole, POCl₃, pyridine, -20°C, 1h; (f) TFA, ACN, 0°C-rt, 1h. 67
- Scheme 2.3. Synthesis of FAP5-DOTA. Reagents and conditions: (a) Mono-Fmoc ethylene diamine, HATU, DIPEA, DMF, rt, 3h; (b) Fragment 1, CuI, DIPEA, DMF, 55°C, 5h; (c) i. Et₂NH, DCM, rt, 1h; ii. NHS ester-PEG₆-NHfmoc, DCM, rt, 3h; (d) i. TFA, ACN, 0°C-rt, 1h; ii. Fragment 2, HATU, DIPEA, DMF, rt, 3h; (e) i. Et₂NH, DCM, rt, 1h; ii. NHS ester DOTA, DMF, rt, 12h.68
- Scheme 2.4. Synthesis of FAP5-IP-DOTA. Reagents and conditions: (a) Fmoc-Lys-OH, HATU, DIPEA, DMF, rt, 3h; (b) Propargyl-PEG₆-NH₂, HATU, DIPEA, DMF, rt, 3h; (c) Fragment 1, CuI, DIPEA, DMF, 55°C, 5h; (d) i. TFA, ACN, 0°C-rt, 1h; ii. Fragment 2, HATU, DIPEA, DMF, rt, 3h; (e) i. Et₂NH, DCM, rt, 1h; ii. NHS-ester DOTA, DMF, rt, 12h. 69
- Scheme 3.1. Synthesis of FAP5-XP-NOTA. Reagents and conditions: (a) Fmoc-Lys-OH, HATU, DIPEA, DMF, rt, 3h; (b) Propargyl-PEG₆-NH₂, HATU, DIPEA, DMF, rt, 3h; (c) Fragment 1, CuI, DIPEA, DMF, 55°C, 5h; (d) i. TFA, ACN, 0°C-rt, 1h; ii. Fragment 2, HATU, DIPEA, DMF, rt, 3h; (e) i. Et₂NH, DCM, rt, 1h; ii. NHS-ester NOTA, DMF, rt, 12h. 108
- Scheme 4.1. Synthesis of Folate-BBM precursor for NIR coupling. Reagents and conditions: a) 2-Chlorotrityl resin, DIPEA, DCM, rt, 2h; b) i. 20% piperidine DMF, Ar, 20 min (x3); ii. Fmoc-Val-OH, HATU, DIPEA, DMF, Ar, 3h (x2); iii. 20% piperidine DMF, Ar, 20 min (x3); iv. Fmoc-Met-OH, HATU, DIPEA, DMF, Ar, 3h (x2); c) i. 20% piperidine DMF, Ar, 20 min (x3); ii. 3-(Tritylthio)propanoic acid, HATU, DIPEA, DMF, Ar, 3h; d) Pd(PPh₃)₄, phenylsilane, DCM, Ar, 1h; e) Fmoc-Glu-OtBu, HATU, DIPEA, DMF, Ar, 3h; f) i. 20% piperidine DMF, Ar, 20 min (x3); ii. N10-TFA-Pteoric acid, HATU, DIPEA, DMF; g) i. 50% NH₄OH DMF, Ar; ii. TCEP, 95/2.5/2.5 TFA/TIPS/H₂O, 1h. 135
- Scheme 4.2. Synthesis of S0456-MVK(Folate)-OH. Reagents and conditions: a) Cl-S0456, CsCO₃, DMSO, rt, 4h; b) i. TFA, rt, 1h; ii. N-Succinimidyl 3-maleimidopropionate, DIPEA, DMSO, rt, 4h; c) SH-MVK(Folate)-OH, DMSO, Ar, rt, 4h..... 136
- Scheme 4.3. Synthesis of Folate-BBM-DOTA precursor for AB coupling. Reagents and conditions: a) 2-Chlorotrityl resin, DIPEA, DCM, rt, 2h; b) i. 20% piperidine DMF, Ar, 20 min (x3); ii. Fmoc-Val-OH, HATU, DIPEA, DMF, Ar, 3h (x2); iii. 20% piperidine DMF, Ar, 20 min (x3); iv. Fmoc-Met-OH, HATU, DIPEA, DMF, Ar, 3h (x2); c) i. 20% piperidine DMF, Ar, 20 min (x3); ii. DOTA-tris (t-Bu ester), HATU, DIPEA, DMF, Ar, 3h; d) Pd(PPh₃)₄, phenylsilane, DCM, Ar, 1h; e) i. Fmoc-Cys-OH, HATU, DIPEA, DMF, Ar, 3h (x2); ii. 20% piperidine DMF, Ar, 20 min (x3); iii. Fmoc-Glu-OtBu, HATU, DIPEA, DMF, Ar, 3h; f) i. 20% piperidine DMF, Ar, 20 min (x3); ii. N10-TFA-Pteoric acid, HATU, DIPEA, DMF; g) i. 50% NH₄OH DMF, Ar; ii. TCEP, 95/2.5/2.5 TFA/TIPS/H₂O, 1h. 143

Scheme 4.4. Synthesis of DOTA-MVK(EB-Folate)-OH. Reagents and conditions: a) Tolidine, HATU, DIPEA, DMF, overnight; b) i. HCl, NaNO₂, ACN, H₂O, 0°C, 30 min; ii. 1-amino-8-naphthol-2,4-disulfonic acid, NaHCO₃, H₂O, 0°C-rt, 1.5h; c) DOTA-MVK(Cys-Folate)-OH, DMSO, Ar, rt, 4h. 144

Scheme 4.5. Synthesis of DOTA-MVK(IP-Folate)-OH. Reagents and conditions: a) 4-iodophenylbutyric acid, HATU, DIPEA, DMF, rt, 3h; b) DOTA-MVK(Cys-Folate)-OH, DMSO, Ar, rt, 4h. 144

LIST OF FIGURES

- Figure 2.1. *In vitro* assays of FAP5-DOTA conjugates. FAP expression was first checked on all cell lines used for this study. Antibody-stained samples are represented by the bright red histograms. Non-staining controls are represented by the dark red histograms. The FAP5 base ligand was then tested with recombinant enzymes for potency and specificity. FAP5-DOTA and FAP5-IP-DOTA were investigated to assess their targeting to human CAFs. 71
- Figure 2.2. Dosing studies of FAP5-DOTA conjugates in 4T1 tumor. White arrows indicate tumor. Red arrows indicate liver. Purple arrows indicate spleen. Yellow arrows indicate kidneys. 73
- Figure 2.3. FAP5-DOTA biodistribution in 4T1 tumor-bearing mice and tumor-to-organ ratios (n = 4–5). White arrows indicate tumor. Red arrows indicate liver. Purple arrows indicate spleen. 74
- Figure 2.4. FAP5-IP-DOTA biodistribution in 4T1 tumor-bearing mice and tumor-to-organ ratios (n = 5). White arrows indicate tumor. Yellow arrows indicate kidneys. 75
- Figure 2.5. Radiotherapy of ¹⁷⁷Lu-FAP5-IP-DOTA in 4T1 tumor-bearing mice (n = 5 per group). Treated mice received a single injection on day 0. The low dose group was injected with 9 MBq of lutetium-177 per mouse, and the high dose group was injected with 18 MBq per mouse. Tumor progression and relative body weights were measured every other day. After the conclusion of the therapy study, mice were euthanized and had their organs fixed for toxicology evaluation. No diagnostic lesions were observed in the selected organs of the control or treated mice. 77
- Figure 2.6. Radiotherapy of ¹⁷⁷Lu-FAP5-DOTA conjugates in human tumor xenografts. Mice bearing U87MG (n = 5), HT29 (n = 4), or KB (n = 5) tumor xenografts received a single injection on day 0. Mice bearing HT29 tumors received a 9 MBq dose of lutetium-177, while mice bearing U87MG or KB tumors received a 18 MBq dose. Survival, tumor progression and relative body weights were measured every other day. After the conclusion of the therapy study, mice were euthanized and had their organs fixed for toxicology evaluation. 79
- Figure 2.7. Effect of ¹⁷⁷Lu-FAP5-IP-DOTA on various tissues. Necrotic collapse was present in all HT29 tumor-bearing mice that received a therapeutic injection, but only mild ulcers were observed in two of the HT29 tumor-bearing mice that received a control injection. No diagnostic lesions were observed in the selected organs of the control or treated mice. 80
- Figure 3.1. Evaluation of binding of FAP5 ligand analogs. A consistent concentration of FAP5-Rhodamine was incubated with HEK-FAP cells and increasing concentrations of either FAP5-PEG₄-DOTA or a FAP5-monofluoro analog. All samples were performed in triplicate. 105
- Figure 3.2. Evaluation of FAP5 ligand binding with modified linkers. A phenyl-triazole linker was compared with two different amide linkers as shown in the structures above. Binding studies were performed, where each conjugate was incubated with HEK-FAP cells in increasing concentrations. All three conjugates were tested in parallel. All samples were performed in triplicate. 106
- Figure 3.3. Evaluation of FAP5-DOTA conjugates with different lengths of PEG spacer. A consistent concentration of FAP5-Rhodamine was incubated with HEK-FAP cells and increasing

concentrations of FAP5-PEG₄-DOTA, FAP5-PEG₆-DOTA, or FAP5-PEG₁₂-DOTA. All samples were performed in triplicate..... 107

Figure 3.4. Evaluation of FAP5-XP-NOTA conjugates with alternative albumin-binders. A consistent concentration of FAP5-Rhodamine was incubated with HEK-FAP cells and increasing concentrations of FAP5-FP-NOTA or FAP5-CP-NOTA. Both conjugates were tested in parallel. All samples were performed in triplicate..... 109

Figure 3.5. Reducing renal uptake of FAP5-IP-DOTA radioconjugates with co-administration of amino acid solution. A concentrated lysine-PBS solution was intraperitoneally injected within minutes of an intravenous tail-vein injection of the FAP5-IP-DOTA radioconjugate. Early time points showed significant reduction in renal uptake compared to previous scans. White arrows indicate tumor. Yellow arrows indicate kidneys..... 110

Figure 3.6. Radiotherapy of 4T1 tumor with high dosing regimen of ¹⁷⁷Lu-FAP5-IP-DOTA. Mice (n = 5 per group) bearing 4T1 tumors were injected with 5 nmol of FAP5-IP-DOTA radiolabeled with 55 MBq of lutetium-177 on day 0 with a coadministration of an amino acid solution into the intraperitoneal cavity. The second group of mice received a second dose of 5 nmol of FAP5-IP-DOTA radiolabeled with 22 MBq of lutetium-177 on day 3 with a coadministration of an amino acid solution into the intraperitoneal cavity..... 111

Figure 3.7. SPECT/CT scans of ¹⁷⁷Lu-FAP5-IP-DOTA in 4T1 tumors. Mice (n = 1) were injected on day 0 with 5 nmol of conjugate radiolabeled with 55 MBq of lutetium-177 and a coadministration of an amino acid solution into the intraperitoneal cavity. The second group of mice received a second dose of 5 nmol of FAP5-IP-DOTA radiolabeled with 22 MBq of lutetium-177 on day 3 with a coadministration of an amino acid solution into the intraperitoneal cavity. White arrows indicate tumor. Yellow arrows indicate kidneys..... 112

Figure 4.1. Binding of Folate-S0456 conjugates to KB cells by FACS analysis. These studies were conducted in parallel. 137

Figure 4.2. Renal clearance of folate-S0456 conjugates from healthy mice (n = 2). A drastic difference in renal fluorescence could be observed within the first hour post-injection. More sensitive scans could no longer detect fluorescence in whole-body scans by six hours post-injection. Biodistribution images show no detectable fluorescence in the kidneys of mice injected with the S0456-MVK(Folate)-OH conjugate by 24 hours p.i., whereas OTL38 was still highly retained. Organs in biodistribution shown from top to bottom: Heart, lungs, liver, spleen, kidneys..... 139

Figure 4.3. Tumor targeting of folate-S0456 in MDA-MB-231 tumor-bearing mice (n = 1–2). An improved tumor-to-kidney ratio can be observed within the first hour for the folate-S0456 conjugate with the BBM-labile linker. Competition mice received an injection of S0456-MVK(Folate)-OH with 100x excess of folate-glucosamine, which blocked tumor fluorescence, demonstrating active receptor targeting. Organs in biodistribution shown from top to bottom: Tumor, heart, lungs, liver, spleen, kidneys. 141

Figure 4.4. Binding of DOTA-MVK(AB-Folate)-OH conjugates radiolabeled with indium-111 to KB cells, measured by gamma counter. These studies were conducted in parallel. All samples were performed in triplicate..... 146

Figure 4.5. SPECT/CT of ^{111}In -DOTA-MVK(AB-Folate)-OH conjugates in healthy mice (n = 1). While ^{111}In -DOTA-MVK(IP-Folate)-OH demonstrated faster clearance than ^{111}In -DOTA-MVK(EB-Folate)-OH, ^{111}In -DOTA-MVK(IP-Folate)-OH also demonstrated low hepatic uptake. Yellow arrows indicate kidneys..... 148

Figure 4.6. SPECT/CT scans of ^{111}In -DOTA-MVK(EB-Folate)-OH in MDA-MB-231 tumor-bearing mouse (n = 1). The conjugate demonstrated long-term tumor retention out to 8 days, as well as a rapid reduction of radioactivity in the kidneys within 12 hours, leading to a favorable tumor-to-kidney ratio. White arrows indicate tumor. Yellow arrows indicate kidneys. 149

Figure 4.7. Radiotherapy of KB tumor with ^{177}Lu -MVK(AB-Folate)-OH conjugates. Mice (n = 5 per group) bearing KB tumors were injected with 5 nmol of ^{177}Lu -MVK(EB-Folate)-OH or ^{177}Lu -MVK(IP-Folate)-OH radiolabeled with 18 MBq of lutetium-177 on day 0..... 150

Figure 4.8. SPECT/CT scans of ^{177}Lu -DOTA-MVK(AB-Folate)-OH conjugates in KB tumor-bearing mice at therapeutic doses (n = 1). White arrows indicate tumors. Yellow arrows indicate kidneys. 151

LIST OF ABBREVIATIONS

CT	Computed Tomography	PD-L1/2	Programmed death-ligand 1/2
SPECT	Single Photon Emission Tomography	B7-H3	B7 Homolog 3
MRI	Magnetic Resonance Imaging	LAG-3	Lymphocyte-activation gene 3
PET	Positron Emission Tomography	TIM-3	T-cell immunoglobulin and mucin domain-containing protein 3
PRRT	Peptide Receptor Radionuclide Therapy	TIGIT	T cell immunoreceptor with Ig and ITIM do
SSTR2	Somatostatin Receptor 2	VISTA	V-domain Ig suppressor of T cell activation
PSMA	Prostate Specific Membrane Antigen	TLR	Toll-like receptor
TAF	Tumor-associated fibroblast	TGF	Transforming growth factor
FR	Folate receptor	CAF	Cancer-associated fibroblast
TAM	Tumor-associated macrophage	ECM	Extra cellular matrix
GLUT1	Glucose Transporter 1	NIR	Near-infrared dye
FDG	2-fluoro-2-deoxy-D-glucose	BFC	Bifunctional chelator
FAP	Fibroblast Activation Protein	SPPS	Solid-phase peptide synthesis
GLP-1R	Glucagon-like peptide-1 receptor	P.I.	Post-injection
BB	Bombesin receptor		
NTSR	Neurotensin receptor		
CCKBR	Cholecystokinin B receptor		
CAIX	Carbonic anhydrase 9		
GI	Gastrointestinal tract		
LHRH-R	Luteinizing hormone-releasing hormone receptor		
LET	Linear Energy Transfer		
ROS	Reactive oxygen species		
BBM	Brush border membrane		
AB	Albumin-binder		
DDR	DNA-damage response		
PARP	Poly (ADP-ribose) Polymerase		
HSP90	Heat shock protein 90		
CTLA-4	Cytotoxic T-lymphocyte-associated protein 4		
PD-1	Programmed cell death protein 1		

ABSTRACT

For any drug candidate to be approved by the U.S. Food and Drug Administration, it must meet strict standards for safety and efficacy. While the field of nuclear medicine is over 100 years old, traditional methods such as external beams or systematic administration have rarely met these standards or have limited application. Ligand-targeted therapy and diagnostics, or “theranostics,” has emerged in the past several decades as an exciting field that offers new possibilities to design drugs that are both safe and effective. When applied to nuclear medicine, the field of ligand-targeted radioactive theranostics is younger still, with many critical lessons being discovered and applied currently. This dissertation outlines the necessary principles of radioactive theranostic drug design, then demonstrates the application of several more recent techniques to improve both the efficacy and safety of radioactive theranostics targeting two high priority oncological targets: fibroblast activation protein alpha and folate receptor.

CHAPTER 1. LIGAND-TARGETED RADIOTHERANOSTICS: A REVIEW

1.1 Abstract

While nuclear medicine as a field is over a century old, research into pairing nuclear medicine with ligand-targeted technology is in its relative infancy. Consequently, integration of many important but distinct advances lags behind mainstream practice. As more radioimaging and radiotherapy conjugates, or radiotheranostics, are approved for human use, it will be essential for interdisciplinary laboratories to rapidly adapt these lessons to the current research space. This Review seeks to encourage the coalescence of important lessons by outlining the current understanding of essential principles for designing a successful radiotheranostic: explanation of relevant receptors in cancer and their respective targeting-ligands, proper selection of radionuclides with compatible chelators, pharmacokinetic enhancements via linker modification, and potential combinations with other therapies. Expanding the understanding of ligand-targeted radiotheranostics will accelerate the progress of this evolving field.

1.2 Introduction

The field of nuclear medicine may date as far back as the late 1800s. Wilhelm Röntgen first discovered X-rays in 1895, and Emil Grubbe likely began using X-rays to treat cancer patients the following year.¹ More possibilities unfolded when Marie Curie discovered the existence of radioactive elements radium and polonium in 1898, followed by the discovery of artificially produced radioactive nuclides in 1934 by Frédéric Joliot-Curie and Irène Joliot-Curie.^{2, 3} The establishment of the Oak Ridge National Laboratory in 1946 by Ernest Lawrence and the ensuing rapid production of reactor-produced radionuclides made the widespread medicinal use of radioactivity possible.

With the advent of radioactivity research, tumor radiotherapy quickly became an application of focus. John Lawrence used phosphorous-32 to treat leukemia, and Saul Hertz and Arthur Roberts used iodine-131 to treat thyroid cancer.⁴ Tumor radioimaging followed thereafter. David Kuhl and Roy Edwards first demonstrated single photon emission computed tomography (SPECT) in 1963.^{5, 6} Godfrey Hounsfield invented computed tomography (CT) in 1971. Raymond

Damadian reported the first magnetic resonance image (MRI) of a tumor in 1971.⁷ Edward Hoffman and Michael Phelps invented positron emission tomography (PET) in 1974.⁸ By this point, most organs of the body could be visualized using some form of nuclear medicine. However, localizing therapeutic radionuclides to tumors remained a challenge. C. L. Edwards wrote in 1979, “We must now look for a new generation of tumor-localizing radiopharmaceuticals and improved detection instruments if we are to make significant progress towards our goal of detecting occult cancers while they are still curable.”⁹

The last several decades have seen a rapid expansion of a new class of anticancer molecules termed ligand-targeted therapeutics.¹⁰ The premise of this class of molecules is that the therapeutic or imaging payload is conjugated to a targeting ligand that binds specifically and with high affinity to a biomarker overexpressed in cancer. Research to identify cell-surface receptors overexpressed in cancer, optimize the structure of their respective targeting ligands, develop suitable isotope and chelator pairings, enhance pharmacokinetic properties, and additional improvements have collectively given rise to a new generation of nuclear medicines deemed radioligands. Whereas older methods relied on external radiation beams, seed implants, or systematic administration followed by passive uptake, radioligands provide the capability to actively concentrate radionuclides in tumors but not healthy tissues. The efficacious yet safe nature of radioligands creates many possibilities to hopefully answer the call of C. L. Edwards.

Herein we review advances of ligand-targeted cancer therapeutics within the context of radioligands. We focus on overexpressed cell-surface receptors found in tumors in preclinical or clinical settings. We summarize radionuclides and common chelator pairings used in nuclear medicine for SPECT, PET, or radiotherapy. We discuss various spacer modifications to improve tumor uptake, retention, and specificity. Finally, we briefly review how radioligands can be used in combination with other cancer therapies to improve overall treatment.

1.3 Oncological Targets & Respective Ligands

Somatostatin receptor 2 (SSTR2) is the oncological target of the first FDA-approved and EMA-approved radiopharmaceutical for peptide receptor radionuclide therapy (PRRT), ¹⁷⁷Lu-DOTATATE (Lutathera®).¹¹ SSTR2 is overexpressed in neuroendocrine tumors and can inhibit growth or stimulate apoptosis in tumors when activated by analogues.¹²⁻¹⁵ These analogs are cyclic peptides, with octreotide (OCT, D-Phe-c(Cys-Phe-D-Trp-Lys-Thr-Cys)-Thr-ol)) being one of the

most extensively researched due to selectivity for SSTR2 over other homologs such as SSTR3 and SSTR5.^{16, 17} Various radioligands that target SSTR2 are derivatized from OCT, such as DOTATATE, DOTATOC, and DOTANOC, are being used to radioimage tumors.¹⁸⁻²² Radiotherapy studies are also being conducted with these ligands.^{23, 24} While SSTR2 expression may also be found in healthy organs such as the pancreas, cerebrum, and kidneys, it shows a significantly higher receptor density in malignant tissues.^{25, 26} The receptor count of SSTR2 may approach 900,000 per cancer cell.²⁷ As a result, SSTR2 is a promising target for radiotheranostics, with many clinical trials currently underway.

Prostate-Specific Membrane Antigen (PSMA) is a highly successful cancer target to date, with many favorable attributes facilitating its success. The PSMA receptor is highly expressed tumor antigen in prostate cancer, often in excess of one million receptors per cell.²⁸ PSMA receptors internalize and recycle rapidly, allowing for high accumulation of radioligand conjugates within the tumor.²⁹ Radioligands that target PSMA are derived from the DUPA molecule, a Glu-ureido inhibitor.³⁰ Although PSMA expression is also found in the salivary glands, the results of PSMA radioligands are nevertheless safe and impressive.³¹ The FDA recently approved ⁶⁸Ga-PSMA-11 for PET imaging in men with prostate cancer.³² It is also expected that the FDA will soon approve ¹⁷⁷Lu-PSMA-617 as a radiotheranostic for patients with prostate cancer based on successful Phase III clinical trials.^{33, 34}

The $\alpha_v\beta$ integrins are another established cancer target. They comprise a family of proteins overexpressed on the vasculature of endothelial cells in solid tumors, tumor-associated fibroblasts (TAFs), and the cells of certain carcinomas.³⁵⁻³⁷ Radioligands targeting $\alpha_v\beta$ integrins, such as $\alpha_v\beta_3$, $\alpha_v\beta_5$, and $\alpha_v\beta_6$, use the RGD peptide sequence.^{38, 39} Multiple clinical trials testing RGD-targeted PET imaging have been completed, with more currently active or recruiting.⁴⁰⁻⁴⁴ The integrin family has also been investigated as a potential target for tumor radiotherapy.^{45, 46}

Folate receptors as a cancer target possess many favorable attributes. Folate receptor alpha (FR α) is overexpressed on approximately 40% of all human cancer cells.⁴⁷⁻⁵⁴ The per cell expression is extremely high, nearing up to 3 million receptors per cancer cell. While FR α also possesses favorable internalization and recycling kinetics, there are several limiting factors. Because the natural ligand for FR α is the vitamin folate, and significant levels of folate can be found in the body, folate competes for the finite binding sites with targeted radiotheranostics that use a derivatized folate molecule.⁵⁵ Furthermore, folate conjugates show prohibitive renal uptake

and retention in the context of radiotherapy.⁵⁶⁻⁵⁹ Nevertheless, folate has shown to still be a valuable target for fluorescent or radioimaging, as well as chemotherapy.^{60, 61} Folate receptor beta (FR β) is another viable oncological target because it is expressed on over 25% of tumor cells, over 50% of tumor-associated macrophages (TAMs), and myeloid leukemia cells.⁶²⁻⁶⁴ However, because the targeting ligand for the beta isoform is also the folate vitamin, the same challenges persist as those for FR α .

Glucose Transporter 1 (GLUT1) is often highly upregulated in cancers compared to expression levels in normal tissue despite its near ubiquitous biodistribution.⁶⁵⁻⁶⁷ Indeed, the modified glucose molecule F-18 2-fluoro-2-deoxy-D-glucose (FDG) has been used to radioimage tumors since the late 1970s. While FDG uptake in tumors may not be strictly dependent on the GLUT1 receptor, FDG uptake is higher in tumors with higher expression of GLUT1.⁶⁸⁻⁷¹ Unfortunately GLUT1 may be limited to radioimaging as a receptor-mediated target. Despite its wide application, GLUT1 demonstrates low sensitivity in certain cancers and poor detection in organs with high glucose metabolism, such as the brain.^{72, 73}

Fibroblast Activation Protein alpha (FAP α , also known as seprase) has emerged in recent years as a promising oncological target.⁷⁴ Expression of FAP α is found primarily on activated fibroblasts such as TAFs, and is negligible in healthy tissues.⁷⁵⁻⁷⁷ A study of hundreds of human biopsies found FAP α expression in 90% of epithelial cancers.⁷⁸ This was further validated *in vivo* where a FAP α targeted PET tracer successfully imaged cancer in patients with 28 different types of tumors among them.⁷⁹ Targeting ligands against FAP α are proline mimetics with an amino acid bridge that bears a small R group on the side chain.⁸⁰⁻⁸⁴ Despite the exciting rise of FAP α radioligands, several challenges remain. The receptor count of FAP α per fibroblast is likely only several hundred thousand, in contrast with previously mentioned receptors, which reduces the theoretical maximum dose deliverable.⁸⁵ Furthermore, FAP α receptors recycle quite slowly, requiring several hours to internalize and up to several days to return to the cell surface.⁸⁶ These dose-limiting attributes are further exacerbated by the distribution of FAP α expression within the tumor microenvironment, which is primarily contained to TAFs, and not typically expressed on cancer cells themselves, though certain exceptions do exist.^{87, 88} As a result, while several FAP radiotherapy studies have been performed with limited success,^{86, 89, 90} the majority of research in targeting FAP α for nuclear medicine has been focused on radioimaging.⁹¹⁻⁹⁸

Glucagon-like peptide-1 receptor (GLP-1R) demonstrates high density in nonmalignant insulinomas.⁹⁹ Among healthy tissues, GLP-1R expression is limited primarily to the pancreas. One ligand for GLP-1R is an endogenous agonist exendin-4, a 39-amino acid peptide.^{100, 101} Exendin-4 has been derivatized for radioimaging of insulinomas, and is currently in clinical trials.¹⁰²⁻¹⁰⁴ Radiotherapeutic applications of Exendin-4 derivatives are also being investigated.^{105, 106} Another class of peptide receptors overexpressed in many tumors is the bombesin receptors (BBs, primarily BB₂; formerly known as Gastrin-Releasing Peptide Receptor, GRPR).¹⁰⁷⁻¹¹³ These tumors include prostate, breast, lung, colon, and ovarian cancers.¹¹⁴ Bombesin is a 27 residue peptide, and various analogs have been studied as targeting ligands for BB receptors in cancer.^{115, 116} To this point, BB₂ is primarily being exploited as a radioimaging target.¹¹⁷⁻¹²¹ A third family of transmembrane proteins that interact with peptides are neurotensin receptors (NTSRs). NTSRs are expressed in various carcinomas, as well as several tissues during embryogenesis.¹²² The receptor density of NTSRs is also high, comparable to that of SSTRs, which suggests close to one million receptors per tumor cell.^{27, 123-125} Because binding of neurotensin peptides to NTSRs can stimulate tumor proliferation and motility, various diarylpyrazole-based, nonpeptidic antagonists have been developed, which were further adapted for nuclear medicinal purposes.¹²⁶⁻¹²⁸ After promising preclinical SPECT/CT images were obtained, the first NTSR-targeted radiotherapy clinical results were recently published.¹²⁹ Cholecystikinin B receptor (CCKBR, also known as CCK2R or CCK₂) is a fourth class of peptide receptors overexpressed in many cancers. CCKBR expression is also found in the brain and epithelial cells of the GI tract.^{130, 131} A number of peptide and small-molecule ligands interact with CCKBR, which have been exploited to deliver radiotheranostic drugs to tumors in numerous preclinical studies and several clinical studies.¹³²⁻¹⁴⁷

Additional cell-surface biomarkers should be noted as potential oncological targets that merit further investigation. Carbonic anhydrase IX (CAIX) is a novel target because it is upregulated in most solid tumors with hypoxic regions and limited to low levels of expression in the gastrointestinal (GI) tract.^{148, 149} Inhibitors of CAIX are typically aromatic sulfonamides that coordinate to an active site zinc.¹⁵⁰ Multiple labs have used CAIX inhibitors as radioligands to image tumors.¹⁵¹⁻¹⁵³ Luteinizing hormone releasing hormone receptor (LHRH-R, also known as gonadotropin-releasing hormone receptor GnRHR) is primarily expressed in the pituitary gland in healthy tissue, but is also significantly upregulated in both hormone-dependent cancers as well as other cancers.¹⁵⁴ Various ligands exist for LHRH-R, such as peptides, agonists, and antagonists,

of which many have been studied to target radionuclides to tumors for imaging in preclinical models, as well as traditional chemotherapy payloads.¹⁵⁴⁻¹⁵⁸

1.4 Radioactive Payloads

Isotope selection requires careful consideration of numerous factors. A list of the properties for commonly used radionuclides with bifunctional chelators is summarized in Table 1.

Table 1.1. Common nuclides currently used in nuclear medicine, and their respective applications, fundamental properties, and common chelators.

Radionuclide	Purpose	$t_{1/2}$	Emission(s)	Max keV	Branching	Common Chelators
Tc-99m	SPECT	6.01 h	γ	141	89%	CIM, TIM, Bocdienac
In-111	SPECT	2.80 d	γ	171, 245	90%, 94%	DOTA, CHX-A''-DTPA
Ga-67	SPECT	3.26 d	γ	93, 184, 300	36%, 20%, 16%	DOTA, NOTA
F-18	PET	1.83 h	β^+	634	97%	NOTA, NETA (+ Al ³⁺)
Ga-68	PET	1.13 h	β^+	1899	88%	DOTA, NOTA
Cu-64	PET	12.7 h	β^+	653	18%	NODAGA, NOTA
Co-55	PET	17.5 h	β^+	1020, 1498	77%	DOTA
Zr-89	PET	3.27 d	β^+	902	23%	DOTA, DFO
Sc-44	PET	4.04 h	β^+	3652	94.3%	DOTA
Mn-52	PET	5.59 d	β^+	572	29%	DOTA
Y-86	PET	14.4 h	β^+	1221, 1545	83%, 33%	DOTA, CHX-A''-DTPA
Lu-177	Therapy/ SPECT	6.73 d	β^- γ	176, 384, 497 113, 210	12%, 9%, 79% 7%, 11%	DOTA, NETA, CHX-A''-DTPA
Bi-212	Therapy	60.6 min	α β^-	6089 2254	36% 64%	3p-CEPA, 3p-C-NETA
Bi-213	Therapy	45.6 min	α β^-	8400 986, 1427	2% 30%, 65%	3p-CEPA, 3p-C-NETA
Cu-67	Therapy	2.58 h	β^-	392, 483, 577	57%, 22%, 20%	NODAGA, NOTA
Sc-47	Therapy	3.35 d	β^-	440, 600	68%, 32%	DOTA
Ho-166	Therapy	1.12 d	β^-	1774, 1854	49%, 50%	DOTA, CHX-A''-DTPA
Pb-212	Therapy	10.6 h	β^-	335, 573	83%, 12%	CB-DO2A
Re-186	Therapy	3.78 d	β^-	939, 1077	22%, 71%	CIM, TIM, Bocdienac
Re-188	Therapy	17.0 h	β^-	1965, 2120	26%, 71%	CIM, TIM, Bocdienac
Y-90	Therapy	2.67 d	β^-	2280	100%	DOTA, CHX-A''-DTPA
Ac-225	Therapy	9.92 d	α	5732, 5791, 5792, 5830	8%, 9%, 18%, 51%	DOTA, DO3A
Th-227	Therapy	18.7 d	α	5708, 5757, 5978, 6038	8%, 20%, 24%, 24%	DOTA, Me-3,2-HOPO

These data surmising the attributes of individual radionuclides were consolidated from various databases belonging to University of Missouri Environmental Health & Safety Isotope Data Sheets, Health Physics Society, and The Lund/LBNL Nuclear Data Search. The compatibility of isotopes with common chelators was drawn from several excellent reviews and other studies.¹⁵⁹⁻

When designing a radioligand conjugate, many factors must be considered. It is essential to first consider which radionuclide is required for the purposes of a study, then select a bifunctional chelator that demonstrates high, long-term stability *in vivo*. Failure to do so will result in premature release of the isotope, uptake, and in some cases, long-term retention in healthy tissue. For radioimaging, PET is generally preferred over SPECT due to higher sensitivity, better spatial resolution and image quality, and the possibility of quantitative assessment of receptor occupancy.¹⁶⁵ Isotopes with higher energy decay suffer from loss of resolution, thus isotopes with relatively low decay energies are preferred specifically for radioimaging.¹⁶⁶ If the radioimaging study is being conducted for diagnostic purposes, then an isotope with a short half-life is ideal; if radioimaging study is being conducted to project how a novel targeting molecule might perform for radiotherapy, then an isotope with a longer half-life is required.^{167, 168} Availability and cost of radionuclides may limit options, particularly for preclinical research. Technetium-99m is an inexpensive medical isotope has been used as a radiotracer since the 1950. It is the most used medical isotope in the world, with tens of millions of diagnostic procedures each year. While fluorine-18 has been in use since the 1960s, gallium-68 has shown rapid growth as a radiodiagnostic in recent years due to the relatively low cost of ⁶⁸Ge/⁶⁸Ga generators.¹⁶⁹⁻¹⁷¹

Regarding radiotherapy, a different set of attributes are desired. Isotopes with high energies and longer half-lives are desirable to increase toxicity against cancer cells. However, the higher the energy, the deeper the tissue penetration, which poses a greater risk to healthy tissues within the surrounding vicinity of the tumor mass. Radiotherapeutic isotopes that undergo alpha decay possess several advantages over isotopes that undergo beta decay. Alpha particles will typically penetrate only 0.05–0.10 mm, whereas beta particles may travel 1–12 mm, hence limiting side effects to neighboring healthy tissue.¹⁷² Alpha particles are classified as high linear energy transfer (LET) (~80 keV/μm), compared to beta particles which are low LET (~0.2 keV/ μm).¹⁷³ Beta particles require the presence of oxygen to form reactive oxygen species (ROS) to damage cancer cells, oxygen which may be lacking in hypoxic regions of a tumor, but alpha particles do not seem to require cellular oxygenation for their cytotoxicity.^{174, 175} Alpha radiotherapy also appears to be independent of factors such as tumor size or cell cycle status.^{173, 176} Alpha emitters even demonstrate significantly less dependency on the effective specific activity dose compared to beta emitters, which can be important in tumors where the receptor count is lower and limits the maximum dose deliverable by targeted radiotherapy.¹⁷⁷ These factors culminate in alpha particles

causing significantly more double strand DNA breaks in cancer cells, which typically cannot be repaired.¹⁷⁷ While the potency of alpha-targeted radiotherapy is exciting, it also necessitates strict specificity in targeting to not cause unacceptable damage to healthy organs.

The daughter isotopes that result from radioactive decay should also be considered. An example of an isotope with an undesirable decay could be cobalt-55, which has a half-life of less than one day but then decays to iron-55, which emits X-rays with a half-life of 2.73 years. Conversely, lead-212 is a beta radiotherapeutic that decays to bismuth-212 and polonium-212, which emit alpha particles that also may serve as a desirable radiotherapy source.¹⁷³ A careful examination of the decay of a radionuclide should always be conducted before selecting a radionuclide to ensure safety and other desired properties.

1.5 Linker Design to Enhance Pharmacokinetics

To optimize the overall structure of a theranostic radioligand conjugate, the linker design must also be carefully considered to achieve desired pharmacokinetic properties. In general, the targeting ligand must be derivatized from a functional group that is exposed to the aqueous medium to preserve integrity of the ligand-receptor binding complex, which can be readily identified if crystal structures are available.¹⁷⁸ The exact structure of the receptor typically requires a minimum spacer length to maintain the high affinity of the targeting molecule.³⁰ Furthermore, undesired intramolecular interactions between the targeting ligand and the radioactive payload may necessitate a rigid linker to prevent such associations.^{179, 180} These factors must always be weighed when designing a radioligand conjugate so as to not compromise the targeting ability of the ligand to the intended receptor. Selecting the appropriate linker with the right modifications can also improve desired pharmacokinetic and biodistribution results.

Targeting ligands are often hydrophobic to maximum receptor affinity, but this hydrophobicity can lead to undesired properties such as passive membrane permeability or nonspecific association with scavenger receptors and lipoproteins. Therefore, a hydrophilic linker that can reduce these hydrophobic interactions is typically preferred. These linkers can be PEGs, hydrophilic amino acids, polysaccharides, or peptidoglycans.¹⁸¹⁻¹⁸⁵ Increased hydrophilicity can also facilitate rapid kidney excretion.¹⁸⁶

Radioligand clearance through the liver, bile duct, and gut are generally not preferred due to slower excretion times, which would increase the potential off-target toxicity.¹⁸⁷ Because the liver

highly expresses organic anion transporters, highly negatively charged linkers should be avoided. Peptide linkers can also lead to unwanted retention due to the presence of peptide scavenger receptors.¹⁸⁸ Liver uptake can be further avoided by using PEG linkers to bias excretion to the kidneys.¹⁸⁹⁻¹⁹⁴

While radioligand clearance through the kidney is preferred due to the faster kinetics of glomerulus extraction from the bloodstream to urinary excretion, residual kidney retention may still occur. It should first be noted that the renal absorbed dose is typically the guiding limitation for determining a maximum dose of radioactivity. The accepted threshold is 23 Gy, with an associated risk of 5% for the development of radiation nephropathy within 5 years (this risk rises to 50% after renal absorbed doses of 28 Gy).¹⁹⁵⁻¹⁹⁸ However, this standard was based on an external beam radiotherapy, which has a higher dose rate, penetration range, and homogeneous effect on the kidneys when compared to radionuclide therapy.¹⁹⁹⁻²⁰¹ Indeed, higher toxicity thresholds of 28 Gy and 40 Gy have been proposed for ligand-targeted radionuclide therapy, depending on other potential risk factors.²⁰² Traditional methods for mitigating kidney retention include the administration of concentrated amino acid solutions, plasma expanders, or diuretics.²⁰³⁻²¹⁰ Nevertheless, efforts to further enhance kidney clearance of the radioligand via judicious linker design are warranted. Because peptide scavengers are present in both the kidneys and liver, peptide linkers should be carefully designed.¹⁸⁸ The Arano lab has published multiple short peptide sequences that are cleaved by brush border membrane (BBM) enzymes found specifically in the kidney. They have demonstrated that by using a BBM-cleavable peptide sequence that links a targeting antibody and the radioactive payload, kidney clearance can be accelerated without significantly reducing tumor uptake.²¹¹⁻²¹⁶ This BBM-cleavable linker has also shown promise with a PSMA-targeted small molecule and a GLP-1R targeting peptide.²¹⁷⁻²¹⁹ If BBM-cleavable linkers are effective for improving the tumor-to-kidney ratio as radioconjugates when translated into the clinic, they could serve as a powerful tool to increase the maximum dose deliverable without simultaneously increasing nephropathy.

Increasing the tumor accumulation and retention of the radioligand is paramount to improving efficacy of radiotherapy. In the past decade, research investigating different appendages to the linker that bind to serum albumin in the blood stream and increase the circulation time of the radioconjugate have shown great promise. Albumin-binders have improved both radioimaging and radiotherapy preclinical results in ligands targeting folate, PSMA, SSTR2, $\alpha_v\beta$ integrins, and

CAIX.^{45, 46, 220-225} The first PSMA-targeted, albumin-binder enhanced clinical results have reflected similar promise.²²⁶ Albumin-binding is a classical technique in medicinal chemistry, and other ligand-targeted conjugates that bear payloads such as fluorescent dyes or signaling pathway inhibitors already show the benefits of increased circulation time.²²⁷⁻²³² However, when the payload is exchanged for a bifunctional chelator, it seems a separate albumin-binding moiety needs to be included in the linker if the ligand is to retain optimal *in vivo* behavior. Further modifications to the linker have been shown to reduce tumor efflux and increase tumor retention in several different ligands, though the exact structural design is likely receptor-specific.²³³⁻²³⁶ Reducing the size of PEG linkers has also been found to significantly increase tumor accumulation.²³⁷⁻²³⁹

The refinement of linker design will likely be a determining factor in the success or failure of radioconjugates with established oncological biomarkers and corresponding targeting ligands.

1.6 Combination Therapies

In cases where a radioconjugate may be insufficient to operate as a curative therapy alone, there can still be additive or even synergistic effects when combined with other therapeutic strategies. Briefly, we will discuss concurrent cancer treatments of radiotherapy with chemotherapy, immunotherapy, or surgery.

Radiotherapy has been used in conjunction with chemotherapy for decades, and significant improvement in survival rates from concurrent therapy has been shown in certain trials compared to single treatments.²⁴⁰⁻²⁴³ Radiotherapy breaks the DNA strands inside tumor cells, and the tumor activates specific pathways to remedy the damage. Typically, the options for DNA repair pathways are more limited in tumor cells compared to healthy cells, providing an opportunity for drugs that target these key pathways to augment the therapeutic efficacy of radiotherapy while simultaneously minimizing negative effects on non-malignant cells.²⁴⁴⁻²⁴⁶ Perhaps the best studied DNA damage response (DDR) target is the enzyme Poly-ADP-Ribose Phosphorylase (PARP), and PARP inhibitors combined with radiotherapy are currently undergoing clinical trials.²⁴⁷⁻²⁵⁰ Another emerging DDR target is the chaperone Heat shock protein 90 (HSP90), which are overexpressed in tumors and contribute to resistance against chemotherapy and radiotherapy.²⁵¹ Several HPS90 inhibitors have demonstrated synergistic effects on radiotherapy results in preclinical studies.^{252, 253} Other chemotherapeutics that modulate the behavior of tumor cells may also enhance radiotherapeutics. One recent study demonstrated that trifluoroperazine blocks the

conversion of glioma cells from a radiosensitive phenotype to a radioresistant phenotype via downregulation of the Yamanaka factors, ultimately extending survival beyond that of radiotherapy alone.²⁵⁴ Finally, it has been demonstrated that radiotherapy combined with a conventional chemotherapy regimen (cyclophosphamide, doxorubicin, prednisone, and vincristine) was effective.²⁵⁵ Other distinguishing features of tumor cells may offer additional pathways to be exploited by chemotherapy in combination with radiotherapy in the future.

A growing field in treating cancer is combining radiotherapy with immunotherapy. When radiation damages or kills tumor cells, specific antigens are exposed or released that can facilitate immune cell recruitment and stimulate activation. This immunoresponse can then propagate and direct itself against metastatic sites, known as the abscopal effect. While the concept itself is over 50 years old, thus far the abscopal effect has rarely been observed.²⁵⁶ However, the advent of checkpoint inhibitors and early clinical studies testing them in combination with radiotherapy seem to have renewed hope that the abscopal effect may become clinically relevant.²⁵⁷ The most well-established immune checkpoint targets are anti-cytotoxic T lymphocyte-associated antigen-4 (CTLA-4), programmed cell death protein-1 (PD-1), and programmed death ligand 1/2 (PD-L1/L2).²⁵⁸ But preclinical and clinical trials are revealing a new generation of potential immune checkpoint targets such as B7 Homolog 3 (B7-H3, or CD276), lymphocyte activation gene-3 (LAG-3), T cell immunoglobulin and mucin-domain containing-3 (TIM-3), T cell immunoglobulin and ITIM domain (TIGIT), and V-domain Ig suppressor of T cell activation (VISTA).²⁵⁹ Aside from immune checkpoints, immunomodulation with toll-like receptor (TLR) agonists and TGF- β antagonists may provide additional tools to induce antitumor immunity in combination with radiotherapy.²⁶⁰⁻²⁶²

Radiotherapy has been combined with surgery for decades. Surgery is employed to remove the obvious tumor mass(es), while radiation eradicates the smaller sites that may go undetected during the procedure as well as metastatic sites.²⁶³ Radioimaging has also been combined with surgery to improve tumor resection, both preoperatively for better mapping of the tumor and intraoperatively with an augmented reality apparatus.²⁶⁴⁻²⁶⁶

1.7 Conclusion

As the field of radiotheranostics has expanded rapidly in the past several decades, many important discoveries have been made. However, they often remain isolated, and adaptation can

be slow due to a variety of logistical challenges.¹⁰ Perhaps the most relevant reason is that the field of radiotheranostics requires highly skilled interdisciplinary research teams, particularly expertise in organic chemistry, biochemistry, animal studies, and radiochemistry. The use of radioactivity is tightly regulated, expensive, and even intimidating from a personal researcher safety standpoint. Radionuclide availability may be limited depending on the country. Instruments and equipment can be prohibitively expensive. The translation of preclinical drugs to the clinic is always difficult, and the complexity of radiotheranostics compared to chemotherapy requires additional training for physicians, nurses, and pharmacists.

While the field of radiotheranostics is challenging, the results are promising, and the potential exciting. We will also note that while this review focused primarily on the application of ligand-targeted radiotheranostics in oncology, additional diseases would also be well-served by the same technologies due to overlap in receptor overexpression. For example, FR β is overexpressed in inflammatory diseases such as rheumatoid arthritis, FAP α and $\alpha_v\beta$ integrins are overexpressed in fibrotic diseases, and GLP1R is overexpressed in diabetes.^{43, 76, 102, 267-270}

As understanding of new oncological targets, refined ligands, additional radionuclides, new chelators, and improved linker pharmacokinetics unfold, it will be essential to incorporate and consolidate these findings if the goal of optimizing the results of radiotheranostic conjugates is to be achieved. Although the field ligand-targeted radiotheranostics is still young, its importance in cancer diagnostics and treatment will likely only continue to grow, as researchers and clinicians rise together to meet the challenges head on.

1.8 References

1. News of Science. *Science* **1957**, *125* (3236), 18-22.
2. Joliot, F.; Curie, I., Artificial Production of a New Kind of Radio-Element. *Nature* **1934**, *133* (3354), 201-202.
3. Janiak, M. K.; Mothersill, C., Marie and Irène Curie, two brilliant women who pioneered the development of nuclear chemistry, radiotherapy, and radiobiology. *International Journal of Radiation Biology* **2021**, 1-4.
4. HERTZ, S.; ROBERTS, A., RADIOACTIVE IODINE IN THE STUDY OF THYROID PHYSIOLOGY: VII. The Use of Radioactive Iodine Therapy in Hyperthyroidism. *Journal of the American Medical Association* **1946**, *131* (2), 81-86.

5. Hutton, B. F., The origins of SPECT and SPECT/CT. *European Journal of Nuclear Medicine and Molecular Imaging* **2014**, *41* (1), 3-16.
6. Kuhl, D. E.; Edwards, R. Q., Image Separation Radioisotope Scanning. *Radiology* **1963**, *80* (4), 653-662.
7. Damadian, R., Tumor Detection by Nuclear Magnetic Resonance. *Science* **1971**, *171* (3976), 1151-1153.
8. Ter-Pogossian, M. M.; Phelps, M. E.; Hoffman, E. J.; Mullani, N. A., A Positron-Emission Transaxial Tomograph for Nuclear Imaging (PETT). *Radiology* **1975**, *114* (1), 89-98.
9. Edwards, C. L., Tumor-localizing radionuclides in retrospect and prospect. *Seminars in Nuclear Medicine* **1979**, *9* (3), 186-189.
10. Herrmann, K.; Schwaiger, M.; Lewis, J. S.; Solomon, S. B.; McNeil, B. J.; Baumann, M.; Gambhir, S. S.; Hricak, H.; Weissleder, R., Radiotheranostics: a roadmap for future development. *The Lancet Oncology* **2020**, *21* (3), e146-e156.
11. Hennrich, U.; Kopka, K., Lutathera®: The First FDA- and EMA-Approved Radiopharmaceutical for Peptide Receptor Radionuclide Therapy. *Pharmaceuticals* **2019**, *12* (3).
12. Reubi, J. C.; Kvolts, L.; Krenning, E.; Lamberts, S. W. J., Distribution of somatostatin receptors in normal and tumor tissue. *Metabolism* **1990**, *39* (9, Supplement 2), 78-81.
13. Reubi, J. C.; Schaer, J. C.; Markwalder, R.; Waser, B.; Horisberger, U.; Laissue, J., Distribution of somatostatin receptors in normal and neoplastic human tissues: recent advances and potential relevance. *Yale J Biol Med* **1997**, *70* (5-6), 471-479.
14. Callison, J. C.; Walker, R. C.; Massion, P. P., Somatostatin Receptors in Lung Cancer: From Function to Molecular Imaging and Therapeutics. *jlc* **2011**, *10* (2), 69-76.
15. Teijeiro, R.; Rios, R.; Costoya, J. A.; Castro, R.; Bello, J. L.; Devesa, J.; Arce, V. M., Activation of Human Somatostatin Receptor 2 Promotes Apoptosis Through a Mechanism that is Independent from Induction of p53. *Cellular Physiology and Biochemistry* **2002**, *12* (1), 31-38.
16. Huo, M.; Zou, A.; Yao, C.; Zhang, Y.; Zhou, J.; Wang, J.; Zhu, Q.; Li, J.; Zhang, Q., Somatostatin receptor-mediated tumor-targeting drug delivery using octreotide-PEG-deoxycholic acid conjugate-modified N-deoxycholic acid-O, N-hydroxyethylation chitosan micelles. *Biomaterials* **2012**, *33* (27), 6393-6407.
17. Xiao, Y.; Jaskula-Sztul, R.; Javadi, A.; Xu, W.; Eide, J.; Dammalapati, A.; Kunnimalaiyaan, M.; Chen, H.; Gong, S., Co-delivery of doxorubicin and siRNA using octreotide-conjugated gold nanorods for targeted neuroendocrine cancer therapy. *Nanoscale* **2012**, *4* (22), 7185-7193.

18. Klinaki, I.; Al-Nahhas, A.; Soneji, N.; Win, Z., ⁶⁸Ga DOTATATE PET/CT Uptake in Spinal Lesions and MRI Correlation on a Patient With Neuroendocrine Tumor: Potential Pitfalls. *Clinical Nuclear Medicine* **2013**, *38* (12).
19. Sounness, B. D.; Schembri, G. P., ⁶⁸Ga-dotatate avid medullary thyroid cancer with occult liver metastases. *Clinical nuclear medicine* **2014**, *39* (1), 87-90.
20. Haug, A. R.; Cindea-Drimus, R.; Auernhammer, C. J.; Reincke, M.; Beuschlein, F.; Wängler, B.; Uebleis, C.; Schmidt, G. P.; Spitzweg, C.; Bartenstein, P.; Hacker, M., Neuroendocrine Tumor Recurrence: Diagnosis with ⁶⁸Ga-DOTATATE PET/CT. *Radiology* **2013**, *270* (2), 517-525.
21. Gayana, S.; Mittal, B. R.; Bhattacharya, A.; Radotra, B. D.; Gupta, A. K., (⁶⁸Ga)-DOTATATE PET/CT imaging in carotid body tumor. *Clinical nuclear medicine* **2013**, *38* (4), e191-3.
22. Sandström, M.; Velikyan, I.; Garske-Román, U.; Sörensen, J.; Eriksson, B.; Granberg, D.; Lundqvist, H.; Sundin, A.; Lubberink, M., Comparative Biodistribution and Radiation Dosimetry of ⁶⁸Ga-DOTATOC and ⁶⁸Ga-DOTATATE in Patients with Neuroendocrine Tumors. *Journal of Nuclear Medicine* **2013**, *54* (10), 1755-1759.
23. Kulkarni, H. R.; Schuchardt, C.; Baum, R. P. In *Peptide Receptor Radionuclide Therapy with ¹⁷⁷Lu Labeled Somatostatin Analogs DOTATATE and DOTATOC: Contrasting Renal Dosimetry in the Same Patient*, Theranostics, Gallium-68, and Other Radionuclides, Berlin, Heidelberg, 2013//; Baum, R. P.; Rösch, F., Eds. Springer Berlin Heidelberg: Berlin, Heidelberg, 2013; pp 551-559.
24. Dobson, R.; Vinjamuri, S.; Hsuan, J.; Banks, M.; Terlizzo, M.; Wiesmann, H.; Daousi, C.; Poston, G. P.; Cuthbertson, D. J., Treatment of Orbital Metastases From a Primary Midgut Neuroendocrine Tumor With Peptide-Receptor Radiolabeled Therapy Using ¹⁷⁷Lutetium-DOTATATE. *Journal of Clinical Oncology* **2013**, *31* (17), e272-e275.
25. Reubi, J. C.; Schaer, J. C.; Waser, B.; Mengod, G., Expression and Localization of Somatostatin Receptor SSTR1, SSTR2, and SSTR3 Messenger RNAs in Primary Human Tumors using *in Situ* Hybridization. *Cancer research* **1994**, *54* (13), 3455-3459.
26. John, M.; Meyerhof, W.; Richter, D.; Waser, B.; Schaer, J. C.; Scherübl, H.; Boese-Landgraf, J.; Neuhaus, P.; Ziske, C.; Mölling, K.; Riecken, E. O.; Reubi, J. C.; Wiedenmann, B., Positive somatostatin receptor scintigraphy correlates with the presence of somatostatin receptor subtype 2. *Gut* **1996**, *38* (1), 33-39.
27. Kuan, C.-T.; Wikstrand, C. J.; McLendon, R. E.; Zalutsky, M. R.; Kumar, U.; Bigner, D. D., Detection of Amino-terminal Extracellular Domain of Somatostatin Receptor 2 by Specific Monoclonal Antibodies and Quantification of Receptor Density in Medulloblastoma. *Hybridoma* **2009**, *28* (6), 389-403.

28. Taylor, R. M.; Severns, V.; Brown, D. C.; Bisoffi, M.; Sillerud, L. O., Prostate cancer targeting motifs: Expression of $\alpha\beta 3$, neurotensin receptor 1, prostate specific membrane antigen, and prostate stem cell antigen in human prostate cancer cell lines and xenografts. *The Prostate* **2012**, 72 (5), 523-532.
29. Liu, T.; Wu, L. Y.; Kazak, M.; Berkman, C. E., Cell-Surface labeling and internalization by a fluorescent inhibitor of prostate-specific membrane antigen. *The Prostate* **2008**, 68 (9), 955-964.
30. Kularatne, S. A.; Zhou, Z.; Yang, J.; Post, C. B.; Low, P. S., Design, Synthesis, and Preclinical Evaluation of Prostate-Specific Membrane Antigen Targeted ^{99m}Tc -Radioimaging Agents. *Molecular Pharmaceutics* **2009**, 6 (3), 790-800.
31. Tönnemann, R.; Meyer, P. T.; Eder, M.; Baranski, A.-C., [(177)Lu]Lu-PSMA-617 Salivary Gland Uptake Characterized by Quantitative In Vitro Autoradiography. *Pharmaceuticals (Basel)* **2019**, 12 (1), 18.
32. Carlucci, G.; Ippisch, R.; Slavik, R.; Mishoe, A.; Blecha, J.; Zhu, S., ^{68}Ga -PSMA-11 NDA Approval: A Novel and Successful Academic Partnership. *Journal of Nuclear Medicine* **2021**, 62 (2), 149-155.
33. Brnjic, A.; Frye, S.; Botkin, C.; Osman, M., Promising ^{177}Lu -PSMA-617 Therapy Results in Patients with Metastatic Castration-Resistant Prostate Cancer. *Journal of Nuclear Medicine* **2021**, 62 (supplement 1), 167-167.
34. Morris, M. J.; De Bono, J. S.; Chi, K. N.; Fizazi, K.; Herrmann, K.; Rahbar, K.; Tagawa, S. T.; Nordquist, L. T.; Vaishampayan, N.; El-Haddad, G.; Park, C. H.; Beer, T. M.; Pérez-Contreras, W. J.; Desilvio, M.; Kpamegan, E. E.; Gericke, G.; Messmann, R. A.; Krause, B. J.; Sartor, A. O., Phase III study of lutetium-177-PSMA-617 in patients with metastatic castration-resistant prostate cancer (VISION). *Journal of Clinical Oncology* **2021**, 39 (18_suppl), LBA4-LBA4.
35. Schittenhelm, J.; Klein, A.; Tatagiba, M. S.; Meyermann, R.; Fend, F.; Goodman, S. L.; Sipos, B., Comparing the expression of integrins $\alpha\beta 3$, $\alpha\beta 5$, $\alpha\beta 6$, $\alpha\beta 8$, fibronectin and fibrinogen in human brain metastases and their corresponding primary tumors. *Int J Clin Exp Pathol* **2013**, 6 (12), 2719-2732.
36. Conroy, K. P.; Kitto, L. J.; Henderson, N. C., αv integrins: key regulators of tissue fibrosis. *Cell and tissue research* **2016**, 365 (3), 511-519.
37. Ruoslahti, E.; Rajotte, D., An address system in the vasculature of normal tissues and tumors. *Annual review of immunology* **2000**, 18 (1), 813-827.
38. Guo, N.; Lang, L.; Li, W.; Kiesewetter, D. O.; Gao, H.; Niu, G.; Xie, Q.; Chen, X., Quantitative analysis and comparison study of [^{18}F] AIF-NOTA-PRGD2, [^{18}F] FPPRGD2 and [^{68}Ga] Ga-NOTA-PRGD2 using a reference tissue model. *PloS one* **2012**, 7 (5), e37506.

39. Gao, S.; Wu, H.; Li, W.; Zhao, S.; Teng, X.; Lu, H.; Hu, X.; Wang, S.; Yu, J.; Yuan, S., A pilot study imaging integrin $\alpha_v\beta_3$ with RGD PET/CT in suspected lung cancer patients. *European Journal of Nuclear Medicine and Molecular Imaging* **2015**, *42* (13), 2029-2037.
40. Beer, A. J.; Schwaiger, M., PET of $\alpha_v\beta_3$ -Integrin and $\alpha_v\beta_3$ -Integrin Expression with ^{18}F -Fluciclatide for Assessment of Response to Targeted Therapy: Ready for Prime Time? *Journal of Nuclear Medicine* **2011**, *52* (3), 335-337.
41. Battle, M. R.; Goggi, J. L.; Allen, L.; Barnett, J.; Morrison, M. S., Monitoring Tumor Response to Antiangiogenic Sunitinib Therapy with ^{18}F -Fluciclatide, an ^{18}F -Labeled $\alpha_v\beta_3$ -Integrin and $\alpha_v\beta_5$ -Integrin Imaging Agent. *Journal of Nuclear Medicine* **2011**, *52* (3), 424-430.
42. Gao, H.; Lang, L.; Guo, N.; Cao, F.; Quan, Q.; Hu, S.; Kiesewetter, D. O.; Niu, G.; Chen, X., PET imaging of angiogenesis after myocardial infarction/reperfusion using a one-step labeled integrin-targeted tracer ^{18}F -AIF-NOTA-PRGD2. *European Journal of Nuclear Medicine and Molecular Imaging* **2012**, *39* (4), 683-692.
43. Kimura, R. H.; Wang, L.; Shen, B.; Huo, L.; Tummers, W.; Filipp, F. V.; Guo, H. H.; Haywood, T.; Abou-Elkacem, L.; Baratto, L.; Habte, F.; Devulapally, R.; Witney, T. H.; Cheng, Y.; Tikole, S.; Chakraborti, S.; Nix, J.; Bonagura, C. A.; Hatami, N.; Mooney, J. J.; Desai, T.; Turner, S.; Gaster, R. S.; Otte, A.; Visser, B. C.; Poultides, G. A.; Norton, J.; Park, W.; Stolowitz, M.; Lau, K.; Yang, E.; Natarajan, A.; Ilovich, O.; Srinivas, S.; Srinivasan, A.; Paulmurugan, R.; Willmann, J.; Chin, F. T.; Cheng, Z.; Iagaru, A.; Li, F.; Gambhir, S. S., Evaluation of integrin $\alpha_v\beta_6$ cystine knot PET tracers to detect cancer and idiopathic pulmonary fibrosis. *Nature Communications* **2019**, *10* (1), 4673.
44. Kenny, L. M.; Coombes, R. C.; Oulie, I.; Contractor, K. B.; Miller, M.; Spinks, T. J.; McParland, B.; Cohen, P. S.; Hui, A.-M.; Palmieri, C.; Osman, S.; Glaser, M.; Turton, D.; Al-Nahhas, A.; Aboagye, E. O., Phase I Trial of the Positron-Emitting Arg-Gly-Asp (RGD) Peptide Radioligand ^{18}F -AH111585 in Breast Cancer Patients. *Journal of Nuclear Medicine* **2008**, *49* (6), 879-886.
45. Tian, R.; Jacobson, O.; Niu, G.; Kiesewetter, D. O.; Wang, Z.; Zhu, G.; Ma, Y.; Liu, G.; Chen, X., Evans Blue Attachment Enhances Somatostatin Receptor Subtype-2 Imaging and Radiotherapy. *Theranostics* **2018**, *8* (3), 735-745.
46. Chen, H.; Jacobson, O.; Niu, G.; Weiss, I. D.; Kiesewetter, D. O.; Liu, Y.; Ma, Y.; Wu, H.; Chen, X., Novel "Add-On" Molecule Based on Evans Blue Confers Superior Pharmacokinetics and Transforms Drugs to Theranostic Agents. *Journal of Nuclear Medicine* **2017**, *58* (4), 590-597.
47. Saul, J. M.; Annapragada, A.; Natarajan, J. V.; Bellamkonda, R. V., Controlled targeting of liposomal doxorubicin via the folate receptor in vitro. *Journal of Controlled Release* **2003**, *92* (1), 49-67.

48. Crane, L. M. A.; Arts, H. J. G.; van Oosten, M.; Low, P. S.; van der Zee, A. G. J.; van Dam, G. M.; Bart, J., The effect of chemotherapy on expression of folate receptor-alpha in ovarian cancer. *Cellular Oncology* **2012**, *35* (1), 9-18.
49. Weitman, S. D.; Lark, R. H.; Coney, L. R.; Fort, D. W.; Frasca, V.; Zurawski, V. R.; Kamen, B. A., Distribution of the Folate Receptor GP38 in Normal and Malignant Cell Lines and Tissues. *Cancer research* **1992**, *52* (12), 3396.
50. Coney, L. R.; Tomassetti, A.; Carayannopoulos, L.; Frasca, V.; Kamen, B. A.; Colnaghi, M. I.; Zurawski, V. R., Cloning of a Tumor-associated Antigen: MOv18 and MOv19 Antibodies Recognize a Folate-binding Protein. *Cancer research* **1991**, *51* (22), 6125.
51. Garin-Chesa, P.; Campbell, I.; Saigo, P. E.; Lewis, J. L., Jr.; Old, L. J.; Rettig, W. J., Trophoblast and ovarian cancer antigen LK26. Sensitivity and specificity in immunopathology and molecular identification as a folate-binding protein. *The American journal of pathology* **1993**, *142* (2), 557-567.
52. Parker, N.; Turk, M. J.; Westrick, E.; Lewis, J. D.; Low, P. S.; Leamon, C. P., Folate receptor expression in carcinomas and normal tissues determined by a quantitative radioligand binding assay. *Analytical Biochemistry* **2005**, *338* (2), 284-293.
53. Low, P. S.; Henne, W. A.; Doorneweerd, D. D., Discovery and Development of Folic-Acid-Based Receptor Targeting for Imaging and Therapy of Cancer and Inflammatory Diseases. *Accounts of Chemical Research* **2008**, *41* (1), 120-129.
54. Low, P. S.; Kularatne, S. A., Folate-targeted therapeutic and imaging agents for cancer. *Current Opinion in Chemical Biology* **2009**, *13* (3), 256-262.
55. Allen, T. M., Ligand-targeted therapeutics in anticancer therapy. *Nature Reviews Cancer* **2002**, *2* (10), 750-763.
56. Holm, J.; Hansen, S. I.; Høier-Madsen, M.; Bostad, L., A high-affinity folate binding protein in proximal tubule cells of human kidney. *Kidney International* **1992**, *41* (1), 50-55.
57. Birn, H.; Spiegelstein, O.; Christensen, E. I.; Finnell, R. H., Renal Tubular Reabsorption of Folate Mediated by Folate Binding Protein 1. *Journal of the American Society of Nephrology* **2005**, *16* (3), 608.
58. Sandoval, R. M.; Kennedy, M. D.; Low, P. S.; Molitoris, B. A., Uptake and trafficking of fluorescent conjugates of folic acid in intact kidney determined using intravital two-photon microscopy. *American Journal of Physiology-Cell Physiology* **2004**, *287* (2), C517-C526.
59. Zhou, P.; Sun, X.; Zhang, Z., Kidney-targeted drug delivery systems. *Acta Pharmaceutica Sinica B* **2014**, *4* (1), 37-42.
60. Bahler, C. D.; Maniar, V.; Marley, K. N.; Kheyfets, S. V.; Shum, C. F.; Sundaram, C. P., OTL-38-Guided Fluorescent Imaging in Renal Cell Cancer Robotic Partial Nephrectomy. *Videourology* **2017**, *31* (3).

61. Fernández, M.; Javaid, F.; Chudasama, V., Advances in targeting the folate receptor in the treatment/imaging of cancers. *Chemical Science* **2018**, *9* (4), 790-810.
62. Shen, J.; Putt, K. S.; Visscher, D. W.; Murphy, L.; Cohen, C.; Singhal, S.; Sandusky, G.; Feng, Y.; Dimitrov, D. S.; Low, P. S., Assessment of folate receptor- β expression in human neoplastic tissues. *Oncotarget* **2015**, *6* (16), 14700-14709.
63. Wang, H.; Zheng, X.; Behm, F. G.; Ratnam, M., Differentiation-independent retinoid induction of folate receptor type β , a potential tumor target in myeloid leukemia. *Blood, The Journal of the American Society of Hematology* **2000**, *96* (10), 3529-3536.
64. Shen, J.; Hu, Y.; Putt, K. S.; Singhal, S.; Han, H.; Visscher, D. W.; Murphy, L. M.; Low, P. S., Assessment of folate receptor alpha and beta expression in selection of lung and pancreatic cancer patients for receptor targeted therapies. *Oncotarget* **2017**, *9* (4), 4485-4495.
65. Kinet, S.; Swainson, L.; Lavanya, M.; Mongellaz, C.; Montel-Hagen, A.; Craveiro, M.; Manel, N.; Battini, J.-L.; Sitbon, M.; Taylor, N., Isolated receptor binding domains of HTLV-1 and HTLV-2 envelopes bind Glut-1 on activated CD4+ and CD8+ T cells. *Retrovirology* **2007**, *4* (1), 31.
66. Avril, N., GLUT1 Expression in Tissue and ¹⁸F-FDG Uptake. *Journal of Nuclear Medicine* **2004**, *45* (6), 930-932.
67. Zambrano, A.; Molt, M.; Uribe, E.; Salas, M., Glut 1 in Cancer Cells and the Inhibitory Action of Resveratrol as A Potential Therapeutic Strategy. *Int J Mol Sci* **2019**, *20* (13), 3374.
68. Som, P.; Ansari, A.; Atkins, H.; Casella, V.; Fowler, J.; Gallagher, B.; Ido, T.; Wan, C.; Wolf, A.; Kuhl, D. In *BIODISTRIBUTION IN NORMAL AND TUMOR BEARING ANIMALS OF F-18-2-DEOXY-2-FLUORO-D-GLUCOSE (F-18-DG)-NEW AGENT FOR MEASURING MYOCARDIAL GLUCOSE-TRANSPORT AND METABOLISM*, JOURNAL OF NUCLEAR MEDICINE, SOC NUCLEAR MEDICINE INC 1850 SAMUEL MORSE DR, RESTON, VA 20190-5316: 1977; pp 618-618.
69. Som, P.; Atkins, H.; Bandoypadhyay, D.; Fowler, J.; MacGregor, R.; Matsui, K.; Oster, Z.; Sacker, D.; Shiue, C.; Turner, H., A fluorinated glucose analog, 2-fluoro-2-deoxy-D-glucose (F-18): nontoxic tracer for rapid tumor detection. *Journal of Nuclear Medicine* **1980**, *21* (7), 670-675.
70. Minn, H.; Joensuu, H.; Ahonen, A.; Klemi, P., Florodeoxyglucose imaging: A method to assess the proliferative activity of human cancer in vivo. Comparison with DNA flow cytometry in head and neck tumors. *Cancer* **1988**, *61* (9), 1776-1781.
71. Mochizuki, T.; Tsukamoto, E.; Kuge, Y.; Kanegae, K.; Zhao, S.; Hikosaka, K.; Hosokawa, M.; Kohanawa, M.; Tamaki, N., FDG Uptake and Glucose Transporter Subtype Expressions in Experimental Tumor and Inflammation Models. *Journal of Nuclear Medicine* **2001**, *42* (10), 1551.

72. Guglielmo, P.; Guerra, L., Radiolabeled fibroblast activation protein inhibitor (FAPI) PET in oncology: has the time come for 18F-fluorodeoxyglucose to think to a well-deserved retirement? *Clinical and Translational Imaging* **2021**, *9* (1), 1-2.
73. Giesel, F. L.; Kratochwil, C.; Lindner, T.; Marschalek, M. M.; Loktev, A.; Lehnert, W.; Debus, J.; Jäger, D.; Flechsig, P.; Altmann, A.; Mier, W.; Haberkorn, U., ⁶⁸Ga-FAPI PET/CT: Biodistribution and Preliminary Dosimetry Estimate of 2 DOTA-Containing FAP-Targeting Agents in Patients with Various Cancers. *Journal of Nuclear Medicine* **2019**, *60* (3), 386-392.
74. Langbein, T.; Weber, W. A.; Eiber, M., Future of Theranostics: An Outlook on Precision Oncology in Nuclear Medicine. *Journal of Nuclear Medicine* **2019**, *60* (Supplement 2), 13S-19S.
75. Brennen, W. N.; Isaacs, J. T.; Denmeade, S. R., Rationale Behind Targeting Fibroblast Activation Protein-Expressing Carcinoma-Associated Fibroblasts as a Novel Chemotherapeutic Strategy. *Molecular Cancer Therapeutics* **2012**, *11* (2), 257.
76. Keane, F. M.; Yao, T.-W.; Seelk, S.; Gall, M. G.; Chowdhury, S.; Poplawski, S. E.; Lai, J. H.; Li, Y.; Wu, W.; Farrell, P.; Vieira de Ribeiro, A. J.; Osborne, B.; Yu, D. M. T.; Seth, D.; Rahman, K.; Haber, P.; Topaloglu, A. K.; Wang, C.; Thomson, S.; Hennessy, A.; Prins, J.; Twigg, S. M.; McLennan, S. V.; McCaughan, G. W.; Bachovchin, W. W.; Gorrell, M. D., Quantitation of fibroblast activation protein (FAP)-specific protease activity in mouse, baboon and human fluids and organs. *FEBS Open Bio* **2014**, *4*, 43-54.
77. Welt, S.; Divgi, C. R.; Scott, A. M.; Garin-Chesa, P.; Finn, R. D.; Graham, M.; Carswell, E. A.; Cohen, A.; Larson, S. M.; Old, L. J., Antibody targeting in metastatic colon cancer: a phase I study of monoclonal antibody F19 against a cell-surface protein of reactive tumor stromal fibroblasts. *Journal of Clinical Oncology* **1994**, *12* (6), 1193-1203.
78. Garin-Chesa, P.; Old, L. J.; Rettig, W. J., Cell surface glycoprotein of reactive stromal fibroblasts as a potential antibody target in human epithelial cancers. *Proceedings of the National Academy of Sciences* **1990**, *87* (18), 7235-7239.
79. Kratochwil, C.; Flechsig, P.; Lindner, T.; Abderrahim, L.; Altmann, A.; Mier, W.; Adeberg, S.; Rathke, H.; Röhrich, M.; Winter, H.; Plinkert, P. K.; Marme, F.; Lang, M.; Kauczor, H.-U.; Jäger, D.; Debus, J.; Haberkorn, U.; Giesel, F. L., ⁶⁸Ga-FAPI PET/CT: Tracer Uptake in 28 Different Kinds of Cancer. *Journal of Nuclear Medicine* **2019**, *60* (6), 801-805.
80. Roy, J.; Hettiarachchi, S. U.; Kaake, M.; Mukkamala, R.; Low, P. S., Design and validation of fibroblast activation protein alpha targeted imaging and therapeutic agents. *Theranostics* **2020**, *10* (13), 5778-5789.

81. Jansen, K.; Heirbaut, L.; Verkerk, R.; Cheng, J. D.; Joossens, J.; Cos, P.; Maes, L.; Lambeir, A.-M.; De Meester, I.; Augustyns, K.; Van der Veken, P., Extended Structure–Activity Relationship and Pharmacokinetic Investigation of (4-Quinolinoyl)glycyl-2-cyanopyrrolidine Inhibitors of Fibroblast Activation Protein (FAP). *Journal of Medicinal Chemistry* **2014**, *57* (7), 3053-3074.
82. Tsai, T.-Y.; Yeh, T.-K.; Chen, X.; Hsu, T.; Jao, Y.-C.; Huang, C.-H.; Song, J.-S.; Huang, Y.-C.; Chien, C.-H.; Chiu, J.-H.; Yen, S.-C.; Tang, H.-K.; Chao, Y.-S.; Jiaang, W.-T., Substituted 4-Carboxymethylpyroglutamic Acid Diamides as Potent and Selective Inhibitors of Fibroblast Activation Protein. *Journal of Medicinal Chemistry* **2010**, *53* (18), 6572-6583.
83. Poplawski, S. E.; Lai, J. H.; Li, Y.; Jin, Z.; Liu, Y.; Wu, W.; Wu, Y.; Zhou, Y.; Sudmeier, J. L.; Sanford, D. G.; Bachovchin, W. W., Identification of Selective and Potent Inhibitors of Fibroblast Activation Protein and Prolyl Oligopeptidase. *Journal of Medicinal Chemistry* **2013**, *56* (9), 3467-3477.
84. Cho, J. M.; Yang, E. H.; Quan, W.; Nam, E. H.; Cheon, H. G., Discovery of a novel fibroblast activation protein (FAP) inhibitor, BR103354, with anti-diabetic and anti-steatotic effects. *Scientific reports* **2020**, *10* (1), 1-17.
85. Christiansen, V. J.; Jackson, K. W.; Lee, K. N.; Downs, T. D.; McKee, P. A., Targeting Inhibition of Fibroblast Activation Protein- α and Prolyl Oligopeptidase Activities on Cells Common to Metastatic Tumor Microenvironments. *Neoplasia* **2013**, *15* (4), 348-358.
86. Fischer, E.; Chaitanya, K.; Wüest, T.; Wadle, A.; Scott, A. M.; van den Broek, M.; Schibli, R.; Bauer, S.; Renner, C., Radioimmunotherapy of Fibroblast Activation Protein Positive Tumors by Rapidly Internalizing Antibodies. *Clinical Cancer Research* **2012**, *18* (22), 6208-6218.
87. Dohi, O.; Ohtani, H.; Hatori, M.; Sato, E.; Hosaka, M.; Nagura, H.; Itoi, E.; Kokubun, S., Histogenesis-specific expression of fibroblast activation protein and dipeptidylpeptidase-IV in human bone and soft tissue tumours. *Histopathology* **2009**, *55* (4), 432-440.
88. Wagner, L.; Klemann, C.; Stephan, M.; von Hörsten, S., Unravelling the immunological roles of dipeptidyl peptidase 4 (DPP4) activity and/or structure homologue (DASH) proteins. *Clinical & Experimental Immunology* **2016**, *184* (3), 265-283.
89. Watabe, T.; Liu, Y.; Kaneda-Nakashima, K.; Shirakami, Y.; Lindner, T.; Ooe, K.; Toyoshima, A.; Nagata, K.; Shimosegawa, E.; Haberkorn, U.; Kratochwil, C.; Shinohara, A.; Giesel, F.; Hatazawa, J., Theranostics Targeting Fibroblast Activation Protein in the Tumor Stroma: ^{64}Cu - and ^{225}Ac -Labeled FAPI-04 in Pancreatic Cancer Xenograft Mouse Models. *Journal of Nuclear Medicine* **2020**, *61* (4), 563-569.
90. Ballal, S.; Yadav, M. P.; Kramer, V.; Moon, E. S.; Roesch, F.; Tripathi, M.; Mallick, S.; ArunRaj, S. T.; Bal, C., A theranostic approach of ^{68}Ga [Ga-DOTA.SA.FAPi PET/CT-guided ^{177}Lu]Lu-DOTA.SA.FAPi radionuclide therapy in an end-stage breast cancer patient: new frontier in targeted radionuclide therapy. *European Journal of Nuclear Medicine and Molecular Imaging* **2021**, *48* (3), 942-944.

91. Lindner, T.; Altmann, A.; Kraemer, S.; Kleist, C.; Loktev, A.; Kratochwil, C.; Giesel, F.; Mier, W.; Marme, F.; Debus, J.; Haberkorn, U., Design and development of ^{99m}Tc labeled FAPI-tracers for SPECT-imaging and ¹⁸⁸Re therapy. *Journal of Nuclear Medicine* **2020**.
92. Lindner, T.; Loktev, A.; Altmann, A.; Giesel, F.; Kratochwil, C.; Debus, J.; Jäger, D.; Mier, W.; Haberkorn, U., Development of Quinoline-Based Theranostic Ligands for the Targeting of Fibroblast Activation Protein. *Journal of Nuclear Medicine* **2018**, *59* (9), 1415-1422.
93. Loktev, A.; Lindner, T.; Mier, W.; Debus, J.; Altmann, A.; Jäger, D.; Giesel, F.; Kratochwil, C.; Barthe, P.; Roumestand, C.; Haberkorn, U., A Tumor-Imaging Method Targeting Cancer-Associated Fibroblasts. *Journal of Nuclear Medicine* **2018**, *59* (9), 1423-1429.
94. Meyer, C.; Dahlbom, M.; Lindner, T.; Vauclin, S.; Mona, C.; Slavik, R.; Czernin, J.; Haberkorn, U.; Calais, J., Radiation Dosimetry and Biodistribution of ⁶⁸Ga-FAPI-46 PET Imaging in Cancer Patients. *Journal of Nuclear Medicine* **2020**, *61* (8), 1171-1177.
95. Giesel, F. L.; Adeberg, S.; Syed, M.; Lindner, T.; Jiménez-Franco, L. D.; Mavriopoulou, E.; Staudinger, F.; Tonndorf-Martini, E.; Regnery, S.; Rieken, S.; El Shafie, R.; Röhrich, M.; Flechsig, P.; Kluge, A.; Altmann, A.; Debus, J.; Haberkorn, U.; Kratochwil, C., FAPI-74 PET/CT Using Either ¹⁸F-ALF or Cold-Kit ⁶⁸Ga Labeling: Biodistribution, Radiation Dosimetry, and Tumor Delineation in Lung Cancer Patients. *Journal of Nuclear Medicine* **2021**, *62* (2), 201-207.
96. Fu, W.; Liu, L.; Liu, H.; Zhou, Z.; Chen, Y., Increased FAPI Uptake in Brain Metastasis From Lung Cancer on ⁶⁸Ga-FAPI PET/CT. *Clinical nuclear medicine* **2021**, *46* (1), e1-e2.
97. Koerber, S. A.; Finck, R.; Dendl, K.; Uhl, M.; Lindner, T.; Kratochwil, C.; Röhrich, M.; Rathke, H.; Ungerechts, G.; Adeberg, S.; Herfarth, K.; Jaeger, D.; Debus, J.; Haberkorn, U.; Giesel, F. L., Novel FAP ligands enable improved imaging contrast in sarcoma patients due to FAPI-PET/CT. *European Journal of Nuclear Medicine and Molecular Imaging* **2021**.
98. Toms, J.; Kogler, J.; Maschauer, S.; Daniel, C.; Schmidkonz, C.; Kuwert, T.; Prante, O., Targeting Fibroblast Activation Protein: Radiosynthesis and Preclinical Evaluation of an ¹⁸F-Labeled FAP Inhibitor. *Journal of Nuclear Medicine* **2020**, *61* (12), 1806-1813.
99. Reubi, J. C.; Waser, B., Concomitant expression of several peptide receptors in neuroendocrine tumours: molecular basis for in vivo multireceptor tumour targeting. *European journal of nuclear medicine and molecular imaging* **2003**, *30* (5), 781-793.
100. Eng, J.; Kleinman, W. A.; Singh, L.; Singh, G.; Raufman, J. P., Isolation and characterization of exendin-4, an exendin-3 analogue, from *Heloderma suspectum* venom. Further evidence for an exendin receptor on dispersed acini from guinea pig pancreas. *Journal of Biological Chemistry* **1992**, *267* (11), 7402-7405.

101. Koole, C.; Reynolds, C. A.; Mobarec, J. C.; Hick, C.; Sexton, P. M.; Sakmar, T. P., Genetically encoded photocross-linkers determine the biological binding site of exendin-4 peptide in the N-terminal domain of the intact human glucagon-like peptide-1 receptor (GLP-1R). *Journal of Biological Chemistry* **2017**, *292* (17), 7131-7144.
102. Christ, E.; Wild, D.; Reubi, J. C., Glucagonlike Peptide-1 Receptor: An Example of Translational Research in Insulinomas: A Review. *Endocrinology and Metabolism Clinics of North America* **2010**, *39* (4), 791-800.
103. Luo, Y.; Pan, Q.; Yao, S.; Yu, M.; Wu, W.; Xue, H.; Kiesewetter, D. O.; Zhu, Z.; Li, F.; Zhao, Y.; Chen, X., Glucagon-Like Peptide-1 Receptor PET/CT with ⁶⁸Ga-NOTA-Exendin-4 for Detecting Localized Insulinoma: A Prospective Cohort Study. *J Nucl Med* **2016**, *57* (5), 715-720.
104. Antwi, K.; Fani, M.; Heye, T.; Nicolas, G.; Rottenburger, C.; Kaul, F.; Merkle, E.; Zech, C. J.; Boll, D.; Vogt, D. R.; Gloor, B.; Christ, E.; Wild, D., Comparison of glucagon-like peptide-1 receptor (GLP-1R) PET/CT, SPECT/CT and 3T MRI for the localisation of occult insulinomas: evaluation of diagnostic accuracy in a prospective crossover imaging study. *European Journal of Nuclear Medicine and Molecular Imaging* **2018**, *45* (13), 2318-2327.
105. Fani, M.; Peitl, P. K.; Velikyan, I., Current Status of Radiopharmaceuticals for the Theranostics of Neuroendocrine Neoplasms. *Pharmaceuticals* **2017**, *10* (1), 30.
106. Velikyan, I.; Eriksson, O., Advances in GLP-1 receptor targeting radiolabeled agent development and prospective of theranostics. *Theranostics* **2020**, *10* (1), 437-461.
107. Preston, S. R.; Miller, G. V.; Primrose, J. N., Bombesin-like peptides and cancer. *Critical Reviews in Oncology/Hematology* **1996**, *23* (3), 225-238.
108. Jensen, R. T.; Battey, J. F.; Spindel, E. R.; Benya, R. V., International Union of Pharmacology. LXVIII. Mammalian Bombesin Receptors: Nomenclature, Distribution, Pharmacology, Signaling, and Functions in Normal and Disease States. *Pharmacological Reviews* **2008**, *60* (1), 1-42.
109. Reubi, J. C.; Körner, M.; Waser, B.; Mazzucchelli, L.; Guillou, L., High expression of peptide receptors as a novel target in gastrointestinal stromal tumours. *European Journal of Nuclear Medicine and Molecular Imaging* **2004**, *31* (6), 803-810.
110. Sun, B.; Halmos, G.; Schally, A. V.; Wang, X.; Martinez, M., Presence of receptors for bombesin/gastrin-releasing peptide and mRNA for three receptor subtypes in human prostate cancers. *The Prostate* **2000**, *42* (4), 295-303.
111. Markwalder, R.; Reubi, J. C., Gastrin-releasing Peptide Receptors in the Human Prostate. *Relation to Neoplastic Transformation* **1999**, *59* (5), 1152-1159.
112. Halmos, G.; Wittliff, J. L.; Schally, A. V., Characterization of Bombesin/Gastrin-releasing Peptide Receptors in Human Breast Cancer and Their Relationship to Steroid Receptor Expression. *Cancer research* **1995**, *55* (2), 280-287.

113. Cuttitta, F.; Carney, D. N.; Mulshine, J.; Moody, T. W.; Fedorko, J.; Fischler, A.; Minna, J. D., Bombesin-like peptides can function as autocrine growth factors in human small-cell lung cancer. *Nature* **1985**, *316* (6031), 823-826.
114. Cornelio, D. B.; Roesler, R.; Schwartzmann, G., Gastrin-releasing peptide receptor as a molecular target in experimental anticancer therapy. *Annals of Oncology* **2007**, *18* (9), 1457-1466.
115. Zhang, H.; Abiraj, K.; Thorek, D. L. J.; Waser, B.; Smith-Jones, P. M.; Honer, M.; Reubi, J. C.; Maecke, H. R., Evolution of Bombesin Conjugates for Targeted PET Imaging of Tumors. *PLOS ONE* **2012**, *7* (9), e44046.
116. Yang, H.; Cai, H.; Wan, L.; Liu, S.; Li, S.; Cheng, J.; Lu, X., Bombesin Analogue-Mediated Delivery Preferentially Enhances the Cytotoxicity of a Mitochondria-Disrupting Peptide in Tumor Cells. *PLOS ONE* **2013**, *8* (2), e57358.
117. Roivainen, A.; Kähkönen, E.; Luoto, P.; Borkowski, S.; Hofmann, B.; Jambor, I.; Lehtiö, K.; Rantala, T.; Rottmann, A.; Sipilä, H.; Sparks, R.; Suilamo, S.; Tolvanen, T.; Valencia, R.; Minn, H., Plasma Pharmacokinetics, Whole-Body Distribution, Metabolism, and Radiation Dosimetry of ⁶⁸Ga Bombesin Antagonist BAY 86-7548 in Healthy Men. *Journal of Nuclear Medicine* **2013**, *54* (6), 867-872.
118. Abiraj, K.; Mansi, R.; Tamma, M.-L.; Fani, M.; Forrer, F.; Nicolas, G.; Cescato, R.; Reubi, J. C.; Maecke, H. R., Bombesin Antagonist-Based Radioligands for Translational Nuclear Imaging of Gastrin-Releasing Peptide Receptor-Positive Tumors. *Journal of Nuclear Medicine* **2011**, *52* (12), 1970-1978.
119. Rinne, S. S.; Abouzayed, A.; Gagnon, K.; Tolmachev, V.; Orlova, A., ⁶⁶Ga-PET-imaging of GRPR-expression in prostate cancer: production and characterization of [⁶⁶Ga]Ga-NOTA-PEG2-RM26. *Scientific Reports* **2021**, *11* (1), 3631.
120. Mitran, B.; Thisgaard, H.; Rosenström, U.; Dam, J. H.; Larhed, M.; Tolmachev, V.; Orlova, A., High Contrast PET Imaging of GRPR Expression in Prostate Cancer Using Cobalt-Labeled Bombesin Antagonist RM26. *Contrast Media & Molecular Imaging* **2017**, *2017*, 6873684.
121. Vahidfar, N.; Aghanejad, A.; Ahmadzadehfar, H.; Farzanehfar, S.; Eppard, E., Theranostic Advances in Breast Cancer in Nuclear Medicine. *Int J Mol Sci* **2021**, *22* (9), 4597.
122. Osadchii, O. E., Emerging role of neurotensin in regulation of the cardiovascular system. *European Journal of Pharmacology* **2015**, *762*, 184-192.
123. Reubi, J. C.; Waser, B.; Friess, H.; Büchler, M.; Laissue, J., Neurotensin receptors: a new marker for human ductal pancreatic adenocarcinoma. *Gut* **1998**, *42* (4), 546-550.
124. Ehlers, R. A.; Kim, S.; Zhang, Y.; Ethridge, R. T.; Murrilo, C.; Hellmich, M. R.; Evans, D. B.; Townsend, C. M., Jr.; Mark Evers, B., Gut peptide receptor expression in human pancreatic cancers. *Ann Surg* **2000**, *231* (6), 838-848.

125. Körner, M.; Waser, B.; Strobel, O.; Büchler, M.; Reubi, J. C., Neurotensin receptors in pancreatic ductal carcinomas. *EJNMMI Research* **2015**, *5* (1), 17.
126. Schulz, J.; Rohracker, M.; Stiebler, M.; Goldschmidt, J.; Grosser, O. S.; Osterkamp, F.; Pethe, A.; Reineke, U.; Smerling, C.; Amthauer, H., Comparative Evaluation of the Biodistribution Profiles of a Series of Nonpeptidic Neurotensin Receptor-1 Antagonists Reveals a Promising Candidate for Theranostic Applications. *Journal of Nuclear Medicine* **2016**, *57* (7), 1120-1123.
127. Gully, D.; Canton, M.; Boigegrain, R.; Jeanjean, F.; Molimard, J. C.; Poncelet, M.; Gueudet, C.; Heaulme, M.; Leyris, R.; Brouard, A., Biochemical and pharmacological profile of a potent and selective nonpeptide antagonist of the neurotensin receptor. *Proceedings of the National Academy of Sciences* **1993**, *90* (1), 65-69.
128. Gully, D.; Labeeuw, B.; Boigegrain, R.; Oury-Donat, F.; Bachy, A.; Poncelet, M.; Steinberg, R.; Suaud-Chagny, M. F.; Santucci, V.; Vita, N.; Pecceu, F.; Labbé-Jullié, C.; Kitabgi, P.; Soubrié, P.; Le Fur, G.; Maffrand, J. P., Biochemical and Pharmacological Activities of SR 142948A, a New Potent Neurotensin Receptor Antagonist. *Journal of Pharmacology and Experimental Therapeutics* **1997**, *280* (2), 802-812.
129. Baum, R. P.; Singh, A.; Schuchardt, C.; Kulkarni, H. R.; Klette, I.; Wiessalla, S.; Osterkamp, F.; Reineke, U.; Smerling, C., ¹⁷⁷Lu-3BP-227 for Neurotensin Receptor 1–Targeted Therapy of Metastatic Pancreatic Adenocarcinoma: First Clinical Results. *Journal of Nuclear Medicine* **2018**, *59* (5), 809-814.
130. Wayua, C.; Roy, J.; Putt, K. S.; Low, P. S., Selective Tumor Targeting of Desacetyl Vinblastine Hydrazide and Tubulysin B via Conjugation to a Cholecystokinin 2 Receptor (CCK2R) Ligand. *Molecular Pharmaceutics* **2015**, *12* (7), 2477-2483.
131. Roy, J.; Putt, K. S.; Coppola, D.; Leon, M. E.; Khalil, F. K.; Centeno, B. A.; Clark, N.; Stark, V. E.; Morse, D. L.; Low, P. S., Assessment of cholecystokinin 2 receptor (CCK2R) in neoplastic tissue. *Oncotarget* **2016**, *7* (12), 14605-14615.
132. Wayua, C.; Low, P. S., Evaluation of a Nonpeptidic Ligand for Imaging of Cholecystokinin 2 Receptor–Expressing Cancers. *Journal of Nuclear Medicine* **2015**, *56* (1), 113-119.
133. Laverman, P.; Roosenburg, S.; Joosten, L.; Eek, A.; van Delft, F.; Rutjes, F.; Oyen, W.; Boerman, O., PET and SPECT imaging of gastrin receptor-expressing tumors with CCK receptor-binding peptides. *Journal of Nuclear Medicine* **2011**, *52* (supplement 1), 1580-1580.
134. Brillouet, S.; Mestre-Voegtle, B.; Dorbes, S.; Caselles, O.; de Medina, P.; Picard, C.; Courbon, F.; Poirot, M.; Silvente-Poirot, S., Preclinical evaluation of new radiolabeled cholecystokinin derivatives for scintigraphic imaging of cholecystokinin/gastrin receptors. *Cancer research* **2007**, *67* (9 Supplement), 5525-5525.
135. Klingler, M.; Hörmann, A. A.; Guggenberg, E. v., Cholecystokinin-2 receptor targeting with radiolabeled peptides: Current status and future directions. *Current medicinal chemistry* **2020**.

136. Klingler, M.; Rangger, C.; Summer, D.; Kaeopookum, P.; Decristoforo, C.; von Guggenberg, E., Cholecystokinin-2 Receptor Targeting with Novel C-terminally Stabilized HYNIC-Minigastrin Analogs Radiolabeled with Technetium-99m. *Pharmaceutics* **2019**, *12* (1), 13.
137. Qin, Y.; Imobersteg, S.; Blanc, A.; Frank, S.; Schibli, R.; Béhé, M. P.; Grzmil, M., Evaluation of Actinium-225 Labeled Minigastrin Analogue [²²⁵Ac]Ac-DOTA-PP-F11N for Targeted Alpha Particle Therapy. *Pharmaceutics* **2020**, *12* (11), 1088.
138. Nock, B. A.; Maina, T.; Béhé, M.; Nikolopoulou, A.; Gotthardt, M.; Schmitt, J. S.; Behr, T. M.; Mäcke, H. R., CCK-2/gastrin receptor-targeted tumor imaging with ^{99m}Tc-labeled minigastrin analogs. *Journal of Nuclear Medicine* **2005**, *46* (10), 1727-1736.
139. Aloj, L.; Caracò, C.; Panico, M.; Zannetti, A.; Del Vecchio, S.; Tesauro, D.; De Luca, S.; Arra, C.; Pedone, C.; Morelli, G., In vitro and in vivo evaluation of ¹¹¹In-DTPAGlu-G-CCK8 for cholecystokinin-B receptor imaging. *Journal of Nuclear Medicine* **2004**, *45* (3), 485-494.
140. Laverman, P.; Roosenburg, S.; Gotthardt, M.; Park, J.; Oyen, W. J. G.; de Jong, M.; Hellmich, M. R.; Rutjes, F. P. J. T.; van Delft, F. L.; Boerman, O. C., Targeting of a CCK2 receptor splice variant with ¹¹¹In-labelled cholecystokinin-8 (CCK8) and ¹¹¹In-labelled minigastrin. *European Journal of Nuclear Medicine and Molecular Imaging* **2008**, *35* (2), 386-392.
141. Laverman, P.; Béhé, M.; Oyen, W. J. G.; Willems, P. H. G. M.; Corstens, F. H. M.; Behr, T. M.; Boerman, O. C., Two Technetium-99m-Labeled Cholecystokinin-8 (CCK8) Peptides for Scintigraphic Imaging of CCK Receptors. *Bioconjugate Chemistry* **2004**, *15* (3), 561-568.
142. de Jong, M.; Bakker, W. H.; Bernard, B. F.; Valkema, R.; Kwekkeboom, D. J.; Reubi, J.-C.; Srinivasan, A.; Schmidt, M.; Krenning, E. P., Preclinical and Initial Clinical Evaluation of ¹¹¹In-Labeled Nonsulfated CCK₈ Analog: A Peptide for CCK-B Receptor-Targeted Scintigraphy and Radionuclide Therapy. *Journal of Nuclear Medicine* **1999**, *40* (12), 2081-2087.
143. Béhé, M.; Becker, W.; Gotthardt, M.; Angerstein, C.; Behr, T. M., Improved kinetic stability of DTPA-dGlu as compared with conventional monofunctional DTPA in chelating indium and yttrium: preclinical and initial clinical evaluation of radiometal labelled minigastrin derivatives. *European Journal of Nuclear Medicine and Molecular Imaging* **2003**, *30* (8), 1140-1146.
144. Béhé, M.; Behr, T. M., Cholecystokinin-B (CCK-B)/gastrin receptor targeting peptides for staging and therapy of medullary thyroid cancer and other CCK-B receptor expressing malignancies. *Peptide Science* **2002**, *66* (6), 399-418.
145. Behr, T. M.; Jenner, N.; Radetzky, S.; Béhe, M.; Gratz, S.; Yücekent, S.; Raue, F.; Becker, W., Targeting of cholecystokinin-B/gastrin receptors in vivo: preclinical and initial clinical evaluation of the diagnostic and therapeutic potential of radiolabelled gastrin. *European Journal of Nuclear Medicine* **1998**, *25* (4), 424-430.

146. Behr, T. M.; Béhé, M. P., Cholecystokinin-B/gastrin receptor-targeting peptides for staging and therapy of medullary thyroid cancer and other cholecystokinin-B receptor-expressing malignancies. *Seminars in Nuclear Medicine* **2002**, *32* (2), 97-109.
147. Behr, T. M.; Jenner, N.; Béhé, M.; Angerstein, C.; Gratz, S.; Raue, F.; Becker, W., Radiolabeled Peptides for Targeting Cholecystokinin-B/Gastrin Receptor-Expressing Tumors. *Journal of Nuclear Medicine* **1999**, *40* (6), 1029-1044.
148. Marks, I. S.; Gardeen, S. S.; Kurdziel, S. J.; Nicolaou, S. T.; Woods, J. E.; Kularatne, S. A.; Low, P. S., Development of a Small Molecule Tubulysin B Conjugate for Treatment of Carbonic Anhydrase IX Receptor Expressing Cancers. *Molecular Pharmaceutics* **2018**, *15* (6), 2289-2296.
149. Strapcova, S.; Takacova, M.; Csaderova, L.; Martinelli, P.; Lukacikova, L.; Gal, V.; Kopacek, J.; Svastova, E., Clinical and Pre-Clinical Evidence of Carbonic Anhydrase IX in Pancreatic Cancer and Its High Expression in Pre-Cancerous Lesions. *Cancers* **2020**, *12* (8), 2005.
150. Dudutienė, V.; Matulienė, J.; Smirnov, A.; Timm, D. D.; Zubrienė, A.; Baranauskienė, L.; Morkūnaitė, V.; Smirnovienė, J.; Michailovienė, V.; Juozapaitienė, V.; Mickevičiūtė, A.; Kazokaitė, J.; Bakšytė, S.; Kasiliauskaitė, A.; Jachno, J.; Revuckienė, J.; Kišonaitė, M.; Pilipuitytė, V.; Ivanauskaitė, E.; Milinavičiūtė, G.; Smirnovas, V.; Petrikaitė, V.; Kairys, V.; Petrauskas, V.; Norvaišas, P.; Lingė, D.; Gibieža, P.; Čapkauskaitė, E.; Zakšauskas, A.; Kazlauskas, E.; Manakova, E.; Gražulis, S.; Ladbury, J. E.; Matulis, D., Discovery and Characterization of Novel Selective Inhibitors of Carbonic Anhydrase IX. *Journal of Medicinal Chemistry* **2014**, *57* (22), 9435-9446.
151. Yang, X.; Minn, I.; Rowe, S. P.; Banerjee, S. R.; Gorin, M. A.; Brummet, M.; Lee, H. S.; Koo, S. M.; Sysa-Shah, P.; Mease, R. C.; Nimmagadda, S.; Allaf, M. E.; Pomper, M. G., Imaging of carbonic anhydrase IX with an ¹¹¹In-labeled dual-motif inhibitor. *Oncotarget* **2015**, *6* (32), 33733-33742.
152. Iikuni, S.; Watanabe, H.; Shimizu, Y.; Nakamoto, Y.; Ono, M., PET imaging and pharmacological therapy targeting carbonic anhydrase-IX high-expressing tumors using US2 platform based on bivalent ureidosulfonamide. *PLOS ONE* **2020**, *15* (12), e0243327.
153. Minn, I.; Koo, S. M.; Lee, H. S.; Brummet, M.; Rowe, S. P.; Gorin, M. A.; Sysa-Shah, P.; Lewis, W. D.; Ahn, H.-H.; Wang, Y., [⁶⁴Cu] XYIMSR-06: A dual-motif CAIX ligand for PET imaging of clear cell renal cell carcinoma. *Oncotarget* **2016**, *7* (35), 56471.
154. Roy, J.; Kaake, M.; Low, P. S., Small molecule targeted NIR dye conjugate for imaging LHRH receptor positive cancers. *Oncotarget* **2019**, *10* (2), 152-160.
155. Vaz, S.; Hadaschik, B.; Gabriel, M.; Herrmann, K.; Eiber, M.; Costa, D., Influence of androgen deprivation therapy on PSMA expression and PSMA-ligand PET imaging of prostate cancer patients. *European Journal of Nuclear Medicine and Molecular Imaging* **2020**, *47* (1), 9-15.

156. Hao, D.; Sun, L.; Hu, X.; Hao, X., (99m)Tc-LHRH in tumor receptor imaging. *Oncol Lett* **2017**, *14* (1), 569-578.
157. Gao, F.; Cai, P.; Yang, W.; Xue, J.; Gao, L.; Liu, R.; Wang, Y.; Zhao, Y.; He, X.; Zhao, L.; Huang, G.; Wu, F.; Zhao, Y.; Chai, Z.; Gao, X., Ultrasmall [64Cu]Cu Nanoclusters for Targeting Orthotopic Lung Tumors Using Accurate Positron Emission Tomography Imaging. *ACS Nano* **2015**, *9* (5), 4976-4986.
158. Föst, C.; Duwe, F.; Hellriegel, M.; Schweyer, S.; Emons, G.; Gründker, C., Targeted chemotherapy for triple-negative breast cancers via LHRH receptor. *Oncol Rep* **2011**, *25* (5), 1481-1487.
159. Price, E. W.; Orvig, C., Matching chelators to radiometals for radiopharmaceuticals. *Chem. Soc. Rev.* **2014**, *43* (1), 260-290.
160. Fersing, C.; Bouhrel, A.; Cantelli, C.; Garrigue, P.; Lisowski, V.; Guillet, B., A Comprehensive Review of Non-Covalent Radiofluorination Approaches Using Aluminum [(18)F]fluoride: Will [(18)F]AlF Replace (68)Ga for Metal Chelate Labeling? *Molecules (Basel, Switzerland)* **2019**, *24* (16), 2866.
161. Klaassen, N. J. M.; Arntz, M. J.; Gil Arranja, A.; Roosen, J.; Nijssen, J. F. W., The various therapeutic applications of the medical isotope holmium-166: a narrative review. *EJNMMI Radiopharmacy and Chemistry* **2019**, *4* (1), 19.
162. Lu, G.; Maresca, K. P.; Hillier, S. M.; Zimmerman, C. N.; Eckelman, W. C.; Joyal, J. L.; Babich, J. W., Synthesis and SAR of 99mTc/Re-labeled small molecule prostate specific membrane antigen inhibitors with novel polar chelates. *Bioorganic & Medicinal Chemistry Letters* **2013**, *23* (5), 1557-1563.
163. Ndinguri, M. W.; Fronczek, F. R.; Marzilli, P. A.; Crowe, W. E.; Hammer, R. P.; Marzilli, L. G., Exploring water-soluble Pt(II) complexes of diethylenetriamine derivatives functionalized at the central nitrogen. Synthesis, characterization, and reaction with 5'-GMP. *Inorganica Chimica Acta* **2010**, *363* (8), 1796-1804.
164. Eychenne, R.; Chérel, M.; Haddad, F.; Guérard, F.; Gestin, J.-F., Overview of the Most Promising Radionuclides for Targeted Alpha Therapy: The “Hopeful Eight”. *Pharmaceutics* **2021**, *13* (6).
165. Rahmim, A.; Zaidi, H., PET versus SPECT: strengths, limitations and challenges. *Nuclear Medicine Communications* **2008**, *29* (3).
166. Conti, M.; Eriksson, L., Physics of pure and non-pure positron emitters for PET: a review and a discussion. *EJNMMI Phys* **2016**, *3* (1), 8-8.
167. Vallabhajosula, S.; Solnes, L.; Vallabhajosula, B., A Broad Overview of Positron Emission Tomography Radiopharmaceuticals and Clinical Applications: What Is New? *Seminars in Nuclear Medicine* **2011**, *41* (4), 246-264.

168. Belov, V. V.; Bonab, A. A.; Fischman, A. J.; Heartlein, M.; Calias, P.; Papisov, M. I., Iodine-124 as a Label for Pharmacological PET Imaging. *Molecular Pharmaceutics* **2011**, *8* (3), 736-747.
169. Velikyan, I., Prospective of ^{68}Ga -radiopharmaceutical development. *Theranostics* **2013**, *4* (1), 47-80.
170. Brandt, M.; Cardinale, J.; Aulsebrook, M. L.; Gasser, G.; Mindt, T. L., An Overview of PET Radiochemistry, Part 2: Radiometals. *Journal of Nuclear Medicine* **2018**, *59* (10), 1500-1506.
171. Blau, M.; Ganatra, R.; Bender, M. A., ^{18}F -fluoride for bone imaging. *Seminars in Nuclear Medicine* **1972**, *2* (1), 31-37.
172. Jurcic, J. G.; Scheinberg, D. A., Monoclonal Antibodies: Leukemia and Lymphoma. In *Encyclopedia of Cancer (Second Edition)*, Bertino, J. R., Ed. Academic Press: New York, 2002; pp 235-245.
173. Poty, S.; Francesconi, L. C.; McDevitt, M. R.; Morris, M. J.; Lewis, J. S., α -Emitters for Radiotherapy: From Basic Radiochemistry to Clinical Studies-Part 1. *J Nucl Med* **2018**, *59* (6), 878-884.
174. Wulbrand, C.; Seidl, C.; Gaertner, F. C.; Bruchertseifer, F.; Morgenstern, A.; Essler, M.; Senekowitsch-Schmidtke, R., Alpha-particle emitting ^{213}Bi -anti-EGFR immunoconjugates eradicate tumor cells independent of oxygenation. *PLoS one* **2013**, *8* (5), e64730-e64730.
175. Vaidyanathan, G.; Zalutsky, M. R., Astatine Radiopharmaceuticals: Prospects and Problems. *Curr Radiopharm* **2008**, *1* (3), 177-177.
176. Hall, E. J.; Giaccia, A. J., *Radiobiology for the Radiologist*. Philadelphia: 2006; Vol. 6.
177. Kampf, G., Induction of DNA double-strand breaks by ionizing radiation of different quality and their relevance for cell inactivation. *Radiobiol., Radiother. (German Democratic Republic)* **1988**, *29* (6).
178. Srinivasarao, M.; Galliford, C. V.; Low, P. S., Principles in the design of ligand-targeted cancer therapeutics and imaging agents. *Nat Rev Drug Discov* **2015**, *14* (3), 203-19.
179. Nakamura, Y.; Inomata, S.; Ebine, M.; Manabe, Y.; Iwakura, I.; Ueda, M., "Click-made" biaryl-linker improving efficiency in protein labelling for the membrane target protein of a bioactive compound. *Organic & biomolecular chemistry* **2010**, *9* (1), 83-85.
180. Tamura, S.; Inomata, S.; Ebine, M.; Genji, T.; Iwakura, I.; Mukai, M.; Shoji, M.; Sugai, T.; Ueda, M., Triazolyl-phenyl linker system enhancing the aqueous solubility of a molecular probe and its efficiency in affinity labeling of a target protein for jasmonate glucoside. *Bioorganic & Medicinal Chemistry Letters* **2013**, *23* (1), 188-193.

181. Changli, D.; Junmei, T.; Shunan, W.; Jie, C.; Xuemei, C.; Yueqing, G. In *Synthesis and Evaluation of a Folate-linked Anti-cancer Prodrug*, 2012 International Conference on Biomedical Engineering and Biotechnology, 28-30 May 2012; 2012; pp 1089-1092.
182. Mikuni, K.; Nakanishi, K.; Hara, K.; Hara, K.; Iwatani, W.; Amano, T.; Nakamura, K.; Tsuchiya, Y.; Okumoto, H.; Mandai, T., *In Vivo* Antitumor Activity of Novel Water-Soluble Taxoids. *Biological and Pharmaceutical Bulletin* **2008**, *31* (6), 1155-1158.
183. Vlahov, I. R.; Leamon, C. P., Engineering Folate–Drug Conjugates to Target Cancer: From Chemistry to Clinic. *Bioconjugate Chemistry* **2012**, *23* (7), 1357-1369.
184. Pinhassi, R. I.; Assaraf, Y. G.; Farber, S.; Stark, M.; Ickowicz, D.; Drori, S.; Domb, A. J.; Livney, Y. D., Arabinogalactan–Folic Acid–Drug Conjugate for Targeted Delivery and Target-Activated Release of Anticancer Drugs to Folate Receptor-Overexpressing Cells. *Biomacromolecules* **2010**, *11* (1), 294-303.
185. Vlahov, I. R.; Santhapuram, H. K. R.; You, F.; Wang, Y.; Kleindl, P. J.; Hahn, S. J.; Vaughn, J. F.; Reno, D. S.; Leamon, C. P., Carbohydrate-Based Synthetic Approach to Control Toxicity Profiles of Folate–Drug Conjugates. *The Journal of Organic Chemistry* **2010**, *75* (11), 3685-3691.
186. Leamon, C. P.; Wang, Y.; Vlahov, I. R.; You, F.; Kleindl, P.; Santhapuram, H. H. R. Conjugates containing hydrophilic spacer linkers. 2008.
187. Leamon, C. P.; Reddy, J. A.; Klein, P. J.; Vlahov, I. R.; Dorton, R.; Bloomfield, A.; Nelson, M.; Westrick, E.; Parker, N.; Bruna, K.; Vetzal, M.; Gehrke, M.; Nicoson, J. S.; Messmann, R. A.; LoRusso, P. M.; Sausville, E. A., Reducing Undesirable Hepatic Clearance of a Tumor-Targeted Vinca Alkaloid via Novel Saccharopeptidic Modifications. *Journal of Pharmacology and Experimental Therapeutics* **2011**, *336* (2), 336-343.
188. Wadhwa, S.; Mumper, R. J., Polypeptide conjugates of d-penicillamine and idarubicin for anticancer therapy. *Journal of Controlled Release* **2012**, *158* (2), 215-223.
189. Webster, R.; Elliott, V.; Park, B. K.; Walker, D.; Hankin, M.; Taupin, P., PEG and PEG conjugates toxicity: towards an understanding of the toxicity of PEG and its relevance to PEGylated biologicals. In *PEGylated Protein Drugs: Basic Science and Clinical Applications*, Veronese, F. M., Ed. Birkhäuser Basel: Basel, 2009; pp 127-146.
190. Bjørnsdottir, I.; Sternebring, O.; Kappers, W. A.; Selvig, H.; Kornø, H. T.; Kristensen, J. B.; Bagger, M. A., Pharmacokinetics, tissue distribution and excretion of 40kDa PEG and PEGylated rFVIII (N8-GP) in rats. *European Journal of Pharmaceutical Sciences* **2016**, *87*, 58-68.
191. Suk, J. S.; Xu, Q.; Kim, N.; Hanes, J.; Ensign, L. M., PEGylation as a strategy for improving nanoparticle-based drug and gene delivery. *Advanced drug delivery reviews* **2016**, *99* (Pt A), 28-51.

192. Gref, R.; Minamitake, Y.; Peracchia, M.; Trubetskoy, V.; Torchilin, V.; Langer, R., Biodegradable long-circulating polymeric nanospheres. *Science* **1994**, *263* (5153), 1600-1603.
193. Mosqueira, V. C. F.; Legrand, P.; Morgat, J.-L.; Vert, M.; Mysiakine, E.; Gref, R.; Devissaguet, J.-P.; Barratt, G., Biodistribution of Long-Circulating PEG-Grafted Nanocapsules in Mice: Effects of PEG Chain Length and Density. *Pharmaceutical Research* **2001**, *18* (10), 1411-1419.
194. Fang, C.; Shi, B.; Pei, Y.-Y.; Hong, M.-H.; Wu, J.; Chen, H.-Z., In vivo tumor targeting of tumor necrosis factor- α -loaded stealth nanoparticles: Effect of MePEG molecular weight and particle size. *European Journal of Pharmaceutical Sciences* **2006**, *27* (1), 27-36.
195. Emami, B.; Lyman, J.; Brown, A.; Cola, L.; Goitein, M.; Munzenrider, J. E.; Shank, B.; Solin, L. J.; Wesson, M., Tolerance of normal tissue to therapeutic irradiation. *International Journal of Radiation Oncology*Biophysics* **1991**, *21* (1), 109-122.
196. Cremonesi, M.; Ferrari, M.; Bodei, L.; Tosi, G.; Paganelli, G., Dosimetry in Peptide Radionuclide Receptor Therapy: A Review. *Journal of Nuclear Medicine* **2006**, *47* (9), 1467-1475.
197. Valkema, R.; Pauwels, S. A.; Kvols, L. K.; Kwekkeboom, D. J.; Jamar, F.; de Jong, M.; Barone, R.; Walrand, S.; Kooij, P. P.; Bakker, W. H., Long-term follow-up of renal function after peptide receptor radiation therapy with ⁹⁰Y-DOTA0, Tyr3-octreotide and ¹⁷⁷Lu-DOTA0, Tyr3-octreotate. *Journal of nuclear medicine* **2005**, *46* (1 suppl), 83S-91S.
198. Sandström, M.; Garske, U.; Granberg, D.; Sundin, A.; Lundqvist, H., Individualized dosimetry in patients undergoing therapy with ¹⁷⁷Lu-DOTA-D-Phe1-Tyr3-octreotate. *European Journal of Nuclear Medicine and Molecular Imaging* **2010**, *37* (2), 212-225.
199. Boerman, O. C.; Oyen, W. J.; Corstens, F. H., Between the Scylla and Charybdis of peptide radionuclide therapy: hitting the tumor and saving the kidney. *European journal of nuclear medicine* **2001**, *28* (10), 1447-1449.
200. O'Donoghue, J., Relevance of External Beam Dose-Response Relationships to Kidney Toxicity Associated with Radionuclide Therapy. *Cancer Biotherapy and Radiopharmaceuticals* **2004**, *19* (3), 378-387.
201. Konijnenberg, M. W., Is the Renal Dosimetry for [⁹⁰Y-DOTA0, Tyr3]Octreotide Accurate Enough to Predict Thresholds for Individual Patients? *Cancer Biotherapy and Radiopharmaceuticals* **2003**, *18* (4), 619-625.
202. Bodei, L.; Cremonesi, M.; Ferrari, M.; Pacifici, M.; Grana, C. M.; Bartolomei, M.; Baio, S. M.; Sansovini, M.; Paganelli, G., Long-term evaluation of renal toxicity after peptide receptor radionuclide therapy with ⁹⁰Y-DOTATOC and ¹⁷⁷Lu-DOTATATE: the role of associated risk factors. *European Journal of Nuclear Medicine and Molecular Imaging* **2008**, *35* (10), 1847-1856.

203. de Jong, M.; Rolleman, E. J.; Bernard, B. F.; Visser, T. J.; Bakker, W. H.; Breeman, W. A.; Krenning, E. P., Inhibition of renal uptake of indium-111-DTPA-octreotide in vivo. *Journal of Nuclear Medicine* **1996**, *37* (8), 1388-1392.
204. Rolleman, E. J.; Valkema, R.; de Jong, M.; Kooij, P. P.; Krenning, E. P., Safe and effective inhibition of renal uptake of radiolabelled octreotide by a combination of lysine and arginine. *European Journal of Nuclear Medicine and Molecular Imaging* **2003**, *30* (1), 9-15.
205. Lin, Y.-C.; Hung, G.-U.; Luo, T.-Y.; Tsai, S.-C.; Sun, S.-S.; Hsia, C.-C.; Chen, S.-L.; Lin, W.-Y., Reducing renal uptake of ^{111}In -DOTATOC: A comparison among various basic amino acids. *Annals of Nuclear Medicine* **2007**, *21* (1), 79.
206. Rolleman, E. J.; Melis, M.; Valkema, R.; Boerman, O. C.; Krenning, E. P.; de Jong, M., Kidney protection during peptide receptor radionuclide therapy with somatostatin analogues. *European Journal of Nuclear Medicine and Molecular Imaging* **2010**, *37* (5), 1018-1031.
207. Kristiansson, A.; Ahlstedt, J.; Holmqvist, B.; Brinte, A.; Tran, T. A.; Forssell-Aronsson, E.; Strand, S.-E.; Gram, M.; Åkerström, B., Protection of Kidney Function with Human Antioxidation Protein $\alpha 1$ -Microglobulin in a Mouse ^{177}Lu -DOTATATE Radiation Therapy Model. *Antioxidants & Redox Signaling* **2018**, *30* (14), 1746-1759.
208. Osterkamp, F.; Zboralski, D.; Schneider, E.; Haase, C.; Paschke, M.; Höhne, A.; Ungewiss, J.; Smerling, C.; Reineke, U.; Bredenbeck, A. Compounds Comprising A Fibroblast Activation Protein Ligand and Use Thereof. 2021.
209. Kobayashi, H.; Yoo, T. M.; Kim, I. S.; Kim, M.-K.; Le, N.; Webber, K. O.; Pastan, I.; Paik, C. H.; Eckelman, W. C.; Carrasquillo, J. A., L-Lysine Effectively Blocks Renal Uptake of ^{125}I - or $^{99\text{m}}\text{Tc}$ -labeled Anti-Tac Disulfide-stabilized Fv Fragment. *Cancer research* **1996**, *56* (16), 3788-3795.
210. Verwijnen, S. M.; Krenning, E. P.; Valkema, R.; Huijmans, J. G. M.; de Jong, M., Oral Versus Intravenous Administration of Lysine: Equal Effectiveness in Reduction of Renal Uptake of [^{111}In -DTPA] Octreotide. *Journal of Nuclear Medicine* **2005**, *46* (12), 2057.
211. Arano, Y.; Fujioka, Y.; Akizawa, H.; Ono, M.; Uehara, T.; Wakisaka, K.; Nakayama, M.; Sakahara, H.; Konishi, J.; Saji, H., Chemical Design of Radiolabeled Antibody Fragments for Low Renal Radioactivity Levels. *Cancer research* **1999**, *59* (1), 128-134.
212. Uehara, T.; Koike, M.; Nakata, H.; Hanaoka, H.; Iida, Y.; Hashimoto, K.; Akizawa, H.; Endo, K.; Arano, Y., Design, Synthesis, and Evaluation of [^{188}Re]Organorhenium-Labeled Antibody Fragments with Renal Enzyme-Cleavable Linkage for Low Renal Radioactivity Levels. *Bioconjugate Chemistry* **2007**, *18* (1), 190-198.
213. Akizawa, H.; Imajima, M.; Hanaoka, H.; Uehara, T.; Satake, S.; Arano, Y., Renal Brush Border Enzyme-Cleavable Linkages for Low Renal Radioactivity Levels of Radiolabeled Antibody Fragments. *Bioconjugate Chemistry* **2013**, *24* (2), 291-299.

214. Uehara, T.; Yokoyama, M.; Suzuki, H.; Hanaoka, H.; Arano, Y., A Gallium-67/68–Labeled Antibody Fragment for Immuno-SPECT/PET Shows Low Renal Radioactivity Without Loss of Tumor Uptake. *Clinical Cancer Research* **2018**, *24* (14), 3309-3316.
215. Suzuki, C.; Uehara, T.; Kanazawa, N.; Wada, S.; Suzuki, H.; Arano, Y., Preferential Cleavage of a Tripeptide Linkage by Enzymes on Renal Brush Border Membrane To Reduce Renal Radioactivity Levels of Radiolabeled Antibody Fragments. *Journal of Medicinal Chemistry* **2018**, *61* (12), 5257-5268.
216. Uehara, T.; Kanazawa, N.; Suzuki, C.; Mizuno, Y.; Suzuki, H.; Hanaoka, H.; Arano, Y., Renal Handling of ^{99m}Tc-Labeled Antibody Fab Fragments with a Linkage Cleavable by Enzymes on Brush Border Membrane. *Bioconjugate Chemistry* **2020**, *31* (11), 2618-2627.
217. Vaidyanathan, G.; Kang, C. M.; McDougald, D.; Minn, I.; Brummet, M.; Pomper, M. G.; Zalutsky, M. R., Brush border enzyme-cleavable linkers: Evaluation for reducing renal uptake of radiolabeled prostate-specific membrane antigen inhibitors. *Nuclear Medicine and Biology* **2018**, *62-63*, 18-30.
218. Bendre, S.; Zhang, Z.; Kuo, H.-T.; Rousseau, J.; Zhang, C.; Merkens, H.; Roxin, Á.; Bénard, F.; Lin, K.-S., Evaluation of Met-Val-Lys as a Renal Brush Border Enzyme-Cleavable Linker to Reduce Kidney Uptake of ⁶⁸Ga-Labeled DOTA-Conjugated Peptides and Peptidomimetics. *Molecules* **2020**, *25* (17), 3854.
219. Zhang, M.; Jacobson, O.; Kiesewetter, D. O.; Ma, Y.; Wang, Z.; Lang, L.; Tang, L.; Kang, F.; Deng, H.; Yang, W.; Niu, G.; Wang, J.; Chen, X., Improving the Theranostic Potential of Exendin 4 by Reducing the Renal Radioactivity through Brush Border Membrane Enzyme-Mediated Degradation. *Bioconjugate Chemistry* **2019**, *30* (6), 1745-1753.
220. Müller, C.; Struthers, H.; Winiger, C.; Zhernosekov, K.; Schibli, R., DOTA Conjugate with an Albumin-Binding Entity Enables the First Folic Acid–Targeted ¹⁷⁷Lu-Radionuclide Tumor Therapy in Mice. *Journal of Nuclear Medicine* **2013**, *54* (1), 124-131.
221. Kuo, H.-T.; Merkens, H.; Zhang, Z.; Uribe, C. F.; Lau, J.; Zhang, C.; Colpo, N.; Lin, K.-S.; Bénard, F., Enhancing Treatment Efficacy of ¹⁷⁷Lu-PSMA-617 with the Conjugation of an Albumin-Binding Motif: Preclinical Dosimetry and Endoradiotherapy Studies. *Molecular Pharmaceutics* **2018**, *15* (11), 5183-5191.
222. Wang, Z.; Tian, R.; Niu, G.; Ma, Y.; Lang, L.; Szajek, L. P.; Kiesewetter, D. O.; Jacobson, O.; Chen, X., Single Low-Dose Injection of Evans Blue Modified PSMA-617 Radioligand Therapy Eliminates Prostate-Specific Membrane Antigen Positive Tumors. *Bioconjugate Chemistry* **2018**, *29* (9), 3213-3221.
223. Kelly, J. M.; Amor-Coarasa, A.; Ponnala, S.; Nikolopoulou, A.; Williams, C.; Thiele, N. A.; Schlyer, D.; Wilson, J. J.; DiMagno, S. G.; Babich, J. W., A Single Dose of ²²⁵Ac-RPS-074 Induces a Complete Tumor Response in an LNCaP Xenograft Model. *Journal of Nuclear Medicine* **2019**, *60* (5), 649-655.

224. Deberle, L. M.; Benešová, M.; Umbricht, C. A.; Borgna, F.; Büchler, M.; Zhernosekov, K.; Schibli, R.; Müller, C., Development of a new class of PSMA radioligands comprising ibuprofen as an albumin-binding entity. *Theranostics* **2020**, *10* (4), 1678-1693.
225. Wen, X.; Shi, C.; Yang, L.; Zeng, X.; Lin, X.; Huang, J.; Li, Y.; Zhuang, R.; Zhu, H.; Guo, Z.; Zhang, X., A radioiodinated FR- β -targeted tracer with improved pharmacokinetics through modification with an albumin binder for imaging of macrophages in AS and NAFL. *European Journal of Nuclear Medicine and Molecular Imaging* **2021**.
226. Zang, J.; Fan, X.; Wang, H.; Liu, Q.; Wang, J.; Li, H.; Li, F.; Jacobson, O.; Niu, G.; Zhu, Z.; Chen, X., First-in-human study of ^{177}Lu -EB-PSMA-617 in patients with metastatic castration-resistant prostate cancer. *European Journal of Nuclear Medicine and Molecular Imaging* **2019**, *46* (1), 148-158.
227. Dennis, M. S.; Zhang, M.; Meng, Y. G.; Kadkhodayan, M.; Kirchhofer, D.; Combs, D.; Damico, L. A., Albumin Binding as a General Strategy for Improving the Pharmacokinetics of Proteins*. *Journal of Biological Chemistry* **2002**, *277* (38), 35035-35043.
228. Dumelin, C. E.; Trüssel, S.; Buller, F.; Trachsel, E.; Bootz, F.; Zhang, Y.; Mannocci, L.; Beck, S. C.; Drumea-Mirancea, M.; Seeliger, M. W.; Baltes, C.; Müggler, T.; Kranz, F.; Rudin, M.; Melkko, S.; Scheuermann, J.; Neri, D., A Portable Albumin Binder from a DNA-Encoded Chemical Library. *Angewandte Chemie International Edition* **2008**, *47* (17), 3196-3201.
229. Eskew, M. W.; Benight, A. S., Evaluation of Drug/Ligand Binding Constants for Human Serum Albumin Using Differential Scanning Calorimetry. *bioRxiv* **2021**, 2021.01.22.427858.
230. Tian, R.; Zeng, Q.; Zhu, S.; Lau, J.; Chandra, S.; Ertsey, R.; Hettie, K. S.; Teraphongphom, T.; Hu, Z.; Niu, G.; Kiesewetter, D. O.; Sun, H.; Zhang, X.; Antaris, A. L.; Brooks, B. R.; Chen, X., Albumin-chaperoned cyanine dye yields superbright NIR-II fluorophore with enhanced pharmacokinetics. *Science Advances* **2019**, *5* (9), eaaw0672.
231. Chen, Q.; Liu, Z., Albumin Carriers for Cancer Theranostics: A Conventional Platform with New Promise. *Advanced Materials* **2016**, *28* (47), 10557-10566.
232. Chen, Q.; Liang, C.; Wang, C.; Liu, Z., An Imagable and Photothermal “Abraxane-Like” Nanodrug for Combination Cancer Therapy to Treat Subcutaneous and Metastatic Breast Tumors. *Advanced Materials* **2015**, *27* (5), 903-910.
233. Benešová, M.; Bauder-Wüst, U.; Schäfer, M.; Klika, K. D.; Mier, W.; Haberkorn, U.; Kopka, K.; Eder, M., Linker Modification Strategies To Control the Prostate-Specific Membrane Antigen (PSMA)-Targeting and Pharmacokinetic Properties of DOTA-Conjugated PSMA Inhibitors. *Journal of Medicinal Chemistry* **2016**, *59* (5), 1761-1775.
234. Loktev, A.; Lindner, T.; Burger, E.-M.; Altmann, A.; Giesel, F.; Kratochwil, C.; Debus, J.; Marmé, F.; Jäger, D.; Mier, W.; Haberkorn, U., Development of Fibroblast Activation Protein-Targeted Radiotracers with Improved Tumor Retention. *Journal of Nuclear Medicine* **2019**, *60* (10), 1421-1429.

235. Kuo, H.-T.; Lin, K.-S.; Zhang, Z.; Uribe, C. F.; Merkens, H.; Zhang, C.; Benard, F., Novel ¹⁷⁷Lu-labeled Albumin-binder-conjugated PSMA-targeting Agents with Extremely High Tumor Uptake and Enhanced Tumor-to-kidney Absorbed Dose Ratio. *Journal of Nuclear Medicine* **2020**, jnumed.120.2507.
236. Moon, E. S.; Elvas, F.; Vliegen, G.; De Lombaerde, S.; Vangestel, C.; De Bruycker, S.; Bracke, A.; Eppard, E.; Greifenstein, L.; Klasen, B.; Kramer, V.; Staelens, S.; De Meester, I.; Van der Veken, P.; Rösch, F., Targeting fibroblast activation protein (FAP): next generation PET radiotracers using squaramide coupled bifunctional DOTA and DATA5m chelators. *EJNMMI Radiopharmacy and Chemistry* **2020**, 5 (1), 19.
237. Vlashi, E.; Kelderhouse, L. E.; Sturgis, J. E.; Low, P. S., Effect of Folate-Targeted Nanoparticle Size on Their Rates of Penetration into Solid Tumors. *ACS Nano* **2013**, 7 (10), 8573-8582.
238. Wang, B.; Galliford, C. V.; Low, P. S., Guiding principles in the design of ligand-targeted nanomedicines. *Nanomedicine* **2014**, 9 (2), 313-330.
239. Verhoef, J. J. F.; Anchordoquy, T. J., Questioning the Use of PEGylation for Drug Delivery. *Drug delivery and translational research* **2013**, 3 (6), 499-503.
240. Gordon Steel, G.; Peckham, M. J., Exploitable mechanisms in combined radiotherapy-chemotherapy: The concept of additivity. *International Journal of Radiation Oncology*Biological*Physics* **1979**, 5 (1), 85-91.
241. Le Chevalier, T.; Arriagada, R.; Quoix, E.; Ruffle, P.; Martin, M.; Tarayre, M.; Marie-José, L.-T.; Douillard, J.-Y.; Laplanche, A., Radiotherapy Alone Versus Combined Chemotherapy and Radiotherapy in Nonresectable Non-Small-Cell Lung Cancer: First Analysis of a Randomized Trial in 353 Patients. *JNCI: Journal of the National Cancer Institute* **1991**, 83 (6), 417-423.
242. Herskovic, A.; Martz, K.; Al-Sarraf, M.; Leichman, L.; Brindle, J.; Vaitkevicius, V.; Cooper, J.; Byhardt, R.; Davis, L.; Emami, B., Combined chemotherapy and radiotherapy compared with radiotherapy alone in patients with cancer of the esophagus. *New England Journal of Medicine* **1992**, 326 (24), 1593-1598.
243. Chin, V.; Nagrial, A.; Sjoquist, K.; O'Connor, C. A.; Chantrill, L.; Biankin, A. V.; Scholten, R. J.; Yip, D., Chemotherapy and radiotherapy for advanced pancreatic cancer. *Cochrane Database of Systematic Reviews* **2018**, (3).
244. Alhmod, J. F.; Woolley, J. F.; Al Moustafa, A.-E.; Malki, M. I., DNA Damage/Repair Management in Cancers. *Cancers* **2020**, 12 (4), 1050.
245. Brown, J. S.; O'Carrigan, B.; Jackson, S. P.; Yap, T. A., Targeting DNA Repair in Cancer: Beyond PARP Inhibitors. *Cancer Discovery* **2017**, 7 (1), 20-37.

246. Ma, J.; Setton, J.; Lee, N. Y.; Riaz, N.; Powell, S. N., The therapeutic significance of mutational signatures from DNA repair deficiency in cancer. *Nature Communications* **2018**, *9* (1), 3292.
247. Chalmers, A. J.; Gutierrez-Quintana, R.; Walker, D. J.; Williams, K.; Forster, D.; Jackson, M. R.; Derby, S.; Stobo, J.; Sweeting, L.; Kelly, C.; Durant, S.; Williams, K. J., Abstract IA-006: Enhancing the therapeutic ratio for glioblastoma by combining radiation therapy with PARP inhibitors. *Clinical Cancer Research* **2021**, *27* (8 Supplement), IA-006-IA-006.
248. Chalmers, A. J.; Short, S.; Watts, C.; Herbert, C.; Morris, A.; Stobo, J.; Cruickshank, G.; Dunn, L.; Erridge, S.; Godfrey, L.; Jefferies, S.; Lopez, J. S.; McBain, C.; Pittman, M.; Dillon, S.; James, A.; Nowicki, S. A.; Williamson, A.; Kelly, C.; Halford, S. E. R., Phase I clinical trials evaluating olaparib in combination with radiotherapy (RT) and/or temozolomide (TMZ) in glioblastoma patients: Results of OPARATIC and PARADIGM phase I and early results of PARADIGM-2. *Journal of Clinical Oncology* **2018**, *36* (15_suppl), 2018-2018.
249. Fulton, B.; Short, S. C.; James, A.; Nowicki, S.; McBain, C.; Jefferies, S.; Kelly, C.; Stobo, J.; Morris, A.; Williamson, A.; Chalmers, A. J., PARADIGM-2: Two parallel phase I studies of olaparib and radiotherapy or olaparib and radiotherapy plus temozolomide in patients with newly diagnosed glioblastoma, with treatment stratified by MGMT status. *Clinical and Translational Radiation Oncology* **2018**, *8*, 12-16.
250. Walls, G. M.; Oughton, J. B.; Chalmers, A. J.; Brown, S.; Collinson, F.; Forster, M. D.; Franks, K. N.; Gilbert, A.; Hanna, G. G.; Hannaway, N.; Harrow, S.; Haswell, T.; Hiley, C. T.; Hinsley, S.; Krebs, M.; Murden, G.; Phillip, R.; Ryan, A. J.; Salem, A.; Sebag-Montefiore, D.; Shaw, P.; Twelves, C. J.; Walker, K.; Young, R. J.; Faivre-Finn, C.; Greystoke, A., CONCORDE: A phase I platform study of novel agents in combination with conventional radiotherapy in non-small-cell lung cancer. *Clinical and Translational Radiation Oncology* **2020**, *25*, 61-66.
251. Pennisi, R.; Ascenzi, P.; Di Masi, A., Hsp90: A New Player in DNA Repair? *Biomolecules* **2015**, *5* (4), 2589-2618.
252. Spiegelberg, D.; Dascalu, A.; Mortensen, A. C.; Abramenkova, A.; Kuku, G.; Nestor, M.; Stenerlöv, B., The novel HSP90 inhibitor AT13387 potentiates radiation effects in squamous cell carcinoma and adenocarcinoma cells. *Oncotarget* **2015**, *6* (34), 35652-35666.
253. Spiegelberg, D.; Abramenkova, A.; Mortensen, A. C. L.; Lundsten, S.; Nestor, M.; Stenerlöv, B., The HSP90 inhibitor Onalespib exerts synergistic anti-cancer effects when combined with radiotherapy: an in vitro and in vivo approach. *Scientific Reports* **2020**, *10* (1), 5923.
254. Bhat, K.; Saki, M.; Vlashi, E.; Cheng, F.; Duhachek-Muggy, S.; Alli, C.; Yu, G.; Medina, P.; He, L.; Damoiseaux, R.; Pellegrini, M.; Zemke, N. R.; Nghiemphu, P. L.; Cloughesy, T. F.; Liau, L. M.; Kornblum, H. I.; Pajonk, F., The dopamine receptor antagonist trifluoperazine prevents phenotype conversion and improves survival in mouse models of glioblastoma. *Proceedings of the National Academy of Sciences* **2020**, *117* (20), 11085-11096.

255. Wei, W.; Wu, P.; Li, L.; Zhang, Z.-h., Effectiveness of pegaspargase, gemcitabine, and oxaliplatin (P-GEMOX) chemotherapy combined with radiotherapy in newly diagnosed, stage IE to IIE, nasal-type, extranodal natural killer/T-cell lymphoma. *Hematology* **2017**, *22* (6), 320-329.
256. Ng, J.; Dai, T., Radiation therapy and the abscopal effect: a concept comes of age. *Ann Transl Med* **2016**, *4* (6), 118-118.
257. Reynders, K.; Illidge, T.; Siva, S.; Chang, J. Y.; De Ruyscher, D., The abscopal effect of local radiotherapy: using immunotherapy to make a rare event clinically relevant. *Cancer Treat Rev* **2015**, *41* (6), 503-510.
258. Wang, Y.; Deng, W.; Li, N.; Neri, S.; Sharma, A.; Jiang, W.; Lin, S. H., Combining Immunotherapy and Radiotherapy for Cancer Treatment: Current Challenges and Future Directions. *Front Pharmacol* **2018**, *9*, 185-185.
259. Qin, S.; Xu, L.; Yi, M.; Yu, S.; Wu, K.; Luo, S., Novel immune checkpoint targets: moving beyond PD-1 and CTLA-4. *Molecular Cancer* **2019**, *18* (1), 155.
260. Vanpouille-Box, C.; Diamond, J. M.; Piones, K. A.; Zavadil, J.; Babb, J. S.; Formenti, S. C.; Barcellos-Hoff, M. H.; Demaria, S., TGF β Is a Master Regulator of Radiation Therapy-Induced Antitumor Immunity. *Cancer research* **2015**, *75* (11), 2232-2242.
261. Sharma, P.; Wagner, K.; Wolchok, J. D.; Allison, J. P., Novel cancer immunotherapy agents with survival benefit: recent successes and next steps. *Nature Reviews Cancer* **2011**, *11* (11), 805-812.
262. Ganesh, K.; Massagué, J., TGF- β Inhibition and Immunotherapy: Checkmate. *Immunity* **2018**, *48* (4), 626-628.
263. Suit, H. D.; Todoroki, T., Rationale for combining surgery and radiation therapy. *Cancer* **1985**, *55* (S9), 2246-2249.
264. Olmos, R. V.; Vidal-Sicart, S.; Giammarile, F.; Zaknun, J.; Leeuwen, F.; Mariani, G., The GOSTT concept and hybrid mixed/virtual/augmented reality environment radioguided surgery. *QJ Nucl Med Mol Imaging* **2014**, *58* (2), 207-215.
265. Wang, L.; Wu, Y.; Deng, Y.; Kim, B.; Pierce, L.; Krilov, G.; Lupyan, D.; Robinson, S.; Dahlgren, M. K.; Greenwood, J.; Romero, D. L.; Masse, C.; Knight, J. L.; Steinbrecher, T.; Beuming, T.; Damm, W.; Harder, E.; Sherman, W.; Brewer, M.; Wester, R.; Murcko, M.; Frye, L.; Farid, R.; Lin, T.; Mobley, D. L.; Jorgensen, W. L.; Berne, B. J.; Friesner, R. A.; Abel, R., Accurate and Reliable Prediction of Relative Ligand Binding Potency in Prospective Drug Discovery by Way of a Modern Free-Energy Calculation Protocol and Force Field. *Journal of the American Chemical Society* **2015**, *137* (7), 2695-2703.

266. Ilgan, S.; Öztürk, E.; Yildiz, R.; Emer, Ö.; Ayan, A.; Görgülü, S.; Alagöz, E.; Deveci, S.; Özgüven, M. A.; Tufan, T., Combination of Preoperative Ultrasonographic Mapping and Radioguided Occult Lesion Localization in Patients With Locally Recurrent/Persistent Papillary Thyroid Carcinoma: A Practical Method for Central Compartment Reoperations. *Clinical Nuclear Medicine* **2010**, *35* (11), 847-852.
267. Xia, W.; Hilgenbrink, A. R.; Matteson, E. L.; Lockwood, M. B.; Cheng, J.-X.; Low, P. S., A functional folate receptor is induced during macrophage activation and can be used to target drugs to activated macrophages. *Blood* **2009**, *113* (2), 438-446.
268. Chandrupatla, D. M. S. H.; Molthoff, C. F. M.; Lammertsma, A. A.; van der Laken, C. J.; Jansen, G., The folate receptor β as a macrophage-mediated imaging and therapeutic target in rheumatoid arthritis. *Drug Delivery and Translational Research* **2019**, *9* (1), 366-378.
269. Egger, C.; Cannet, C.; Gerard, C.; Suply, T.; Ksiazek, I.; Jarman, E.; Beckmann, N., Effects of the fibroblast activation protein inhibitor, PT100, in a murine model of pulmonary fibrosis. *Eur J Pharmacol* **2017**, *809*, 64-72.
270. Henderson, N. C.; Arnold, T. D.; Katamura, Y.; Giacomini, M. M.; Rodriguez, J. D.; McCarty, J. H.; Pellicoro, A.; Raschperger, E.; Betsholtz, C.; Ruminiski, P. G.; Griggs, D. W.; Prinsen, M. J.; Maher, J. J.; Iredale, J. P.; Lacy-Hulbert, A.; Adams, R. H.; Sheppard, D., Targeting of α v integrin identifies a core molecular pathway that regulates fibrosis in several organs. *Nature Medicine* **2013**, *19* (12), 1617-1624.

CHAPTER 2. ALBUMIN-BINDING MOTIF ENHANCES THERANOSTIC TARGETING OF FIBROBLAST ACTIVATION PROTEIN RADIOLIGAND: PRECLINICAL EVALUATION IN MULTIPLE TUMORS

2.1 Abstract

Cancer-associated fibroblasts (CAFs) play a consistent role in the development of a wide variety of tumors by secreting growth factors, suppressing the immune system, and facilitating metastasis. Fibroblast activation protein alpha (FAP α) is an excellent oncological target due to its selective expression on activated fibroblasts such as CAFs, which are found in almost all tumor types but are nearly nonexistent in healthy tissues. While albumin-binding motifs have been used to improve the radioactive theranostics of ligands targeting other receptors, this technique has been only superficially investigated with FAP α ligands. We synthesized a novel FAP α -targeted ligand FAP5, then conjugated it to a DOTA chelator with or without the established albumin-binder 4-(*p*-iodophenyl)butyric acid. The FAP5 conjugates exhibited high binding affinity to FAP α in the low nanomolar range. After *in vitro* validation of the synthesized products, we conducted *in vivo* studies using both murine tumor and human xenograft models to assess the radioimaging and radiotherapy performance. SPECT/CT scans and biodistribution results showed increased tumor uptake and retention. Administration of the conjugate radiolabeled with ^{177}Lu indicated promising tumor therapy results. We conclude that the new FAP5 radioligand with an albumin-binder demonstrates unprecedented tumor uptake and retention.

2.2 Introduction

The fibroblast activation protein alpha (FAP α) is a robust biomarker in cancer. Human biopsies showed FAP α to be present in 90% of epithelial cancers, and radioimaging demonstrated FAP α is present in 28 different kinds of cancer.^{1,2} FAP α expression in healthy tissue is negligible, rendering FAP α an ideal oncological target for theranostics.^{3,4} Many FAP α -targeted drugs are in research or development for cancer, such as antibodies,^{5,6} prodrugs,⁷⁻¹⁰ imaging agents,¹¹⁻¹³ and therapeutic agents.¹⁴⁻¹⁷

While several tumor types such as sarcoma, melanoma, glioblastoma, and osteosarcoma do express FAP α directly on the cancer cells,¹⁸⁻²⁰ FAP α is primarily overexpressed on activated

fibroblasts such as cancer associated fibroblasts (CAFs).¹⁵ Therefore, any FAP α -targeted therapy will require a by-stander effect to optimally eliminate both cancer and stromal cells alike. Radiotherapy is an ideal payload for FAP α -targeted conjugates in cancer treatment due to the ability of the radiation to damage neighboring cancer cells from within CAFs. Radiotherapeutic results are optimized by maximizing tumor uptake and retention. Several labs have successfully made improvements to FAP α ligand uptake and retention in the tumor with linker modifications, but further improvements are necessary.^{21, 22}

Serum protein binding is a well-established technique to improve the pharmacokinetics of pharmaceuticals that otherwise may be cleared too rapidly to exert a proper therapeutic effect.²³ The low-molecular-weight albumin-binder 4-(*p*-iodophenyl)butyric acid was reported as a portable albumin-binder,²⁴ and has since been applied to targeting ligands such as FAP,²⁵ folate,²⁶⁻²⁹ PSMA,^{30, 31} CAIX,³² antibody fragments,³³ or for passive albumin uptake into diseased tissues.^{34, 35} These conjugates form stable noncovalent interactions with serum albumin, greatly enhance tumor uptake and retention, and result in superior radioactive theranostics in both mice and humans. However, this technique did not seem to demonstrate improved tumor uptake compared to other linker modifications on the FAPI radioligand and has yet to be tested in radiotherapy.^{21, 25, 36}

Herein, we report a novel FAP α -targeted radioligand with an albumin-binding moiety to improve the pharmacokinetics and thus overall radiotheranostic performance. We also conjugated the new FAP α radioligand to 4-(*p*-iodophenyl)butyric acid. The goal of this study was to evaluate the tumor uptake and retention of the FAP5-IP-DOTA conjugate using both SPECT/CT and tissue distribution. The anticancer radiotherapeutic efficacy was also investigated for multiple tumors in mice using ¹⁷⁷Lu as the therapeutic isotope.

2.3 Materials and Methods

2.3.1 Materials

4-methyl isoindoline-4-carboxylate hydrochloride was purchased from PharmaBlock (Hatfield, PA). Boc-L-pyroglutamic acid benzyl ester was purchased from Accela ChemBio (San Diego, CA). 4-(*p*-iodophenyl)butyric acid was purchased from AstaTech, Inc (Bristol, PA). Fmoc-Lys-OH HCl was purchased from Aapptec. NHS-ester-PEG₆-NHfmoc and Propargyl-PEG₆-amine were purchased from BroadPharm. DOTA-NHS ester was purchased from Macrocyclics. Lysine was purchased from AAPPTec (Louisville, KY). 4,4-Difluoro-L-prolinamide

hydrochloride and HATU were purchased from Chem-Impex International (Chicago, IL). 4-Ethynylbenzoic acid and mono-Fmoc ethylene diamine hydrochloride were purchased from AA Blocks LLC (San Diego, CA). Di-tert-butyl dicarbonate was purchased from Oakwood Chemical (Estill, SC). Palladium, 10% on carbon, was purchased from Alfa Aesar (Haverhill, MA). Sodium borohydride, N-bromosuccinimide, triphenylphosphine, sodium azide, lithium bis(trimethylsilyl)amide, tert-butyl-bromoacetate, 1,8-diazabicyclo[5.4.0]undec-7-ene, pyridine, imidazole, phosphoryl chloride, diethyl ether, DIPEA, TFA, THF, DMF, DCM, MeOH, DMSO, and all other reagents were purchased from Sigma-Aldrich (St. Louis, MO). All molecules were purified using either flash chromatography (CombiFlash RF, Teledyne) or RP-HPLC (Agilent 1200 Instrument) with an XBridge OBD preparative column (19 x 150 mm, 5 μ m) purchased from Waters (Milford, MA). LRMS-LC/MS was performed with an Agilent 1220 Infinity LC with a reverse-phase XBridge Shield RP18 column (3.0 x 50 mm, 3.5 μ m).

FAP, DPP4, and PREP recombinant enzymes were purchased from R&D Systems (Minneapolis, MN). Enzyme buffer was purchased from BPS Bioscience (San Diego, CA). H-Gly-Pro-AMC and Z-Gly-Pro-AMC were purchased from Bachem Americas, Inc (Torrance, CA). All cell lines were originally purchased from ATCC. Cell culture media such as Eagle's Minimum Essential Medium (EMEM), Dulbecco's Modified Eagle's Medium (DMEM, and Roswell Park Memorial Institute medium 1640 (RPMI-1640) were purchased from GIBCO. All other cell culture reagents such as fetal bovine serum (FBS), 1% penicillin-streptomycin, and 2 mM glutamine were purchased from Life Technologies. Amine-coated 24-well cultureware plates were purchased from BD Biosciences (San Jose, CA). Accutase was purchased from BioLegend (San Diego, CA). Human FAP α APC-conjugated and murine FAP α monoclonal rat IgG antibodies were purchased from R&D Systems (Minneapolis, MN). Common cell culture materials such as culture flasks and syringes were purchased from VWR (Chicago, IL). Fluorescence based assays were measured with a BioTek Synergy Neo2 plate reader. FACS analysis was performed with an Attune NxT Acoustic Focusing Flow Cytometer

Indium-111 was purchased from Cardinal Health (Indianapolis, IN). Lutetium-177 was purchased from RadioMedix (Houston, TX and Garching, Germany). Chelations were done using a Fisherbrand Isotemp Digital Dry Bath/Block Heater (Waltham, MA). Radio-HPLC analysis was performed with an Agilent 1260 Infinity II with a Flow-RAM detector purchased from LabLogic (Brandon, FL) and a reverse-phase XBridge Shield RP18 column (3.0 x 50 mm, 3.5 μ m).

SPECT/CT scans were acquired with a VECTor/CT system with a clustered multi-pinhole high-energy collimator (MILabs, Utrecht, The Netherlands). Radioactive binding and biodistribution studies were done with a Packard Cobra Gamma Counter (Niederösterreich, Austria).

2.3.2 Synthesis of FAP5 intermediates

Synthesis of Fragment 1. 4-methyl isoindoline-4-carboxylate hydrochloride was dissolved in DCM. To the solution were added Boc_2O (4 eq) and TEA (4 eq). The reaction was stirred overnight under inert conditions, then purified by flash chromatography [A=Hex, B=EtOAc, solvent gradient 0% B to 50% B in 25 minutes, retention time = 16 minutes] to yield the product as a yellow oil.

The Boc-protected isoindoline was dissolved in a THF:MeOH (50:50, v/v) solution. Portionwise, NaBH_4 (10 equivalents) was added, then the reaction was refluxed for 5 hours. The crude product was extracted, then purified by flash chromatography [A=Hex, B=EtOAc, solvent gradient 0% B to 50% B in 25 minutes, retention time = 20 minutes] to yield the product as a pale-yellow oil.

The hydroxyl-bearing isoindoline was dissolved in DMF, then PPh_3 (1.5 eq) and NBS (1.5 eq) were added. The solution was stirred for 6 hours at RT. The crude product was extracted, then purified by flash chromatography [A=Hex, B=EtOAc, solvent gradient 0% B to 50% B in 25 minutes, retention time = 12 minutes] to yield the product as a yellow oil.

The brominated-isoindoline was dissolved in DMF, then NaN_3 (5 eq) was added. The reaction was heated to 65°C and reacted overnight. The crude product was extracted and purified by flash chromatography [A=Hex, B=EtOAc, solvent gradient 0% B to 40% B in 25 minutes, retention time = 15 minutes] to yield the product as a pale-yellow solid. LC/MS (m/z): $[\text{M}+\text{H}]^+$ calculated for $\text{C}_{14}\text{H}_{18}\text{N}_4\text{O}_2$, 274.3; observed mass 219 (m- 56 for tBu fragmentation from Boc group).

Synthesis of Fragment 2. Benzyl-(2S)-N-tert-butoxycarbonylpyroglutamate was dissolved in THF and then chilled to -78°C and placed under inert gas. Dropwise, 1.0 M LHMDS in THF (2.2 eq) was added then stirred for 1 hour. After 1 hour, tert-butyl-bromoacetate (2 eq) was added dropwise then stirred for several hours. The crude product was extracted and then purified by flash chromatography [A=Hex, B=EtOAc, solvent gradient 0% B to 100% B in 30 minutes, retention time = 15 minutes] to yield the product as a yellow oil.

The product was completely converted to the trans isomer by dissolving it in DCM and cooling it to 0°C before adding DBU (3 eq) and stirring it for 24 hours. The trans product was washed then purified by flash chromatography [A=Hex, B=EtOAc, solvent gradient 0% B to 100% B in 30 minutes, retention time = 15 minutes] to yield the product as a yellow oil.

The trans product was then dissolved in MeOH, placed under inert gas, then 1:10 (w/w) of 10% Pd/C:trans product was added. The vessel was then purged with H₂ gas and stirred overnight. The debenzylated product was purified by flash chromatography [A=Hex, B=EtOAc, solvent gradient 0% B to 100% B in 30 minutes, retention time = 15 minutes] to yield the product as a pale-yellow solid.

The debenzylated product was dissolved in DMF with DIPEA (3 eq) and HATU (1.2 eq) and stirred for 10 minutes. Difluoroprolineamide in DMF and DIPEA (1.5 eq) was then added, and the mixture was stirred for 3 hours. The crude amide product was extracted, then purified on flash chromatography [A=Hex, B=EtOAc, solvent gradient 0% B to 100% B in 15 minutes, C=DCM, D=MeOH, solvent gradient 0% B to 20% B in 20 minutes, retention time = 30 minutes] to yield the product as a pale-yellow solid.

The amide product was dissolved in pyridine (2 eq) and imidazole (1.125 eq), then cooled to -20°C and placed under inert conditions. Phosphoryl chloride (2.6 eq) was added, and the reaction was stirred for 30 minutes. The reaction was dried under vacuum, resulting in a brown solid. The nitrile product was extracted, resulting in a viscous oil, which was then purified by flash chromatography [A=Hex, B=EtOAc, solvent gradient 0% B to 100% B in 25 minutes, retention time = 15 minutes] to yield the product as a white solid.

The nitrile product was dissolved in ACN, and chilled to 0°C. Dropwise, TFA was added dropwise to achieve a v/v ratio of 1:1. The reaction was then allowed to warm to room temperature and stirred for 1 hour. The crude product, Fragment 2, was isolated under vacuum then precipitated with ice cold ether, after which it was filtered and dried overnight. LC/MS (m/z): [M+H]⁺ calculated for C₁₂H₁₃F₂N₃O₄, 301.3; observed mass 302.

2.3.3 Synthesis of FAP5-DOTA conjugates

Synthesis of FAP5-DOTA. 4-Ethynylbenzoic acid was dissolved in anhydrous DMF with HATU (1 eq) and anhydrous DIPEA (3 eq) for 10 minutes. Mono-Fmoc ethylene diamine was dissolved in anhydrous DMF and DIPEA (1.5 eq), then added to the reaction mixture. The resulting solution

was stirred under inert atmosphere for 2h. The product was precipitated out with ice cold water, then filtered and dried under vacuum. The propargyl-benzene-NHFmoc product was dissolved in anhydrous DMF, then CuI (0.5 eq) and DIPEA (2.0 eq) were added. The reaction mixture was heated to to 55°C and stirred for 5 hours. The crude product was extracted with EtOAc, washed with ice cold brine, then purified by flash chromatography [A=Hex, B=EtOAc, solvent gradient 0% B to 100% B in 20 minutes] to yield the product Frag1-Bz-NHFmoc. LC/MS (m/z): [M+H]⁺ calculated for C₄₀H₄₀N₆O₅, 684.8; observed mass 685.

The Frag1-Bz-NHFmoc was dissolved in DCM and diethylamine (20 eq) then stirred for 1 hour. LC/MS (m/z): [M+H]⁺ calculated for C₂₅H₃₀N₆O₃, 462.6; observed mass 463. Upon completion of the deprotection, the product was isolated via rotary evaporation, washed several times with ice cold diethyl ether, then put on a high vacuum for several hours, after which it was used without further purification. NHS ester-PEG₆-NHFmoc (1.1 eq) and DIPEA (3 eq) were added and stirred for several hours. The crude product was washed, then purified by flash chromatography [A=DCM, B=MeOH, solvent gradient 0% B to 30% B in 25 minutes] to yield the product Frag1-Bz-PEG₆-NHFmoc. LC/MS (m/z): [M+H]⁺ calculated for C₅₅H₆₉N₆O₁₂, 1020.2; observed mass 1021.

Frag1-Bz-PEG₆-NHFmoc was dissolved in ACN and cooled to 0°C. An equal volume of TFA was added and the reaction mixture was stirred at room temperature for 1h. Progress of the reaction was monitored via LC/MS. LC/MS (m/z): [M+H]⁺ calculated for C₅₀H₆₁N₇O₁₀, 920.1; observed mass 921. Upon completion of the deprotection, TFA was removed by rotary evaporation and the deprotected product was used without further purification. Fragment 2 was dissolved in anhydrous DMF and DIPEA (3 eq) for 10 minutes. The previously deprotected product was dissolved in anhydrous DMF and excess DIPEA, then added to the reaction mixture and stirred under inert atmosphere for 2h. The crude product was extracted with EtOAc, washed with ice cold brine, then purified by flash chromatography [A=DCM, B=MeOH, solvent gradient 0% B to 30% B in 25 minutes] to yield the product FAP5-NHFmoc. [M+H]⁺ calculated for C₆₂H₇₂F₂N₁₀O₁₃, 1203.3; observed mass 1204.

FAP5-NHFmoc was dissolved in DCM and diethylamine (20 eq) then stirred for 1 hour. LC/MS (m/z): [M+H]⁺ calculated for C₄₇H₆₂F₂N₁₀O₁₁, 981.1; observed mass 982. Upon completion of the deprotection, the product was isolated via rotary evaporation, washed several times with ice cold diethyl ether, then put on a high vacuum for several hours, after which it was

used without further purification. The deprotected product was dissolved in anhydrous DMF and DIPEA (3 eq) with DOTA-NHS ester (1.2 eq) and stirred under inert atmosphere for 12h. The crude product was purified via RP-HPLC [A = 20 mM ammonium acetate buffer (pH 5.0) and B = CH₃CN, solvent gradient 5% B to 55% B in 45 minutes] to yield the product FAP5-DOTA. [M+H]⁺ calculated for C₆₃H₈₈F₂N₁₄O₁₈, 1203.3; observed mass 1204.

Synthesis of FAP5-IP-DOTA. 4-(*p*-iodophenyl)butyric acid was dissolved in anhydrous DMF with HATU (1 eq) and anhydrous DIPEA (3 eq) for 10 minutes. Fmoc-Lys-OH HCl (1 eq) was dissolved in anhydrous DMF and DIPEA (1.5 eq), then added to the reaction mixture. The resulting solution was stirred under inert atmosphere for 2h. The product was extracted with EtOAc, washed with ice cold brine, then purified by flash chromatography [A=DCM, B=MeOH, solvent gradient 0% B to 20% B in 25 minutes] to yield NHFmoc-Lys(IP)-OH. LC/MS (m/z): [M+H]⁺ calculated for C₃₁H₃₃IN₂O₅, 640.5; observed mass 641.

NHFmoc-Lys(IP)-OH was dissolved in anhydrous DMF with HATU (1 eq) and anhydrous DIPEA (3 eq) for 10 minutes. Propargyl-PEG₆-amine was dissolved in anhydrous DMF and DIEPA (1.5 eq), then added to the reaction mixture. The resulting solution was stirred under inert atmosphere for 2h. The product was extracted with EtOAc, washed with ice cold brine, then purified by flash chromatography [A=DCM, B=MeOH, solvent gradient 0% B to 20% B in 25 minutes] to yield NHFmoc-Lys(IP)-Pro. LC/MS (m/z): [M+H]⁺ calculated for C₄₆H₆₀IN₃O₁₀, 941.9; observed mass 943. Progress of the reaction was monitored by LC/MS.

Fragment 1 (1.2 eq) was dissolved in anhydrous DMF with NHFmoc-Lys(IP)-OH, then CuI (0.5 eq) and DIPEA (2.0 eq) were added. The reaction mixture was heated to 55°C and stirred for 5 hours. The product was extracted with EtOAc, washed with ice cold brine, then purified by flash chromatography [A=DCM, B=MeOH, solvent gradient 0% B to 20% B in 25 minutes] to yield NHFmoc-Lys(IP)-Frag1. LC/MS (m/z): [M+H]⁺ calculated for C₆₀H₇₈IN₇O₁₂, 1216.2; observed mass 1217.

NHFmoc-Lys(IP)-Frag1 was dissolved in ACN and cooled to 0°C. An equal volume of TFA was added and the reaction mixture was stirred at room temperature for 1h. Progress of the reaction was monitored via LC/MS. LC/MS (m/z): [M+H]⁺ calculated for C₅₅H₇₀IN₇O₁₀, 1116.11; observed mass 1117. Upon completion of the deprotection, TFA was removed by rotary evaporation and the deprotected product was used without further purification. Fragment 2 was dissolved in anhydrous DMF and DIPEA (3 eq) for 10 minutes. The previously deprotected

product was dissolved in anhydrous DMF and excess DIPEA, then added to the reaction mixture and stirred under inert atmosphere for 2h. The crude product was extracted with EtOAc, washed with ice cold brine, then purified by flash chromatography [A=DCM, B=MeOH, solvent gradient 0% B to 30% B in 25 minutes] to yield FAP5-LysIP-NHFmoc. LC/MS (m/z): [M+H]⁺ calculated for C₆₇H₈₁IN₁₀O₁₃, 1399.3; observed mass 1400.

FAP5-LysIP-NHFmoc was dissolved in DCM and diethylamine (20 eq) then stirred for 1h. Progress of the reaction was monitored via LC/MS. LC/MS (m/z): [M+H]⁺ calculated for C₅₂H₇₁F₂IN₁₀O₁₀, 1177.11; observed mass 1178. Upon completion of the deprotection, the product was isolated via rotary evaporation, washed several times with ice cold diethyl ether, then put on a high vacuum for several hours, after which it was used without further purification. The deprotected product was dissolved in anhydrous DMF and DIPEA (3 eq) with DOTA-NHS ester (1.2 eq) and stirred under inert atmosphere for 12h. The product was purified via RP-HPLC [A = 20 mM ammonium acetate buffer (pH 5.0) and B = CH₃CN, solvent gradient 5% B to 55% B in 45 minutes] to yield FAP5-IP-DOTA. LC/MS (m/z): [M+H]⁺ calculated for C₆₈H₉₇F₂IN₁₄O₁₈, 1563.6; observed mass 1564.

2.3.4 Enzyme Inhibition Assays

Enzyme inhibition assays were conducted similarly to previous reports.^{37, 38} Briefly, FAP5 ligand (ranging between 10⁻⁴ and 10⁻¹¹ M) was incubated with enzyme, 1 μM substrate, and buffer in a total volume of 100 μL for 30 minutes at 37°C. Final enzyme concentrations were 50 ng, 25 ng, and 10 ng for FAP, PREP, and DPP4 respectively. The FAP5 ligand was preincubated with the enzyme for 10 minutes at room temperature before addition of substrate. Fluorescence was measured with a BioTek Synergy Neo2 plate reader in the Chemical Genomics Facility. The excitation wavelength was 365 nm and the emission wavelength was 450 nm. Conditions were tested in triplicate. FAP5 ligand stock solution (10 mM) was prepared in 5% DMSO and PBS.

2.3.5 Cell Culture

HEK and Hs894 cells were cultured in DMEM media. HT1080 and U87MG were cultured in EMEM media. 4T1 and KB cells were cultured in RPMI-1640 media. 10% FBS and 1% penicillin-streptomycin were added to all media. 1% 2 mM glutamine was also added to RPMI-

1640 media. All cells were cultured at 37°C in a 5% CO₂ and 95% humidified atmosphere. All cells used in this study were thawed from frozen vials saved in a master stock.

2.3.6 Transfection and Cell Sorting

Six million HEK293T cells were cultured in 100 mm petri dishes with media consisting of DMEM and 10% FBS. The transfection solution was prepared by first mixing 30 µg of Lipofectamine per milliliter of Opti-MEM media. A second solution was prepared by mixing 4 µg FAP expression vector with 10 µg packing plasmid per milliliter of Opti-MEM media, then added to the Lipofectamine solution in drop-wise fashion. The culture media was aspirated from the petri dish, then two milliliters of the resulting solution were added dropwise onto the cells. DMEM media was added, and the cells were returned to the incubator. After 24 hours, the media was removed and chilled on ice. The media was centrifuged at 500 rcf, then filtered with a 0.45 µm membrane to remove cellular debris. 1 mL of Lenti-X Concentrator was added for every 3 mL of media, and the solution was incubated overnight at 4°C. The virus was concentrated by centrifuging the solution at 1500 rcf and 4°C. The supernatant was discarded, and the virus was redissolved in cold PBS.

The virus was diluted with media consisting of DMEM or EMEM, 10% FBS, and 1% penicillin-streptomycin. The solution was added to a small flask containing 250,000 HEK or HT1080 cells. After incubating overnight, the virus-containing media was replaced with complete EMEM and 1 µg of Puromycin per milliliter of media to select for transduced cells. HEK-FAP or HT1080-FAP cells were cultured and passaged under the same conditions for several weeks. Ten million Transfected cells were then harvested with Accutase, concentrated in staining buffer, and stained with human FAP α APC-conjugated antibody for 20 minutes at 4°C. After washing 3x with staining buffer, dead cells were marked with 7-AAD. The cells were sorted with a BD LSRFortessa Flow Cytometer in the Bindley Bioscience Center to isolate HT1080 cells expressing high quantities of FAP receptor. The high FAP expressing cells were cultured and stored for subsequent confocal and binding studies.

2.3.7 Chelation and Radiolabeling

FAP5-IP-DOTA was mixed with ammonium acetate (0.5 M, pH 8.0) to reach a final DOTA concentration of 0.5 mM. Cold chelations were performed by adding natural indium or lutetium in a dilute HCl solution in excess, heated to 90°C for 10 minutes, then analyzed using LC/MS. ^{111}In ($^{111}\text{InCl}_3$) was added to obtain a specific activity of up to 3 MBq/nmol. ^{177}Lu ($^{177}\text{LuCl}_3$) was added to obtain a specific activity of up to 4 MBq/nmol. Sodium-diethylenetriamine pentaacetate solution (5 mM, pH 7.0) was added to complex any unreacted traces of radioactive isotope. Radiochemical purities were analyzed using radio-HPLC. The mobile phase consisted of a 20 mM ammonium acetate aqueous buffer (pH 7) (A) and acetonitrile (B) with a linear gradient from 5% B to 95% B over 15 minutes. Radiochemical purities were over 95% for all studies.

2.3.8 Computational Docking

The crystal structure for FAP (PDB id: 1Z68) was prepared with Protein Preparation Wizard in Glide of the Schrödinger Maestro Suite (11.2.014, MMshare 3.8.014) by preprocessing the structures to fill in any missing loops or side chains, assigning bond orders, generating possible Epik states at a target pH of 7.0 ± 2.0 and removing crystallization artifacts. The structures were then refined by optimizing hydrogen bond (HB) assignments and minimizing the energy of the protein structure with the OPLS3 force field. The docking zones to specify the locales of FAP ligands were designed as a 25 Å³ cube encompassing the binding pocket of FAP and calculated by Receptor Grid Generation in Glide. The catalytic serine S624 was selected for covalent docking. Other key residues in the binding pocket such as R123, E203, E204, Y656, and H734 were used as additional reference residues.

2.3.9 Cell Binding Studies

Binding curves: 100,000 Hs894 CAFs or 200,000 HT1080-hFAP cells were seeded in 24 well plates. 250,000 HEK-hFAP cells were seed in 24 well amine-coated plates. Once the cells reached confluency, they were incubated with FAP5-DOTA conjugates labeled with indium-111 in the absence or presence of excess FAP5 ligand. After incubation for 1h at room temperature, the cells were washed 3x with PBS to remove unbound radioactivity and dissolved in 1.0 M NaOH. The samples were transferred to tubes and cell-bound radioactivity was measured using a gamma

counter. A specific binding constant was calculated using one-site specific binding nonlinear regression after subtracting competition counts from total binding counts. Alternatively, a total binding constant was calculated using one-site total binding nonlinear regression. All samples were performed in triplicate.

Displacement assay: 250,000 HEK-hFAP cells were seeded in amine-coated 24 well plates. Once the cells reached confluency, they were incubated with FAP5-Rhodamine at a concentration of 10 nM in the presence of increasing concentrations of FAP5-IP-DOTA. After incubation for 1h at 4°C, the cells were washed 3x with PBS to remove unbound fluorescence and dissolved in 1% SDS. The samples were transferred to a 96 well clear bottom, black wall plate. Cell-bound fluorescence was measured with a BioTek Synergy Neo2 plate reader in the Chemical Genomics Facility at the Purdue Institute for Drug Discovery. Wavelengths were set to $\lambda_{ex} = 552$ nm and $\lambda_{em} = 575$ nm. Cell-bound fluorescence was plotted against the logarithm of the concentrations of FAP5-IP-DOTA in nM. A K_d of 2.67 nM for FAP5-Rhodamine was used to calculate the K_i of FAP5-IP-DOTA using one-site binding nonlinear fit. All samples were performed in triplicate.

2.3.10 Animal Husbandry

6-week-old (16-19 g) female mice Balb/cJ were purchased from Charles River. 12-week-old female athymic nu/nu mice (23-27 g) were purchased from Envigo. All mice were given access to normal rodent chow and water ad libitum. The mice were maintained on a standard 12h light-dark cycle. All animal procedures were approved by the Purdue Animal Care and Use Committee.

2.3.11 Tumor Models

Mouse tumor: Balb/cJ mice were inoculated on their shoulder with 1×10^5 cells of 4T1 cells in sterile PBS.

Human xenograft: Nu/nu mice were inoculated on their shoulder with 5×10^6 cells of HT29, KB, or U87MG cells in sterile PBS.

2.3.12 SPECT/CT scans

4T1 tumors were allowed to grow to approximately 1 cm^3 before initiating SPECT/CT scans. Each tumor-bearing mouse was intravenously injected with up to 6 nmol of FAP5-IP-

DOTA radiolabeled with 13 MBq of indium-111 via the tail vein. Animals were anesthetized with isoflurane and scanned at 4, 24, 48, 72, 96, and 120 h after injection. The emission scan was conducted for 20-60 min using the MILabs VECTor/CT system in the Purdue Imaging Facility of Bindley Bioscience Center at Purdue University. The CT scans were acquired with an X-ray source set at 60 kV and 615 μ A. The SPECT images were reconstructed with U-SPECT II software and ^{111}In γ -energy windows of 171 and 241 keV or ^{177}Lu γ -energy window of 208 keV. A POS-EM algorithm was used with 16 subsets and 4 iterations on a 0.8 mm voxel grid. The CT images were reconstructed using NRecon software. The datasets were fused and filtered using PMOD software (version 3.2).

2.3.13 Radioactive Biodistribution

4T1 tumors were allowed to grow to approximately 100 mm³ before initiating biodistribution studies. Each tumor-bearing mouse was intravenously injected with 5 nmol of FAP5-IP-DOTA radiolabeled with 3.7 MBq of lutetium-177 via the tail vein. Animals (n = 4-5) were euthanized by CO₂ asphyxiation at 1, 4, 24, 72, 120, and 168 h post injection. Organs of interest were harvested, washed with PBS, weighed, and analyzed on a gamma counter to quantitate radioactive uptake. Results were normalized as percentages of the injected dose per gram of tissue (%ID /g).

2.3.14 Radiotherapy

4T1 tumors were grown to approximately 72 mm³ (n = 5 per group). HT29 tumors were grown to approximately 169 mm³ (n = 4 per group). KB tumors were grown to approximately 52 mm³ (n = 5 per group). U87MG tumors were grown to approximately 173 mm³ (n = 5 per group). All mice were randomly divided into control or treatment groups prior to the initiation of the therapy studies. Mice received a single intravenous dose of sterile saline or 5 nmol of FAP5-IP-DOTA radiolabeled with 9 or 18 MBq of lutetium-177 via the tail vein on day 0. Tumors were measured in two perpendicular directions every other day during therapy, and their volumes were calculated as $0.5 \times L \times W^2$, where L is the longest axis (in millimeters), and W is the axis perpendicular to L (in millimeters). Humane endpoint criteria were defined as weight loss of more

than 20% of the initial body weight, a tumor volume of more than 1,800 mm³, or open ulceration. Mice were euthanized on reaching one of the predefined endpoint criteria.

2.3.15 Toxicology

Mice were weighed every other day during the therapy studies as a gross measurement of toxicology. Mice were randomly selected from control and treated groups for further toxicology evaluation. Organs of interest were harvested immediately post euthanasia, washed, then fixed in a 10% formalin solution for 48-72 hours. Organs were then maintained in a 70% ethanol solution until radioactivity had fully decayed, after which they were submitted to the Histology Laboratory at Purdue University to be embedded in paraffin, sectioned, and stained with H&E. Tissue sections (n = 4–8 per organ per mouse) were examined in a blinded manner for lesions by a licensed pathologist at the Purdue University Department of Comparative Pathobiology.

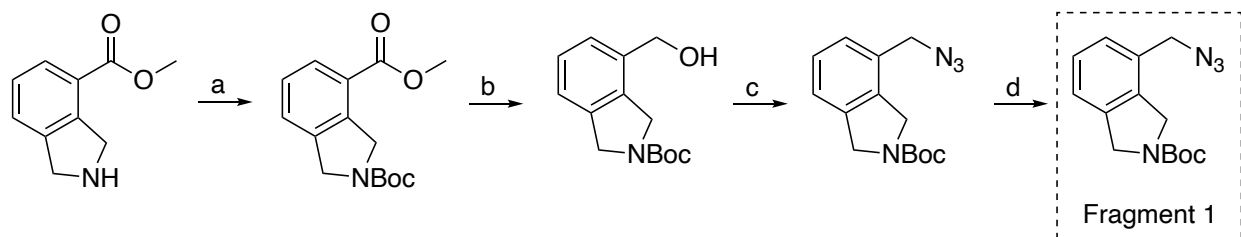
2.3.16 Statistical Analysis

Data were analyzed using on GraphPad Prism 8 unless otherwise stated. Results are shown as mean ± SE.

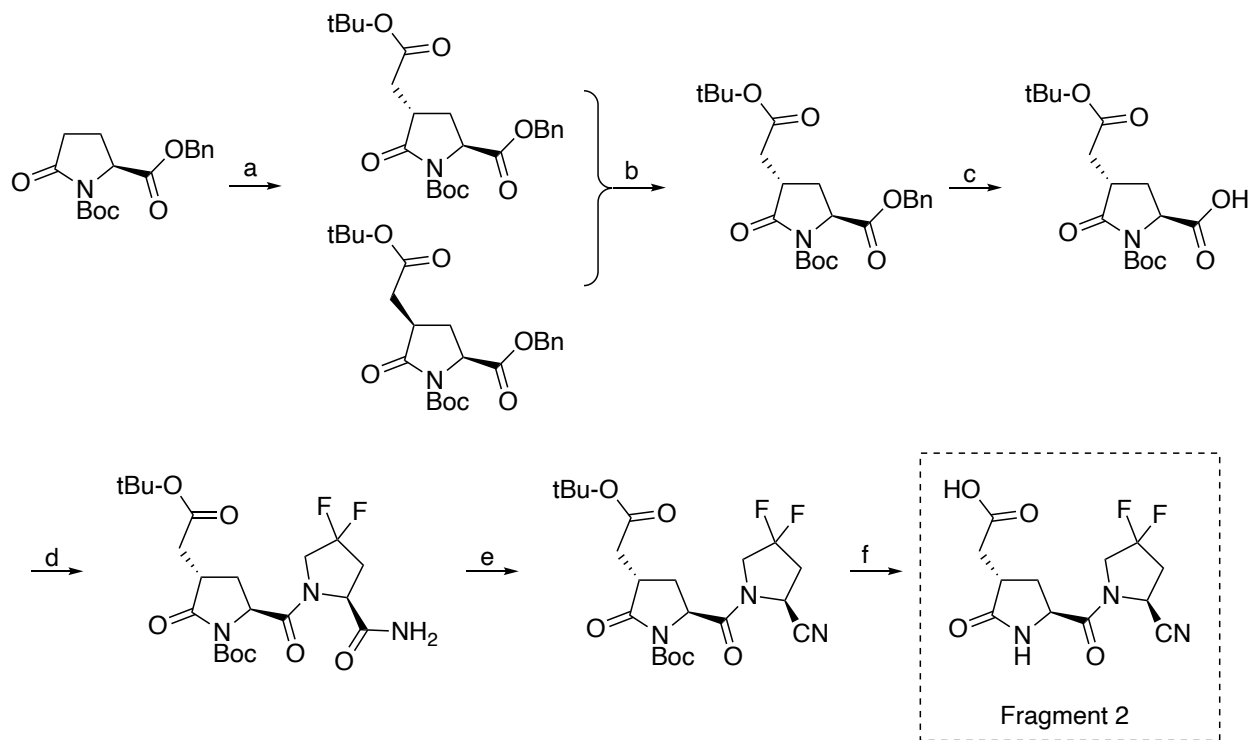
2.4 Results

2.4.1 Synthesis of FAP-Targeted Drug Conjugates

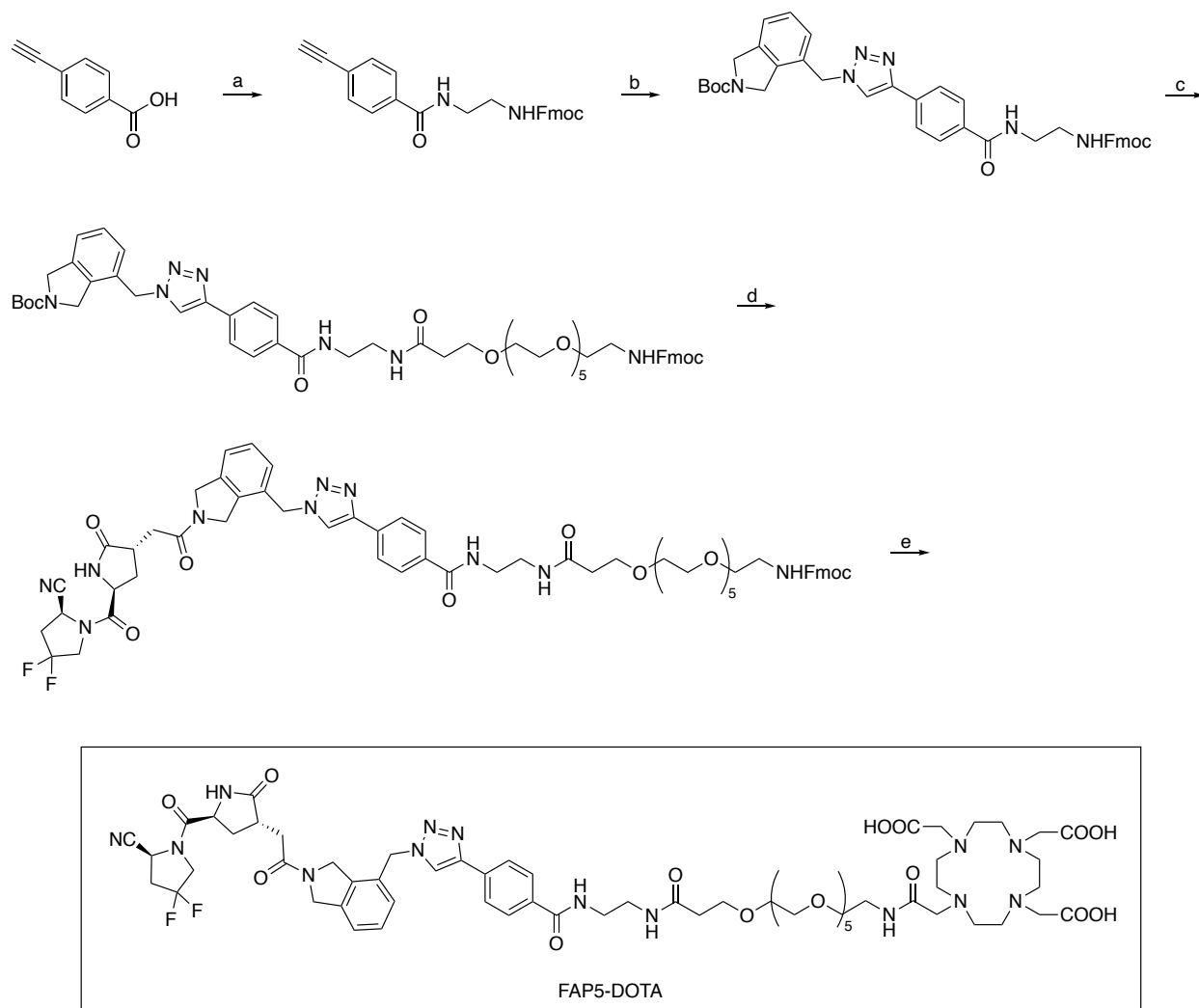
After reviewing various fibroblast activation protein inhibitors as reported in the literature, and some previous internal comparisons in our lab, the diamide 4,4-difluoro-2-carbonitrile-pyrroldine ring with a 4-carboxymethylpyroglutamic acid isoindoline was selected due to its high potency against FAP (~20 nM) and selectivity against homologous enzymes such as DPP-IV and PREP (> 10,000 fold).^{38, 39} Scheme 2.1 and Scheme 2.2 depicts the synthesis of the two key fragments of this inhibitor, with an azide derivatization on the 4 position of the solvent-exposed isoindoline moiety. The azide facilitates a facile coupling to a functional linker via click chemistry, after which the two fragments could be conjugated together by amide coupling to form the FAP5 ligand. Further functionalization with DOTA alone or with DOTA and an albumin-binder are depicted in Scheme 2.3 and Scheme 2.4. respectively.



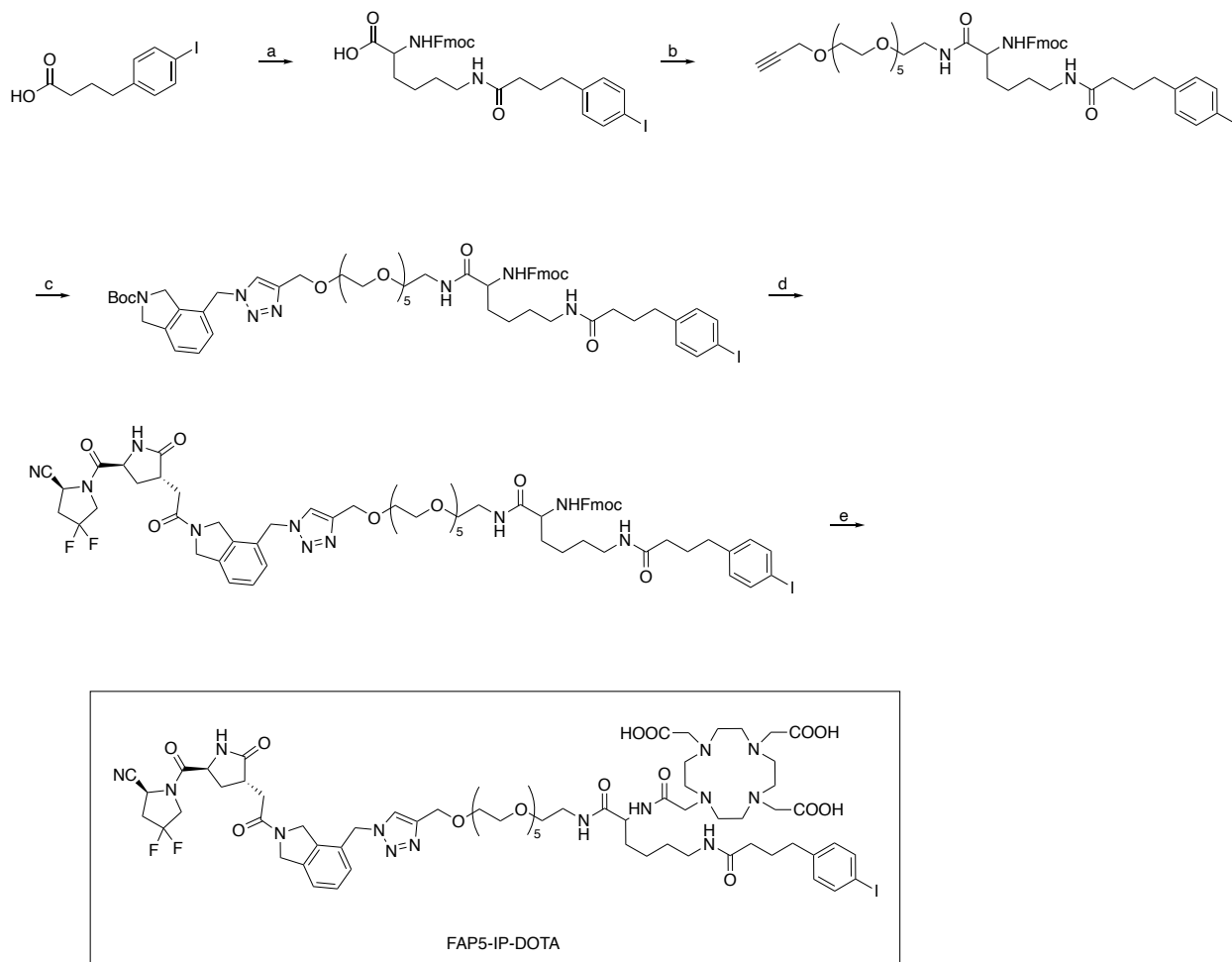
Scheme 2.1. Synthesis of FAP5 Final Intermediate 1. Reagents and conditions for Fragment 1: (a) Boc_2O , TEA, DCM, rt, overnight; (b) NaBH_4 , MeOH, THF, 55°C , 5h; (c) NBS, PPh_3 , DMF, rt, 6h; (d) NaN_3 , DMF, 65°C , overnight.



Scheme 2.2. Synthesis of FAP5 Final Intermediate 2. Reagents and conditions for Fragment 2: (a) i. LiHMDS, THF, -78°C , 1h; ii. tert-butyl-bromoacetate, 2h; (b) DBU, DCM, 0°C -rt, 24h; (c) $\text{H}_2/\text{Pd-C}$, MeOH, rt, overnight; (d) 4,4-difluoro-L-prolinamide, HATU, DIPEA, DMF, rt, 3h; (e) imidazole, POCl_3 , pyridine, -20°C , 1h; (f) TFA, ACN, 0°C -rt, 1h.



Scheme 2.3. Synthesis of FAP5-DOTA. Reagents and conditions: (a) Mono-Fmoc ethylene diamine, HATU, DIPEA, DMF, rt, 3h; (b) Fragment 1, CuI, DIPEA, DMF, 55°C, 5h; (c) i. Et₂NH, DCM, rt, 1h; ii. NHS ester-PEG₆-NHFmoc, DCM, rt, 3h; (d) i. TFA, ACN, 0°C-rt, 1h; ii. Fragment 2, HATU, DIPEA, DMF, rt, 3h; (e) i. Et₂NH, DCM, rt, 1h; ii. NHS ester DOTA, DMF, rt, 12h.



Scheme 2.4. Synthesis of FAP5-IP-DOTA. Reagents and conditions: (a) Fmoc-Lys-OH, HATU, DIPEA, DMF, rt, 3h; (b) Propargyl-PEG₆-NH₂, HATU, DIPEA, DMF, rt, 3h; (c) Fragment 1, CuI, DIPEA, DMF, 55°C, 5h; (d) i. TFA, ACN, 0°C-rt, 1h; ii. Fragment 2, HATU, DIPEA, DMF, rt, 3h; (e) i. Et₂NH, DCM, rt, 1h; ii. NHS-ester DOTA, DMF, rt, 12h.

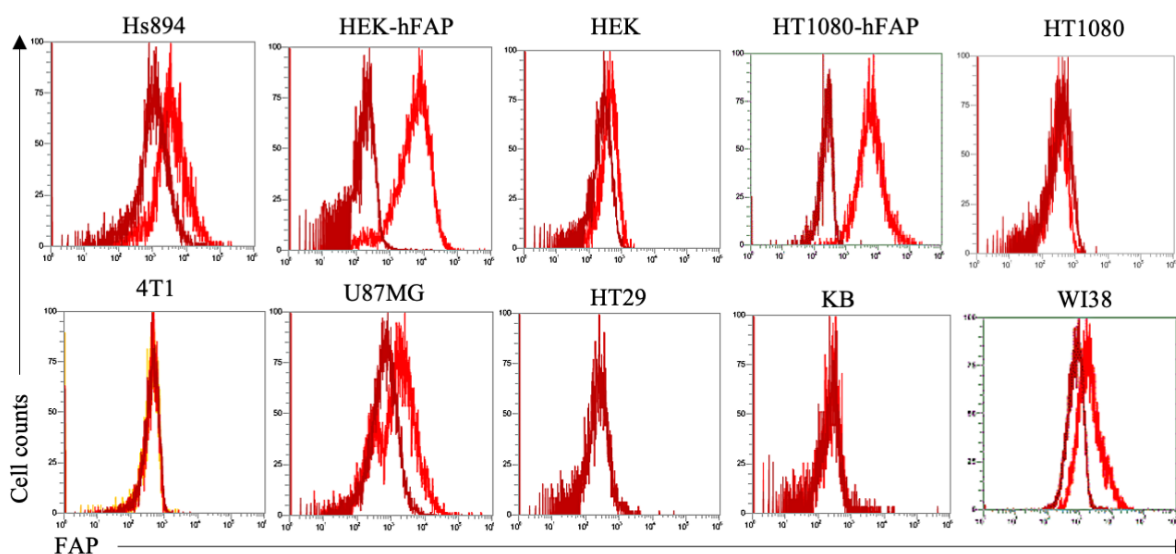
All final products were characterized by LC/MS, and representative spectra are given in Supplemental Figure S2.1. The chelation of FAP5-DOTA and FAP5-IP-DOTA were validated by incubating aliquots of each conjugate dissolved in buffer with either natural indium or natural lutetium in a dilute HCl solution, then analyzing the samples on LC/MS, as shown in Supplemental Figure S2.2. Once confirmed, each conjugate was radiolabeled with indium-111 or lutetium-177, and >95% radiopurity was confirmed on radio-HPLC as shown in Supplemental Figures S2.3 and 2.4 before conducting radioactive studies.

2.4.2 *In vitro* assays of FAP5-DOTA Conjugates

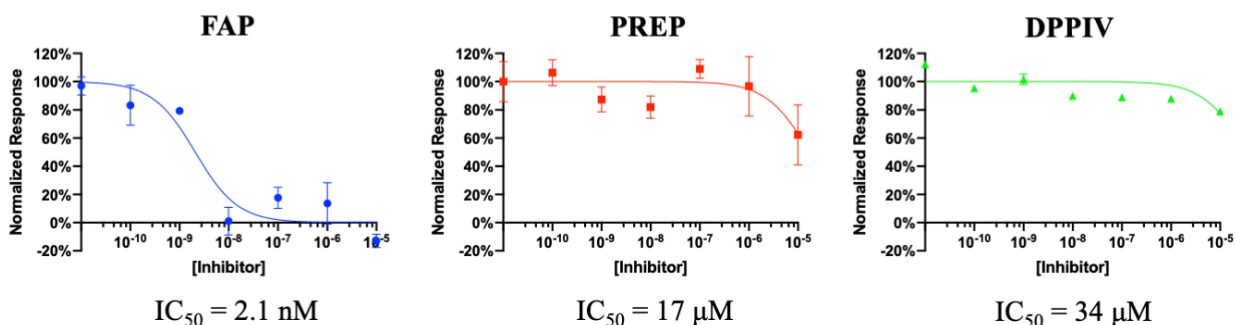
Various cell lines were first investigated for FAP expression by FACS analysis. As shown in Figure 2.1, the commercially available fibroblast cell lines Hs894 and WI38 express low levels of endogenous FAP, as well as the glioblastoma cell line U87MG. Although various tumor models have been proven to be FAP⁺ *in vivo*, such as 4T1,^{40, 41} HT29,³⁶ and KB,¹⁷ these cell lines did not demonstrate positive FAP expression *in vitro*.

The synthesized FAP5 ligand demonstrated strong FAP inhibition in our enzyme assay ($IC_{50} = 2.1$ nM), as well as high selectivity for FAP over other homologous enzymes such as DPPIV and PREP (~1000 fold). When radiolabeled with indium-111, both FAP5-DOTA and FAP5-IP-DOTA demonstrated high binding affinities to the CAF cell line Hs894 ($K_d = 1.2$ nM and $K_d = 0.92$ nM respectively). Incubation of these conjugates with a hundred-fold excess of competition FAP5 ligand to competitively block all available FAP receptors abolished all targeting, further validating that the targeting of our FAP5-DOTA conjugates is receptor-mediated. Additional cellular assays found in Supplemental Figure S2.5 such as displacement assays using a FAP5-Rhodamine conjugate as a reporter, and binding studies with two different cell lines transfected with human FAP further substantiate FAP5 as a novel targeting ligand.

FACS Analysis of FAP expression in cell lines



Enzyme Inhibition Assays



Binding Curves with hCAF Cell Line Hs894

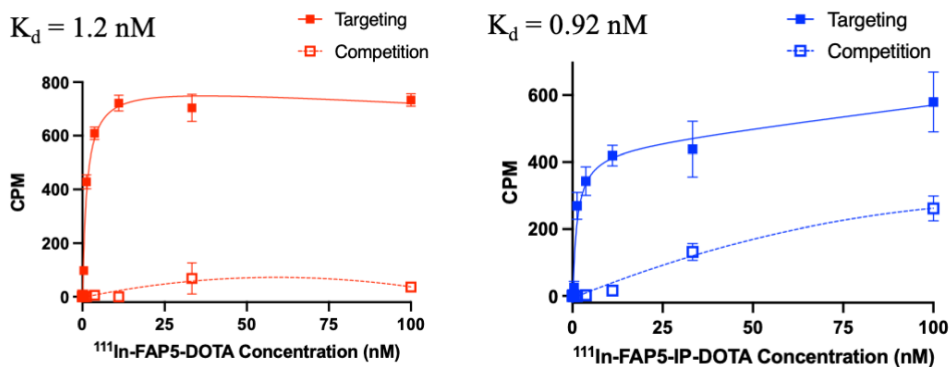


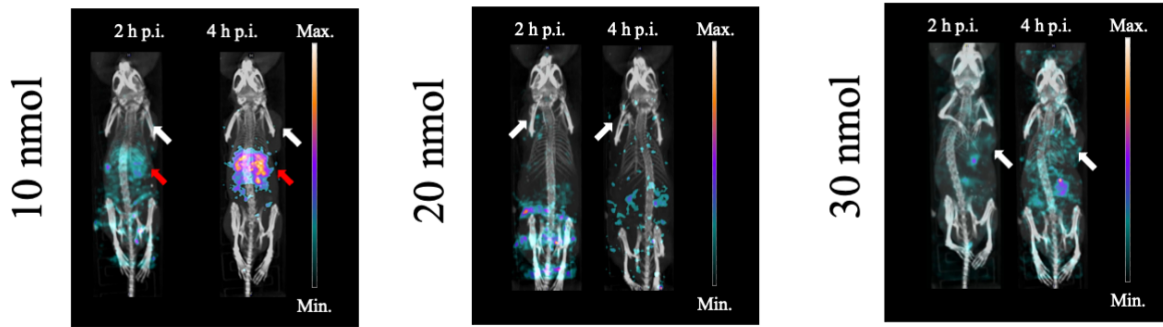
Figure 2.1. *In vitro* assays of FAP5-DOTA conjugates. FAP expression was first checked on all cell lines used for this study. Antibody-stained samples are represented by the bright red histograms. Non-staining controls are represented by the dark red histograms. The FAP5 base ligand was then tested with recombinant enzymes for potency and specificity. FAP5-DOTA and FAP5-IP-DOTA were investigated to assess their targeting to human CAFs.

2.4.3 *In vivo* evaluation of the tumor retention, biodistribution, and pharmacokinetics of FAP5-DOTA conjugates

Having thoroughly vetted FAP5 as a targeting ligand using several *in vitro* methods, we proceeded to study the *in vivo* properties of FAP5, particularly the effect of the iodophenyl albumin-binder. Dosing studies were first conducted to optimize the nmol of conjugate required for radioimaging and radiotherapy. Balb/c mice bearing 4T1 tumors received an intravenous tail-vein injection of 1–30 nmol FAP5-DOTA or FAP5-IP-DOTA radiolabeled with ~11 MBq of In-111, after which SPECT/CT scans were performed to assess the biodistribution and pharmacokinetics. The results of these dosing studies are given in Figure 2.2. The SPECT/CT scans indicate that even high doses of FAP5-DOTA resulted in poor tumor uptake and retention. However, the presence of the iodophenyl albumin-binder facilitated high tumor uptake and long-term retention of FAP5 radioligand when injected in sufficient quantities. Similar results were found in the human tumor xenograft HT29, as shown in Supplemental Figure S2.6.

The biodistribution FAP5-DOTA conjugates were next quantitatively studied by *ex vivo* analysis. FAP5-DOTA (5 nmol) was radiolabeled with Lu-177 and injected intravenously into 4T1-bearing Balb/c mice (n = 4–5) via the tail vein. FAP5-IP-DOTA (5 nmol) was radiolabeled with In-111 and injected intravenously into 4T1-bearing Balb/c mice (n = 5) via the tail vein. At various times, the mice were euthanized, and organs of interest were harvested for radioactive measurements using a gamma counter. The results of FAP5-DOTA versus FAP5-IP-DOTA are given in Figure 2.3 and Figure 2.4 respectively, and parallel what was expected based on the SPECT/CT scans. FAP5-DOTA possesses a short half-life *in vivo*, appearing to entirely clear from the bloodstream in under an hour via the liver and spleen, thus limiting the tumor uptake of the radioconjugate. Conversely, the addition of the iodophenyl albumin-binder allows the FAP5 radioligand to persist in the bloodstream for more than 24 hours, enabling FAP receptor saturation in the tumor stroma and consequently long-term tumor retention. Retention in the tumor persisted for up to 120 hours. FAP5-IP-DOTA cleared from most off-target organs within the first 24 hours via renal excretion, with the notable exception of the kidneys. Ratios of tumors to important organs at the tested time points are also provided.

SPECT/CT of ^{111}In -FAP5-DOTA



SPECT/CT of ^{111}In -FAP5-IP-DOTA

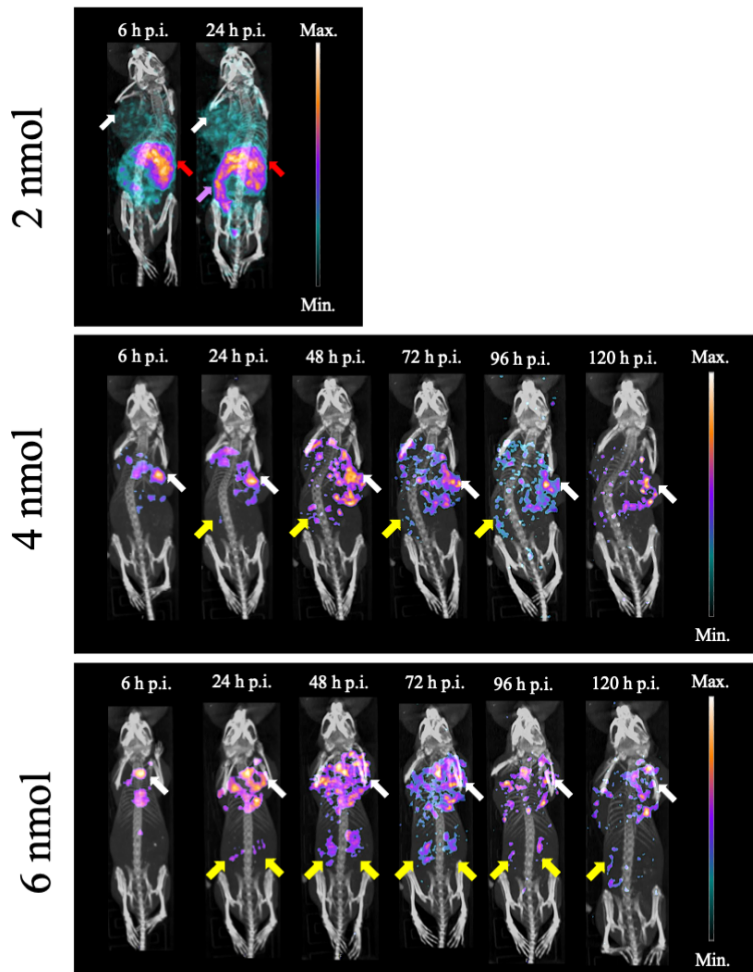
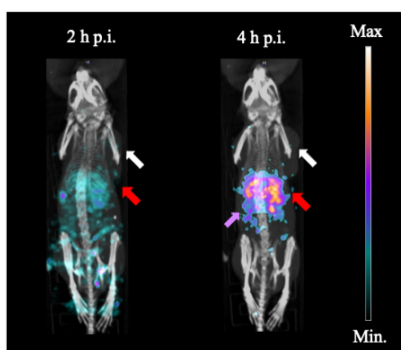
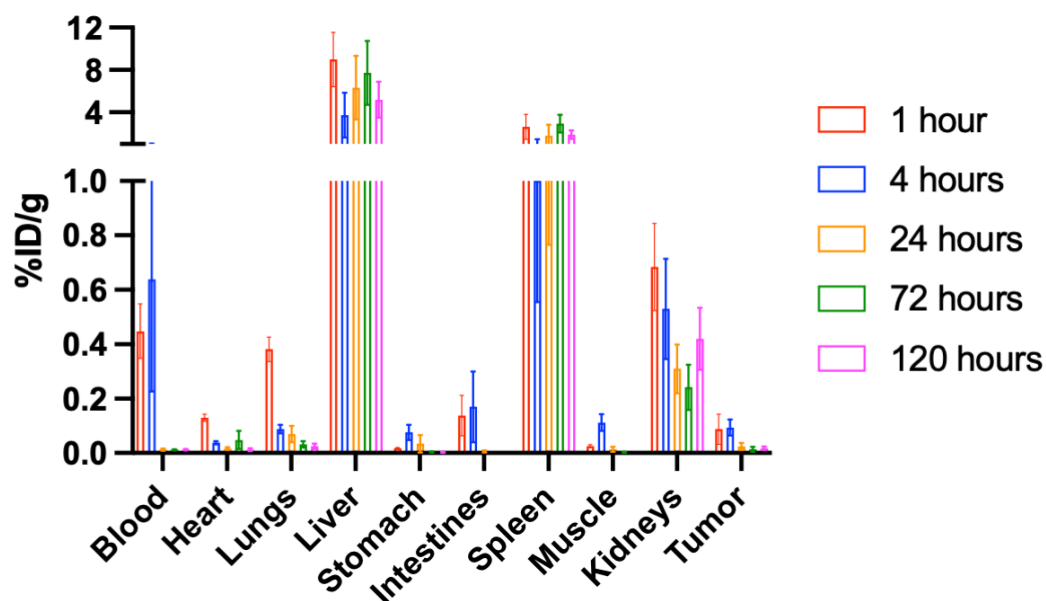


Figure 2.2. Dosing studies of FAP5-DOTA conjugates in 4T1 tumor. White arrows indicate tumor. Red arrows indicate liver. Purple arrows indicate spleen. Yellow arrows indicate kidneys.

SPECT/CT in 4T1 tumor



Biodistribution in 4T1 tumor



Tumor-to-organ ratios

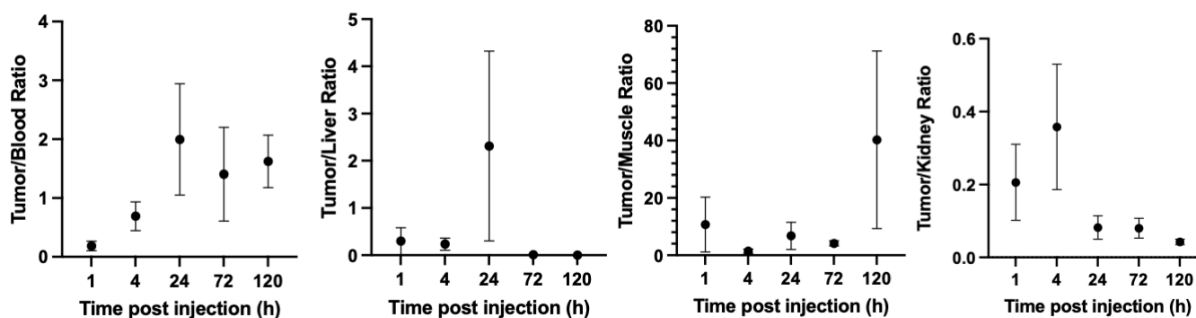
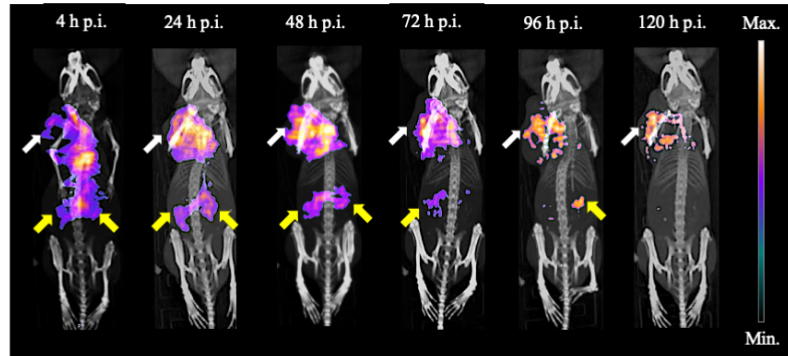
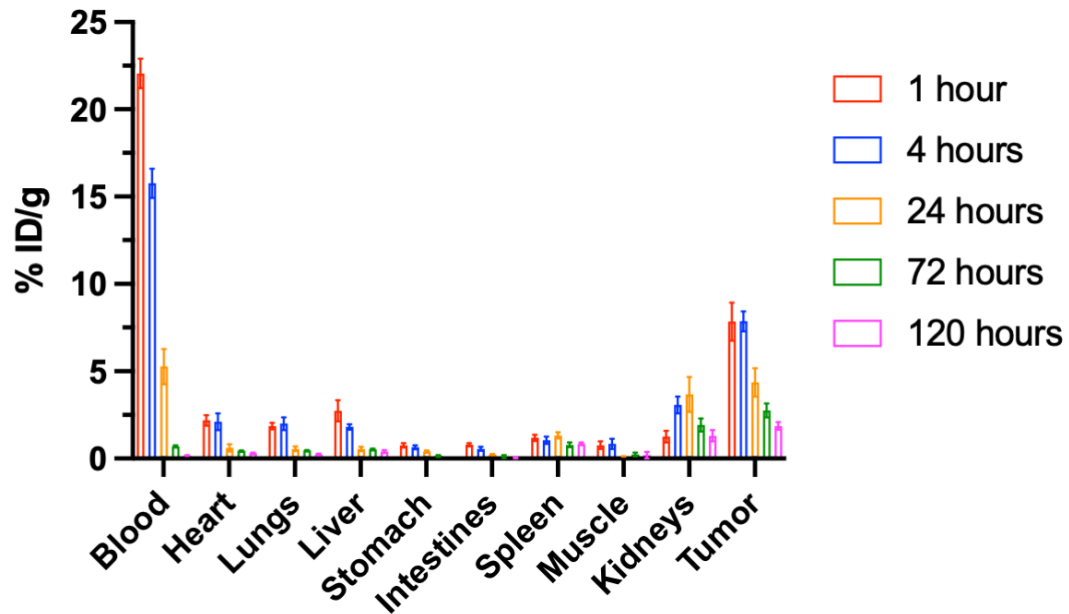


Figure 2.3. FAP5-DOTA biodistribution in 4T1 tumor-bearing mice and tumor-to-organ ratios (n = 4–5). White arrows indicate tumor. Red arrows indicate liver. Purple arrows indicate spleen.

SPECT/CT in 4T1 tumor



Biodistribution in 4T1 tumor



Tumor-to-organ ratios

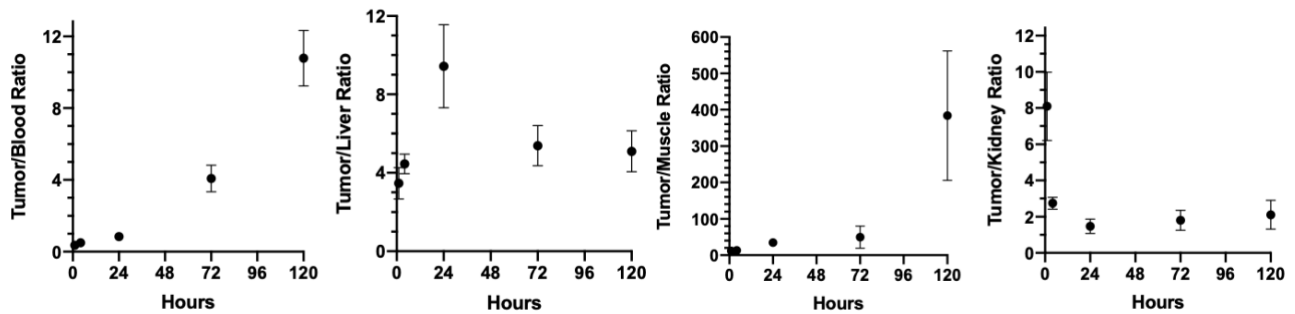
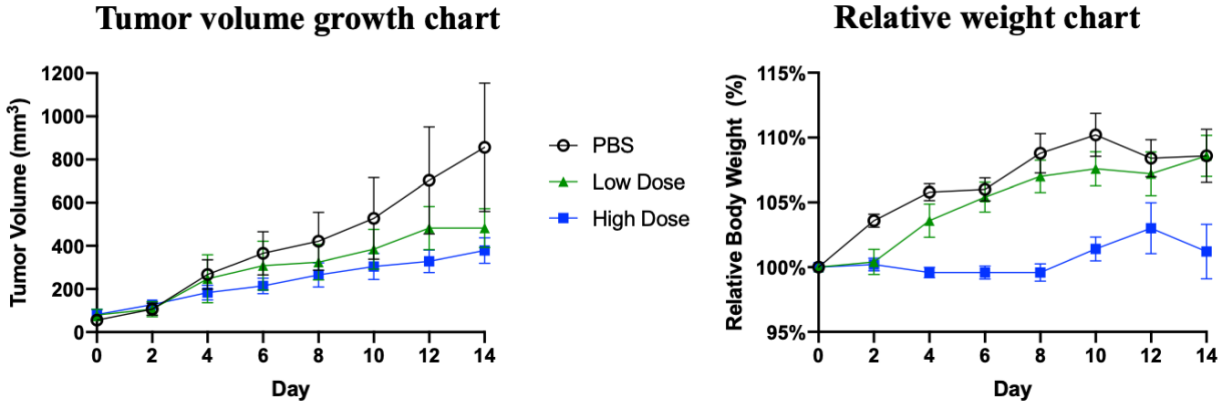


Figure 2.4. FAP5-IP-DOTA biodistribution in 4T1 tumor-bearing mice and tumor-to-organ ratios (n=5). White arrows indicate tumor. Yellow arrows indicate kidneys.

2.4.4 Radiotherapy of ¹⁷⁷Lu-FAP5-IP-DOTA in 4T1 tumor-bearing mice

Encouraged by the high tumor uptake and retention FAP5-IP-DOTA demonstrated *in vivo*, we next pursued radiotherapy with the conjugate. Balb/c mice were implanted with 4T1 tumors approximately one week prior to initiation of the radiotherapy. Mice were randomized into different experimental groups to ensure equal starting tumor size. Mice then received a single intravenous injection via tail vein of 5% ethanol in PBS as a control, or 5% ethanol in PBS containing 5 nmol of FAP5-IP-DOTA radiolabeled with either 9 MBq (low dose) or 18 MBq (high dose) of lutetium-177. Tumors and body weights were measured every other day for two weeks, after which the mice were sacrificed and select organs were fixed and prepared for toxicology evaluation. Both doses limited growth of the murine breast cancer 4T1 relative to the control, and were well tolerated, as shown in Figure 2.5. SPECT/CT scans were also taken of one treated mouse from the therapy study, which is shown in Supplemental Figure S2.7. Further evaluation of sections from the heart, liver, and kidneys post-radiotherapy showed no diagnostic lesions nor other significant differences between the treated and control mice.



H&E staining of select organs

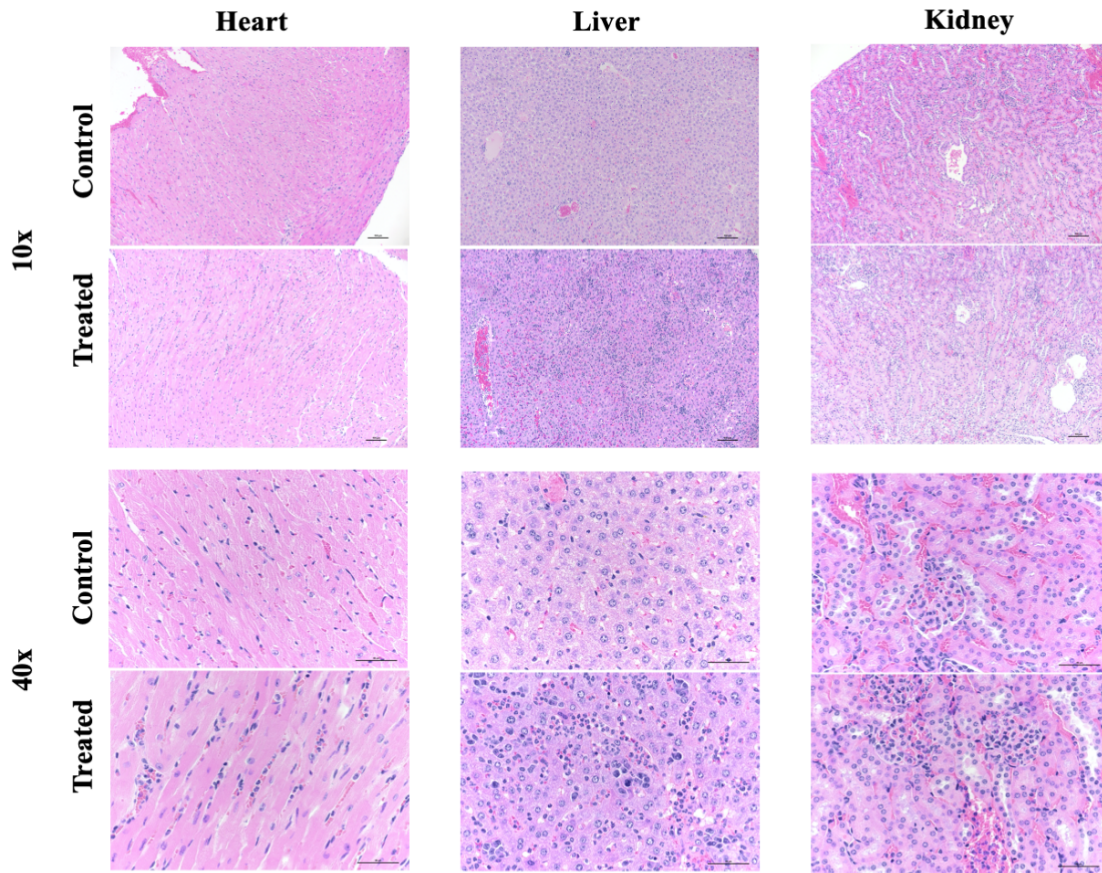


Figure 2.5. Radiotherapy of ¹⁷⁷Lu-FAP5-IP-DOTA in 4T1 tumor-bearing mice (n = 5 per group). Treated mice received a single injection on day 0. The low dose group was injected with 9 MBq of lutetium-177 per mouse, and the high dose group was injected with 18 MBq per mouse.

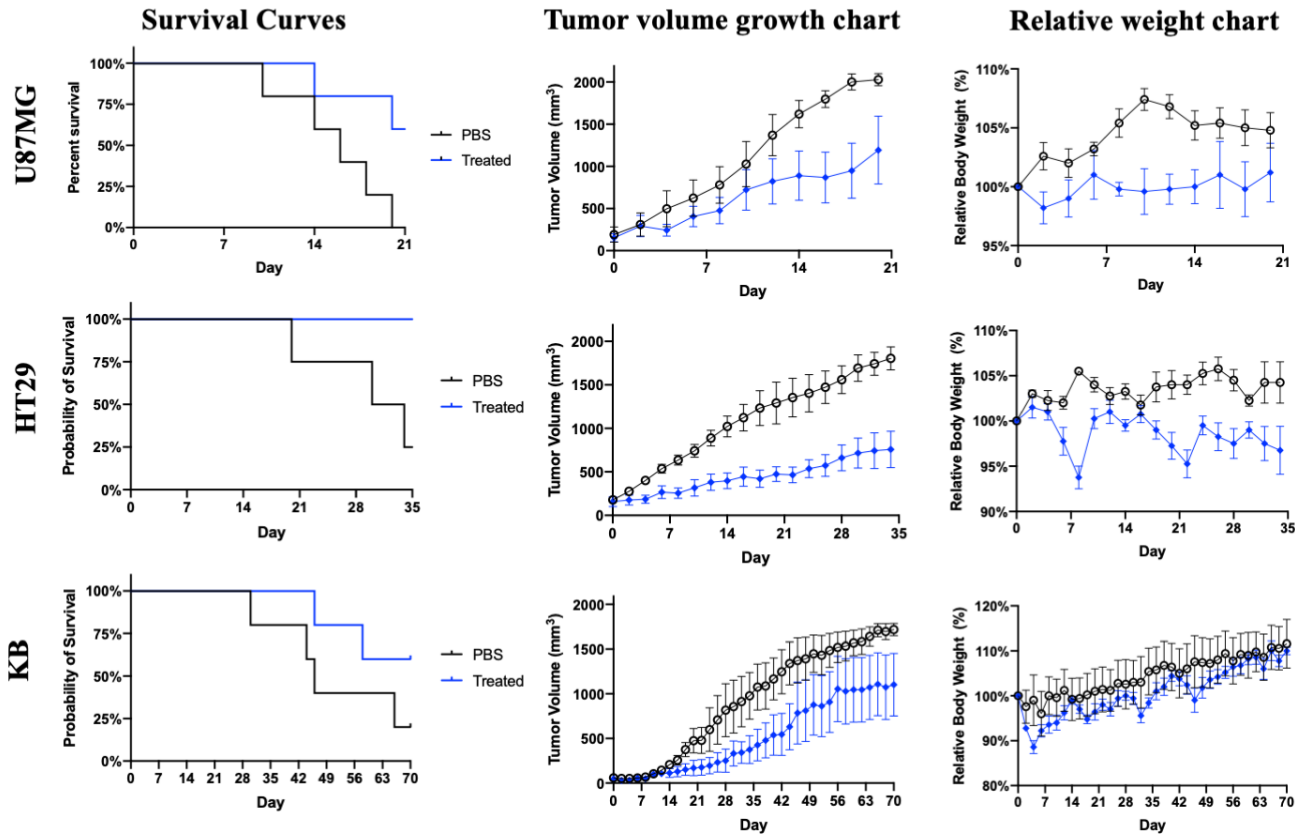
Tumor progression and relative body weights were measured every other day. After the conclusion of the therapy study, mice were euthanized and had their organs fixed for toxicology evaluation. No diagnostic lesions were observed in the selected organs of the control or treated mice.

2.4.5 Radiotherapy of ^{177}Lu -FAP5-DOTA Conjugates in Human Tumor Xenografts

Radiotherapy with FAP5-IP-DOTA against three human tumor xenografts using lutetium-177 as the radionuclide was next investigated. Mice were randomized into different experimental groups to ensure equal starting tumor size. Mice then received a single intravenous injection via tail vein of 5% ethanol in PBS as a control, or 5% ethanol in PBS containing 5 nmol of FAP5-IP-DOTA radiolabeled with either 9 MBq (HT29) or 18 MBq (U87MG and KB) of lutetium-177. Survival, tumor sizes, and body weights were measured every other day until mice reached a critical endpoint as shown in Figure 2.6. After euthanasia, random mice were selected to immediately harvest and fix important organs for toxicology evaluation. In all 3 tumor models, ^{177}Lu -FAP5-IP-DOTA suppressed tumor growth compared to the control mice. Mice treated with ^{177}Lu -FAP5-IP-DOTA also experienced a weight loss within the first week post injection but recovered thereafter. Survival curves show that ^{177}Lu -FAP5-IP-DOTA therapy extended the survival time of treated mice relative to controls. SPECT/CT scans in all 3 tumor models with FAP5-IP-DOTA are also shown in Supplemental Figure S2.7. Necrotic collapse was observed specifically in HT29-tumor bearing mice that received FAP-targeted radiotherapy, but not control mice. Representative pictures are provided in Figure 2.7. Post-radiotherapy evaluation of sections from the heart, liver, and kidneys showed no diagnostic lesions nor other significant differences between the treated and control mice. Representative slides from the diagnostic lesion evaluation are shown in Figure 2.7.

FAP5-DOTA radiotherapy without an albumin-binder was also investigated in one tumor model using ^{177}Lu as the radionuclide. A separate group of KB tumor-bearing mice received a single intravenous injection via tail vein of 5% ethanol in PBS containing 5 nmol of FAP5-DOTA with 18 MBq of lutetium-177. Tumor sizes and body weights were measured every other day until mice reached a critical endpoint, after which the mice were euthanized. No discernible difference between the ^{177}Lu -FAP5-DOTA and the control group was observed with regards to survival time, tumor sizes, or body weights. Results from the FAP5-DOTA radiotherapy study in KB tumors are also presented in Figure 2.6.

^{177}Lu -FAP5-IP-DOTA



^{177}Lu -FAP5-DOTA

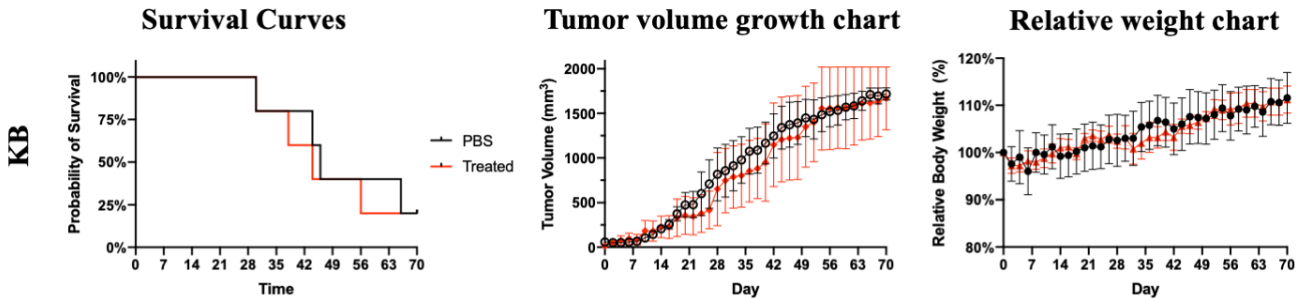


Figure 2.6. Radiotherapy of ^{177}Lu -FAP5-DOTA conjugates in human tumor xenografts. Mice bearing U87MG (n = 5), HT29 (n = 4), or KB (n = 5) tumor xenografts received a single injection on day 0. Mice bearing HT29 tumors received a 9 MBq dose of lutetium-177, while mice bearing U87MG or KB tumors received a 18 MBq dose. Survival, tumor progression and relative body weights were measured every other day. After the conclusion of the therapy study, mice were euthanized and had their organs fixed for toxicology evaluation.

HT29 Tumors Post-Radiotherapy



H&E staining of select organs

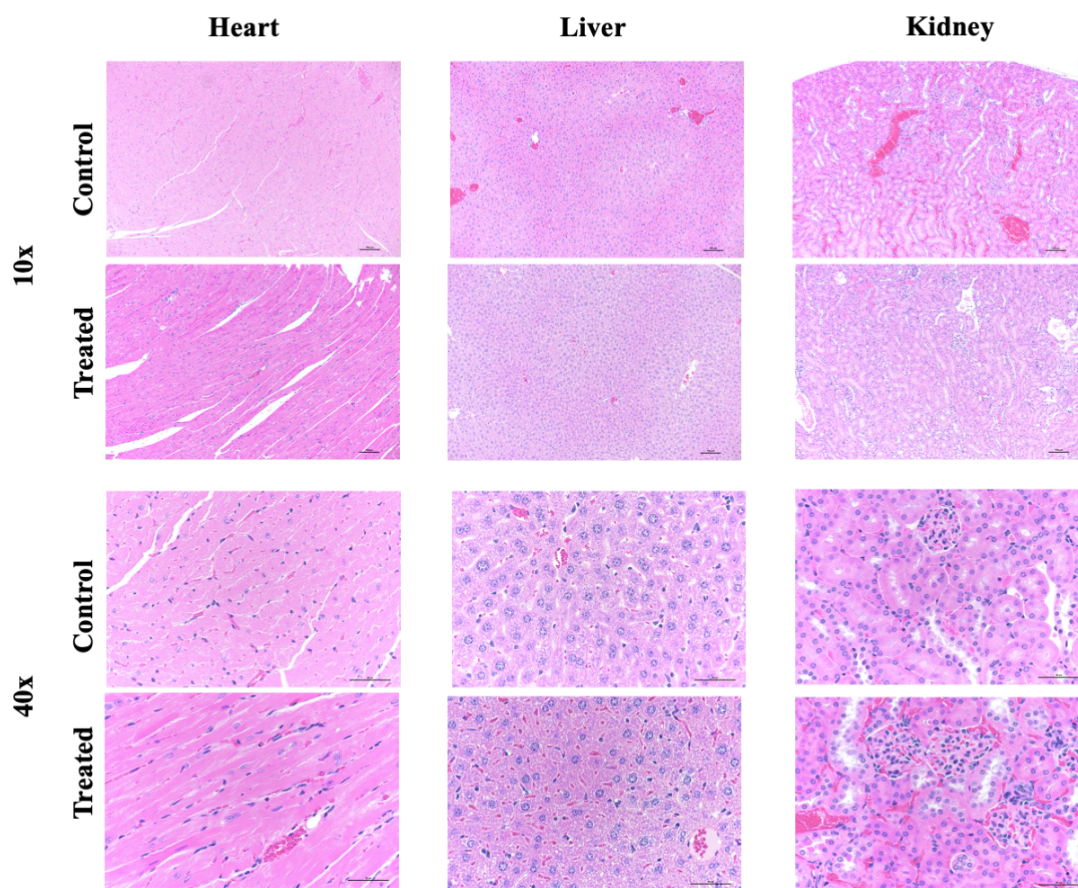


Figure 2.7. Effect of ^{177}Lu -FAP5-IP-DOTA on various tissues. Necrotic collapse was present in all HT29 tumor-bearing mice that received a therapeutic injection, but only mild ulcers were observed in two of the HT29 tumor-bearing mice that received a control injection. No diagnostic lesions were observed in the selected organs of the control or treated mice.

2.5 Discussion

The quinoline-based FAP ligand FAPI has been investigated extensively in recent years for radiotheranostic purposes.^{2, 42-44} However, tumor uptake and retention have proven problematic.^{21, 22, 45} In an effort to identify alternative FAP ligands with improved tumor uptake and retention, we conducted an *in silico* comparison of FAPI to other reported FAP inhibitors. Based on reported IC₅₀ values and our computational results (see Supplemental Figure S2.8), we selected and synthesized a 4-carboxymethylpyroglutamic acid diamide-based FAP ligand (see Sch. 2.1–4). Our analysis of FAP expression on the various cell lines used to test this novel ligand match those previously reported.^{20, 46, 47} The lack of positive staining shown by 4T1, HT29, and KB tumor models with FAP antibodies (see Fig. 2.1) suggest that the apparent FAP overexpression *in vivo* is primarily due to recruiting and or activating FAP⁺ CAFs. U87MG cells do express FAP α directly, although at somewhat lower levels than CAFs.²⁰

In recent years, our lab has focused on developing new FAP ligands for targeting activated fibroblasts with various payloads such as fluorescent dyes, cell signaling pathway inhibitors, and radioactivity.^{17, 48} While fluorescent dyes and inhibitors generally contain albumin-binding moieties within their structures,^{23, 24, 49-54} radioactive chelators do not appear to provide the same pharmacokinetic benefits. We performed parallel studies with FAP5-DOTA and FAP5-IP-DOTA and did not observe similar tumor uptake, retention, or biodistribution profile *in vivo* (see Fig. 2.2–4) despite demonstrating near identical FAP α binding affinity *in vitro* (Fig. 2.1, see also Suppl. Fig. S2.5). Our results parallel the improvements shown in the literature with other targeting ligands (e.g., folate, PSMA) that used the iodophenyl albumin-binder to improve radioactive theranostics.^{26, 30}

Previous FAP α -targeted radiotherapy studies have attempted to compensate for lack of tumor uptake with experimental models using either tumor cell lines where FAP α is expressed directly on the cancer cells,^{14, 55} or using very large tumors.⁵⁶ While these models can be useful as a proof-of-concept, they can also be problematic for translation into the clinic. Most tumor types do not express FAP α directly on the cancer cells, so the interpretation of research in preclinical evaluation that uses FAP-expressing cell lines may be overly optimistic. Larger tumors and advanced grades correlate significantly with CAF density and high FAP stroma intensity,⁵⁷⁻⁵⁹ but radiotherapy is less effective in such tumors.⁶⁰ Additionally, targeted therapies that use large tumor models may rely more on the enhanced permeability and retention (EPR) effect than ligand-

receptor mediated targeting to deliver their drug.⁶¹ Relevant tumor models that provide more representative results for translation into the clinic should be encouraged.

We initiated radiotherapy studies with 4T1 tumors and found that a single dose of 9 or 18 MBq of ¹⁷⁷Lu-FAP5-IP-DOTA was sufficient to suppress tumor growth after 2 weeks without major side effects (see Fig. 2.5). We then investigated the radiotherapeutic effects of ¹⁷⁷Lu-FAP5-IP-DOTA in several human tumor xenograft models (see Fig. 2.6). After several weeks, we observed significant suppression of tumor growth in all models. Slight weight loss, followed by recovery, was also observed within the first week post injection. This is likely due to the low but enduring kidney retention observed in both our SPECT/CT and biodistribution studies. Survival was extended in all treatment groups compared to the controls. It should be noted that the U87MG cell line does express FAP α directly on the cancer cells. However, U87MG cells do not express significantly more FAP α receptors compared to CAFs,²⁰ and the therapeutic benefits observed were not seemingly different compared to the FAP α tumor models 4T1, KB, or HT29. Furthermore, FAP5-IP-DOTA showed discernible radiotoxic effects on the tumor, but not healthy tissues (see Fig. 2.7). A blinded evaluation of various sections of the myocardium, liver, and kidneys from randomly selected control and treated mice displayed no discernible toxic lesions resulting from the therapy nor any other significant morphological differences (see Table 2.1). While hepatic extramedullary hematopoiesis (EMH) was observed in certain mice, it is expected. Increased circulating neutrophils were also observed in certain mice, though no necrosis was noted. Future studies with a complete blood count (CBC) will be required to determine the cause.

Table 2.1. Summary of histopathology of necropsy tissues from ¹⁷⁷Lu-FAP5-IP-DOTA radiotherapy studies. # Examined refers to total number of sections examined from multiple mice. DL = Diagnostic Lesions.

Species	Group	Organ	# Examined	DL
Balb/c	Control (n = 4)	Liver	22	0
		R. Kidney	16	0
		L. Kidney	16	0
		Myocardium	16	0
	Treated (n = 4)	Liver	24	0
		R. Kidney	16	0
		L. Kidney	16	0
		Myocardium	16	0
Athymic nu/nu	Control (n = 2)	Liver	8	0
		R. Kidney	8	0
		L. Kidney	8	0
		Myocardium	8	0
	Treated (n = 7)	Liver	38	0
		R. Kidney	28	0
		L. Kidney	28	0
		Myocardium	28	0

While attaching an albumin-binder attachment to our FAP α radioligand resulted in increased tumor uptake and retention, further optimization is required. The most critical need to address will be investigating methods to increase the therapeutic effect of FAP-targeted radioligands. While FAP α is highly specific for tumor tissue, there are potential concerns regarding the receptor count, as well as the internalization and recycling kinetics. Christiansen et. al estimated ~117,000 FAP α cell-surface receptors per fibroblast based on their enzymatic activity assays with the WI38 cell line, and our FACS analysis indicates a similar level of FAP expression between the WI38 human embryonic lung fibroblast cell line and the Hs894 human CAF cell line (see Fig. 2.1).⁴⁶ Fischer et. al showed that ~5 hours was necessary to internalize 80% of cell-surface FAP α upon binding with a FAP internalizing antibody, and over 60 hours passed before ~90% FAP cell-surface expression was restored.¹⁴ These FAP α attributes are significantly inferior compared to other receptors such as FR and PSMA, and will require creative solutions to maximize tumor uptake and retention.⁶²⁻⁶⁴

Based on the apparent lack of toxicity of ¹⁷⁷Lu-FAP5-IP-DOTA, tumor radiotherapy results could be readily improved by using higher doses, multiple doses, and/or more potent isotopes such as ⁹⁰Y or ²²⁵Ac.^{56, 65, 66} Another facile method for increasing therapeutic potency would be combining ¹⁷⁷Lu-FAP5-IP-DOTA radiotherapy with chemo- or immunotherapy.⁶⁷⁻⁷⁴ Structural

modifications to enhance FAP radioligand internalization and/or retention should be explored. Finally, the low yet persistent renal retention of radioactivity needs to be addressed. Protection of the kidneys may be achieved through the administration of high amounts of lysine and/or arginine, plasma expanders, or diuretics to elevate the rate of urination.⁷⁵⁻⁸²

2.6 Conclusion

In this study, we synthesized a novel FAP α targeted ligand with an albumin-binding domain for radioactive theranostics using 4-(*p*-iodophenyl)butyric acid. The albumin-binder was the driving force in improving the pharmacokinetics of the FAP α radioligand, which resulted in increased tumor uptake and retention. This effect provided for SPECT/CT scans with higher tumor-to-background contrast, more favorable biodistribution, and enhanced tumor therapy in both mouse and human tumor models. The results are encouraging, and further research is warranted for the development of FAP α -targeted radioligands with albumin-binding moieties to provide better radiotheranostic options to cancer patients.

2.7 References

1. Garin-Chesa, P.; Old, L. J.; Rettig, W. J., Cell surface glycoprotein of reactive stromal fibroblasts as a potential antibody target in human epithelial cancers. *Proceedings of the National Academy of Sciences* **1990**, *87* (18), 7235-7239.
2. Kratochwil, C.; Flechsig, P.; Lindner, T.; Abderrahim, L.; Altmann, A.; Mier, W.; Adeberg, S.; Rathke, H.; Röhrich, M.; Winter, H.; Plinkert, P. K.; Marme, F.; Lang, M.; Kauczor, H.-U.; Jäger, D.; Debus, J.; Haberkorn, U.; Giesel, F. L., 68Ga-FAPI PET/CT: Tracer Uptake in 28 Different Kinds of Cancer. *Journal of Nuclear Medicine* **2019**, *60* (6), 801-805.
3. Brennen, W. N.; Isaacs, J. T.; Denmeade, S. R., Rationale Behind Targeting Fibroblast Activation Protein-Expressing Carcinoma-Associated Fibroblasts as a Novel Chemotherapeutic Strategy. *Molecular Cancer Therapeutics* **2012**, *11* (2), 257.
4. Keane, F. M.; Yao, T.-W.; Seelk, S.; Gall, M. G.; Chowdhury, S.; Poplawski, S. E.; Lai, J. H.; Li, Y.; Wu, W.; Farrell, P.; Vieira de Ribeiro, A. J.; Osborne, B.; Yu, D. M. T.; Seth, D.; Rahman, K.; Haber, P.; Topaloglu, A. K.; Wang, C.; Thomson, S.; Hennessy, A.; Prins, J.; Twigg, S. M.; McLennan, S. V.; McCaughan, G. W.; Bachovchin, W. W.; Gorrell, M. D., Quantitation of fibroblast activation protein (FAP)-specific protease activity in mouse, baboon and human fluids and organs. *FEBS Open Bio* **2014**, *4*, 43-54.

5. Fang, J.; Xiao, L.; Joo, K.-I.; Liu, Y.; Zhang, C.; Liu, S.; Conti, P. S.; Li, Z.; Wang, P., A potent immunotoxin targeting fibroblast activation protein for treatment of breast cancer in mice. *International Journal of Cancer* **2016**, *138* (4), 1013-1023.
6. Scott, A. M.; Wiseman, G.; Welt, S.; Adjei, A.; Lee, F.-T.; Hopkins, W.; Divgi, C. R.; Hanson, L. H.; Mitchell, P.; Gansen, D. N.; Larson, S. M.; Ingle, J. N.; Hoffman, E. W.; Tanswell, P.; Ritter, G.; Cohen, L. S.; Bette, P.; Arvay, L.; Amelsberg, A.; Vlock, D.; Rettig, W. J.; Old, L. J., A Phase I Dose-Escalation Study of Sibrotuzumab in Patients with Advanced or Metastatic Fibroblast Activation Protein-positive Cancer. *Clinical Cancer Research* **2003**, *9* (5), 1639.
7. LeBeau, A. M.; Brennen, W. N.; Aggarwal, S.; Denmeade, S. R., Targeting the cancer stroma with a fibroblast activation protein-activated promelittin protoxin. *Molecular Cancer Therapeutics* **2009**, *8* (5), 1378.
8. Peng, X.-H.; Chen, S.-F.; Xu, C.-H.; Zheng, B.-Y.; Ke, M.-R.; Huang, J.-D., Synthesis, Spectroscopic and Fibroblast Activation Protein (FAP)-Responsive Properties of Phthalocyanine-Doxorubicin Conjugates. *ChemistrySelect* **2018**, *3* (19), 5405-5411.
9. Brennen, W. N.; Rosen, D. M.; Wang, H.; Isaacs, J. T.; Denmeade, S. R., Targeting Carcinoma-Associated Fibroblasts Within the Tumor Stroma With a Fibroblast Activation Protein-Activated Prodrug. *JNCI: Journal of the National Cancer Institute* **2012**, *104* (17), 1320-1334.
10. Santos, A. M.; Jung, J.; Aziz, N.; Kissil, J. L.; Puré, E., Targeting fibroblast activation protein inhibits tumor stromagenesis and growth in mice. *The Journal of Clinical Investigation* **2009**, *119* (12), 3613-3625.
11. Lindner, T.; Loktev, A.; Altmann, A.; Giesel, F.; Kratochwil, C.; Debus, J.; Jäger, D.; Mier, W.; Haberkorn, U., Development of Quinoline-Based Theranostic Ligands for the Targeting of Fibroblast Activation Protein. *Journal of Nuclear Medicine* **2018**, *59* (9), 1415-1422.
12. Tsionou, M. I.; Knapp, C. E.; Foley, C. A.; Munteanu, C. R.; Cakebread, A.; Imberti, C.; Eykyn, T. R.; Young, J. D.; Paterson, B. M.; Blower, P. J.; Ma, M. T., Comparison of macrocyclic and acyclic chelators for gallium-68 radiolabelling. *RSC Adv* **2017**, *7* (78), 49586-49599.
13. Li, J.; Chen, K.; Liu, H.; Cheng, K.; Yang, M.; Zhang, J.; Cheng, J. D.; Zhang, Y.; Cheng, Z., Activatable Near-Infrared Fluorescent Probe for In Vivo Imaging of Fibroblast Activation Protein- α . *Bioconjugate Chemistry* **2012**, *23* (8), 1704-1711.
14. Fischer, E.; Chaitanya, K.; Wüest, T.; Wadle, A.; Scott, A. M.; van den Broek, M.; Schibli, R.; Bauer, S.; Renner, C., Radioimmunotherapy of Fibroblast Activation Protein Positive Tumors by Rapidly Internalizing Antibodies. *Clinical Cancer Research* **2012**, *18* (22), 6208-6218.

15. Welt, S.; Divgi, C. R.; Scott, A. M.; Garin-Chesa, P.; Finn, R. D.; Graham, M.; Carswell, E. A.; Cohen, A.; Larson, S. M.; Old, L. J., Antibody targeting in metastatic colon cancer: a phase I study of monoclonal antibody F19 against a cell-surface protein of reactive tumor stromal fibroblasts. *Journal of Clinical Oncology* **1994**, *12* (6), 1193-1203.
16. Meletta, R.; Müller Herde, A.; Chiotellis, A.; Isa, M.; Rancic, Z.; Borel, N.; Ametamey, S. M.; Krämer, S. D.; Schibli, R., Evaluation of the Radiolabeled Boronic Acid-Based FAP Inhibitor MIP-1232 for Atherosclerotic Plaque Imaging. *Molecules* **2015**, *20* (2).
17. Roy, J.; Hettiarachchi, S. U.; Kaake, M.; Mukkamala, R.; Low, P. S., Design and validation of fibroblast activation protein alpha targeted imaging and therapeutic agents. *Theranostics* **2020**, *10* (13), 5778-5789.
18. Dohi, O.; Ohtani, H.; Hatori, M.; Sato, E.; Hosaka, M.; Nagura, H.; Itoi, E.; Kokubun, S., Histogenesis-specific expression of fibroblast activation protein and dipeptidylpeptidase-IV in human bone and soft tissue tumours. *Histopathology* **2009**, *55* (4), 432-440.
19. Huber, M. A.; Schubert, R. D.; Peter, R. U.; Kraut, N.; Park, J. E.; Rettig, W. J.; Garin-Chesa, P., Fibroblast Activation Protein: Differential Expression and Serine Protease Activity in Reactive Stromal Fibroblasts of Melanocytic Skin Tumors. *Journal of Investigative Dermatology* **2003**, *120* (2), 182-188.
20. Kakarla, S.; Chow, K. K. H.; Mata, M.; Shaffer, D. R.; Song, X.-T.; Wu, M.-F.; Liu, H.; Wang, L. L.; Rowley, D. R.; Pfizenmaier, K.; Gottschalk, S., Antitumor Effects of Chimeric Receptor Engineered Human T Cells Directed to Tumor Stroma. *Molecular Therapy* **2013**, *21* (8), 1611-1620.
21. Loktev, A.; Lindner, T.; Burger, E.-M.; Altmann, A.; Giesel, F.; Kratochwil, C.; Debus, J.; Marmé, F.; Jäger, D.; Mier, W.; Haberkorn, U., Development of Fibroblast Activation Protein-Targeted Radiotracers with Improved Tumor Retention. *Journal of Nuclear Medicine* **2019**, *60* (10), 1421-1429.
22. Moon, E. S.; Elvas, F.; Vliegen, G.; De Lombaerde, S.; Vangestel, C.; De Bruycker, S.; Bracke, A.; Eppard, E.; Greifenstein, L.; Klasen, B.; Kramer, V.; Staelens, S.; De Meester, I.; Van der Veken, P.; Rösch, F., Targeting fibroblast activation protein (FAP): next generation PET radiotracers using squaramide coupled bifunctional DOTA and DATA5m chelators. *EJNMMI Radiopharmacy and Chemistry* **2020**, *5* (1), 19.
23. Dennis, M. S.; Zhang, M.; Meng, Y. G.; Kadkhodayan, M.; Kirchofer, D.; Combs, D.; Damico, L. A., Albumin Binding as a General Strategy for Improving the Pharmacokinetics of Proteins*. *Journal of Biological Chemistry* **2002**, *277* (38), 35035-35043.
24. Dumelin, C. E.; Trüssel, S.; Buller, F.; Trachsel, E.; Bootz, F.; Zhang, Y.; Mannocci, L.; Beck, S. C.; Drumea-Mirancea, M.; Seeliger, M. W.; Baltes, C.; Müggler, T.; Kranz, F.; Rudin, M.; Melkko, S.; Scheuermann, J.; Neri, D., A Portable Albumin Binder from a DNA-Encoded Chemical Library. *Angewandte Chemie International Edition* **2008**, *47* (17), 3196-3201.

25. Kelly, J. M.; Jeitner, T. M.; Ponnala, S.; Williams, C.; Nikolopoulou, A.; DiMagno, S. G.; Babich, J. W., A Trifunctional Theranostic Ligand Targeting Fibroblast Activation Protein- α (FAP α). *Molecular Imaging and Biology* **2021**.
26. Müller, C.; Struthers, H.; Winiger, C.; Zhernosekov, K.; Schibli, R., DOTA Conjugate with an Albumin-Binding Entity Enables the First Folic Acid-Targeted ^{177}Lu -Radionuclide Tumor Therapy in Mice. *Journal of Nuclear Medicine* **2013**, *54* (1), 124-131.
27. Farkas, R.; Siwowska, K.; Ametamey, S. M.; Schibli, R.; van der Meulen, N. P.; Müller, C., ^{64}Cu - and ^{68}Ga -Based PET Imaging of Folate Receptor-Positive Tumors: Development and Evaluation of an Albumin-Binding NODAGA-Folate. *Molecular Pharmaceutics* **2016**, *13* (6), 1979-1987.
28. Radford, L. L.; Fernandez, S.; Beacham, R.; El Sayed, R.; Farkas, R.; Benešová, M.; Müller, C.; Lapi, S. E., New ^{55}Co -labeled Albumin-Binding Folate Derivatives as Potential PET Agents for Folate Receptor Imaging. *Pharmaceutics* **2019**, *12* (4).
29. Wen, X.; Shi, C.; Yang, L.; Zeng, X.; Lin, X.; Huang, J.; Li, Y.; Zhuang, R.; Zhu, H.; Guo, Z.; Zhang, X., A radioiodinated FR- β -targeted tracer with improved pharmacokinetics through modification with an albumin binder for imaging of macrophages in AS and NAFL. *European Journal of Nuclear Medicine and Molecular Imaging* **2021**.
30. Kuo, H.-T.; Merkens, H.; Zhang, Z.; Uribe, C. F.; Lau, J.; Zhang, C.; Colpo, N.; Lin, K.-S.; Bénard, F., Enhancing Treatment Efficacy of ^{177}Lu -PSMA-617 with the Conjugation of an Albumin-Binding Motif: Preclinical Dosimetry and Endoradiotherapy Studies. *Molecular Pharmaceutics* **2018**, *15* (11), 5183-5191.
31. Nakashima, K.; Iikuni, S.; Watanabe, H.; Ono, M., Development of a novel radiotheranostic platform with a DOTA-based trifunctional chelating agent. *Chemical Communications* **2021**.
32. Iikuni, S.; Okada, Y.; Shimizu, Y.; Watanabe, H.; Ono, M., Modulation of the Pharmacokinetics of a Radioligand Targeting Carbonic Anhydrase-IX with Albumin-Binding Moieties. *Molecular Pharmaceutics* **2021**.
33. Trüssel, S.; Dumelin, C.; Frey, K.; Villa, A.; Buller, F.; Neri, D., New Strategy for the Extension of the Serum Half-Life of Antibody Fragments. *Bioconjugate Chemistry* **2009**, *20* (12), 2286-2292.
34. Schniering, J.; Borgna, F.; Siwowska, K.; Benešová, M.; Cohrs, S.; Hasler, R.; van der Meulen, N. P.; Maurer, B.; Schibli, R.; Müller, C., In Vivo Labeling of Plasma Proteins for Imaging of Enhanced Vascular Permeability in the Lungs. *Molecular Pharmaceutics* **2018**, *15* (11), 4995-5004.
35. Wen, X.; Shi, C.; Xu, D.; Zhang, P.; Li, Z.; Li, J.; Su, X.; Zhuang, R.; Liu, T.; Guo, Z.; Zhang, X., Radioiodinated Portable Albumin Binder as a Versatile Agent for in Vivo Imaging with Single-Photon Emission Computed Tomography. *Molecular Pharmaceutics* **2019**, *16* (2), 816-824.

36. Moon, E. S.; Elvas, F.; Vliegen, G.; Lombaerde, S. D.; Vangestel, C.; Bruycker, S. D.; Bracke, A.; Eppart, E.; Greifenstein, L.; Klasen, B.; Krmaer, V.; Staelens, S.; Deester, I. D.; Veken, P. V. d.; Roesch, F., Targeting fibroblast activation protein (FAP): next generation PET radiotracers using squaramide coupled bifunctional DOTA and DATA5m chelators. **2020**.
37. Poplawski, S. E.; Lai, J. H.; Li, Y.; Jin, Z.; Liu, Y.; Wu, W.; Wu, Y.; Zhou, Y.; Sudmeier, J. L.; Sanford, D. G.; Bachovchin, W. W., Identification of Selective and Potent Inhibitors of Fibroblast Activation Protein and Prolyl Oligopeptidase. *Journal of Medicinal Chemistry* **2013**, *56* (9), 3467-3477.
38. Jansen, K.; Heirbaut, L.; Verkerk, R.; Cheng, J. D.; Joossens, J.; Cos, P.; Maes, L.; Lambeir, A.-M.; De Meester, I.; Augustyns, K.; Van der Veken, P., Extended Structure–Activity Relationship and Pharmacokinetic Investigation of (4-Quinolinoyl)glycyl-2-cyanopyrrolidine Inhibitors of Fibroblast Activation Protein (FAP). *Journal of Medicinal Chemistry* **2014**, *57* (7), 3053-3074.
39. Tsai, T.-Y.; Yeh, T.-K.; Chen, X.; Hsu, T.; Jao, Y.-C.; Huang, C.-H.; Song, J.-S.; Huang, Y.-C.; Chien, C.-H.; Chiu, J.-H.; Yen, S.-C.; Tang, H.-K.; Chao, Y.-S.; Jiaang, W.-T., Substituted 4-Carboxymethylpyroglutamic Acid Diamides as Potent and Selective Inhibitors of Fibroblast Activation Protein. *Journal of Medicinal Chemistry* **2010**, *53* (18), 6572-6583.
40. Liao, D.; Luo, Y.; Markowitz, D.; Xiang, R.; Reisfeld, R. A., Cancer Associated Fibroblasts Promote Tumor Growth and Metastasis by Modulating the Tumor Immune Microenvironment in a 4T1 Murine Breast Cancer Model. *PLoS ONE* **2009**, *4* (11), e7965.
41. Lee, J.; Fassnacht, M.; Nair, S.; Boczkowski, D.; Gilboa, E., Tumor Immunotherapy Targeting Fibroblast Activation Protein, a Product Expressed in Tumor-Associated Fibroblasts. *Cancer research* **2005**, *65* (23), 11156-11163.
42. Loktev, A.; Lindner, T.; Mier, W.; Debus, J.; Altmann, A.; Jäger, D.; Giesel, F.; Kratochwil, C.; Barthe, P.; Roumestand, C.; Haberkorn, U., A Tumor-Imaging Method Targeting Cancer-Associated Fibroblasts. *Journal of Nuclear Medicine* **2018**, *59* (9), 1423-1429.
43. Chen, H.; Zhao, L.; Ruan, D.; Pang, Y.; Hao, B.; Dai, Y.; Wu, X.; Guo, W.; Fan, C.; Wu, J.; Huang, W.; Lin, Q.; Sun, L.; Wu, H., Usefulness of [68Ga]Ga-DOTA-FAPI-04 PET/CT in patients presenting with inconclusive [18F]FDG PET/CT findings. *European Journal of Nuclear Medicine and Molecular Imaging* **2020**.
44. Fu, W.; Liu, L.; Liu, H.; Zhou, Z.; Chen, Y., Increased FAPI Uptake in Brain Metastasis From Lung Cancer on 68Ga-FAPI PET/CT. *Clinical nuclear medicine* **2021**, *46* (1), e1-e2.
45. Slania, S. L.; Das, D.; Lisok, A.; Du, Y.; Jiang, Z.; Mease, R. C.; Rowe, S. P.; Nimmagadda, S.; Yang, X.; Pomper, M. G., Imaging of Fibroblast Activation Protein in Cancer Xenografts Using Novel (4-Quinolinoyl)-glycyl-2-cyanopyrrolidine-Based Small Molecules. *Journal of Medicinal Chemistry* **2021**, *64* (7), 4059-4070.

46. Christiansen, V. J.; Jackson, K. W.; Lee, K. N.; Downs, T. D.; McKee, P. A., Targeting Inhibition of Fibroblast Activation Protein- α and Prolyl Oligopeptidase Activities on Cells Common to Metastatic Tumor Microenvironments. *Neoplasia* **2013**, *15* (4), 348-358.
47. Zhang, B.; Liu, F.; Yang, M.-F.; Xu, J.; Wang, Z.; Zhang, J.; Wang, R.; Yang, X., A cell-based fluorescent assay for FAP inhibitor discovery. *Bioorganic & Medicinal Chemistry Letters* **2020**, *30* (14), 127253.
48. Hettiarachchi, S. U.; Li, Y.-H.; Roy, J.; Zhang, F.; Puchulu-Campanella, E.; Lindeman, S. D.; Srinivasarao, M.; Tsoyi, K.; Liang, X.; Ayaub, E. A.; Nickerson-Nutter, C.; Rosas, I. O.; Low, P. S., Targeted inhibition of PI3 kinase/mTOR specifically in fibrotic lung fibroblasts suppresses pulmonary fibrosis in experimental models. *Science Translational Medicine* **2020**, *12* (567), eaay3724.
49. Eskew, M. W.; Benight, A. S., Evaluation of Drug/Ligand Binding Constants for Human Serum Albumin Using Differential Scanning Calorimetry. *bioRxiv* **2021**, 2021.01.22.427858.
50. Tian, R.; Zeng, Q.; Zhu, S.; Lau, J.; Chandra, S.; Ertsey, R.; Hettie, K. S.; Teraphongphom, T.; Hu, Z.; Niu, G.; Kiesewetter, D. O.; Sun, H.; Zhang, X.; Antaris, A. L.; Brooks, B. R.; Chen, X., Albumin-chaperoned cyanine dye yields superbright NIR-II fluorophore with enhanced pharmacokinetics. *Science Advances* **2019**, *5* (9), eaaw0672.
51. Chen, Q.; Liu, Z., Albumin Carriers for Cancer Theranostics: A Conventional Platform with New Promise. *Advanced Materials* **2016**, *28* (47), 10557-10566.
52. Chen, Q.; Liang, C.; Wang, C.; Liu, Z., An Imagable and Photothermal “Abraxane-Like” Nanodrug for Combination Cancer Therapy to Treat Subcutaneous and Metastatic Breast Tumors. *Advanced Materials* **2015**, *27* (5), 903-910.
53. Khan, M. N.; Goel, S., Binding study of different drugs with serum albumins.
54. Usama, S. M.; Thapaliya, E. R.; Luciano, M. P.; Schnermann, M. J., Not so innocent: Impact of fluorophore chemistry on the in vivo properties of bioconjugates. *Current Opinion in Chemical Biology* **2021**, *63*, 38-45.
55. Zboralski, D.; Osterkamp, F.; Simmons, A.; Bredenbeck, A.; Schumann, A.; Paschke, M.; Beindorff, N.; Mohan, A.; Nguyen, M.; Xiao, J., 571P Preclinical evaluation of FAP-2286, a peptide-targeted radionuclide therapy (PRT) to fibroblast activation protein alpha (FAP). *Annals of Oncology* **2020**, *31*, S488.
56. Watabe, T.; Liu, Y.; Kaneda-Nakashima, K.; Shirakami, Y.; Lindner, T.; Ooe, K.; Toyoshima, A.; Nagata, K.; Shimosegawa, E.; Haberkorn, U.; Kratochwil, C.; Shinohara, A.; Giesel, F.; Hatazawa, J., Theranostics Targeting Fibroblast Activation Protein in the Tumor Stroma: ^{64}Cu - and ^{225}Ac -Labeled FAPI-04 in Pancreatic Cancer Xenograft Mouse Models. *Journal of Nuclear Medicine* **2020**, *61* (4), 563-569.

57. Moreno-Ruiz, P.; Corvigno, S.; te Grootenhuis, N. C.; La Fleur, L.; Backman, M.; Strell, C.; Mezheyeuski, A.; Hoelzlwimmer, G.; Klein, C.; Botling, J.; Micke, P.; Östman, A., Stromal FAP is an independent poor prognosis marker in non-small cell lung adenocarcinoma and associated with p53 mutation. *Lung Cancer* **2021**.
58. Chen, L.; Qin, Y.; Zhang, T.; Ding, N.; Chen, Y.; Zhang, Z.; Guo, C., Clinical significance of cancer-associated fibroblasts and their correlation with microvessel and lymphatic vessel density in lung adenocarcinoma. *J Clin Lab Anal* **2019**, *33* (4), e22832-e22832.
59. Jia-Jia, L.; Chia-Pao, C.; Jia-Yu, L.; Feng-Ting, H.; chiun-wei, H., Development and preclinical evaluation of [⁶⁸Ga]Ga-Alb-FAPtp-01, a novel tumour-associated fibroblast activation protein tracer for PET imaging of xenograft glioma. *Research Square* **2021**.
60. Ito, H.; Kutuki, S.; Nishiguchi, I.; Shigematsu, N.; Kuribayashi, T.; Uematsu, M.; Nakayama, T.; Ka, W.-J.; Takemasa, K.; Ando, Y.; Kubo, A., Radiotherapy for cervical cancer with high-dose rate brachytherapy — correlation between tumor size, dose and failure. *Radiotherapy and Oncology* **1994**, *31* (3), 240-247.
61. Natfji, A. A.; Ravishankar, D.; Osborn, H. M. I.; Greco, F., Parameters Affecting the Enhanced Permeability and Retention Effect: The Need for Patient Selection. *Journal of Pharmaceutical Sciences* **2017**, *106* (11), 3179-3187.
62. Srinivasarao, M.; Galliford, C. V.; Low, P. S., Principles in the design of ligand-targeted cancer therapeutics and imaging agents. *Nat Rev Drug Discov* **2015**, *14* (3), 203-19.
63. Taylor, R. M.; Severns, V.; Brown, D. C.; Bisoffi, M.; Sillerud, L. O., Prostate cancer targeting motifs: Expression of $\alpha\beta 3$, neurotensin receptor 1, prostate specific membrane antigen, and prostate stem cell antigen in human prostate cancer cell lines and xenografts. *The Prostate* **2012**, *72* (5), 523-532.
64. Liu, T.; Wu, L. Y.; Kazak, M.; Berkman, C. E., Cell-Surface labeling and internalization by a fluorescent inhibitor of prostate-specific membrane antigen. *The Prostate* **2008**, *68* (9), 955-964.
65. Wang, Z.; Tian, R.; Niu, G.; Ma, Y.; Lang, L.; Szajek, L. P.; Kiesewetter, D. O.; Jacobson, O.; Chen, X., Single Low-Dose Injection of Evans Blue Modified PSMA-617 Radioligand Therapy Eliminates Prostate-Specific Membrane Antigen Positive Tumors. *Bioconjugate Chemistry* **2018**, *29* (9), 3213-3221.
66. Chen, H.; Jacobson, O.; Niu, G.; Weiss, I. D.; Kiesewetter, D. O.; Liu, Y.; Ma, Y.; Wu, H.; Chen, X., Novel “Add-On” Molecule Based on Evans Blue Confers Superior Pharmacokinetics and Transforms Drugs to Theranostic Agents. *Journal of Nuclear Medicine* **2017**, *58* (4), 590-597.
67. Gordon Steel, G.; Peckham, M. J., Exploitable mechanisms in combined radiotherapy-chemotherapy: The concept of additivity. *International Journal of Radiation Oncology*Biophysics* **1979**, *5* (1), 85-91.

68. Le Chevalier, T.; Arriagada, R.; Quoix, E.; Ruffle, P.; Martin, M.; Tarayre, M.; Marie-José, L.-T.; Douillard, J.-Y.; Laplanche, A., Radiotherapy Alone Versus Combined Chemotherapy and Radiotherapy in Nonresectable Non-Small-Cell Lung Cancer: First Analysis of a Randomized Trial in 353 Patients. *JNCI: Journal of the National Cancer Institute* **1991**, *83* (6), 417-423.
69. Herskovic, A.; Martz, K.; Al-Sarraf, M.; Leichman, L.; Brindle, J.; Vaitkevicius, V.; Cooper, J.; Byhardt, R.; Davis, L.; Emami, B., Combined chemotherapy and radiotherapy compared with radiotherapy alone in patients with cancer of the esophagus. *New England Journal of Medicine* **1992**, *326* (24), 1593-1598.
70. Chin, V.; Nagrial, A.; Sjoquist, K.; O'Connor, C. A.; Chantrill, L.; Biankin, A. V.; Scholten, R.; Yip, D., Chemotherapy and radiotherapy for advanced pancreatic cancer. *Cochrane Database of Systematic Reviews* **2018**, (3).
71. Reynders, K.; Illidge, T.; Siva, S.; Chang, J. Y.; De Ruyscher, D., The abscopal effect of local radiotherapy: using immunotherapy to make a rare event clinically relevant. *Cancer Treat Rev* **2015**, *41* (6), 503-510.
72. Vanpouille-Box, C.; Diamond, J. M.; Pilonis, K. A.; Zavadil, J.; Babb, J. S.; Formenti, S. C.; Barcellos-Hoff, M. H.; Demaria, S., TGF β Is a Master Regulator of Radiation Therapy-Induced Antitumor Immunity. *Cancer research* **2015**, *75* (11), 2232-2242.
73. Sharma, P.; Wagner, K.; Wolchok, J. D.; Allison, J. P., Novel cancer immunotherapy agents with survival benefit: recent successes and next steps. *Nature Reviews Cancer* **2011**, *11* (11), 805-812.
74. Ganesh, K.; Massagué, J., TGF- β Inhibition and Immunotherapy: Checkmate. *Immunity* **2018**, *48* (4), 626-628.
75. de Jong, M.; Rolleman, E. J.; Bernard, B. F.; Visser, T. J.; Bakker, W. H.; Breeman, W. A.; Krenning, E. P., Inhibition of renal uptake of indium-111-DTPA-octreotide in vivo. *Journal of Nuclear Medicine* **1996**, *37* (8), 1388-1392.
76. Kobayashi, H.; Yoo, T. M.; Kim, I. S.; Kim, M.-K.; Le, N.; Webber, K. O.; Pastan, I.; Paik, C. H.; Eckelman, W. C.; Carrasquillo, J. A., L-Lysine Effectively Blocks Renal Uptake of ¹²⁵I- or ^{99m}Tc-labeled Anti-Tac Disulfide-stabilized Fv Fragment. *Cancer research* **1996**, *56* (16), 3788-3795.
77. Rolleman, E. J.; Valkema, R.; de Jong, M.; Kooij, P. P.; Krenning, E. P., Safe and effective inhibition of renal uptake of radiolabelled octreotide by a combination of lysine and arginine. *European Journal of Nuclear Medicine and Molecular Imaging* **2003**, *30* (1), 9-15.
78. Verwijnen, S. M.; Krenning, E. P.; Valkema, R.; Huijmans, J. G. M.; de Jong, M., Oral Versus Intravenous Administration of Lysine: Equal Effectiveness in Reduction of Renal Uptake of [¹¹¹In-DTPA] Octreotide. *Journal of Nuclear Medicine* **2005**, *46* (12), 2057.

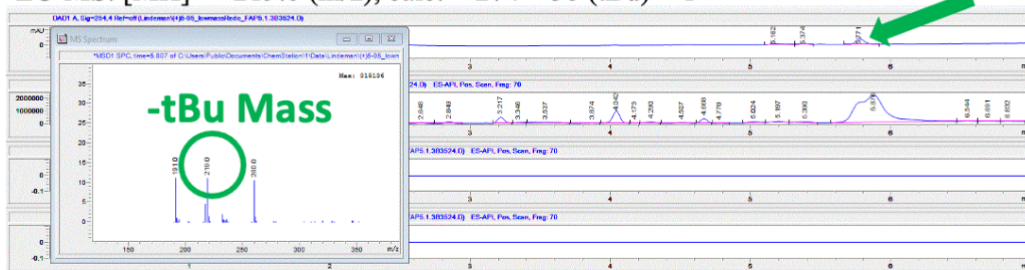
79. Lin, Y.-C.; Hung, G.-U.; Luo, T.-Y.; Tsai, S.-C.; Sun, S.-S.; Hsia, C.-C.; Chen, S.-L.; Lin, W.-Y., Reducing renal uptake of ^{111}In -DOTATOC: A comparison among various basic amino acids. *Annals of Nuclear Medicine* **2007**, *21* (1), 79.
80. Rolleman, E. J.; Melis, M.; Valkema, R.; Boerman, O. C.; Krenning, E. P.; de Jong, M., Kidney protection during peptide receptor radionuclide therapy with somatostatin analogues. *European Journal of Nuclear Medicine and Molecular Imaging* **2010**, *37* (5), 1018-1031.
81. Kristiansson, A.; Ahlstedt, J.; Holmqvist, B.; Brinte, A.; Tran, T. A.; Forssell-Aronsson, E.; Strand, S.-E.; Gram, M.; Åkerström, B., Protection of Kidney Function with Human Antioxidation Protein α 1-Microglobulin in a Mouse ^{177}Lu -DOTATATE Radiation Therapy Model. *Antioxidants & Redox Signaling* **2018**, *30* (14), 1746-1759.
82. Osterkamp, F.; Zboralski, D.; Schneider, E.; Haase, C.; Paschke, M.; Höhne, A.; Ungewiss, J.; Smerling, C.; Reineke, U.; Bredenbeck, A. Compounds Comprising A Fibroblast Activation Protein Ligand and Use Thereof. 2021.

2.8 Appendix A. Supplemental Information

Additional data further supporting our results are provided below.

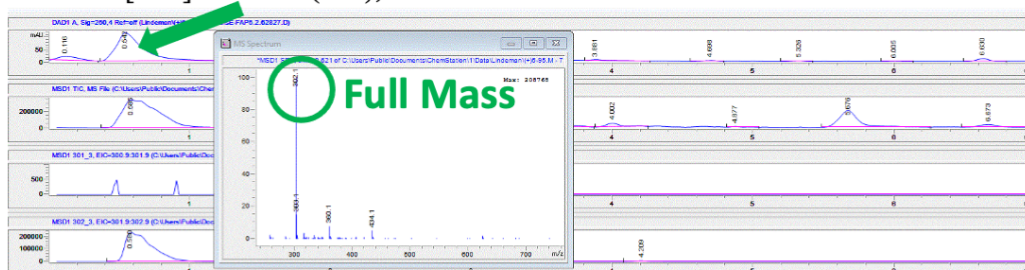
FAP5 Final Intermediate 1 (Fragment 1)

LC-MS: $[MH]^+ = 219.0$ (m/z), calc. = $274 - 56$ (tBu) + 1



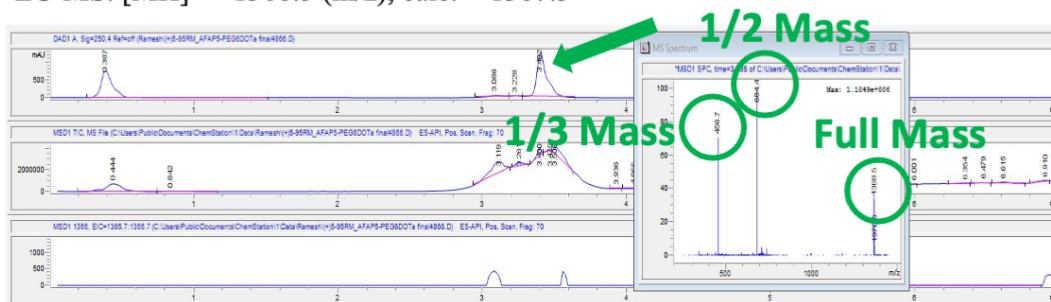
FAP5 Final Intermediate (Fragment 2)

LC-MS: $[MH]^+ = 302.1$ (m/z), calc. = 301.3



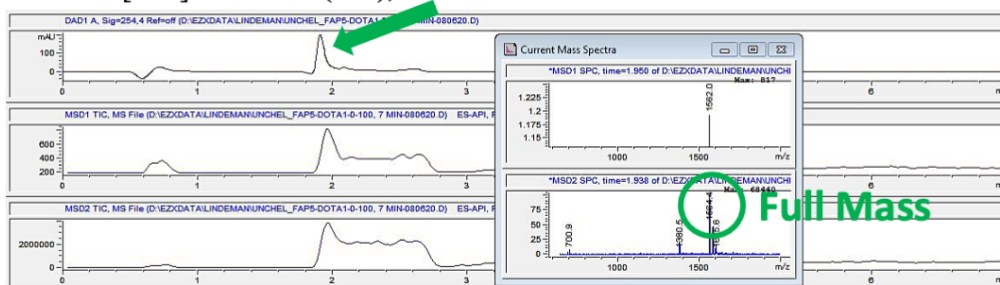
FAP5-DOTA

LC-MS: $[MH]^+ = 1368.5$ (m/z), calc. = 1367.5



FAP5-IP-DOTA

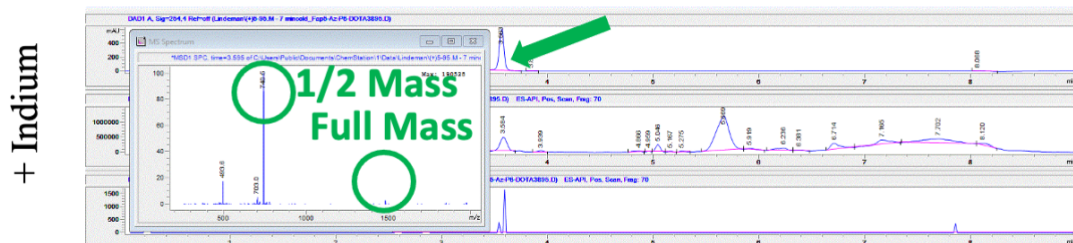
LC-MS: $[MH]^+ = 1563.4$ (m/z), calc. = 1562.6



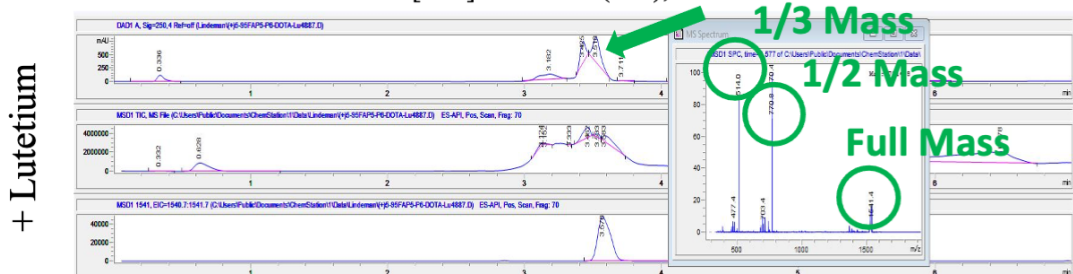
Supplemental Figure S2.1: LC/MS characterization of final products of Schemes 2.1-4.

FAP5-DOTA

^{nat}In -FAP5-DOTA. LC-MS: $[\text{MH}]^+ = 740.5$ (m/z), calc. = $1367.5 - 3 + 114.8 = 1479.3$

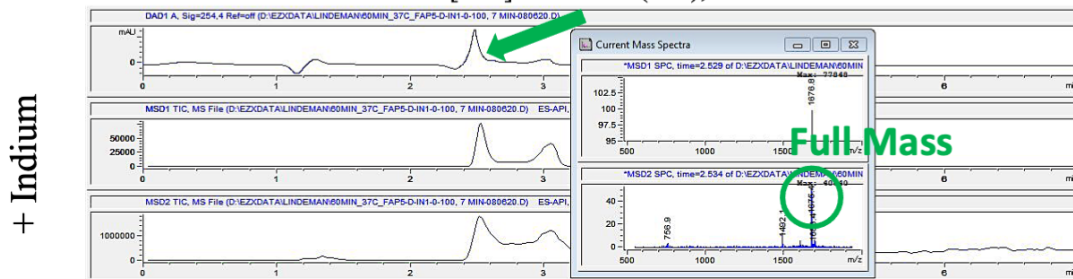


^{nat}Lu -FAP5-DOTA. LC-MS: $[\text{MH}]^+ = 1541.4$ (m/z), calc. = $1367.5 - 3 + 175.0 = 1539.5$

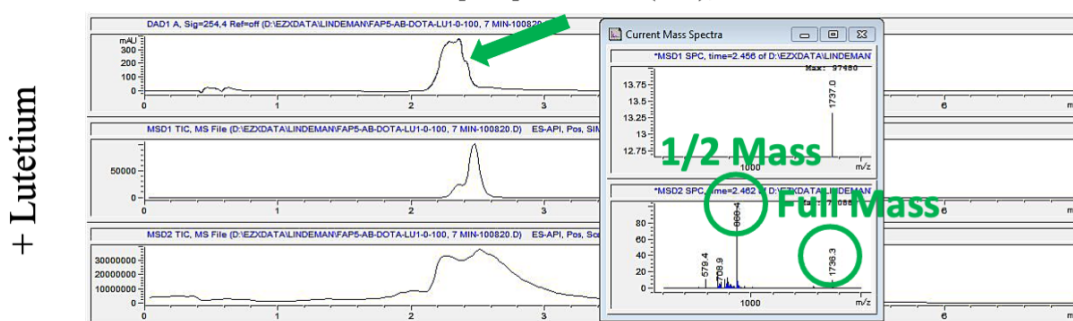


FAP5-IP-DOTA

^{nat}In -FAP5-IP-DOTA. LC-MS: $[\text{MH}]^+ = 1675.4$ (m/z), calc. = $1562.6 - 3 + 114.8 = 1674.4$

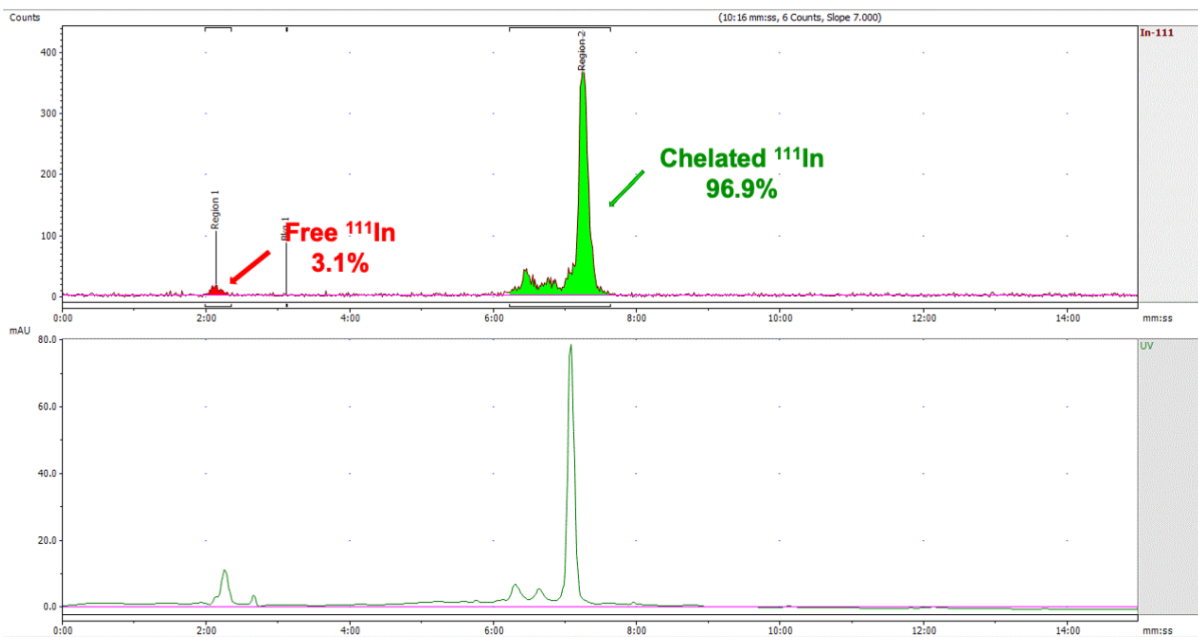


^{nat}Lu -FAP5-IP-DOTA. LC-MS: $[\text{MH}]^+ = 1736.3$ (m/z), calc. = $1562.6 - 3 + 175.0 = 1734.6$

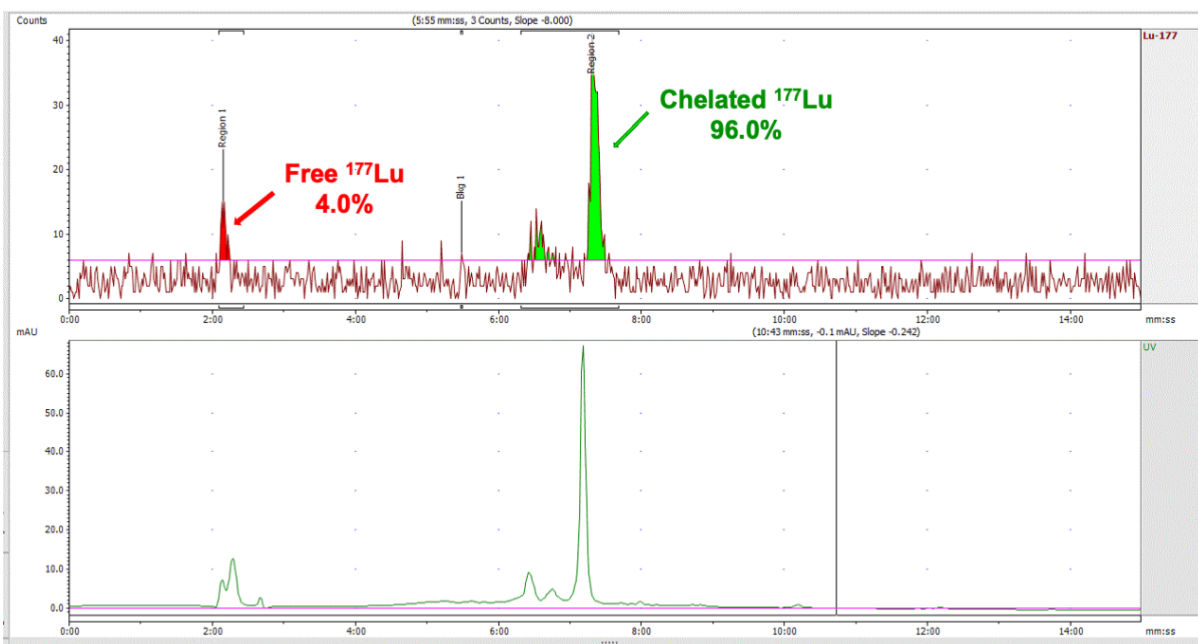


Supplemental Figure S2.2: LC/MS analysis of cold chelations with FAP5-DOTA conjugates.

^{111}In -FAP5-DOTA

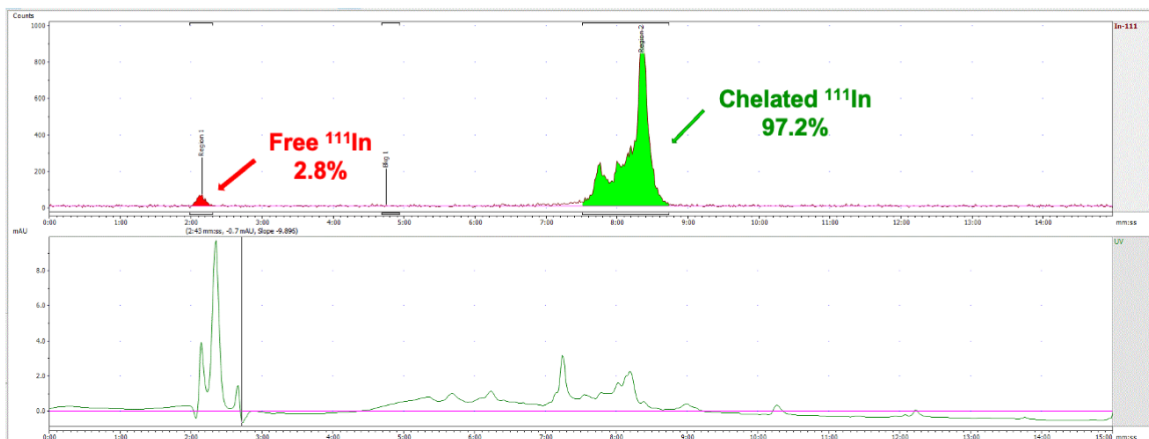


^{177}Lu -FAP5-DOTA

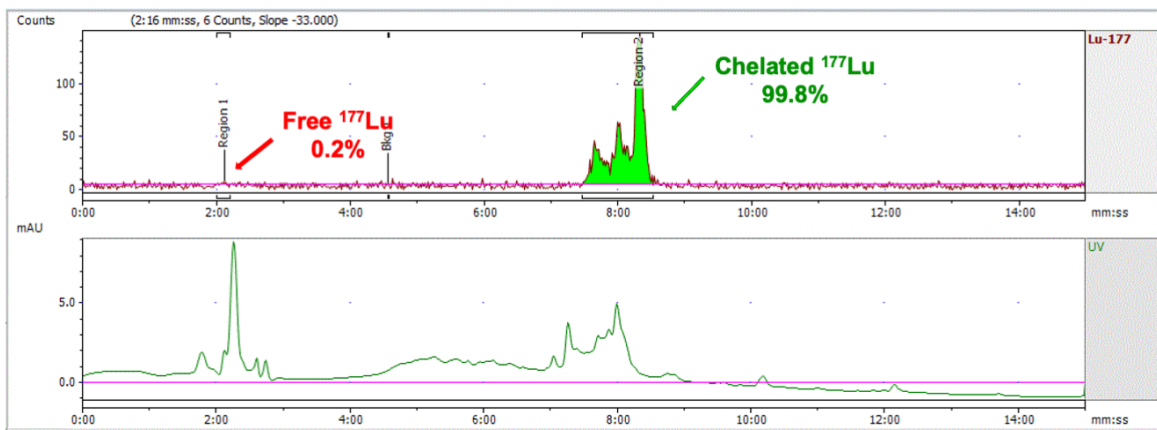


Supplemental Figure S2.3: Representative radiochromatograms of FAP5-DOTA radiolabeled with either indium-111 or lutetium-177.

^{111}In -FAP5-IP-DOTA

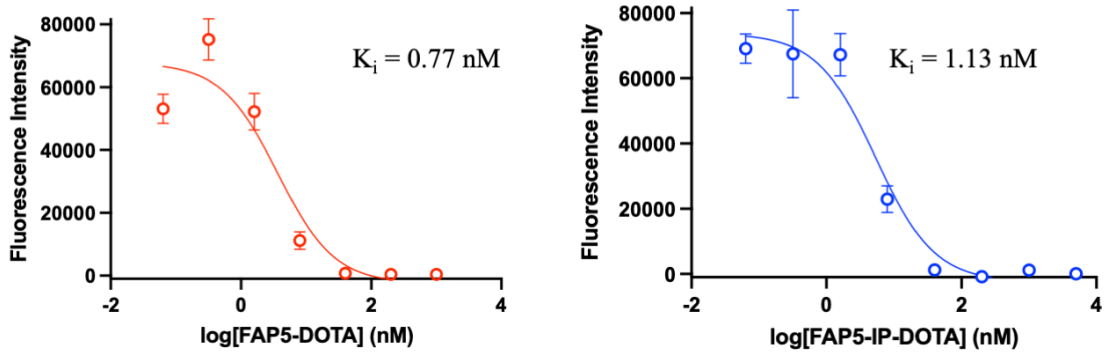


^{177}Lu -FAP5-IP-DOTA

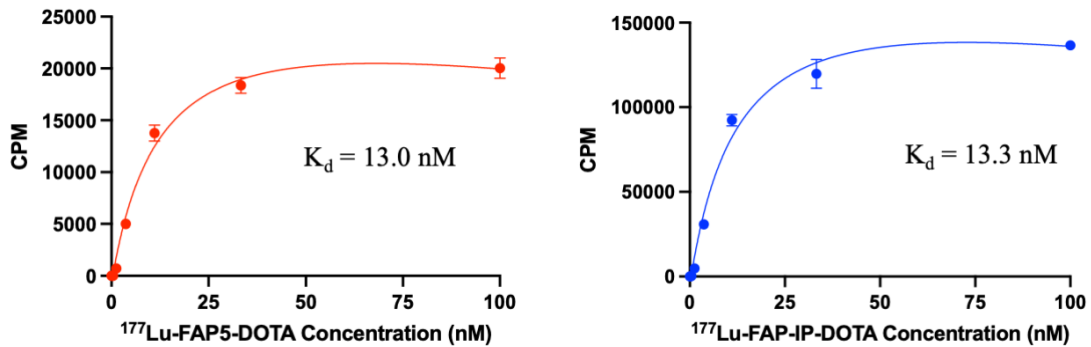


Supplemental Figure S2.4: Representative radiochromatograms of FAP5-IP-DOTA radiolabeled with either indium-111 or lutetium-177.

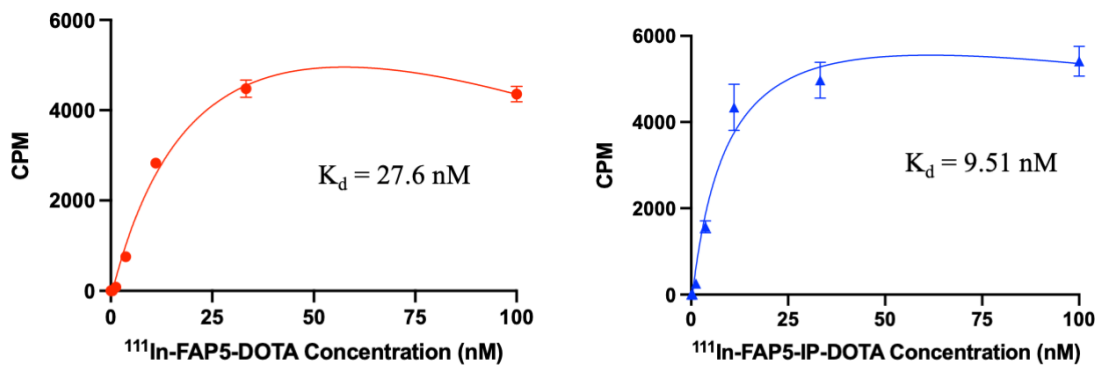
Displacement Assays with HEK-hFAP cells



Binding Curves with HEK-hFAP Cells

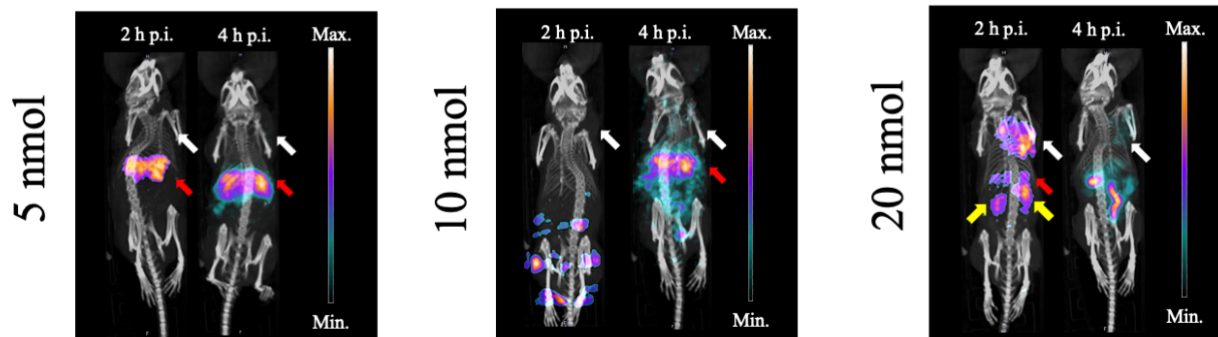


Binding Curves with HT1080-hFAP Cells

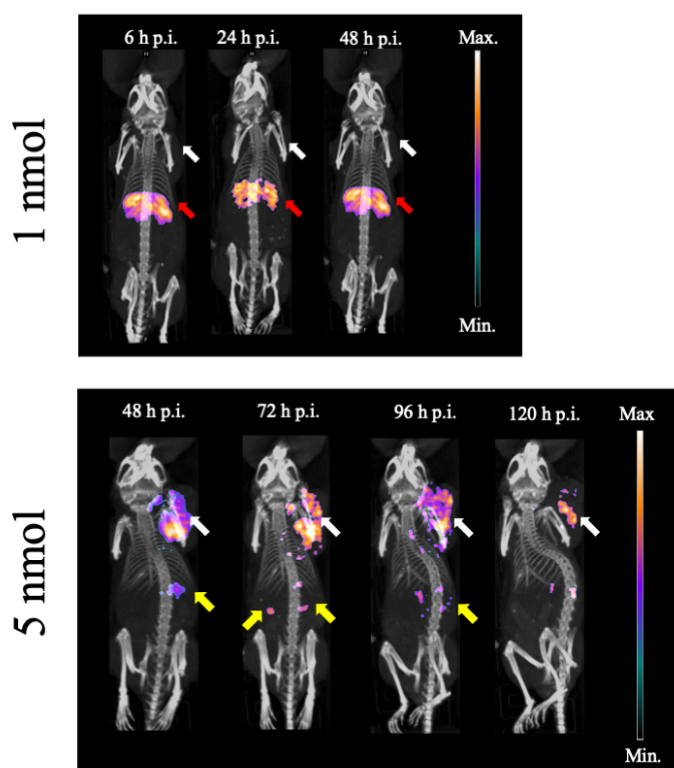


Supplemental Figure S2.5. FAP5-DOTA and FAP5-IP-DOTA were incubated with HEK-hFAP cells at increasing concentrations to displace a constant concentration of FAP5-Rhodamine conjugate. FAP5-DOTA and FAP5-IP-DOTA were radiolabeled with either Lu-177 or In-111 and incubated with HEK-hFAP or HT1080-hFAP at increasing concentrations to generate total binding curves. All samples were performed in triplicate.

SPECT/CT of ^{111}In -FAP5-DOTA

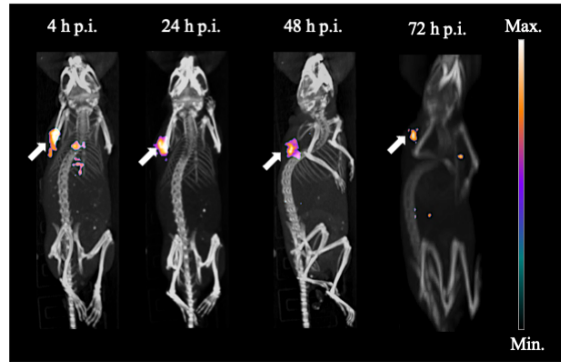


SPECT/CT of ^{111}In -FAP5-IP-DOTA

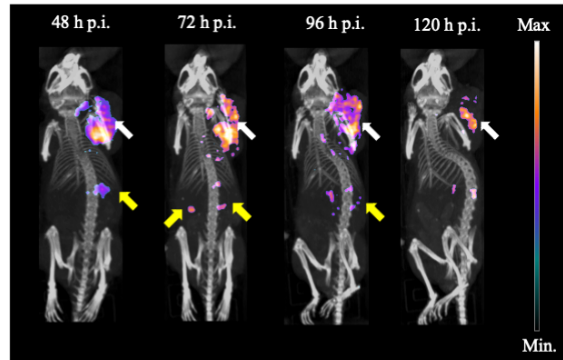


Supplemental Figure S2.6. Dosing studies of FAP5-DOTA conjugates in HT29 tumor xenografts. White arrows indicate tumor. Red arrows indicate liver. Yellow arrows indicate kidneys.

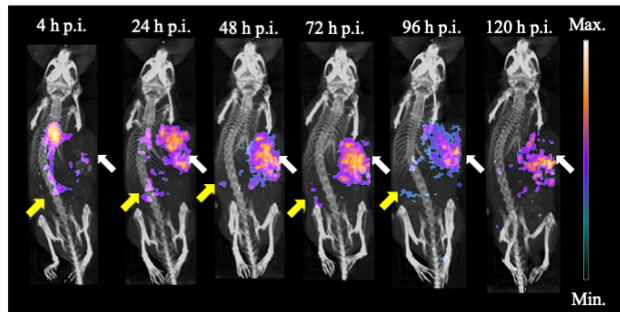
^{177}Lu -FAP5-IP-DOTA therapy in 4T1 tumor



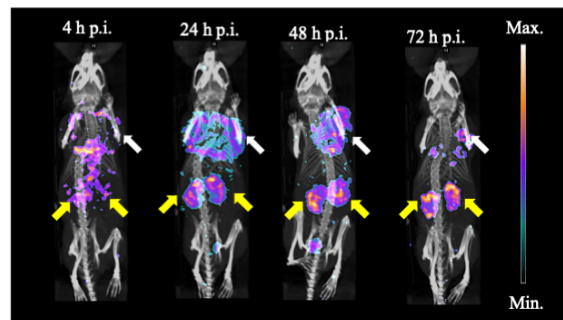
^{111}In -FAP5-IP-DOTA SPECT/CT in HT29 tumor



^{111}In -FAP5-IP-DOTA SPECT/CT in KB tumor

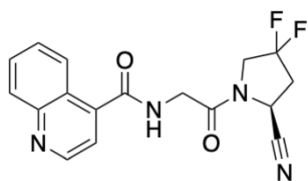


^{111}In -FAP5-IP-DOTA SPECT/CT in U87MG tumor



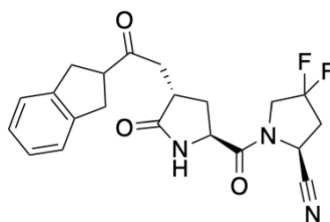
Supplemental Figure S2.7. Additional SPECT/CT scans with FAP5-IP-DOTA. White arrows indicate tumor. Yellow arrows indicate kidneys.

FAPI-04



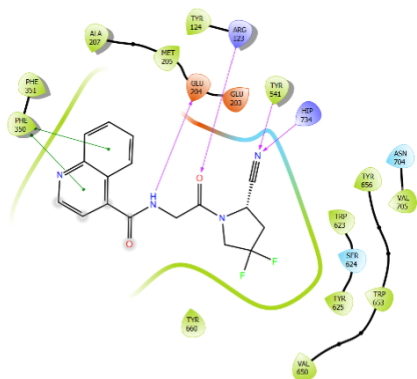
Reported $K_d = 3.2$ nM

FAP5

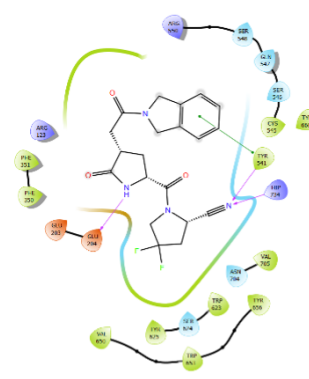


Reported $K_d = 22$ nM

Induced Fit Docking

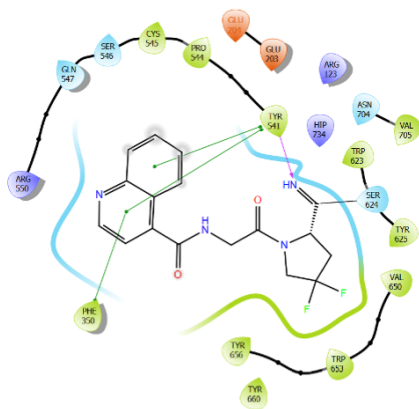


Docking Score = -8.5 kcal/mol

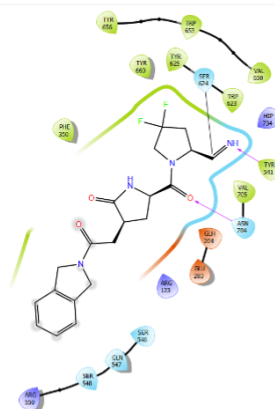


Docking Score = -8.2 kcal/mol

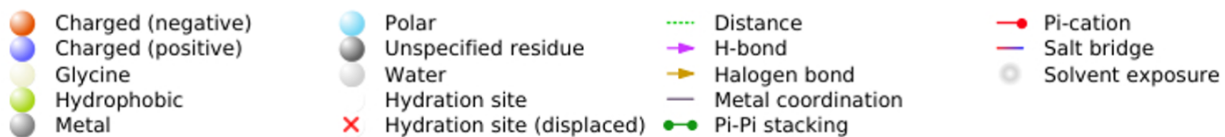
Covalent Docking



Docking Score = -7.3 kcal/mol



Docking Score = -7.2 kcal/mol



Supplemental Figure S2.8. *In silico* comparison of FAPI-04 vs. FAP5 docking to FAP protein.

CHAPTER 3. PRECLINICAL INVESTIGATION OF THERANOSTIC FIBROBLAST ACTIVATION PROTEIN RADIOLIGANDS: FURTHER OPTIMIZATIONS

3.1 Abstract

Fibroblast activation protein alpha (FAP α) is an excellent oncological target due to its selective expression on activated fibroblasts such as cancer-associated fibroblasts (CAFs) and nearly nonexistent expression in healthy tissues. Like other stromal cells, CAFs consistently accumulate in and play a key role in the development of a wide variety of tumors. We previously reported a safe and effective FAP-targeted radioligand for imaging and therapy, but further improvements are warranted. Structural modifications to the ligand and/or linker are a vital strategy for enhancing radiotheranostic results. More aggressive dosing strategies are also possible due to the low toxicity of FAP5-IP-DOTA. In this study we explore a variety of approaches for improving the radiotheranostic results of the FAP5 radioligand. We report key insights into the optimization of FAP5 radiotherapy based via structural modifications and dosing regimens.

3.2 Introduction

Fibroblast activation protein (FAP) is an ideal target for cancer due to the near ubiquitous expression in cancerous tissue and coinciding lack of expression in healthy tissues.¹⁻⁴ Cancer associated fibroblasts (CAFs) are manipulated by tumor cells to secrete growth factors, promote angiogenesis, release immunosuppressive agents, and produce extracellular matrix (ECM) proteins that act as a physical barrier against immune cells and antibodies.⁵⁻¹⁰ Increased FAP expression and CAF differentiation are negative prognostic markers for patient survival.¹¹⁻¹⁵

Research into optimizing FAP-targeting ligands for radiotheranostics is ongoing, primarily with linker modifications but also recently with albumin-binder attachments.¹⁶⁻¹⁹ We previously demonstrated a novel, 4-carboxymethylpyroglutamic acid diamide-based structure, FAP5, was an effective FAP ligand. Though the FAP5 ligand is quite potent *in vitro*, we found that an albumin-binding moiety was pharmacokinetically expedient for desirable *in vivo* targeting. The FAP5-IP-DOTA conjugate showed high tumor uptake, long-term retention, and negligible toxicity when radiolabeled with the beta-emitting radionuclide lutetium-177. However, maximizing tumor

uptake and retention are essential for ideal radiotherapeutic results, and further investigation to optimize these desired attributes are merited.

In this study, we explore a variety of structural and procedural modifications to further improve the radiotheranostic results with FAP5. We began with rational structural modifications to the FAP5 ligand, the linker, and spacer based on the literature.²⁰⁻²⁵ We investigated additional albumin-binder moieties based on recent reports.²⁶⁻²⁹ We co-injected an amino acid solution to further improve the biodistribution of FAP5-IP-DOTA.³⁰⁻³⁵ Finally, we explored several more aggressive dosing regimens with ¹⁷⁷Lu-FAP5-IP-DOTA.

3.3 Materials and Methods

Materials were purchased from the same vendors as reported previously (2.3.1). Syntheses, purifications, and characterizations were performed with procedures analogous to what we have reported previously (2.3.2, 2.3.3). Cell culture (2.3.5), radiolabelings (2.3.7), computational docking (2.3.8), cell binding assays (2.3.9), animal husbandry (2.3.10), tumor implantations (2.3.11), radioimaging (2.3.12), radiotherapy (2.3.14), and statistical analyses (2.3.15) were all performed as previously reported. Some noteworthy distinctions are detailed below.

3.3.1 Materials

Rhodamine NHS ester was purchased from Thermo Fisher Scientific (Waltham, MA). Additional PEG linkers were purchased from BroadPharm. NOTA-NHS ester was purchased from CheMatech (Dijon, France). 4-(*p*-fluorophenyl)butyric acid was purchased from A2B (San Diego, CA). 2-(*p*-chlorophenyl)butyric acid was purchased from AK Scientific (Union City, CA). Fmoc-Lys-OtBu was purchased from ChemImpex (Wood Dale, IL). L-Lysine monohydrochloride was purchased from Millipore Sigma (St. Louis, MO).

3.3.2 Chelation

FAP5-NOTA conjugates were diluted with ammonium acetate (0.5 M, pH 8.0) to reach a final conjugate concentration of 0.5 mM. Cold chelations were performed by adding natural copper in a dilute HCl solution in excess, agitated for 30 minutes, then analyzed using LC/MS. The mobile phase consisted of a 20 mM ammonium acetate aqueous buffer (pH 7) (A) and acetonitrile (B) with a linear gradient from 5% B to 95% B over 15 minutes.

3.3.3 Formulation

Sodium ascorbate (100 mg/mL) and L-methionine (5 mg/mL) were freshly dissolved in a 5% EtOH in PBS solution just prior to dilution. Conjugates were diluted to the correct concentration upon confirmation of successful radiolabeling via radio-HPLC analysis. Further radio-HPLC analysis over a one-week period at room temperature showed the presence of radiolytic stabilizers allowed the conjugate to maintain radiochemical purity.

3.3.4 Amino Acid Solution Administration

An amino acid solution was made with 30 mg of L-Lysine per 200 μ L of PBS. Mice were injected intraperitoneally with 30 mg of L-Lysine within 5 minutes of intravenous tail-vein injection of the radioconjugate, either pre- or post-injection.

3.3.5 Radiotherapy

4T1 tumors were grown to approximately 200 mm³ (n = 5 per group). All mice were randomly divided into control or treatment groups prior to the initiation of the therapy studies. Mice received a single intravenous dose of formulation buffer alone or with 5 nmol of FAP5-IP-DOTA radiolabeled with ~50 MBq of lutetium-177 via the tail vein on day 0. One group of mice received a second intravenous dose of 5 nmol of FAP5-IP-DOTA radiolabeled with ~22 MBq of lutetium-177 via the tail vein on day 3. All mice were administered a dose of amino acid solution with each radioactive injection. Tumors were measured in two perpendicular directions every other day during therapy, and their volumes were calculated as $0.5 \times L \times W^2$, where L is the longest axis (in millimeters), and W is the axis perpendicular to L (in millimeters). Humane endpoint criteria were defined as weight loss of more than 20% of the initial body weight, a tumor volume of more than 1,800 mm³, or open ulceration. Mice were euthanized on reaching one of the predefined endpoint criteria.

3.3.6 NIR Imaging

Fluorescence imaging and biodistribution was performed with a Caliper IVIS Luminal II. 4T1 tumors were treated for approximately 3.5 weeks before conducting NIR dye scans. Each mouse was injected intravenously via tail vein with 10 nmol of FAP5-S0456. Mice (n = 2 per

group) were anesthetized with 3% isoflurane in oxygen and whole-body images were taken at 3 hours post-injection. Imaging acquisition parameters were: Lamp Level = high; Excitation = 745 nm; Emission = 810 nm; Binning (M) = 4M; F-stop = 4; FOV = 12.5; Acquisition time \leq 5 seconds.

3.3.7 Murine pulmonary fibrosis model

Pulmonary fibrosis was induced in C57BL/6 mice as reported previously.^{36,37} Radiolabeling, SPECT/CT scans, and image processing were performed using the same procedures as in the tumor model.

3.4 Results

3.4.1 *In vitro* Evaluation of Binding of FAP5 Ligand Analogs

A mono-fluoro analog of FAP5 was synthesized for comparison to our FAP5 ligand, based on the original report of similar or even slightly improved binding to FAP α .²⁰ The two were compared by incubating increasing concentrations of either analog with a constant concentration of FAP5-Rhodamine in HEK-FAP cells. The results are provided in Figure 3.1. Our difluoro-FAP5 ligand demonstrated \sim 20x better binding to FAP than the mono-fluoro analog, with inhibitory constants of 0.37 nM and 8.65 nM respectively.

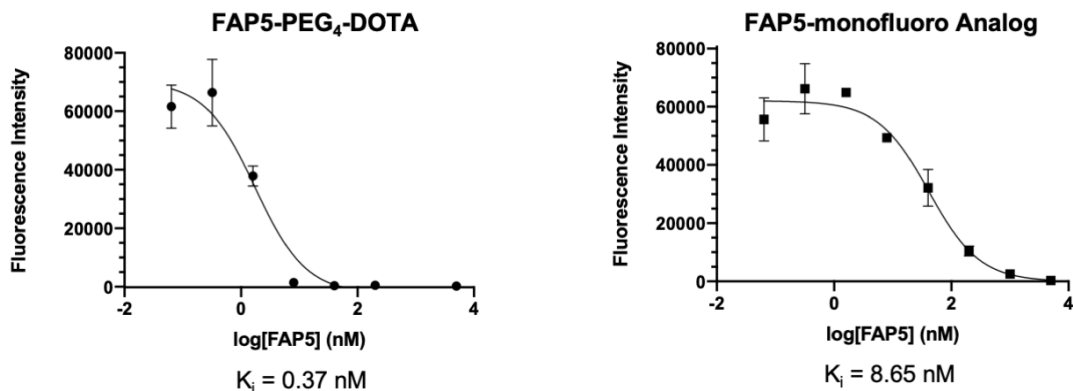
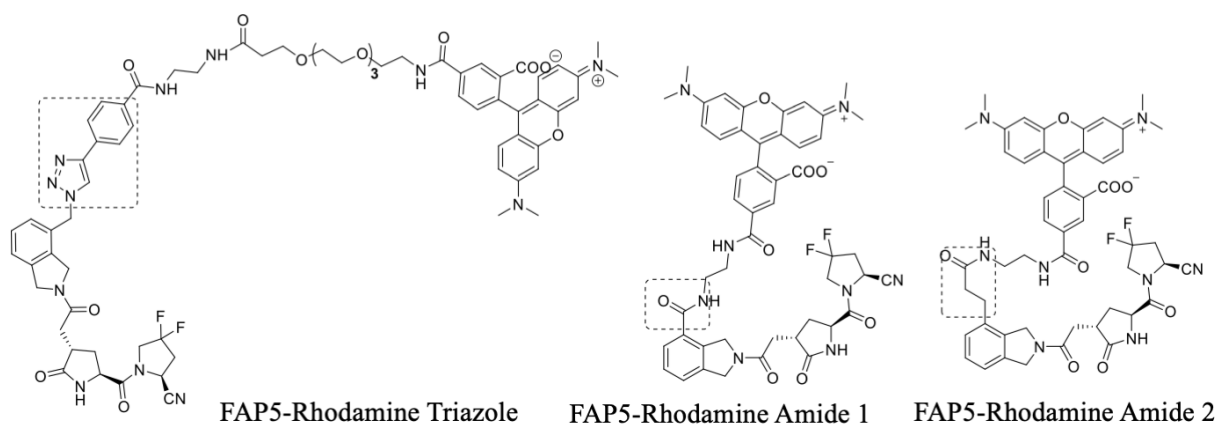


Figure 3.1. Evaluation of binding of FAP5 ligand analogs. A consistent concentration of FAP5-Rhodamine was incubated with HEK-FAP cells and increasing concentrations of either FAP5-PEG₄-DOTA or a FAP5-monofluoro analog. All samples were performed in triplicate.

3.4.2 *In vitro* Evaluation of FAP5 Ligand Binding with Modified Linkers

Several FAP5-Rhodamine conjugates with different linkers were synthesized. A triazole linker was compared to two amide linkers of different lengths via binding curves in HEK-FAP cells. The final structures and binding curves are provided in Figure 3.2. The triazole-phenyl linker conjugate demonstrated a binding affinity of 1.4 nM, while both amide linker conjugates showed binding affinities above 10 nM (12.1 and 10.8 nM respectively).

FAP5-Rhodamine Modified Linkers



Binding Curves

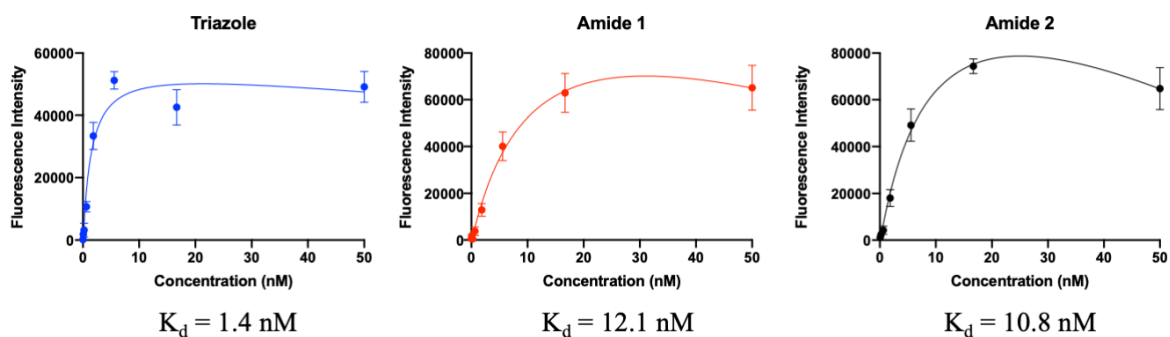


Figure 3.2. Evaluation of FAP5 ligand binding with modified linkers. A phenyl-triazole linker was compared with two different amide linkers as shown in the structures above. Binding studies were performed, where each conjugate was incubated with HEK-FAP cells in increasing concentrations. All three conjugates were tested in parallel. All samples were performed in triplicate.

3.4.3 *In vitro* Evaluation of FAP5-DOTA Conjugates with Different Spacer Lengths

Several FAP5-DOTA conjugates with different spacer lengths were next synthesized to investigate the influence of the spacer on the binding of FAP5. Polyethylene glycol (PEG) spacers with 4, 6, and 12 units were evaluated. Binding to FAP was determined in HEK-FAP cells by displacing a constant concentration of FAP5-Rhodamine with increasing concentrations of FAP5-PEG₄-DOTA, FAP5-PEG₆-DOTA, or FAP5-PEG₁₂-DOTA. The results of the displacement assay are provided in Figure 3.3. While FAP5 maintained inhibitory binding constants of less than 1 nM with a PEG₄ or PEG₆ spacer (0.37 nM and 0.77 nM respectively), a PEG₁₂ spacer caused a severe reduction in FAP binding affinity (>200,000 nM).

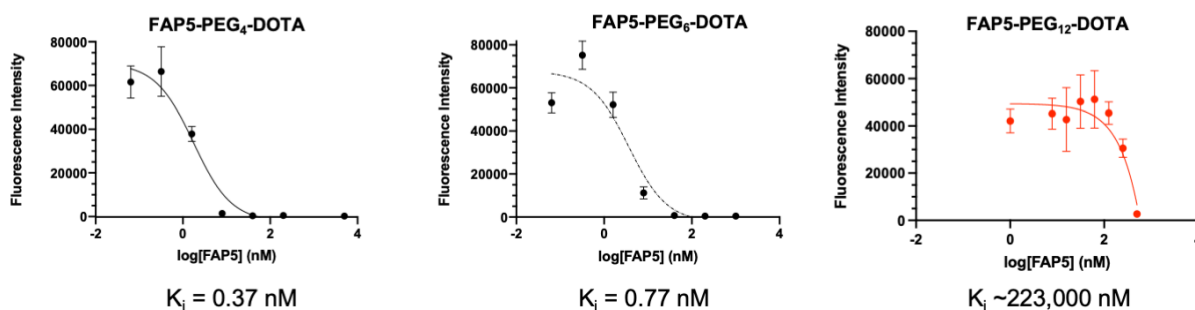
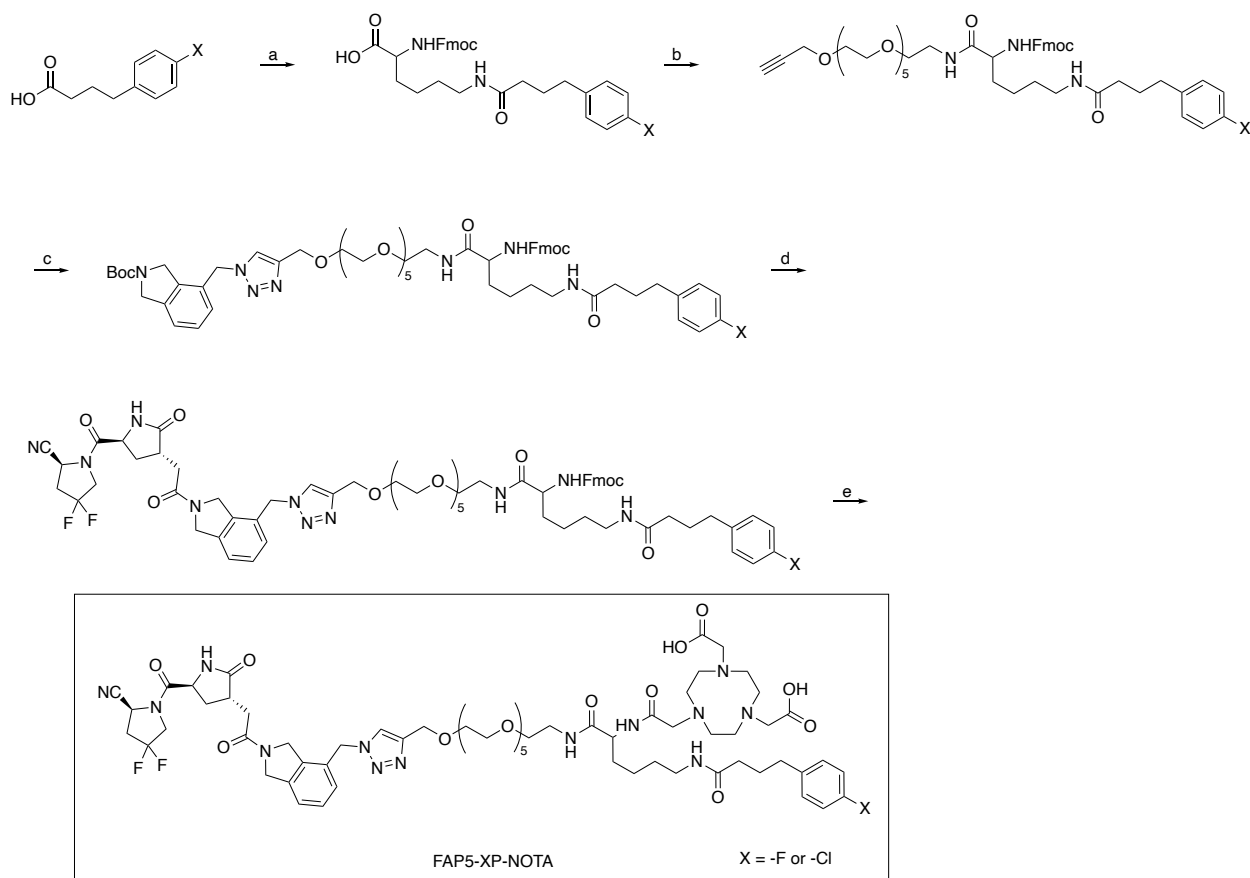


Figure 3.3. Evaluation of FAP5-DOTA conjugates with different lengths of PEG spacer. A consistent concentration of FAP5-Rhodamine was incubated with HEK-FAP cells and increasing concentrations of FAP5-PEG₄-DOTA, FAP5-PEG₆-DOTA, or FAP5-PEG₁₂-DOTA. All samples were performed in triplicate.

3.4.4 Synthesis and Evaluation of FAP5-NOTA Conjugates with Alternative Phenyl-based Albumin Binders

Based on previous reports, we synthesized several FAP5-NOTA conjugates with alternative substituents at *para* position of phenyl-butyric acid.^{26, 27} Faster tumor uptake and clearance from healthy tissues are ideal pharmacokinetics for radiodiagnostics. PET radionuclides such as F-18, Ga-68, and Cu-64 are generally preferred to SPECT radionuclides, and NOTA is a more suitable chelator for these specific isotopes.^{38, 39} The synthesis for these conjugates is provided in Scheme 3.1. LC/MS characterization of final conjugates and cold chelation with natural copper are provided in Supplementary Figure S3.1.



Scheme 3.1. Synthesis of FAP5-XP-NOTA. Reagents and conditions: (a) Fmoc-Lys-OH, HATU, DIPEA, DMF, rt, 3h; (b) Propargyl-PEG₆-NH₂, HATU, DIPEA, DMF, rt, 3h; (c) Fragment 1, CuI, DIPEA, DMF, 55°C, 5h; (d) i. TFA, ACN, 0°C-rt, 1h; ii. Fragment 2, HATU, DIPEA, DMF, rt, 3h; (e) i. Et₂NH, DCM, rt, 1h; ii. NHS-ester NOTA, DMF, rt, 12h.

The conjugates were evaluated *in vitro* by displacement assay. HEK-FAP cells were incubated with a constant concentration of FAP5-Rhodamine and increasing concentrations of either FAP5-FP-NOTA or FAP5-CP-NOTA. The results are provided in Figure 3.4. Both conjugates displaced high affinity for FAP, with inhibitory constants of 0.90 nM and 2.3 nM respectively.

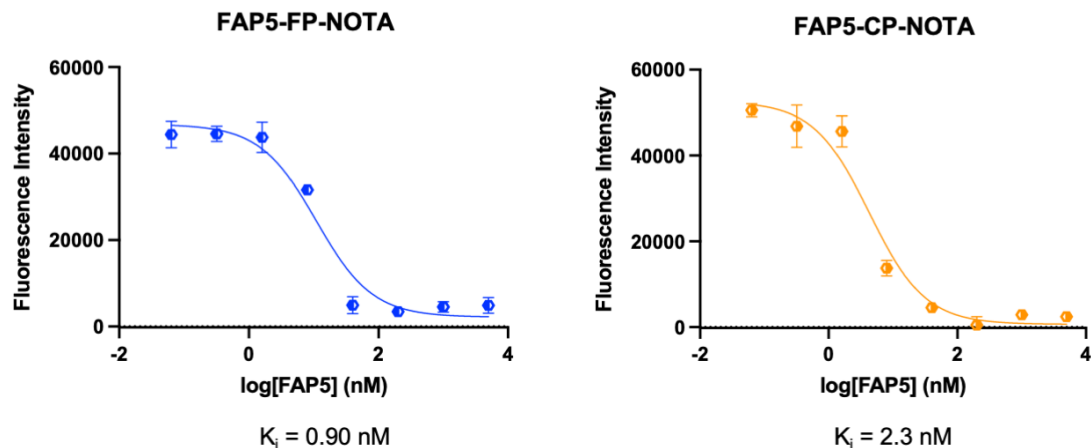
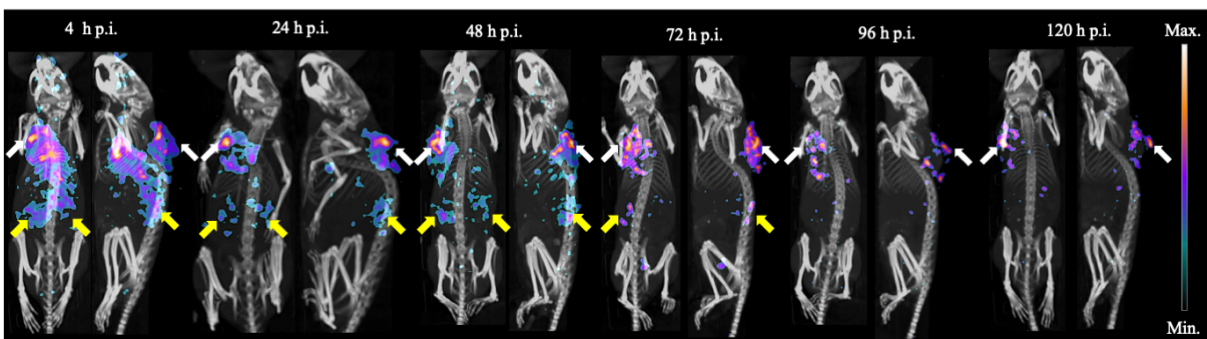


Figure 3.4. Evaluation of FAP5-XP-NOTA conjugates with alternative albumin-binders. A consistent concentration of FAP5-Rhodamine was incubated with HEK-FAP cells and increasing concentrations of FAP5-FP-NOTA or FAP5-CP-NOTA. Both conjugates were tested in parallel. All samples were performed in triplicate.

3.4.5 Reducing Renal Uptake of FAP5-IP-DOTA with Co-Administration of Amino Acid Solution

We have previously demonstrated that FAP5-IP-DOTA has high and sustained tumor retention. While FAP5-IP-DOTA is cleared relatively quickly from most other organs, the kidneys do experience prolonged exposure to radioactivity, likely due to the long circulation time of FAP5-IP-DOTA as well as slow clearance from the tumor. Other studies reported that the administration of amino acid solutions both reduce renal uptake and increase tumor uptake.³⁴ We injected a lysine solution into the intraperitoneal cavity of mice with several different tumors within minutes of an intravenous tail-vein injection of radiolabeled FAP5-IP-DOTA. We then performed SPECT/CT scans to investigate whether this technique might also improve the renal clearance of FAP5-IP-DOTA. The resulting scans are provided in Figure 3.5. In both Balb/c mouse bearing a 4T1 tumor and an athymic nu/nu mouse bearing a KB tumor, renal uptake appeared reduced relative to previous scans, particularly at early time points (see Figures 2.4, S2.7).

SPECT/CT of ^{177}Lu -FAP5-IP-DOTA + Lysine Injection 4T1 Tumor



SPECT/CT of ^{111}In -FAP5-IP-DOTA + Lysine Injection KB Tumor

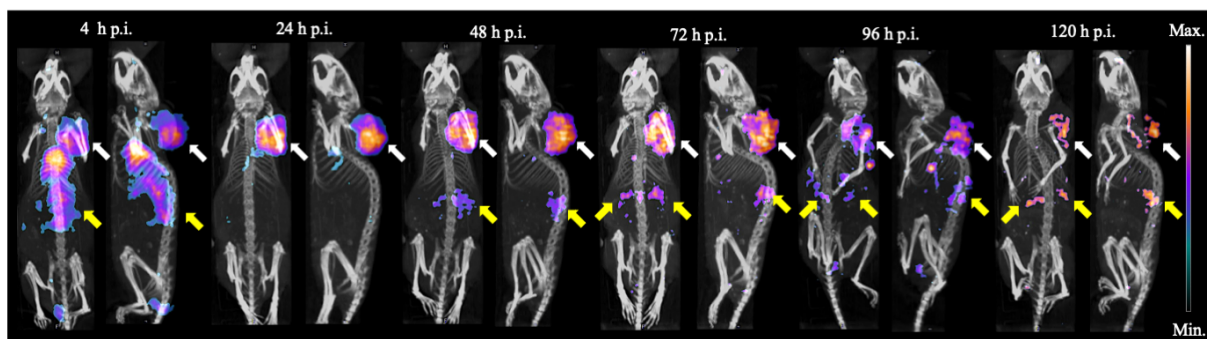


Figure 3.5. Reducing renal uptake of FAP5-IP-DOTA radioconjugates with co-administration of amino acid solution. A concentrated lysine-PBS solution was intraperitoneally injected within minutes of an intravenous tail-vein injection of the FAP5-IP-DOTA radioconjugate. Early time points showed significant reduction in renal uptake compared to previous scans. White arrows indicate tumor. Yellow arrows indicate kidneys.

3.4.6 Improved Radiotherapy with High Dosing Regimen of ^{177}Lu -FAP5-IP-DOTA

Balb/c mice were implanted with 4T1 tumors, which were grown to approximately 200 mm³ before initiation of the radiotherapy. Mice received an intravenous injection of either 5% EtOH in PBS alone or 5% EtOH in PBS containing FAP5-IP-DOTA radiolabeled with 55 MBq of lutetium-177 on day 0. A second group of mice received a second dose of FAP5-IP-DOTA radiolabeled with 22 MBq on day 3. All radioactive injections were accompanied with an injection of amino acid solution into the intraperitoneal cavity. Tumor sizes and body weights were measured every other day, which are provided in Figure 3.6. Both treatment groups show

significant reduction of tumor growth compared to the controls, but not a significant difference is observed between the mice that received one dose versus two doses. While neither treatment group suffered significant weight loss, the treatment group that received a second dose appears to have experienced a slower recovery than the mice that received one dose.

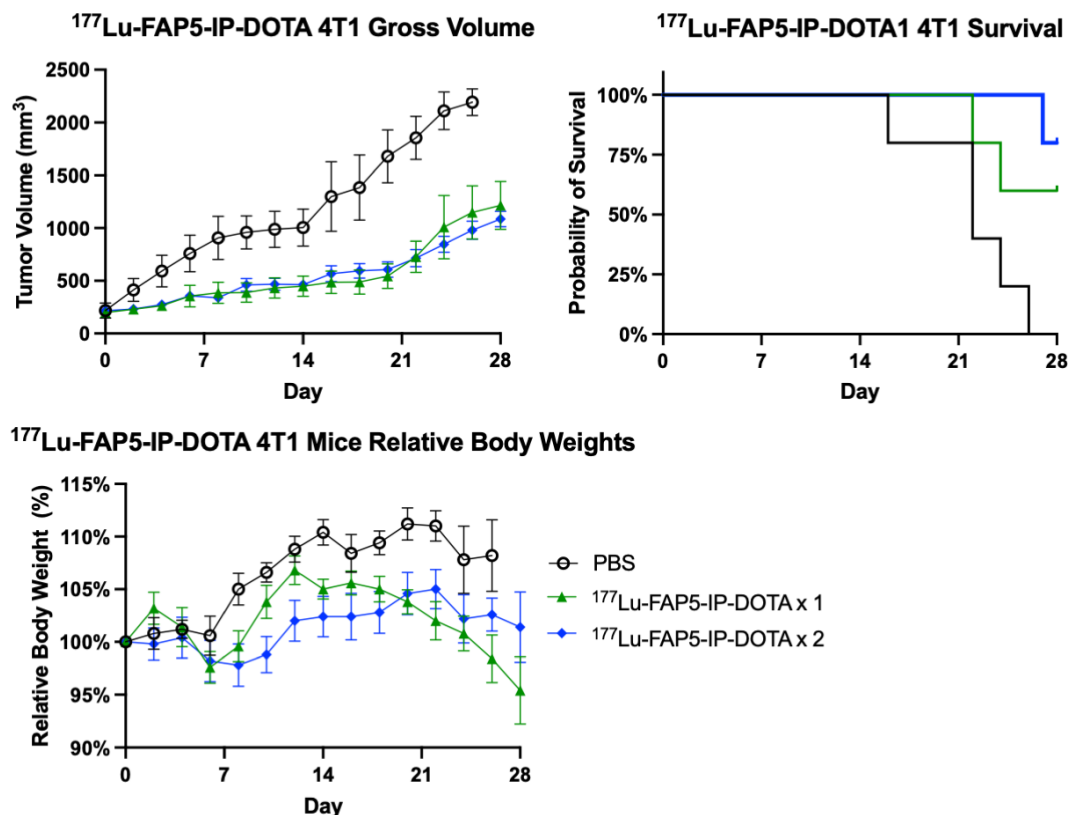
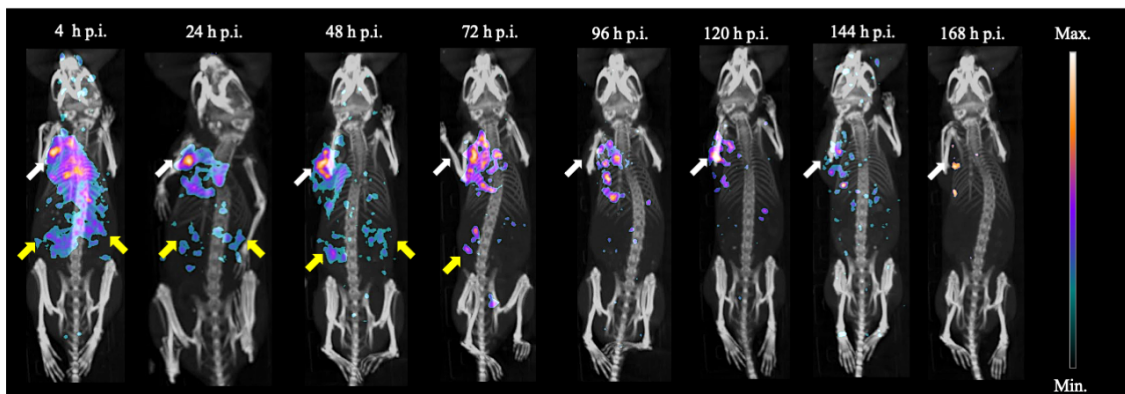


Figure 3.6. Radiotherapy of 4T1 tumor with high dosing regimen of ¹⁷⁷Lu-FAP5-IP-DOTA. Mice (n = 5 per group) bearing 4T1 tumors were injected with 5 nmol of FAP5-IP-DOTA radiolabeled with 55 MBq of lutetium-177 on day 0 with a coadministration of an amino acid solution into the intraperitoneal cavity. The second group of mice received a second dose of 5 nmol of FAP5-IP-DOTA radiolabeled with 22 MBq of lutetium-177 on day 3 with a coadministration of an amino acid solution into the intraperitoneal cavity.

SPECT/CT scans were taken of one mouse from each radiotherapy group daily during the first week to evaluate tumor retention and kidney clearance, which are provided in Figure 3.7. Radioactivity was cleared from the tumor of the single dose mouse by 168 hours post injection, while there is still significant radioactivity in the tumor of the mouse that received a second, smaller dose on day 3 after 168 hours post-injection of the first dose.

SPECT/CT of ^{177}Lu -FAP5-IP-DOTA + Lysine Injection



SPECT/CT of ^{177}Lu -FAP5-IP-DOTA x 2 + Lysine Injection

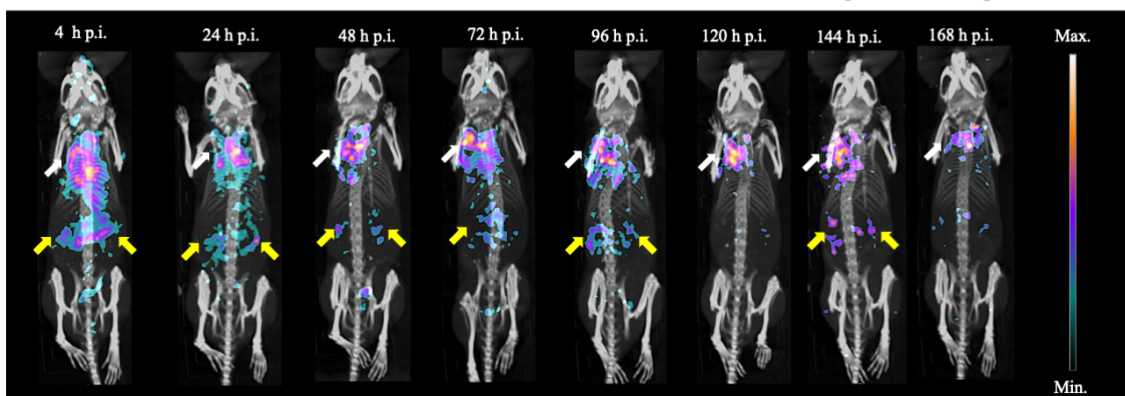


Figure 3.7. SPECT/CT scans of ^{177}Lu -FAP5-IP-DOTA in 4T1 tumors. Mice ($n = 1$) were injected on day 0 with 5 nmol of conjugate radiolabeled with 55 MBq of lutetium-177 and a coadministration of an amino acid solution into the intraperitoneal cavity. The second group of mice received a second dose of 5 nmol of FAP5-IP-DOTA radiolabeled with 22 MBq of lutetium-177 on day 3 with a coadministration of an amino acid solution into the intraperitoneal cavity. White arrows indicate tumor. Yellow arrows indicate kidneys.

3.5 Discussion

In this study, we investigated both structural modifications and procedural adjustments to optimize FAP-targeted radiotheranostics. We found that modifying the structure of the FAP5 ligand did not improve binding (see Fig. 3.1) despite previous SAR studies intimating otherwise.²⁰ Modification of the linker from the triazole-benzene to a more hydrophilic amide bond resulted in a reduction of FAP binding affinity (see Fig. 3.2), likely due to loss of Pi-Pi stacking in the FAP

binding pocket (see Supplementary Figure S3.1). Little difference in FAP binding affinity was observed between a PEG₄ and a PEG₆ spacer. However, a drastic reduction in FAP binding affinity was observed with a PEG₁₂ linker (see Fig. 3.3). This is likely due to intramolecular interactions between key functional groups on the FAP5 ligand and other parts of the conjugate afforded by the additional length and flexibility of PEG₁₂. In the past, we have observed that reducing the length and flexibility of the spacer greatly influences the binding of other targeting ligands.²¹⁻²⁵

We synthesized several novel FAP-targeted conjugates which were optimized for radioimaging. While the 4-*p*-iodophenyl albumin-binding moiety demonstrates a circulation time of 18-24 hours, which is suitable for radiotherapy, the relatively slow clearance renders it suboptimal for radioimaging, which requires a high tumor-to-background ratio at early time points. We rationalized that different albumin-binders would be required to optimize radioligands for radioimaging vs. radiotherapy. Based on several other studies comparing different 4-*p*-substituted phenyl groups,^{18, 19, 26, 27} we selected fluoro- and chloro- substituents for further investigation with FAP5. Both conjugates demonstrated strong affinity to FAP (see Fig. 3.4).

Satisfied with what we learned from our structural modification studies we next turned our attention to procedural alterations to further improve FAP-targeted radiotheranostic results. We first altered our formulation buffer to include radiolytic stabilizers. Radio-HPLC analysis showed that the radiolabeled conjugate in the new formulation buffer was stable for at least one week (see Supplementary Figure S3.2), whereas previous studies without radiolytic stabilizers were not successful if the radiolabeled conjugate was not used within the first day. Another simple improvement was the co-injection of an amino acid solution, which is reported to both reduce kidney retention and increase tumor uptake.^{31, 34, 35} The co-injection of a lysine solution with FAP5-IP-DOTA appears to mitigate radioactive retention in the kidneys (see Fig. 3.5) compared to previous results (Figure 2.2 and Figure 2.4, see also Supplementary Figure S2.7). The apparent inhibition of radioactive renal uptake could facilitate higher doses of radioactivity for radiotherapy studies with FAP5-IP-DOTA.

Our previous studies demonstrated suppressed tumor growth of multiple tumor types investigated with a single dose of ¹⁷⁷Lu-FAP5-IP-DOTA. However, complete tumor regression was not consistently achieved. Because the radiotherapy was well tolerated based on both relative body weight changes as well as post-radiotherapy toxicology evaluations, we determined to increase the amount of radioactivity delivered. Indeed, other reported FAP-targeted radiotherapies

have used higher amounts of radioactivity compared to other targeting ligands.^{28, 40-45} This is likely necessary due to several biological attributes of the FAP receptor. FAP receptors recycle quite slowly relative to other receptors, requiring 5 hours to fully internalize and 60 hours to restore full cell-surface expression.⁴⁶ Furthermore, it seems that fibroblasts express fewer than 150,000 FAP receptors per cell,⁴⁷ which is significantly lower compared to other receptors exploited for ligand-targeting.⁴⁸ Similarly, an $\alpha_v\beta$ integrin-targeted radiotherapeutic, another receptor expressed on CAFs, required multiple high doses to achieve complete tumor remission.⁴⁹

We injected groups of 4T1 mice with saline, 1 dose of ¹⁷⁷Lu-FAP5-IP-DOTA (50 MBq) on day 0, or 2 doses of ¹⁷⁷Lu-FAP5-IP-DOTA (50 + 22 MBq) on day 0 and day 3 with a coadministration of a lysine solution (see Fig. 3.6). Day 3 was chosen for the second dose because we believed it to be the first day full cell-surface expression of the FAP receptor would be restored.⁴⁶ The body weights did not significantly decrease in the treated mice despite the increase in radioactivity, suggesting negligible toxicity. The body weight changes were also comparable to previous studies with lower doses (Figure 2.5), which is likely due to the coadministration of the lysine solution reducing radioactive retention in the kidneys (see Fig. 3.7). The 4T1 tumor growth was drastically reduced in the treated groups versus the control and compared to mice treated with lower doses in previous studies (Figure 2.5). Pictures of the tumors were also taken on a weekly basis for the first 3 weeks, which are provided in Supplementary Figure S3.3.

While the second dose does appear to contribute to extended radioactivity in the tumor (see Fig. 3.7), no significant changes in tumor growth were observed throughout the study between the two treatment groups. We supposed that this may be due to the single high dose being sufficient to deplete the tumors of the initial CAF population. To assess the CAF population in the tumors of the different groups post-radiotherapy, we performed NIR imaging in a subset of mice from each group with FAP5-S0456. Somewhat surprisingly, most scans showed higher FAP5-S0456 uptake in the treated groups compared to the controls (see Supplementary Figure S3.4), suggesting that there were more FAP⁺ CAFs in the tumors of treated mice. It is a well-established phenomenon in the literature that radiotherapy promotes tissue fibrosis,⁵⁰ and that radiotherapy leads to the activation of CAFs as part of the DNA Damage Response (DDR) pathway.⁵¹ Our initial hypothesis that multiple doses in rapid succession would be optimal regimen appears to have been incorrect. A second dose should likely be delayed for several weeks to allow the tumor time to activate a new generation of CAFs as part of the DDR. Indeed, a one report that targeted a family of CAF

biomarkers $\alpha_v\beta$ integrins with a radiotherapeutic found that a second dose 2 weeks after the first dose resulted in complete tumor regression.⁴⁹

Finally, it should be noted that the potential application of FAP5 radioligands for other diseases as not escaped our notice. We have previously investigated FAP-targeted theranostic agents for fibrosis.³⁶ A pilot examination of FAP5-IP-DOTA radioimaging in pulmonary fibrosis offers encouraging results as a diagnostic agent (see Supplementary Figure S3.5), where early diagnosis is critical and noninvasive methods are needed.⁵²⁻⁵⁸

3.6 Conclusion

FAP is a highly promising oncological target with great potential for radiotheranostics. However, several biological limitations of the receptor pose significant challenges to improve preclinical results before translation to the clinic. We have conducted varied approaches to enhance the performance of our FAP5 radioligand for radioimaging and radiotherapy each. Lessons to optimize the structure of the FAP ligand, linker, and spacer have been observed. Coadministration of a lysine solution significantly reduces the kidney retention of FAP5-IP-DOTA. This reduction in renal radioactivity, in turn, facilitates higher and multiple doses of FAP5-IP-DOTA radiotherapy, ultimately resulting in improved tumor eradication.

3.7 References

1. Garin-Chesa, P.; Old, L. J.; Rettig, W. J., Cell surface glycoprotein of reactive stromal fibroblasts as a potential antibody target in human epithelial cancers. *Proceedings of the National Academy of Sciences* **1990**, *87* (18), 7235-7239.
2. Kratochwil, C.; Flechsig, P.; Lindner, T.; Abderrahim, L.; Altmann, A.; Mier, W.; Adeberg, S.; Rathke, H.; Röhrich, M.; Winter, H.; Plinkert, P. K.; Marme, F.; Lang, M.; Kauczor, H.-U.; Jäger, D.; Debus, J.; Haberkorn, U.; Giesel, F. L., 68Ga-FAPI PET/CT: Tracer Uptake in 28 Different Kinds of Cancer. *Journal of Nuclear Medicine* **2019**, *60* (6), 801-805.
3. Brennen, W. N.; Isaacs, J. T.; Denmeade, S. R., Rationale Behind Targeting Fibroblast Activation Protein-Expressing Carcinoma-Associated Fibroblasts as a Novel Chemotherapeutic Strategy. *Molecular Cancer Therapeutics* **2012**, *11* (2), 257.

4. Keane, F. M.; Yao, T.-W.; Seelk, S.; Gall, M. G.; Chowdhury, S.; Poplawski, S. E.; Lai, J. H.; Li, Y.; Wu, W.; Farrell, P.; Vieira de Ribeiro, A. J.; Osborne, B.; Yu, D. M. T.; Seth, D.; Rahman, K.; Haber, P.; Topaloglu, A. K.; Wang, C.; Thomson, S.; Hennessy, A.; Prins, J.; Twigg, S. M.; McLennan, S. V.; McCaughan, G. W.; Bachovchin, W. W.; Gorrell, M. D., Quantitation of fibroblast activation protein (FAP)-specific protease activity in mouse, baboon and human fluids and organs. *FEBS Open Bio* **2014**, *4*, 43-54.
5. Bussard, K. M.; Mutkus, L.; Stumpf, K.; Gomez-Manzano, C.; Marini, F. C., Tumor-associated stromal cells as key contributors to the tumor microenvironment. *Breast Cancer Research* **2016**, *18* (1), 84.
6. Blankenstein, T., The role of tumor stroma in the interaction between tumor and immune system. *Current Opinion in Immunology* **2005**, *17* (2), 180-186.
7. Tao, L.; Huang, G.; Song, H.; Chen, Y.; Chen, L., Cancer associated fibroblasts: An essential role in the tumor microenvironment. *Oncol Lett* **2017**, *14* (3), 2611-2620.
8. Ziani, L.; Chouaib, S.; Thiery, J., Alteration of the Antitumor Immune Response by Cancer-Associated Fibroblasts. *Frontiers in Immunology* **2018**, *9*, 414.
9. Barbazán, J.; Matic Vignjevic, D., Cancer associated fibroblasts: is the force the path to the dark side? *Current Opinion in Cell Biology* **2019**, *56*, 71-79.
10. Li, X. Y.; Hu, S. Q.; Xiao, L., The cancer-associated fibroblasts and drug resistance. *Eur. Rev. Med. Pharmacol. Sci* **2015**, *19* (11), 2112-2119.
11. Puré, E.; Blomberg, R., Pro-tumorigenic roles of fibroblast activation protein in cancer: back to the basics. *Oncogene* **2018**, *37* (32), 4343-4357.
12. Busek, P.; Mateu, R.; Zubal, M.; Kotackova, L.; Sedo, A., Targeting fibroblast activation protein in cancer-prospects and caveats. *Front Biosci (Landmark Ed)* **2018**, *23*, 1933-1968.
13. Kilvaer, T. K.; Khanekhenari, M. R.; Hellevik, T.; Al-Saad, S.; Paulsen, E.-E.; Bremnes, R. M.; Busund, L.-T.; Donnem, T.; Martinez, I. Z., Cancer associated fibroblasts in stage I-III A NSCLC: prognostic impact and their correlations with tumor molecular markers. *PloS one* **2015**, *10* (8), e0134965.
14. Cheng, Y.; Wang, K.; Ma, W.; Zhang, X.; Song, Y.; Wang, J.; Wang, N.; Song, Q.; Cao, F.; Tan, B.; Yu, J., Cancer-associated fibroblasts are associated with poor prognosis in esophageal squamous cell carcinoma after surgery. *Int J Clin Exp Med* **2015**, *8* (2), 1896-1903.
15. Sun, Q.; Zhang, B.; Hu, Q.; Qin, Y.; Xu, W.; Liu, W.; Yu, X.; Xu, J., The impact of cancer-associated fibroblasts on major hallmarks of pancreatic cancer. *Theranostics* **2018**, *8* (18), 5072-5087.

16. Loktev, A.; Lindner, T.; Burger, E.-M.; Altmann, A.; Giesel, F.; Kratochwil, C.; Debus, J.; Marmé, F.; Jäger, D.; Mier, W.; Haberkorn, U., Development of Fibroblast Activation Protein–Targeted Radiotracers with Improved Tumor Retention. *Journal of Nuclear Medicine* **2019**, *60* (10), 1421-1429.
17. Moon, E. S.; Elvas, F.; Vliegen, G.; Lombaerde, S. D.; Vangestel, C.; Bruycker, S. D.; Bracke, A.; Eppart, E.; Greifenstein, L.; Klasen, B.; Krmaer, V.; Staelens, S.; Deester, I. D.; Veken, P. V. d.; Roesch, F., Targeting fibroblast activation protein (FAP): next generation PET radiotracers using squaramide coupled bifunctional DOTA and DATA5m chelators. **2020**.
18. Kelly, J. M.; Jeitner, T. M.; Ponnala, S.; Williams, C.; Nikolopoulou, A.; DiMagno, S. G.; Babich, J. W., A Trifunctional Theranostic Ligand Targeting Fibroblast Activation Protein- α (FAP α). *Molecular Imaging and Biology* **2021**.
19. Jia-Jia, L.; Chia-Pao, C.; Jia-Yu, L.; Feng-Ting, H.; chiun-wei, H., Development and preclinical evaluation of [⁶⁸Ga]Ga-Alb-FAPtp-01, a novel tumour-associated fibroblast activation protein tracer for PET imaging of xenograft glioma. *Research Square* **2021**.
20. Tsai, T.-Y.; Yeh, T.-K.; Chen, X.; Hsu, T.; Jao, Y.-C.; Huang, C.-H.; Song, J.-S.; Huang, Y.-C.; Chien, C.-H.; Chiu, J.-H.; Yen, S.-C.; Tang, H.-K.; Chao, Y.-S.; Jiaang, W.-T., Substituted 4-Carboxymethylpyroglutamic Acid Diamides as Potent and Selective Inhibitors of Fibroblast Activation Protein. *Journal of Medicinal Chemistry* **2010**, *53* (18), 6572-6583.
21. Nakamura, Y.; Inomata, S.; Ebine, M.; Manabe, Y.; Iwakura, I.; Ueda, M., “Click-made” biaryl-linker improving efficiency in protein labelling for the membrane target protein of a bioactive compound. *Organic & biomolecular chemistry* **2010**, *9* (1), 83-85.
22. Tamura, S.; Inomata, S.; Ebine, M.; Genji, T.; Iwakura, I.; Mukai, M.; Shoji, M.; Sugai, T.; Ueda, M., Triazolyl–phenyl linker system enhancing the aqueous solubility of a molecular probe and its efficiency in affinity labeling of a target protein for jasmonate glucoside. *Bioorganic & Medicinal Chemistry Letters* **2013**, *23* (1), 188-193.
23. Vlashi, E.; Kelderhouse, L. E.; Sturgis, J. E.; Low, P. S., Effect of Folate-Targeted Nanoparticle Size on Their Rates of Penetration into Solid Tumors. *ACS Nano* **2013**, *7* (10), 8573-8582.
24. Wang, B.; Galliford, C. V.; Low, P. S., Guiding principles in the design of ligand-targeted nanomedicines. *Nanomedicine* **2014**, *9* (2), 313-330.
25. Verhoef, J. J. F.; Anchordoquy, T. J., Questioning the Use of PEGylation for Drug Delivery. *Drug delivery and translational research* **2013**, *3* (6), 499-503.
26. Kuo, H.-T.; Lin, K.-S.; Zhang, Z.; Uribe, C. F.; Merkens, H.; Zhang, C.; Benard, F., Novel ¹⁷⁷Lu-labeled Albumin-binder-conjugated PSMA-targeting Agents with Extremely High Tumor Uptake and Enhanced Tumor-to-kidney Absorbed Dose Ratio. *Journal of Nuclear Medicine* **2020**, jnumed.120.2507.

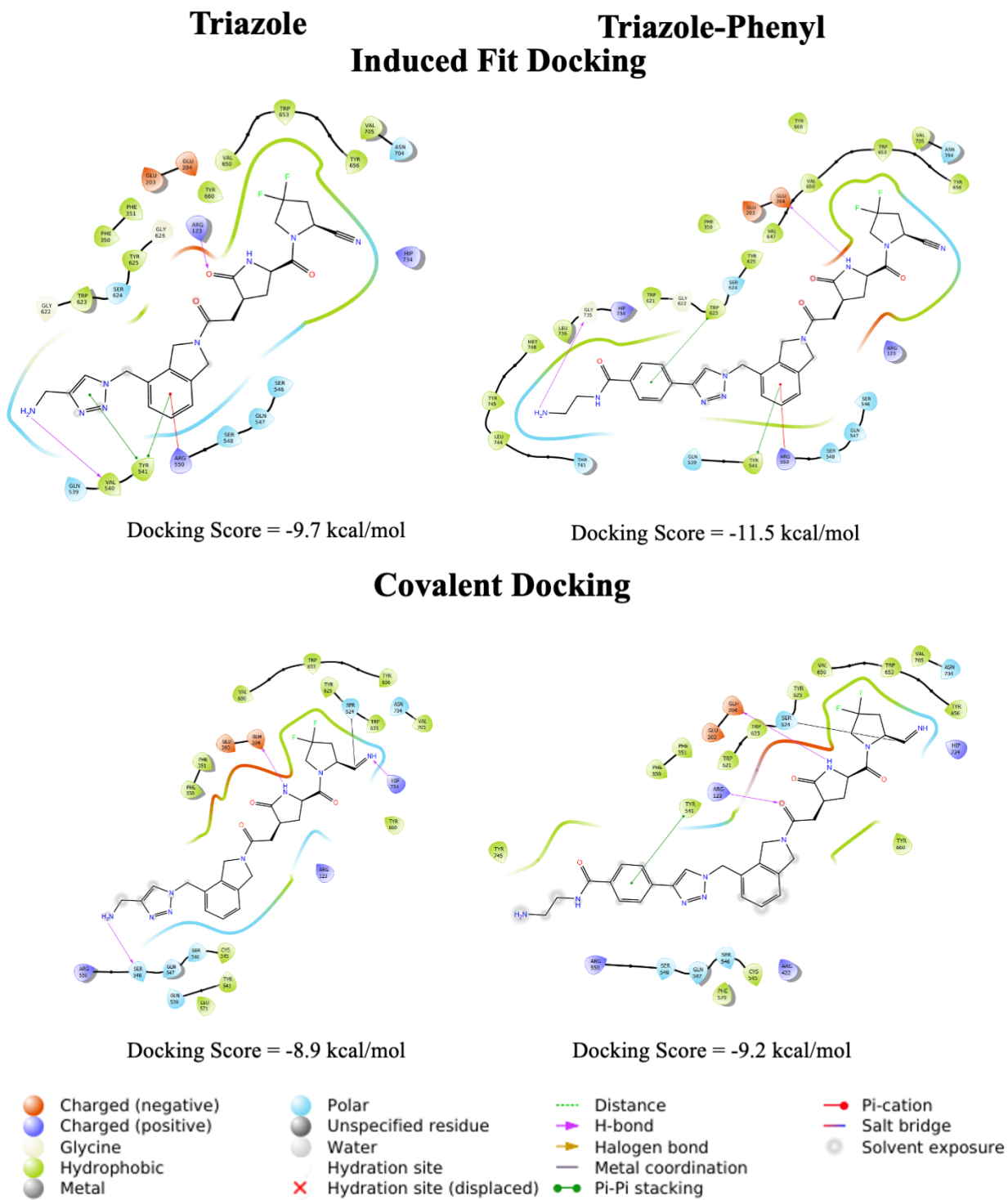
27. Iikuni, S.; Okada, Y.; Shimizu, Y.; Watanabe, H.; Ono, M., Modulation of the Pharmacokinetics of a Radioligand Targeting Carbonic Anhydrase-IX with Albumin-Binding Moieties. *Molecular Pharmaceutics* **2021**.
28. Umbricht, C. A.; Benešová, M.; Schibli, R.; Müller, C., Preclinical Development of Novel PSMA-Targeting Radioligands: Modulation of Albumin-Binding Properties To Improve Prostate Cancer Therapy. *Molecular Pharmaceutics* **2018**, *15* (6), 2297-2306.
29. Deberle, L. M.; Benešová, M.; Umbricht, C. A.; Borgna, F.; Büchler, M.; Zhernosekov, K.; Schibli, R.; Müller, C., Development of a new class of PSMA radioligands comprising ibuprofen as an albumin-binding entity. *Theranostics* **2020**, *10* (4), 1678-1693.
30. de Jong, M.; Rolleman, E. J.; Bernard, B. F.; Visser, T. J.; Bakker, W. H.; Breeman, W. A.; Krenning, E. P., Inhibition of renal uptake of indium-111-DTPA-octreotide in vivo. *Journal of Nuclear Medicine* **1996**, *37* (8), 1388-1392.
31. Rolleman, E. J.; Valkema, R.; de Jong, M.; Kooij, P. P.; Krenning, E. P., Safe and effective inhibition of renal uptake of radiolabelled octreotide by a combination of lysine and arginine. *European Journal of Nuclear Medicine and Molecular Imaging* **2003**, *30* (1), 9-15.
32. Rolleman, E. J.; Melis, M.; Valkema, R.; Boerman, O. C.; Krenning, E. P.; de Jong, M., Kidney protection during peptide receptor radionuclide therapy with somatostatin analogues. *European Journal of Nuclear Medicine and Molecular Imaging* **2010**, *37* (5), 1018-1031.
33. Lin, Y.-C.; Hung, G.-U.; Luo, T.-Y.; Tsai, S.-C.; Sun, S.-S.; Hsia, C.-C.; Chen, S.-L.; Lin, W.-Y., Reducing renal uptake of ¹¹¹In-DOTATOC: A comparison among various basic amino acids. *Annals of Nuclear Medicine* **2007**, *21* (1), 79.
34. Kobayashi, H.; Yoo, T. M.; Kim, I. S.; Kim, M.-K.; Le, N.; Webber, K. O.; Pastan, I.; Paik, C. H.; Eckelman, W. C.; Carrasquillo, J. A., L-Lysine Effectively Blocks Renal Uptake of ¹²⁵I- or ^{99m}Tc-labeled Anti-Tac Disulfide-stabilized Fv Fragment. *Cancer research* **1996**, *56* (16), 3788-3795.
35. Verwijnen, S. M.; Krenning, E. P.; Valkema, R.; Huijmans, J. G. M.; de Jong, M., Oral Versus Intravenous Administration of Lysine: Equal Effectiveness in Reduction of Renal Uptake of [¹¹¹In-DTPA] Octreotide. *Journal of Nuclear Medicine* **2005**, *46* (12), 2057.
36. Hettiarachchi, S. U.; Li, Y.-H.; Roy, J.; Zhang, F.; Puchulu-Campanella, E.; Lindeman, S. D.; Srinivasarao, M.; Tsoyi, K.; Liang, X.; Ayaub, E. A.; Nickerson-Nutter, C.; Rosas, I. O.; Low, P. S., Targeted inhibition of PI3 kinase/mTOR specifically in fibrotic lung fibroblasts suppresses pulmonary fibrosis in experimental models. *Science Translational Medicine* **2020**, *12* (567), eaay3724.
37. Zhang, F.; Ayaub, E. A.; Wang, B.; Puchulu-Campanella, E.; Li, Y.-H.; Hettiarachchi, S. U.; Lindeman, S. D.; Luo, Q.; Rout, S.; Srinivasarao, M.; Cox, A.; Tsoyi, K.; Nickerson-Nutter, C.; Rosas, I. O.; Low, P. S., Reprogramming of profibrotic macrophages for treatment of bleomycin-induced pulmonary fibrosis. *EMBO Molecular Medicine* **2020**, *12* (8), e12034.

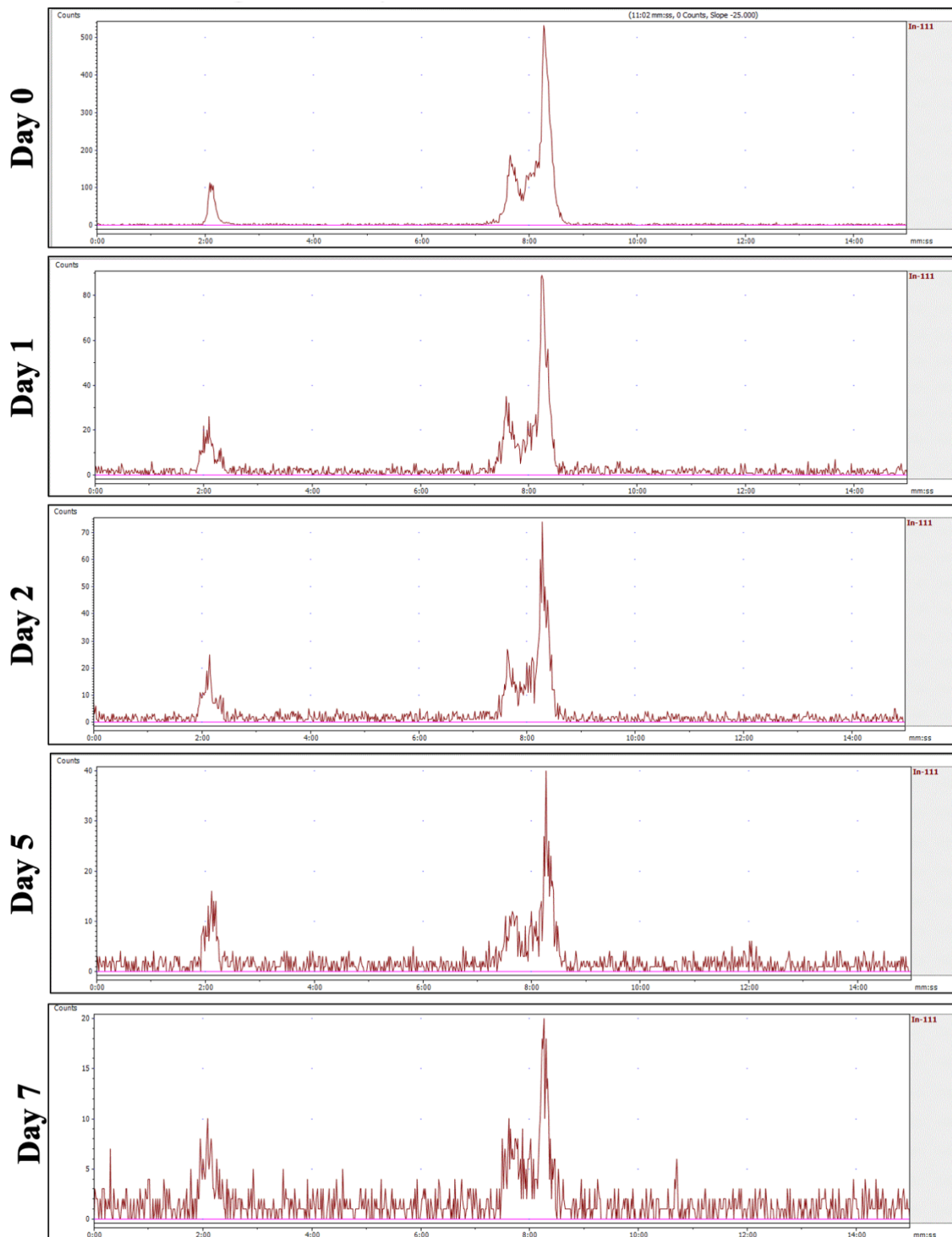
38. Price, E. W.; Orvig, C., Matching chelators to radiometals for radiopharmaceuticals. *Chem. Soc. Rev.* **2014**, *43* (1), 260-290.
39. Rahmim, A.; Zaidi, H., PET versus SPECT: strengths, limitations and challenges. *Nuclear Medicine Communications* **2008**, *29* (3).
40. Watabe, T.; Liu, Y.; Kaneda-Nakashima, K.; Shirakami, Y.; Lindner, T.; Ooe, K.; Toyoshima, A.; Nagata, K.; Shimosegawa, E.; Haberkorn, U.; Kratochwil, C.; Shinohara, A.; Giesel, F.; Hatazawa, J., Theranostics Targeting Fibroblast Activation Protein in the Tumor Stroma: ⁶⁴Cu- and ²²⁵Ac-Labeled FAPI-04 in Pancreatic Cancer Xenograft Mouse Models. *Journal of Nuclear Medicine* **2020**, *61* (4), 563-569.
41. Yuwei, L.; Tadashi, W.; Kazuko, K.-N.; Yoshifumi, S.; Sadahiro, N.; Kazuhiro, O.; Atsushi, T.; Kojiro, N.; Uwe, H.; Clemens, K.; Atsushi, S.; Jun, H.; Frederik, G., Fibroblast Activation Protein Targeted Therapy Using [¹⁷⁷Lu]FAPI-46 Compared with [²²⁵Ac]FAPI-46 in a Pancreatic Cancer Model. *European Journal of Nuclear Medicine and Molecular Imaging* **2021**.
42. Zboralski, D.; Osterkamp, F.; Simmons, A.; Bredenbeck, A.; Schumann, A.; Paschke, M.; Beindorff, N.; Mohan, A.; Nguyen, M.; Xiao, J., ⁵⁷¹P Preclinical evaluation of FAP-2286, a peptide-targeted radionuclide therapy (PTRT) to fibroblast activation protein alpha (FAP). *Annals of Oncology* **2020**, *31*, S488.
43. Müller, C.; Struthers, H.; Winiger, C.; Zhernosekov, K.; Schibli, R., DOTA Conjugate with an Albumin-Binding Entity Enables the First Folic Acid-Targeted ¹⁷⁷Lu-Radionuclide Tumor Therapy in Mice. *Journal of Nuclear Medicine* **2013**, *54* (1), 124-131.
44. Kuo, H.-T.; Merkens, H.; Zhang, Z.; Uribe, C. F.; Lau, J.; Zhang, C.; Colpo, N.; Lin, K.-S.; Bénard, F., Enhancing Treatment Efficacy of ¹⁷⁷Lu-PSMA-617 with the Conjugation of an Albumin-Binding Motif: Preclinical Dosimetry and Endoradiotherapy Studies. *Molecular Pharmaceutics* **2018**, *15* (11), 5183-5191.
45. Kelly, J. M.; Amor-Coarasa, A.; Ponnala, S.; Nikolopoulou, A.; Williams, C.; Thiele, N. A.; Schlyer, D.; Wilson, J. J.; DiMagno, S. G.; Babich, J. W., A Single Dose of ²²⁵Ac-RPS-074 Induces a Complete Tumor Response in an LNCaP Xenograft Model. *Journal of Nuclear Medicine* **2019**, *60* (5), 649-655.
46. Fischer, E.; Chaitanya, K.; Wüest, T.; Wadle, A.; Scott, A. M.; van den Broek, M.; Schibli, R.; Bauer, S.; Renner, C., Radioimmunotherapy of Fibroblast Activation Protein Positive Tumors by Rapidly Internalizing Antibodies. *Clinical Cancer Research* **2012**, *18* (22), 6208-6218.
47. Christiansen, V. J.; Jackson, K. W.; Lee, K. N.; Downs, T. D.; McKee, P. A., Targeting Inhibition of Fibroblast Activation Protein- α and Prolyl Oligopeptidase Activities on Cells Common to Metastatic Tumor Microenvironments. *Neoplasia* **2013**, *15* (4), 348-358.
48. Srinivasarao, M.; Galliford, C. V.; Low, P. S., Principles in the design of ligand-targeted cancer therapeutics and imaging agents. *Nat Rev Drug Discov* **2015**, *14* (3), 203-19.

49. Chen, H.; Jacobson, O.; Niu, G.; Weiss, I. D.; Kiesewetter, D. O.; Liu, Y.; Ma, Y.; Wu, H.; Chen, X., Novel “Add-On” Molecule Based on Evans Blue Confers Superior Pharmacokinetics and Transforms Drugs to Theranostic Agents. *Journal of Nuclear Medicine* **2017**, *58* (4), 590-597.
50. Nguyen, H. Q.; To, N. H.; Zadigue, P.; Kerbrat, S.; De La Taille, A.; Le Gouvello, S.; Belkacemi, Y., Ionizing radiation-induced cellular senescence promotes tissue fibrosis after radiotherapy. A review. *Critical Reviews in Oncology/Hematology* **2018**, *129*, 13-26.
51. Tommelein, J.; De Vlieghere, E.; Verset, L.; Melsens, E.; Leenders, J.; Descamps, B.; Debucquoy, A.; Vanhove, C.; Pauwels, P.; Gespach, C. P.; Vral, A.; De Boeck, A.; Haustermans, K.; de Tullio, P.; Ceelen, W.; Demetter, P.; Boterberg, T.; Bracke, M.; De Wever, O., Radiotherapy-Activated Cancer-Associated Fibroblasts Promote Tumor Progression through Paracrine IGF1R Activation. *Cancer research* **2018**, *78* (3), 659.
52. Zibrak, J. D.; Price, D., Interstitial lung disease: raising the index of suspicion in primary care. *NPJ primary care respiratory medicine* **2014**, *24*, 14054.
53. Collard, H. R.; Tino, G.; Noble, P. W.; Shreve, M. A.; Michaels, M.; Carlson, B.; Schwarz, M. I., Patient experiences with pulmonary fibrosis. *Respiratory Medicine* **2007**, *101* (6), 1350-1354.
54. Sverzellati, N., Highlights of HRCT imaging in IPF. *Respiratory Research* **2013**, *14* (1), S3.
55. Fisher, M.; Nathan, S. D.; Hill, C.; Marshall, J.; Dejonckheere, F.; Thuresson, P.-O.; Maher, T. M., Predicting Life Expectancy for Pirfenidone in Idiopathic Pulmonary Fibrosis. *Journal of Managed Care & Specialty Pharmacy* **2017**, *23* (3-b Suppl), S17-S24.
56. King, T. E.; Bradford, W. Z.; Castro-Bernardini, S.; Fagan, E. A.; Glaspole, I.; Glassberg, M. K.; Gorina, E.; Hopkins, P. M.; Kardatzke, D.; Lancaster, L.; Lederer, D. J.; Nathan, S. D.; Pereira, C. A.; Sahn, S. A.; Sussman, R.; Swigris, J. J.; Noble, P. W., A Phase 3 Trial of Pirfenidone in Patients with Idiopathic Pulmonary Fibrosis. *New England Journal of Medicine* **2014**, *370* (22), 2083-2092.
57. Richeldi, L.; du Bois, R. M.; Raghu, G.; Azuma, A.; Brown, K. K.; Costabel, U.; Cottin, V.; Flaherty, K. R.; Hansell, D. M.; Inoue, Y.; Kim, D. S.; Kolb, M.; Nicholson, A. G.; Noble, P. W.; Selman, M.; Taniguchi, H.; Brun, M.; Le Maulf, F.; Girard, M.; Stowasser, S.; Schlenker-Herceg, R.; Disse, B.; Collard, H. R., Efficacy and Safety of Nintedanib in Idiopathic Pulmonary Fibrosis. *New England Journal of Medicine* **2014**, *370* (22), 2071-2082.
58. Raghu, G.; Wells, A.; Nicholson, A. G.; Richeldi, L.; Flaherty, K. R.; Le Maulf, F.; Stowasser, S.; Schlenker-Herceg, R.; Hansell, D. M., S106 Consistent effect of nintedanib on decline in FVC in patients across subgroups based on HRCT diagnostic criteria: results from the INPULSIS® trials in IPF. *Thorax* **2015**, *70* (Suppl 3), A60.

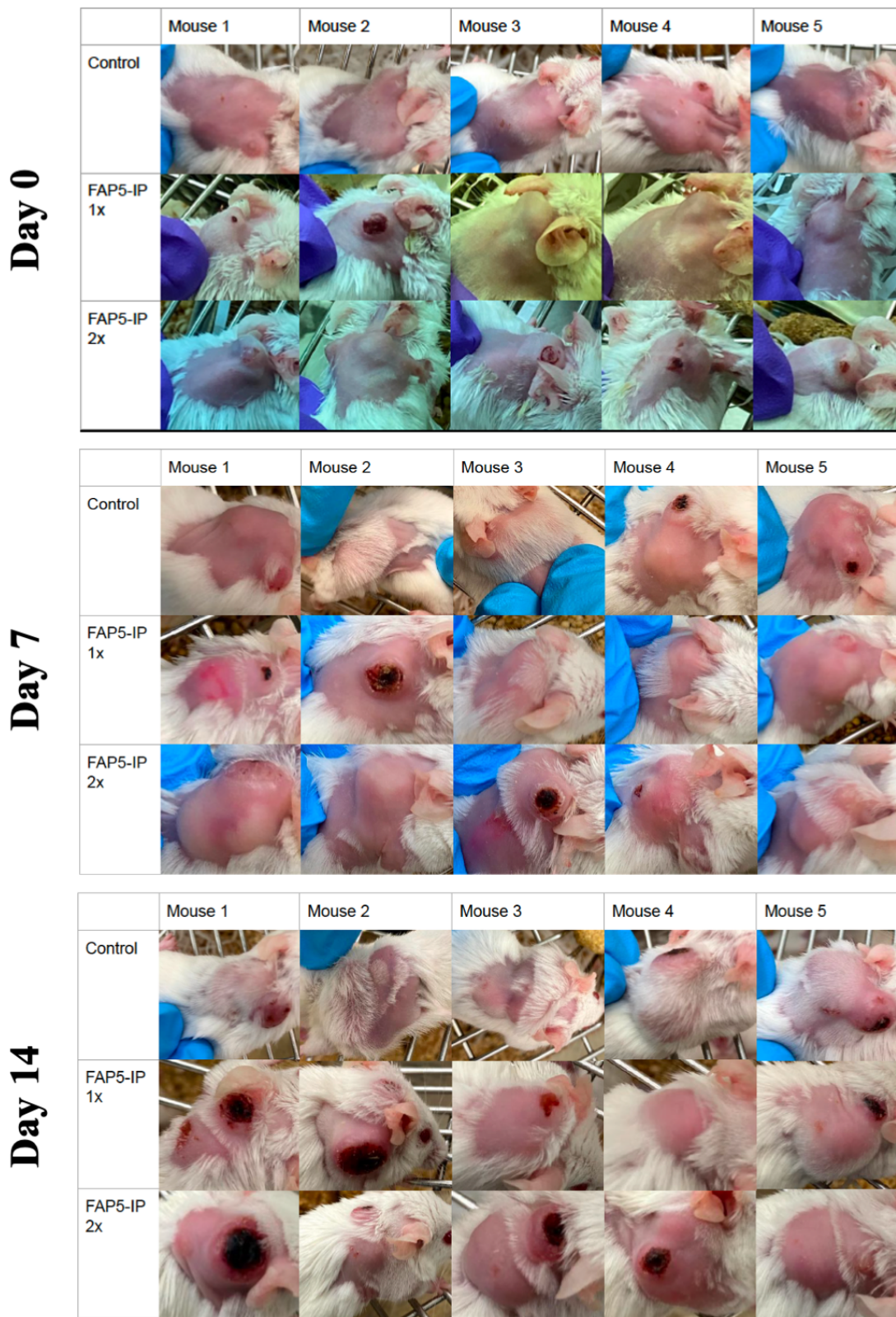
3.8 Appendix B. Supplemental Information

Additional data further validating our findings are provided below.



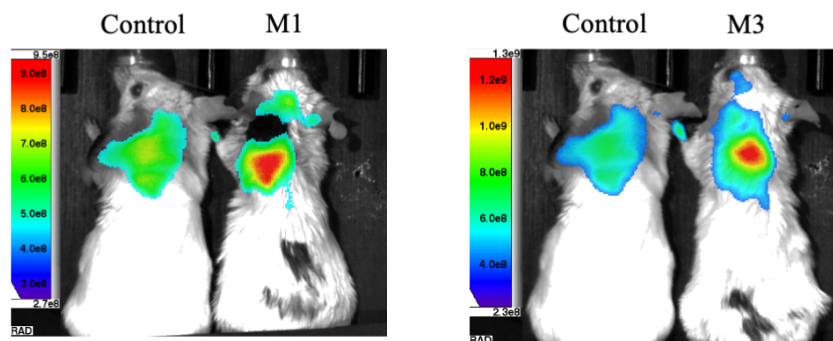


Supplementary Figure S3.2. Radiochromatogram analyses of the stability of the ^{111}In -FAP5-IP-DOTA complex in the presence of radiolytic stabilizers (100 mg/mL of ascorbate, 5 mg/mL of methionine) in PBS at room temperature.

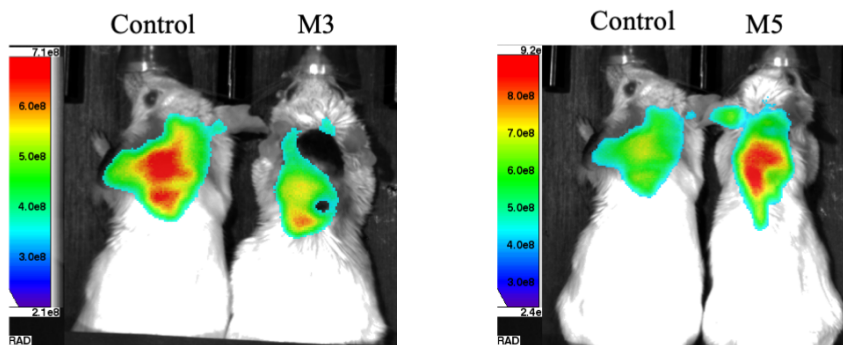


Supplementary Figure S3.3. Pictures of 4T1 tumors throughout radiotherapy study with high doses of ^{177}Lu -FAP5-IP-DOTA.

NIR Imaging of ^{177}Lu -FAP5-IP-DOTA + Lysine Injection

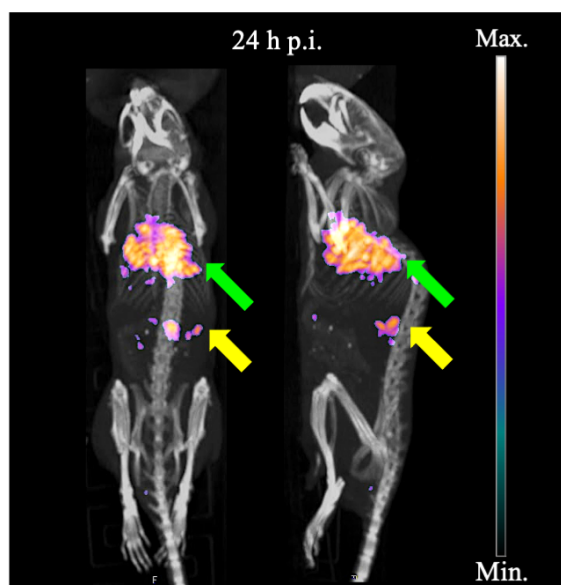


NIR Imaging ^{177}Lu -FAP5-IP-DOTA x 2 + Lysine Injection



Supplementary Figure S3.4. NIR imaging with FAP5-S0456 of ^{177}Lu -FAP5-IP-DOTA treated 4T1 tumors at 3.5 weeks post injection.

SPECT/CT Scans of ^{111}In -FAP5-IP-DOTA in Pulmonary Fibrosis



Supplementary Figure S3.5. SPECT/CT scan of ^{111}In -FAP5-IP-DOTA in a murine pulmonary fibrosis model (n = 1). Green arrows indicate lung. Yellow arrows indicate kidneys.

CHAPTER 4. FACILITATING RENAL CLEARANCE OF FOLATE CONJUGATES VIA BRUSH BORDER MEMBRANE ENZYME-MEDIATED DEGRADATION: PRECLINICAL EVALUATION FOR CANCER THERANOSTICS

4.1 Abstract

Folate receptor is a well-validated oncological target with many desirable properties for ligand-targeting. However, the high and sustained renal retention of folate radioconjugates precludes radiotherapeutic applications with the folate-targeting ligand. Several labs have demonstrated that certain peptide sequences are specifically cleaved by enzymes found on the brush border membrane (BBM) of the kidneys and can be exploited to accelerate renal clearance of radioligands targeting other receptors. We present the first incorporation of BBM-cleavable linkers into folate conjugates and demonstrate rapid renal clearance of both near infrared (NIR) dye and radioactive payloads via imaging scans. We also report the first quadri-functional radioligand, comprised of a targeting ligand, bifunctional chelator (BFC), an albumin binder (AB), and a BBM enzyme-labile linker. We investigate the effect of two albumin-binders, Evans Blue and 4-(*p*-iodophenyl)butyric acid, on BBM facilitated renal clearance, particularly within the context of radiotherapy. Our data show promising results for reducing the kidney retention of folate conjugates.

4.2 Introduction

Folate receptor (FR) is highly overexpressed on ~40% of human cancer cells and over 50% of tumor-associated macrophages (TAMs).¹⁻⁸ Folic acid conjugates bind to FR with low nanomolar affinity and internalize rapidly, which are ideal attributes for ligand-targeted radiotheranostics.^{9, 10} As a result, many folate-targeted imaging agents and drugs have entered clinical trials.¹¹ While FR expression is limited in most healthy tissues, folate conjugates have shown high renal accumulation both in preclinical models and clinical studies.¹²⁻¹⁴ This disqualifies all radiotherapeutic applications of folate-targeted ligands, as well as imaging applications of folate-targeted ligands in renal carcinomas.

Various strategies have been attempted to achieve acceptable tumor-to-kidney ratios with folate-targeted radioligands. Conventional methods for blocking renal uptake of radioligands such

as amino acid administration or diuretics failed to reduce kidney retention of folate-targeted radioconjugates.¹⁵ Administration of antifolates such as pemetrexed improved the tumor-to-kidney ratio by ~5 fold, but the ratio is still less than 1, indicating that further improvements are necessary.¹⁵⁻¹⁹ The incorporation of albumin-binders into the linker has also improved the tumor-to-kidney ratio relative to radiofolates without an albumin-binder, but the ratio is also less than 1.²⁰⁻²² A recent publication demonstrated that the 6R-isomer of folic acid analog 5-methyltetrahydrofolate (5-MTHF) achieved a tumor-to-kidney ratio of ~2.²³ However, the improvement in the ratio is due to a higher accumulation of tumor uptake rather than a reduction in kidney uptake based on their quantitative biodistribution results. Therefore, reducing renal accumulation of radiofolates remains a need.

One potential solution that has emerged is the presence of enzymes expressed specifically in the brush border membrane (BBM). The BBM is an epithelial surface covered by microvilli, which is found mainly in the kidney, as well the small and large intestines. These BBM enzymes cleave specific substrates such as peptides and sugars.²⁴ This concept was first applied to targeted radioconjugates by the Arano lab, where a short peptide sequence that is specifically cleaved by BBM enzymes was used to link an antibody fragment to a radiolabeled molecule. They successfully demonstrated rapid kidney clearance of the conjugate with the BBM-cleavable linker relative to controls.²⁵ Since then, they have identified additional peptide sequences that also facilitate renal clearance of radioactivity without compromising tumor uptake.²⁶⁻³¹ Several other labs have also demonstrated this concept of BBM-cleavable linkers was translatable to PSMA radioligands and targeting peptides.³²⁻³⁴ However, Arano opined that this technology, “may be limited to LMW Abs and peptides that undergo no or slow rates of internalization...”³⁰ Furthermore, it was unclear whether the BBM enzyme kinetics would successfully cleave radionuclides from folate due to receptors actively binding and recirculating folate conjugates into the bloodstream, unlike other radioligands.

Herein we report the first folate conjugates that use a BBM-cleavable substrate as the linker. We demonstrate a facile synthesis for incorporating BBM-cleavable peptides into folate conjugates with different potential payloads. We evaluate the renal clearance of a folate-targeted conjugate with a BBM-cleavable linker using the near-infrared (NIR) dye S0456 as a reporter for images of both healthy and tumor-bearing mice. We also report the first quadri-functional radioligand, consisting of folate as the targeting ligand, DOTA as the bifunctional chelator, a BBM-cleavable

peptide for a linker, and one of several albumin-binders. Albumin-binders have been shown to improve folate uptake in the tumor and simultaneously reduce kidney uptake, but different albumin binders can affect kidney retention.^{20, 21, 35} We evaluate the renal clearance of a folate radioligand with a BBM-cleavable linker with either Evans Blue or 4-(*p*-iodophenyl)butyric acid for both radioimaging and radiotherapy purposes in preclinical models.

4.3 Materials & Methods

4.3.1 Materials

2-chlorotrityl resin and all amino acids were purchased from AAPPTec (Louisville, KY). 3-Maleimido-propionic acid, HATU, PyBOP, TIPS, and Pd(PPh₃)₄ were purchased from Chem-Impex International (Chicago, IL). N-Succinimidyl 3-maleimido-propionic acid was purchased from A2B Chem LLC (San Diego, CA). 3-(Tritylthio)propanoic acid was purchased from AK Scientific, Inc. (Union City, CA). N-(2-Aminoethyl)maleimide trifluoroacetate salt was purchased from Enamine (Monmouth Jct., NJ). S0456-chloride was purchased from Few Chemicals GmbH (Bitterfeld-Wolfen, Germany). DOTA-tris (t-Bu ester) and 4-(*p*-iodophenyl)butyric acid were purchased from AstaTech, Inc (Bristol, PA). *o*-Tolidine and 1-Amino-8-naphthol-2,4-disulfonic Acid Monosodium Salt Hydrate were purchased from Thermo Fisher Scientific (Waltham, MA). Piperidine, ammonium hydroxide, diethyl ether, CsCO₃, TCEP, DIPEA, TFA, DMF, DCM, MeOH, DMSO, and all other reagents were purchased from Sigma-Aldrich (St. Louis, MO). OTL38 was provided by OnTarget. (West Lafayette, IN). Intermediates and products were purified using either flash chromatography (CombiFlash RF, Teledyne) or RP-HPLC (Agilent 1200 Instrument) with an XBridge OBD preparative column (19 x 150 mm, 5 μm) purchased from Waters (Milford, MA). LRMS-LC/MS was performed with an Agilent 1220 Infinity LC with a reverse-phase XBridge Shield RP18 column (3.0 x 50 mm, 3.5 μm).

KB and MDA-MB-231 cell lines were originally purchased from ATCC and cultured in folate-deficient Roswell Park Memorial Institute medium 1640 (RPMI-1640) purchased from GIBCO. All other cell culture reagents such as fetal bovine serum (FBS), 1% penicillin-streptomycin, and 2 mM glutamine were purchased from Life Technologies. Amine-coated 24-well cultureware plates were purchased from BD Biosciences (San Jose, CA). Accutase was purchased from BioLegend (San Diego, CA). Common cell culture materials such as culture flasks

and syringes were purchased from VWR (Chicago, IL). FACS analysis was performed with an Attune NxT Acoustic Focusing Flow Cytometer.

Indium-111 was purchased from Cardinal Health (Indianapolis, IN). Lutetium-177 was purchased from RadioMedix (Houston, TX and Garching, Germany). Chelations were done using a Fisherbrand Isotemp Digital Dry Bath/Block Heater (Waltham, MA). Radio-HPLC analysis was performed with an Agilent 1260 Infinity II with a Flow-RAM detector purchased from LabLogic (Brandon, FL) and a reverse-phase XBridge Shield RP18 column (3.0 x 50 mm, 3.5 μ m). SPECT/CT scans were acquired with a VECTor/CT system with a clustered multi-pinhole high-energy collimator (MILabs, Utrecht, The Netherlands). Radioactive binding and biodistribution studies were done with a Packard Cobra Gamma Counter (Niederösterreich, Austria).

4.3.2 Synthesis of Folate Conjugates with Brush Border Membrane Cleavable Linker

Solid Phase Synthesis of Folate with Brush Border Membrane Cleavable Linker. Fmoc-Lys(Alloc)-OH was loaded onto 2-Chlorotriyl chloride resin by stirring the resin in 2.0 equivalents of the amino acid, 10 equivalents of DIPEA, and 10 mL of DCM per gram of resin for 2 hours before capping the resin with 0.8 mL of MeOH per gram of resin for an additional 30 minutes. The resin was washed twice with DMF with DCM per use. Amino acid couplings were performed following solid phase peptide synthesis protocols, available on the AAPPTec website. Briefly, the resin was swelled in DCM for 10 minutes, then deprotected 3x with 20% piperidine in DMF for 20 minutes per reaction, with 5 washes of DMF, then DCM, and DMF each between every deprotection. Next, 2.0 equivalents of the appropriate amino acid were activated with 2.0 equivalents of HATU in DMF and 4.0 equivalents of DIPEA for 10 minutes before adding to the resin. The reaction was bubbled for three hours with an inert gas, washed, then repeated for an additional three hours before proceeding to the next step. When the payload was to be coupled (3-Tritylthio-propanoic acid or DOTA-tris t-Bu ester), 3.0 equivalents of the carboxylic acid bearing molecule and 3.0 equivalents of HATU were used with 6.0 equivalents of DIPEA to react with the resin one time for four hours. Alloc deprotection was performed with 1.0 equivalents of Pd(PPh₃)₄ freshly rinsed with MeOH and 20.0 equivalents of phenylsilane in DCM under inert conditions for one hour. The resin was rinsed 3x with DMF, 0.03 M sodium N,N-diethyldithiocarbamate in DMF, and DCM each before proceeding to additional couplings. Protected cysteine coupling was included next for radioactive conjugates but not NIR dye conjugates). Folate synthesis was

performed with 3.0 equivalents of N10-TFA-Pteric acid and 3.0 equivalents of HATU with 6.0 equivalents of DIPEA for four hours. The N10 TFA protecting group was removed using 50:50 NH₄OH:DMF (v/v). The folate intermediate was cleaved from the resin using 95:2.5:2.5 TFA:TIPS:H₂O with 10 mg of TCEP-HCl per 10 mL of solution for two hours. The resulting solution was removed in vacuo, filtered, and precipitated with cold diethyl ether before being purified on RP-HPLC [A = 20 mM ammonium acetate buffer (pH 5.0) and B = CH₃CN, solvent gradient 5% B to 95% B in 45 minutes].

[M+H]⁺ calculated for SH-MVK(Folate)-OH: C₃₈H₅₃N₁₁O₁₀S₂, 888.0; observed mass 889.

[M+H]⁺ calculated for DOTA-MVK(Cys-Folate)-OH: C₅₄H₈₀N₁₆O₁₇S₂, 1289.5; observed mass 1290.

Synthesis of S0456 maleimide. One equivalent of N-Boc-tyramine was dissolved in anhydrous DMSO with 1.0 equivalents of CsCO₃ and 1.0 equivalents of Cl-S0456 and stirred for four hours at room temperature. The product was purified on RP-HPLC [A = 20 mM ammonium acetate buffer (pH 7.0) and B = CH₃CN, solvent gradient 5% B to 95% B in 45 minutes]. [M+H]⁺ calculated for C₅₁H₆₆N₃O₁₅S₄⁺, 1089.3; observed mass 1090.

The amine was deprotected with neat TFA for 1 hour. Progress of the reaction was monitored via LC/MS. LC/MS (m/z): [M+H]⁺ calculated for C₄₆H₅₈N₃O₁₃S₄⁺, 989.2; observed mass 990. After removal of the TFA *in vacuo*, the product was redissolved in anhydrous DMSO with 10.0 equivalents of DIPEA and 1.2 equivalents of N-Succinimidyl 3-maleimidopropionate and stirred for four hours at room temperature under inert gas. The final product was purified on RP-HPLC [A = 20 mM ammonium acetate buffer (pH 7.0) and B = CH₃CN, solvent gradient 5% B to 95% B in 45 minutes]. [M+H]⁺ calculated for C₅₃H₆₃N₄O₁₆S₄⁺, 1140.3; observed mass 1141.

Synthesis of Evans Blue maleimide. Evans Blue maleimide was synthesized as reported previously.^{36, 37} Briefly, 1.0 equivalents of 3-Maleimido-propionic acid was stirred with 1.0 equivalents of HATU in DMF and 4.0 equivalents of DIPEA under inert gas for 10 minutes, then 1.5 equivalents of tolidine were added. The reaction was stirred overnight, then purified by flash chromatography. [M+H]⁺ calculated for C₂₁H₂₁N₃O₃, 363.4; observed mass 364.

The product was dissolved in ACN and cooled to 0°C. Ice cold 0.3 M HCl was added, sufficient for 4.7 equivalents, then ice cold 0.9 M NaNO₂ was added, sufficient for 3.0 equivalents, in dropwise fashion. The solution was stirred for thirty minutes, during which it turned a bright yellow color. Meanwhile, 2.1 equivalents of 1-amino-8-naphthol-2,4-disulfonic acid was

dissolved with 4.0 equivalents of NaHCO₃, and chilled to 0°C. The two solutions were then combined, allowed to reach room temperature, and stirred for 90 minutes. The Evans Blue maleimide was purified on RP-HPLC [A = 20 mM ammonium acetate buffer (pH 7.0) and B = CH₃CN, solvent gradient 5% B to 95% B in 45 minutes]. [M+H]⁺ calculated for C₃₁H₂₇N₅O₁₀S₂, 693.7; observed mass 694.

Synthesis of Iodophenyl maleimide. 4-(*p*-iodophenyl)butyric acid was dissolved with DIPEA (3 eq) and HATU (1 eq) in DMF and stirred for 10 minutes. N-(2-Aminoethyl)maleimide and DIPEA (1.5 eq) were added in DMF then stirred for 2 hours. The crude product was extracted then purified by flash chromatography. [M+H]⁺ calculated for C₁₇H₁₈INO₃, 411.2; observed mass 412.

Synthesis of final Folate conjugates. The thiol-bearing folate molecule was conjugated to the respective maleimide-bearing molecule by dissolving one equivalent of each compound in anhydrous DMSO and stirred under inert gas for four hours. The final folate conjugates were purified on RP-HPLC [A = 20 mM ammonium acetate buffer (pH 7.0) and B = CH₃CN, solvent gradient 5% B to 95% B in 45 minutes].

[M+H]⁺ calculated for S0456-MVK(Folate)-OH: C₉₁H₁₁₆N₁₅O₂₆S₆⁺, 2028.4; observed mass 1014, 676.

[M+H]⁺ calculated for DOTA-MVK(EB-Folate)-OH: C₈₅H₁₀₇N₂₁O₂₇S₄, 1983.2; observed mass 992.

[M+H]⁺ calculated for DOTA-MVK(IP-Folate)-OH: C₇₀H₉₇IN₁₈O₂₀S₂, 1701.7; observed mass 1702, 851, 567.

4.3.3 Cell Culture

KB and MDA-MB-231 cells were cultured in folate-deficient RPMI-1640 media with 10% FBS, 1% penicillin-streptomycin, and 1% 2 mM glutamine. Cells were cultured at 37°C in a 5% CO₂ and 95% humidified atmosphere. All cells used in this study were thawed from frozen vials saved in a master stock

4.3.4 Chelation and Radiolabeling

Folate-DOTA conjugates were diluted with ammonium acetate (0.5 M, pH 8.0) to reach a final conjugate concentration of 0.5 mM. Cold chelations were performed by adding natural

indium or lutetium in a dilute HCl solution in excess, heated to 90°C for 10 minutes, then analyzed using LC/MS. Indium-111 ($^{111}\text{InCl}_3$) was added to obtain a specific activity of up to 2 MBq/nmol, then heated to 90°C for 10 minutes. ^{177}Lu ($^{177}\text{LuCl}_3$) was added to obtain a specific activity of up to 4 MBq/nmol. Sodium-diethylenetriamine pentaacetate solution (5 mM, pH 7.0) was added to complex any unreacted traces of radioactive isotope. Radiochemical purities were analyzed using radio-HPLC. The mobile phase consisted of a 20 mM ammonium acetate aqueous buffer (pH 7) (A) and acetonitrile (B) with a linear gradient from 5% B to 95% B over 15 minutes. Radiochemical purities were $\geq 95\%$ for ^{111}In and ^{177}Lu radiolabeled Folate-DOTA conjugates.

4.3.5 Cell Binding Studies

Fluorescence-based binding curves were measured as follows. 200,000 KB cells were aliquoted into individual Eppendorf tubes suspended in staining buffer. The cells were incubated with increasing concentrations of OTL38 or S0456-MVK(Folate)-OH in the absence or presence of 100x excess of folate-glucosamine for one hour at 4°C. The cells were washed 3x with PBS to remove unbound fluorescence, then analyzed using channel RL3 on the Attune NxT Acoustic Focusing Flow Cytometer of The Chemical Genomics Facility at the Purdue Institute for Drug Discovery. Radioactive-based binding curves were measured as follows. 200,000 KB cells were seeded into 24-well amine coated plates and allowed to adhere overnight. Once the cells reached confluency, they were incubated with increasing concentrations of ^{111}In -DOTA-MVK(EB-Folate)-OH in the absence or presence of 100x excess of folate-glucosamine for one hour at room temperature. After incubation, the cells were washed 3x with PBS to remove unbound radioactivity and dissolved in 1.0 M NaOH. The samples were transferred to tubes and the cell-bound radioactivity was measured using a gamma counter. A specific binding constant was calculated using one-site specific nonlinear fit.

4.3.6 Animal Husbandry

12-week-old female ND4 swiss webster mice and 12-week-old female athymic nu/nu mice were purchased from Envigo. All mice were given access to a folate-deficient diet and water *ad libitum*. The mice were housed on a standard 12-hour light-dark cycle. All animal procedures were approved by the Purdue Animal Care and Use Committee.

4.3.7 Tumor Models

Nu/nu mice were inoculated on their shoulder with 5×10^6 MDA-MB-231 or KB cells in sterile PBS. MDA-MB-231 tumors were grown to 500-1000 mm³ for imaging. KB tumors were grown to ~200 mm³ for therapy.

4.3.8 NIR Imaging

Fluorescence imaging and biodistribution was performed with a Caliper IVIS Luminal II. MDA-MB-231 tumors were allowed to grow to approximately 1 cm³ before conducting NIR dye scans. Each mouse was injected intravenously via tail vein with up to 5 nmol of S0456-MVK(Folate)-OH in the absence or presence of 100x excess of folate-glucosamine. Mice (n=1–2 per group) were anesthetized with 3% isoflurane in oxygen and whole-body images were taken at multiple time points. When kidney fluorescence was no longer detectable, the mice were euthanized by CO₂ asphyxiation and organs of interest were harvested for biodistribution images. Imaging acquisition parameters were: Lamp Level = high; Excitation = 745 nm; Emission = 810 nm; Binning (M) = 4M; F-stop = 4; FOV = 12.5; Acquisition time ≤ 5 seconds.

4.3.9 SPECT/CT scans

Radioactive scans were performed with a VECTor/CT system with a clustered multi-pinhole high-energy collimator (MILabs, Utrecht, The Netherlands) of the Bindley Bioscience Center of Purdue University. MDA-MB-231 tumors were allowed to grow to approximately 1 cm³ before conducting SPECT/CT scans. Each mouse was injected intravenously via tail vein with up to 5 nmol ¹¹¹In-DOTA-MVK(EB-Folate)-OH in the absence or presence of 100x excess of folate-glucosamine. Mice (n=1 per group) were anesthetized with 3% isoflurane in oxygen and whole-body scans were performed at multiple time points. The emission scan was conducted for 15-60 min. The CT scans were acquired with an X-ray source set at 60 kV and 615 μA. The SPECT images were reconstructed with U-SPECT II software and ¹¹¹In γ-energy windows of 171 and 241 keV. A POS-EM algorithm was used with 16 subsets and 4 iterations on a 0.8 mm voxel grid. The CT images were reconstructed using NRecon software. The datasets were fused and filtered using PMOD software (version 3.2).

4.3.10 Radiotherapy

KB tumors were grown to approximately 300 mm³ (n = 5 per group). Mice were randomly sorted into control or treatment groups prior to the initiation of the therapy studies. Mice received a single intravenous dose of sterile saline or 5 nmol of radiofolate labeled with 18 MBq of lutetium-177 via the tail vein on day 0. Tumors were measured in two perpendicular directions every other day during therapy, and their volumes were calculated as $0.5 \times L \times W^2$, where L is the longest axis (in millimeters), and W is the axis perpendicular to L (in millimeters). Humane endpoint criteria were defined as weight loss of more than 20% of the initial body weight, a tumor volume of more than 1,800 mm³, or open ulceration. Mice were euthanized on reaching one of the predefined endpoint criteria.

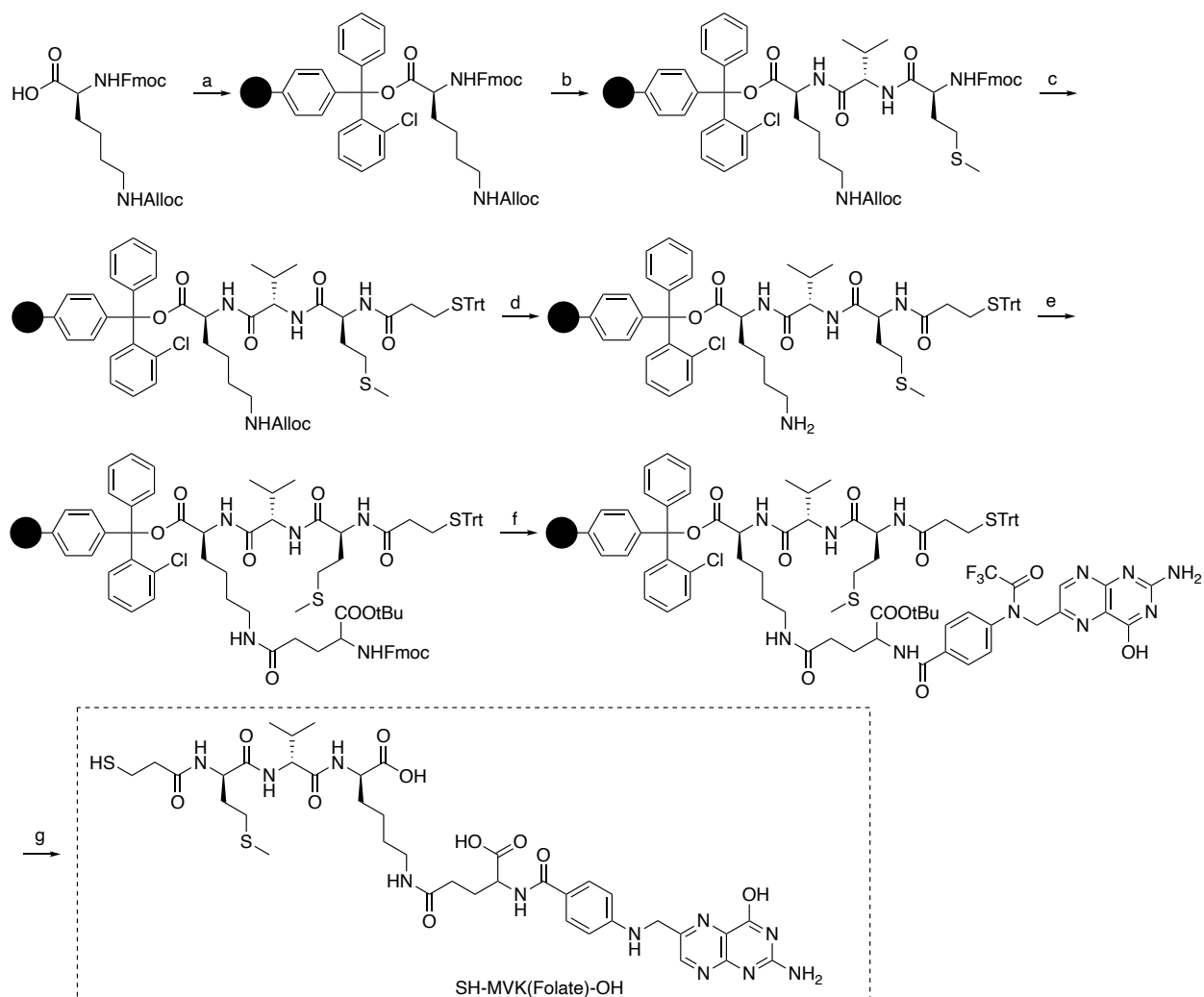
4.3.11 Statistical Analysis

Data were analyzed using on GraphPad Prism 8 unless otherwise stated. Results are shown as mean \pm SE.

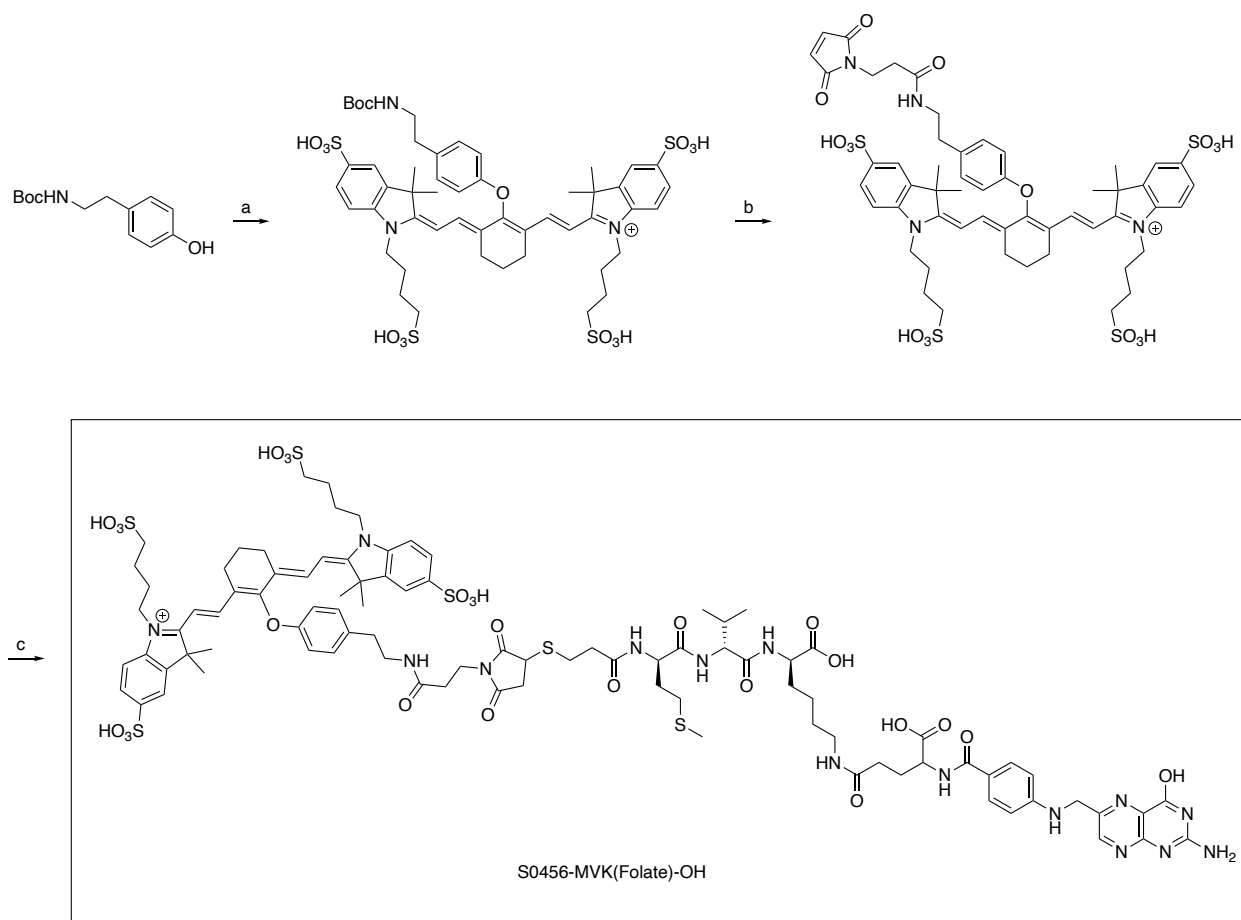
4.4 Results

4.4.1 Synthesis of Folate-Targeted NIR Conjugate with BBM-Cleavable Linkers

After reviewing different BBM-cleavable linkers as reported in the literature, we selected the methionine-valine-lysine (MVK) sequence. Scheme 4.1 depicts the solid-phase synthesis of a folate conjugate with a thiol and BBM-cleavable linker. The targeting molecule folate was conjugated to the side chain of lysine, following similar constructs previously reported.³⁸ The amine of methionine was derivatized for coupling to the NIR dye, also mirroring the overall design of other BBM-cleavable conjugates.^{30, 34, 39} S0456-maleimide synthesis and coupling to the thiol-bearing folate-BBM conjugate was performed as shown in Scheme 4.2, similar to previous reports.^{40, 41} Successful synthesis of the final conjugate was confirmed by LC/MS as shown in Supplemental Figure S4.1.



Scheme 4.1. Synthesis of Folate-BBM precursor for NIR coupling. Reagents and conditions: a) 2-Chlorotrityl resin, DIPEA, DCM, rt, 2h; b) i. 20% piperidine DMF, Ar, 20 min (x3); ii. Fmoc-Val-OH, HATU, DIPEA, DMF, Ar, 3h (x2); iii. 20% piperidine DMF, Ar, 20 min (x3); iv. Fmoc-Met-OH, HATU, DIPEA, DMF, Ar, 3h (x2); c) i. 20% piperidine DMF, Ar, 20 min (x3); ii. 3-(Tritylthio)propanoic acid, HATU, DIPEA, DMF, Ar, 3h; d) Pd(PPh₃)₄, phenylsilane, DCM, Ar, 1h; e) Fmoc-Glu-OtBu, HATU, DIPEA, DMF, Ar, 3h; f) i. 20% piperidine DMF, Ar, 20 min (x3); ii. N10-TFA-Pteoric acid, HATU, DIPEA, DMF; g) i. 50% NH₄OH DMF, Ar; ii. TCEP, 95/2.5/2.5 TFA/TIPS/H₂O, 1h.

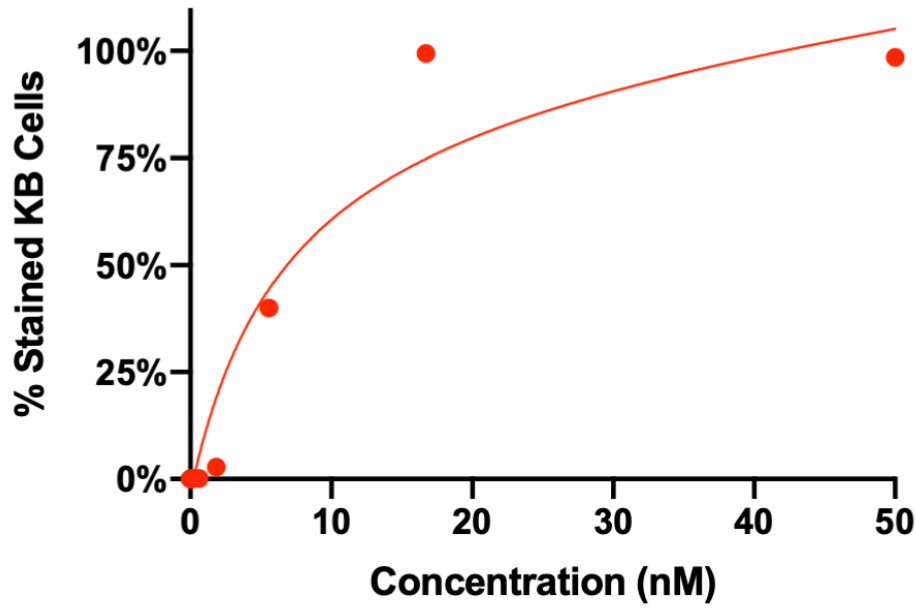


Scheme 4.2. Synthesis of S0456-MVK(Folate)-OH. Reagents and conditions: a) Cl-S0456, CsCO₃, DMSO, rt, 4h; b) i. TFA, rt, 1h; ii. N-Succinimidyl 3-maleimidopropionate, DIPEA, DMSO, rt, 4h; c) SH-MVK(Folate)-OH, DMSO, Ar, rt, 4h.

4.4.2 *In vitro* validation of FR targeting by S0456-MVK(Folate)-OH

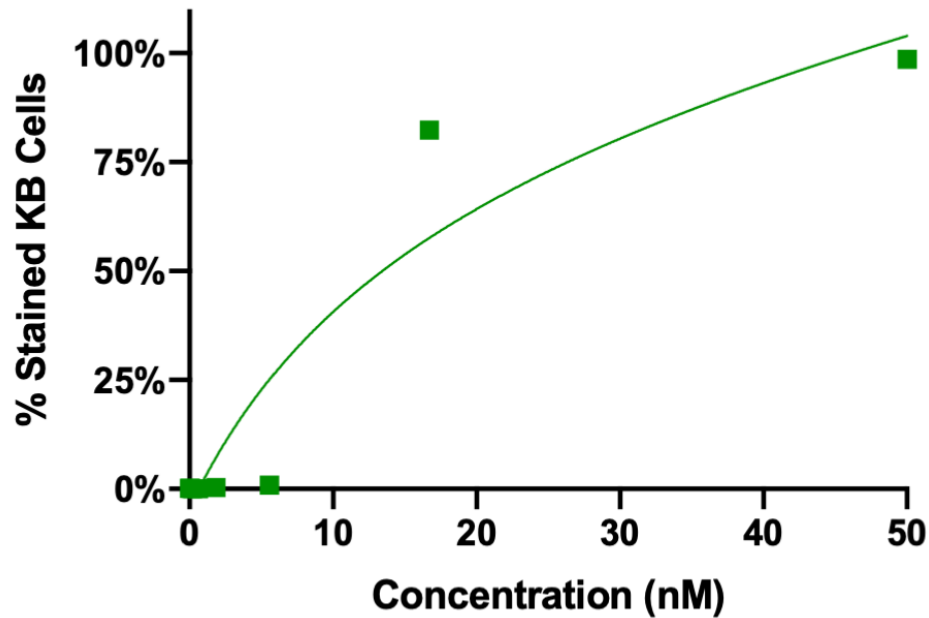
The novel S0456-MVK(Folate)-OH was first compared to the folate-S0456 conjugate OTL38 *in vitro* by performing a FACS-based binding study using KB cells cultured in folate-deficient media. We determined a binding affinity of 6.7 nM for OTL38 and 16.0 nM for S0456-MVK(Folate)-OH as shown in Figure 4.1. Separate KB cell samples incubated with 50 nM of either folate-NIR conjugate and a 100x excess of folate-glucosamine both showed complete abolishment of conjugate binding, as shown in Supplementary Figure S4.2, demonstrating that the binding of both conjugates is receptor-mediated.

OTL38



$K_d = 6.7$ nM

S0456-MVK(Folate)-OH



$K_d = 16.0$ nM

Figure 4.1. Binding of Folate-S0456 conjugates to KB cells by FACS analysis. These studies were conducted in parallel.

4.4.3 *In vivo* evaluation of S0456-MVK(Folate)-OH Renal Clearance and Tumor Targeting

Once we established the functionality of the folate in our novel targeting molecule, we next assessed the renal clearance facilitated by the BBM-labile linker. We injected healthy ND4 Swiss Webster mice housed on folate-deficient diet for several weeks with either OTL38 or S0456-MVK(Folate)-OH intravenously via tail vein injection (n = 2). The lower backs of the mice were shaved to improve visualization of the fluorescence signal. At various time points, mice were anesthetized so whole-body scans could be taken to compare renal NIR fluorescence. Within 1-hour post-injection, a significant difference in renal fluorescence could be observed between OTL38 and S0456-MVK(Folate)-OH. By 6 hours post-injection, heavy-exposure scans could not detect any renal fluorescence in the mice injected with S0456-MVK(Folate)-OH. After 24 hours, the mice were sacrificed for additional biodistribution scans. While OTL38 was still highly retained in the kidneys, S0456-MVK(Folate)-OH was no longer detectable. All scans are shown in Figure 4.2

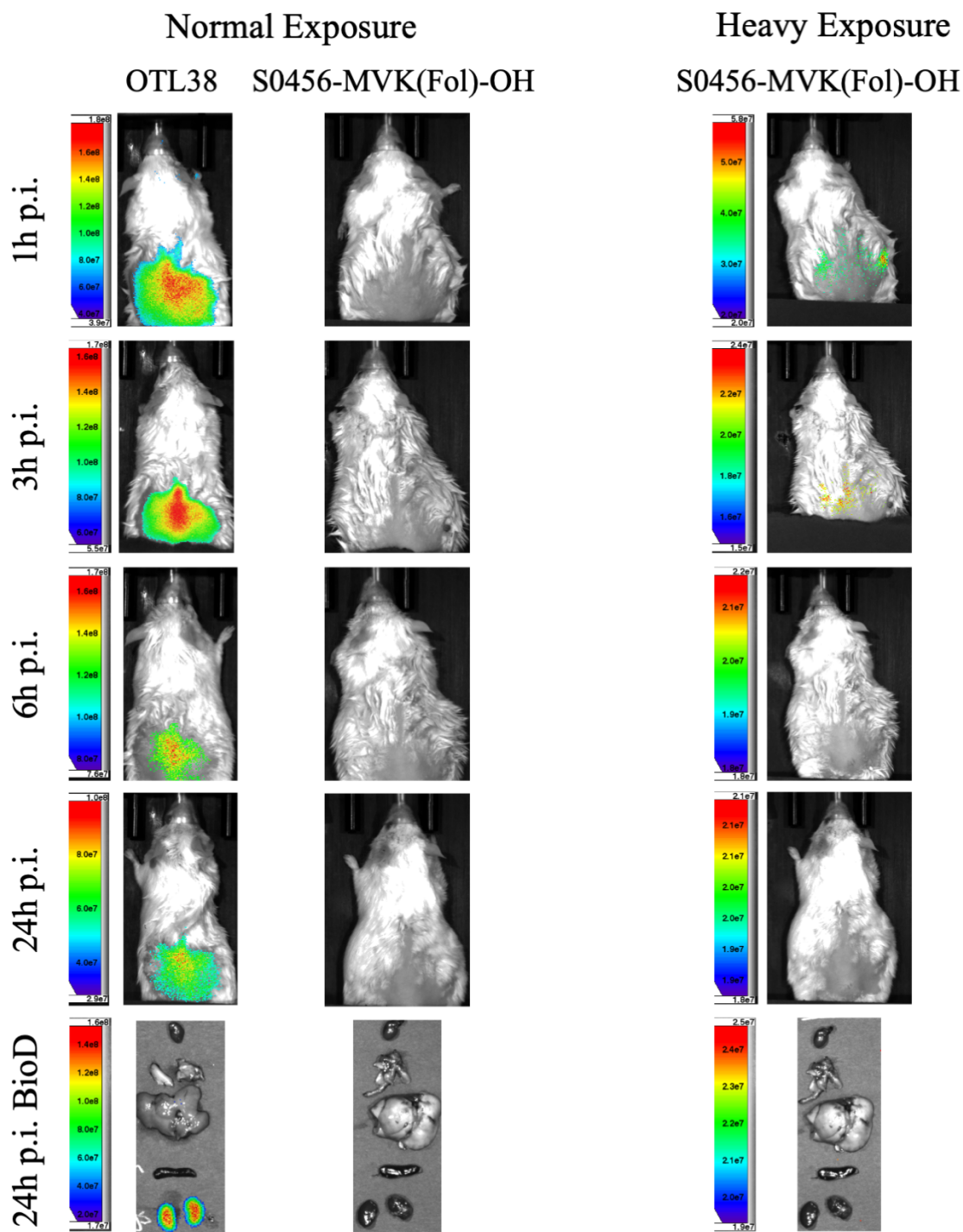


Figure 4.2. Renal clearance of folate-S0456 conjugates from healthy mice (n = 2). A drastic difference in renal fluorescence could be observed within the first hour post-injection. More sensitive scans could no longer detect fluorescence in whole-body scans by six hours post-injection. Biodistribution images show no detectable fluorescence in the kidneys of mice injected with the S0456-MVK(Folate)-OH conjugate by 24 hours p.i., whereas OTL38 was still highly retained. Organs in biodistribution shown from top to bottom: Heart, lungs, liver, spleen, kidneys.

Encouraged by the rapid renal clearance of S0456-MVK(Folate)-OH compared to OTL38, we next investigated the tumor uptake and retention. We used athymic nu/nu mice bearing MDA-MB-231 tumors as our model. After housing these mice on folate-deficient diet for several weeks, we injected these mice with either OTL38 or S0456-MVK(Folate)-OH in the absence or presence of 100x excess of folate-glucosamine (n = 1–2). At various time points, the mice were anesthetized so whole-body scans could be taken to compare renal NIR fluorescence. Within 1-hour post-injection, a significant difference in fluorescent tumor-to-kidney ratio could be observed between OTL38 and S0456-MVK(Folate)-OH. Competition mice lacked tumor fluorescence, thus demonstrating that tumor uptake by S0456-MVK(Folate)-OH is receptor mediated. After 24 hours, the mice were sacrificed for additional biodistribution scans. Small, kidney-sized tumor sections were used for comparison to kidney fluorescence. While OTL38 still showed significant kidney retention, S0456-MVK(Folate)-OH was barely detectable in the kidneys. All scans are shown in Figure 4.3.

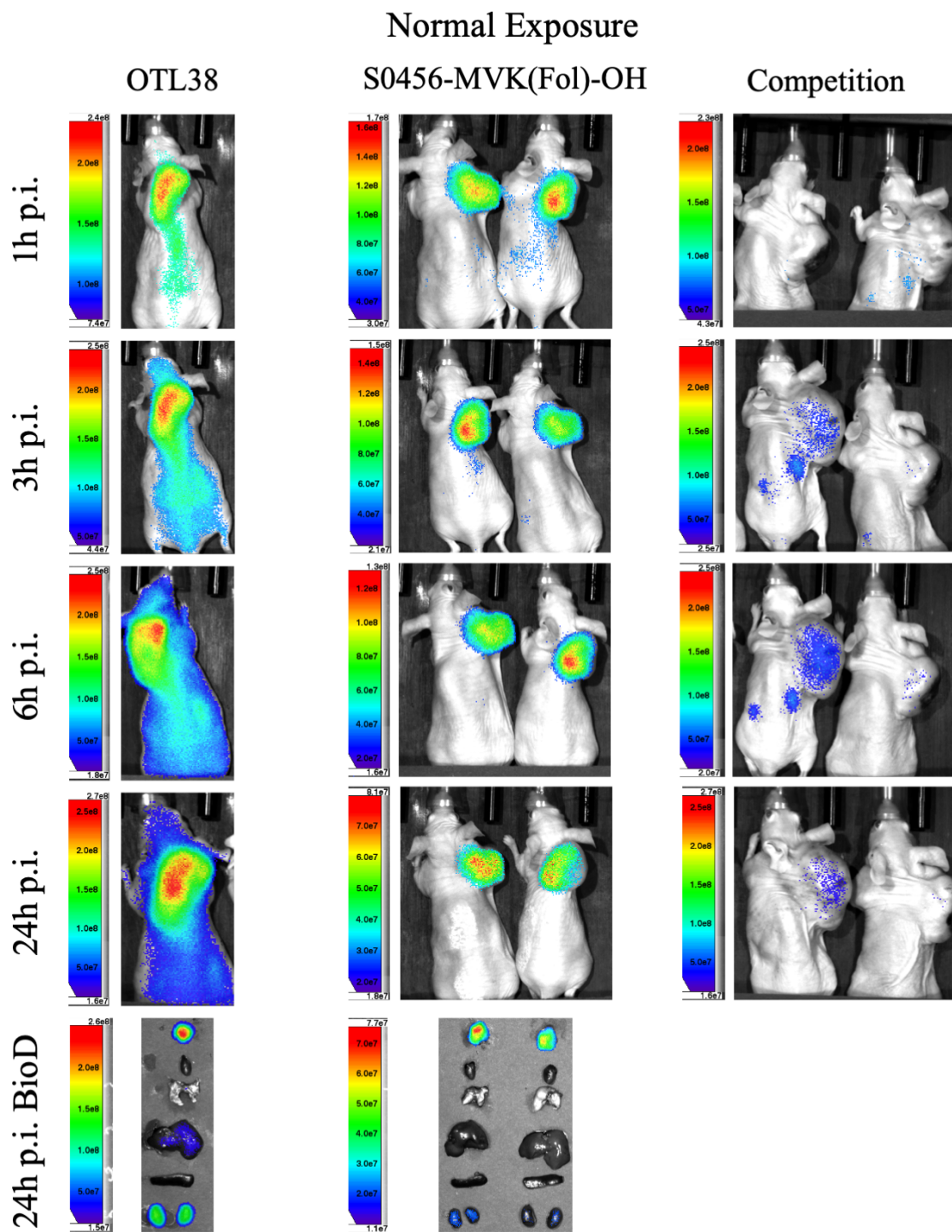
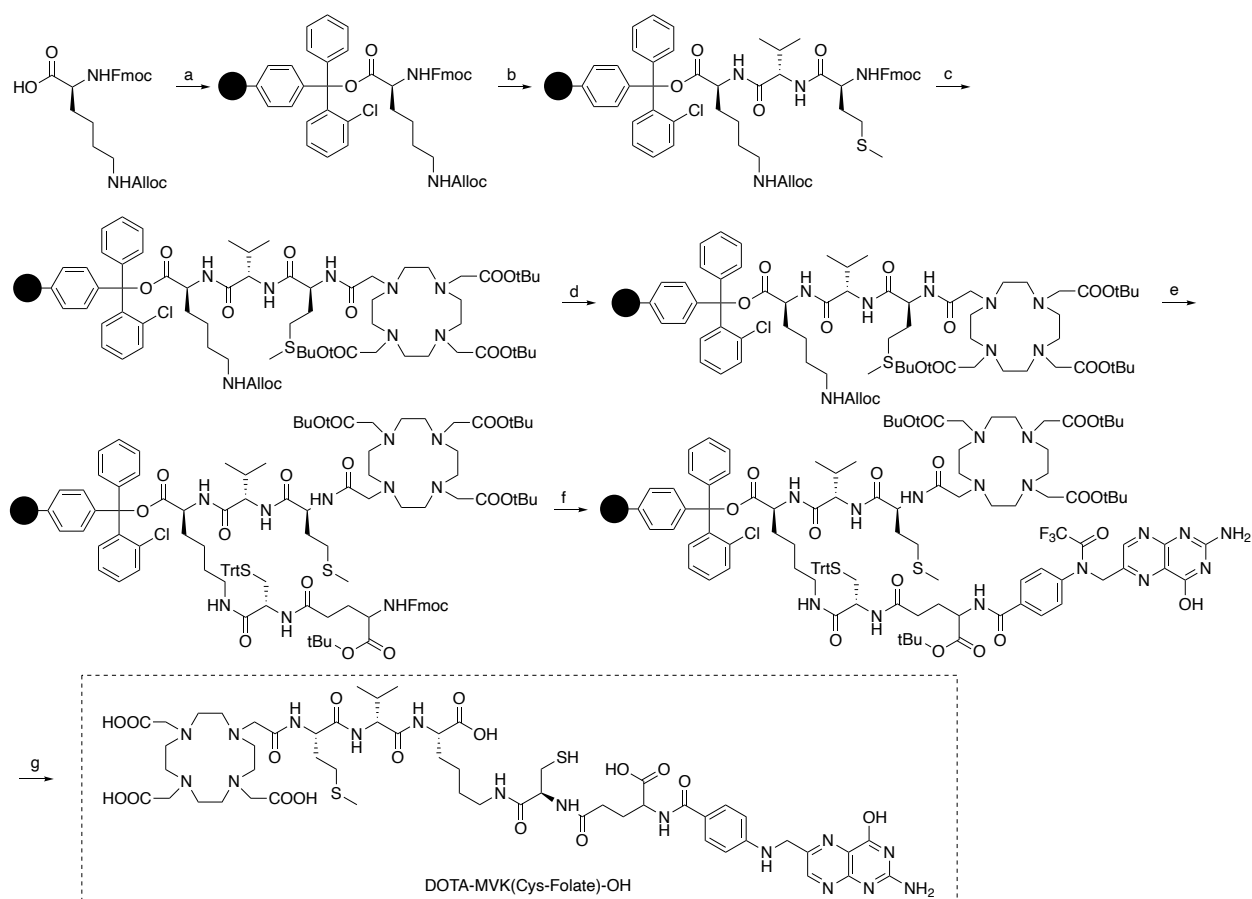


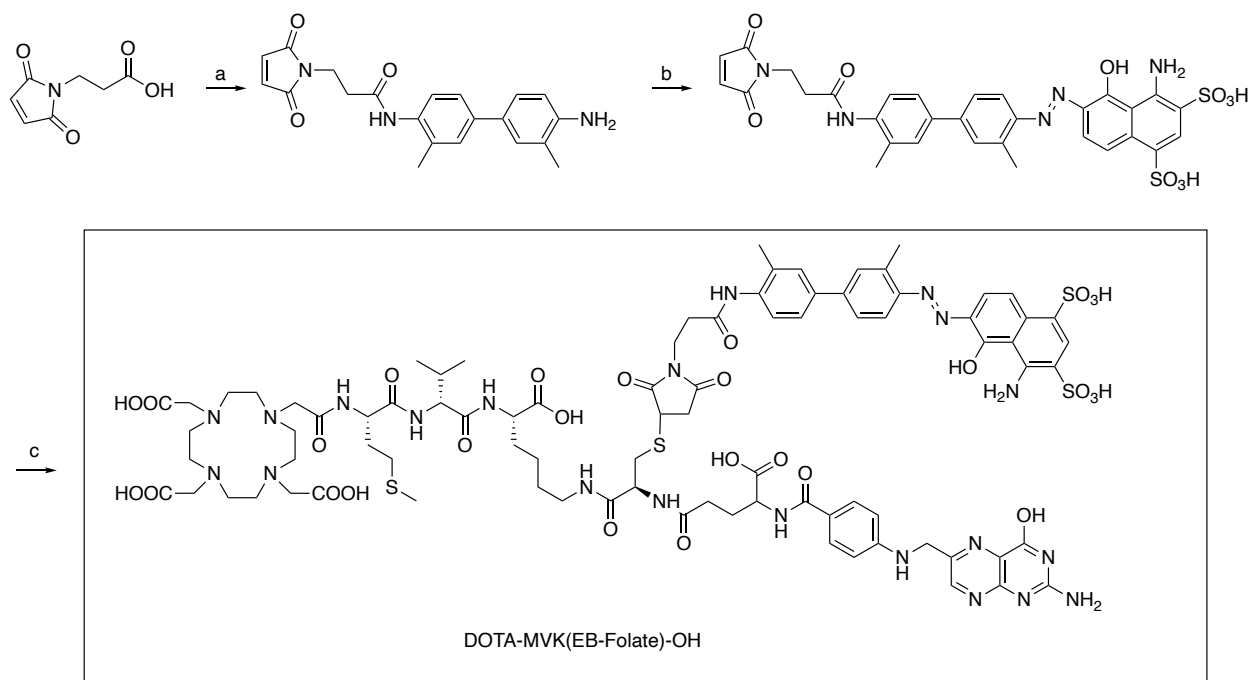
Figure 4.3. Tumor targeting of folate-S0456 in MDA-MB-231 tumor-bearing mice (n = 1–2). An improved tumor-to-kidney ratio can be observed within the first hour for the folate-S0456 conjugate with the BBM-labile linker. Competition mice received an injection of S0456-MVK(Folate)-OH with 100x excess of folate-glucosamine, which blocked tumor fluorescence, demonstrating active receptor targeting. Organs in biodistribution shown from top to bottom: Tumor, heart, lungs, liver, spleen, kidneys.

4.4.4 Synthesis of DOTA-MVK(AB-Folate) Conjugates with Several Albumin-Binders

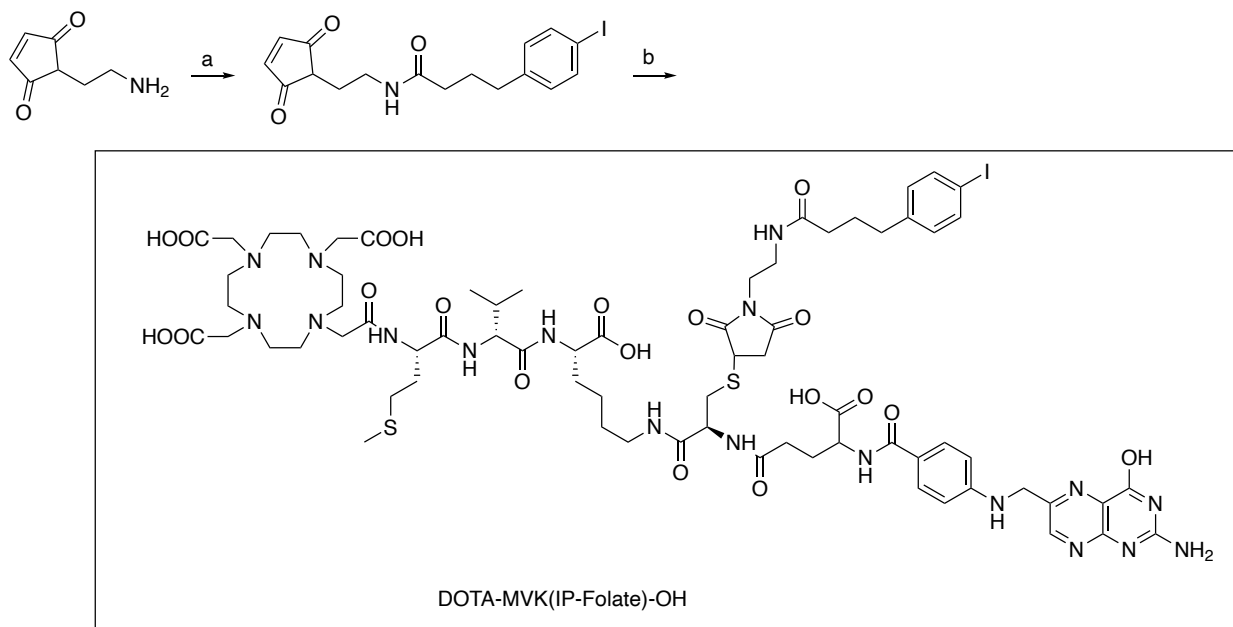
Satisfied with our preliminary findings that folate conjugate payloads could be cleared rapidly from tumors using BBM-cleavable linkers, we next sought to adapt this technology to radiotheranostics. The synthesis shown in Scheme 4.3 closely parallels that which we employed previously, with the notable exception of an inclusion of a cysteine residue on the lysine side chain before the synthesis of folate. The thiol would be exploited for coupling to one of several albumin-binders (ABs) conjugated to a maleimide, as shown in Schemes 4.4–4.5. Successful synthesis of the final conjugates was confirmed by LC/MS as shown in Supplementary Figure S.4.1.



Scheme 4.3. Synthesis of Folate-BBM-DOTA precursor for AB coupling. Reagents and conditions: a) 2-Chlorotrityl resin, DIPEA, DCM, rt, 2h; b) i. 20% piperidine DMF, Ar, 20 min (x3); ii. Fmoc-Val-OH, HATU, DIPEA, DMF, Ar, 3h (x2); iii. 20% piperidine DMF, Ar, 20 min (x3); iv. Fmoc-Met-OH, HATU, DIPEA, DMF, Ar, 3h (x2); c) i. 20% piperidine DMF, Ar, 20 min (x3); ii. DOTA-tris (t-Bu ester), HATU, DIPEA, DMF, Ar, 3h; d) Pd(PPh₃)₄, phenylsilane, DCM, Ar, 1h; e) i. Fmoc-Cys-OH, HATU, DIPEA, DMF, Ar, 3h (x2); ii. 20% piperidine DMF, Ar, 20 min (x3); iii. Fmoc-Glu-OtBu, HATU, DIPEA, DMF, Ar, 3h; f) i. 20% piperidine DMF, Ar, 20 min (x3); ii. N10-TFA-Pteoric acid, HATU, DIPEA, DMF; g) i. 50% NH₄OH DMF, Ar; ii. TCEP, 95/2.5/2.5 TFA/TIPS/H₂O, 1h.



Scheme 4.4. Synthesis of DOTA-MVK(EB-Folate)-OH. Reagents and conditions: a) Tolidine, HATU, DIPEA, DMF, overnight; b) i. HCl, NaNO₂, ACN, H₂O, 0°C, 30 min; ii. 1-amino-8-naphthol-2,4-disulfonic acid, NaHCO₃, H₂O, 0°C-rt, 1.5h; c) DOTA-MVK(Cys-Folate)-OH, DMSO, Ar, rt, 4h.

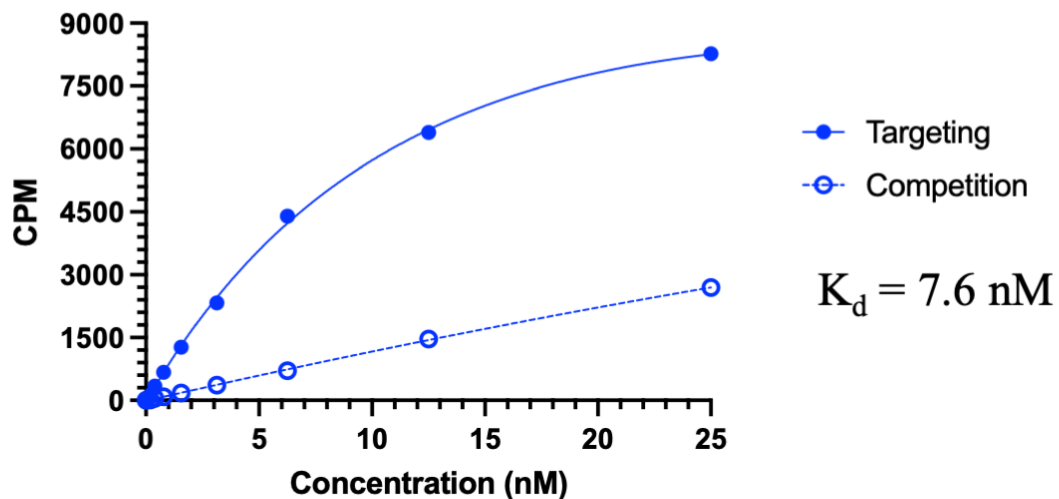


Scheme 4.5. Synthesis of DOTA-MVK(IP-Folate)-OH. Reagents and conditions: a) 4-iodophenylbutyric acid, HATU, DIPEA, DMF, rt, 3h; b) DOTA-MVK(Cys-Folate)-OH, DMSO, Ar, rt, 4h.

4.4.5 *In vitro* validation of FR targeting by DOTA-MVK(AB-Folate)-OH conjugates

We first sought to validate the functionality of our DOTA-MVK(AB-Folate)-OH conjugates through several *in vitro* assays. First, we incubated each conjugate with natural indium or lutetium then submitted samples to LC/MS for mass verification of DOTA chelation. The results of these tests are provided in Supplementary Figure S4.3. The folate targeting was next assessed by labeling each conjugate with indium-111 then performing binding studies with KB cells in the absence or presence of 100x excess of folate-glucosamine. DOTA-MVK(EB-Folate)-OH demonstrated a binding affinity of 7.6 nM, and DOTA-MVK(IP-Folate)-OH demonstrated a binding affinity of 14.0 nM. The binding of both conjugates to FR was blockaded by the incubation of folate-glucosamine, illustrating the active receptor-targeting of our conjugates. The results of these binding studies are reported in Figure 4.4. The radiopurities of these conjugates are provided in Supplementary Figure S4.4.

¹¹¹In-DOTA-MVK(EB-Folate)-OH



¹¹¹In-DOTA-MVK(IP-Folate)-OH

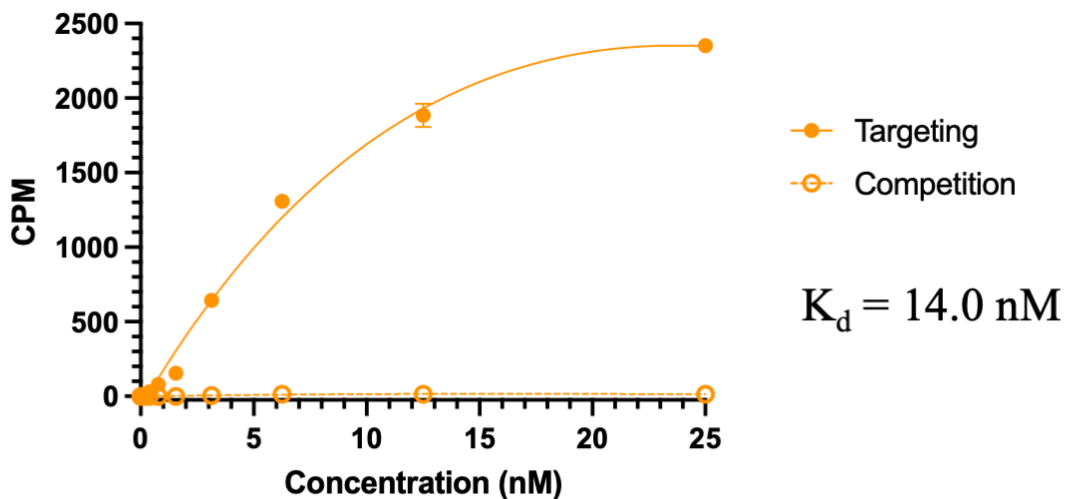
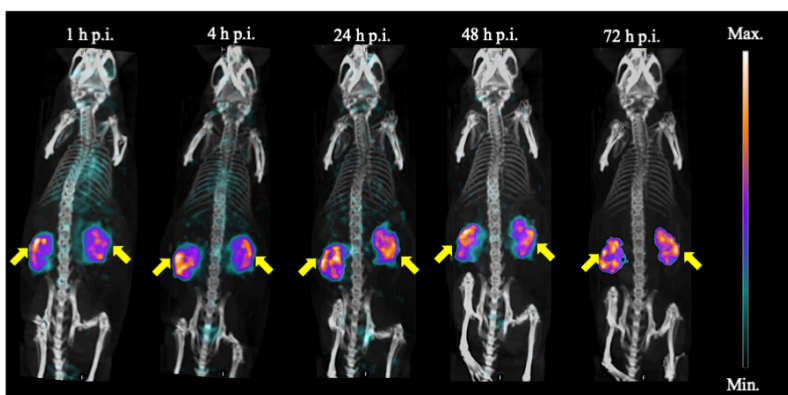


Figure 4.4. Binding of DOTA-MVK(AB-Folate)-OH conjugates radiolabeled with indium-111 to KB cells, measured by gamma counter. These studies were conducted in parallel. All samples were performed in triplicate.

4.4.6 *In vivo* evaluation of Renal Clearance and Tumor Targeting of DOTA-MVK(AB-Folate)-OH conjugates

Once we were vetted the folate-targeting of our DOTA-MVK(AB-Folate)-OH conjugates, we next evaluated their renal clearance in healthy mice. We injected healthy ND4 Swiss Webster mice, housed on folate-deficient diet for several weeks, with either ^{111}In -DOTA-MVK(EB-Folate)-OH or ^{111}In -DOTA-MVK(IP-Folate)-OH intravenously via tail vein injection ($n = 1$). At various time points, mice were anesthetized so whole-body SPECT/CT scans could be taken to compare radioactive renal retention. Both conjugates showed relatively comparable amounts of radioactivity for the first 24 hours, after which the ^{111}In -DOTA-MVK(IP-Folate)-OH appeared to clear from the kidneys, while the ^{111}In -DOTA-MVK(EB-Folate)-OH only saw modest renal clearance by 96 hours. Surprisingly however, ^{111}In -DOTA-MVK(IP-Folate)-OH showed low levels of liver uptake, unlike ^{111}In -DOTA-MVK(EB-Folate)-OH which was limited exclusively to the kidneys. All scans are shown in Figure 4.5

SPECT/CT of ^{111}In -DOTA-MVK(EB-Folate)-OH



SPECT/CT of ^{111}In -DOTA-MVK(IP-Folate)-OH

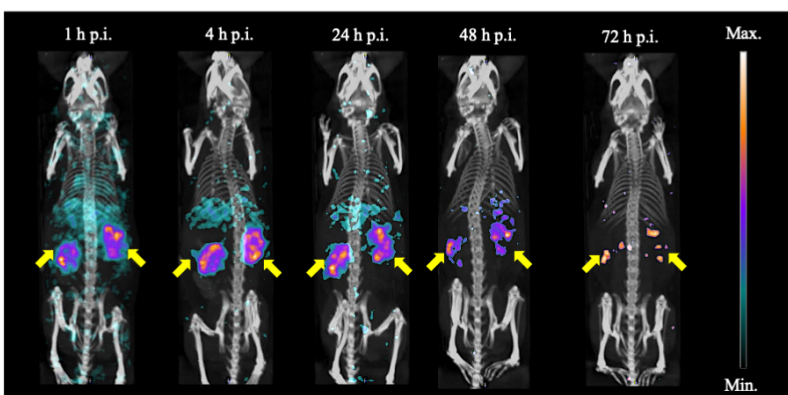


Figure 4.5. SPECT/CT of ^{111}In -DOTA-MVK(EB-Folate)-OH conjugates in healthy mice ($n = 1$). While ^{111}In -DOTA-MVK(IP-Folate)-OH demonstrated faster clearance than ^{111}In -DOTA-MVK(EB-Folate)-OH, ^{111}In -DOTA-MVK(IP-Folate)-OH also demonstrated low hepatic uptake. Yellow arrows indicate kidneys.

We were encouraged by the significant reduction in kidney retention of the DOTA-MVK(IP-Folate)-OH conjugate within 48–72 hours. Puzzled by lack of kidney clearance demonstrated by the DOTA-MVK(EB-Folate)-OH conjugate, we next sought to ascertain if there was a significant difference in tumor-to-kidney ratio with the DOTA-MVK(EB-Folate)-OH. We injected the Evans Blue conjugate radiolabeled with indium-111 into an athymic nu/nu mouse bearing an MDA-MB-231 previously housed on a folate-deficient diet for several weeks. At various time points, the mouse was anesthetized so SPECT/CT scans could be taken to compare

tumor vs. kidney retention. All scans are shown in Figure 4.6. A favorable tumor-to-kidney ratio can be visualized within 12 hours post injection.

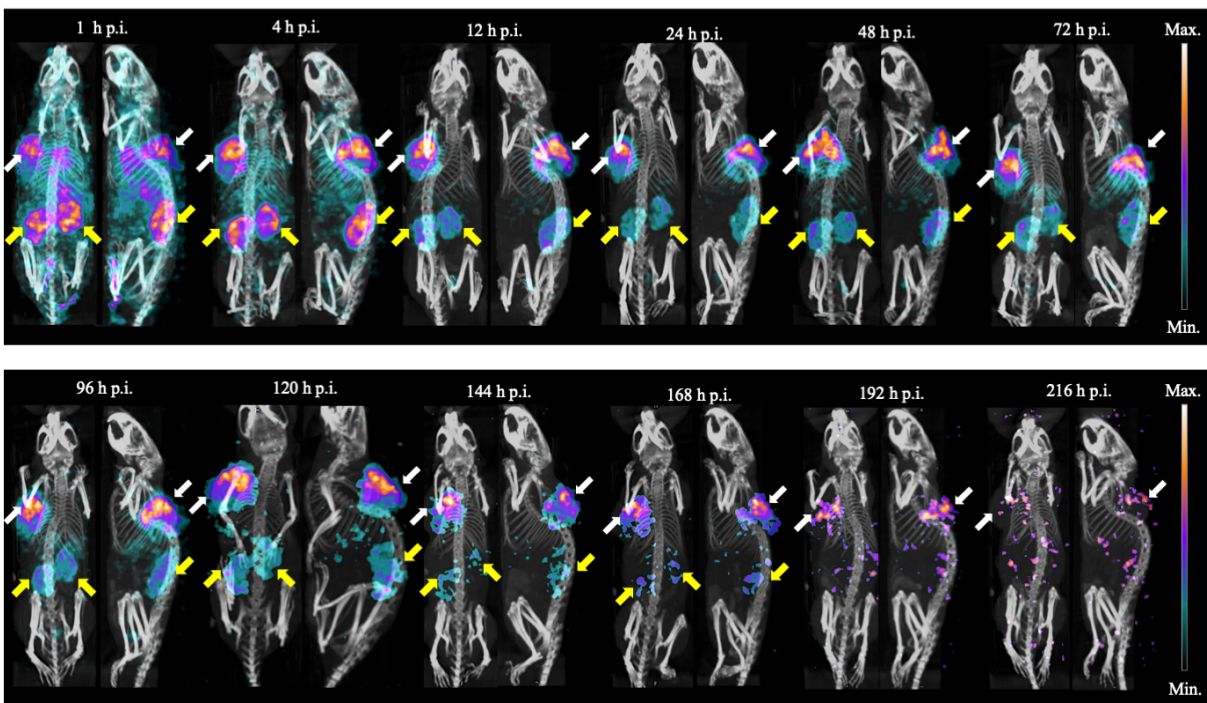


Figure 4.6. SPECT/CT scans of ^{111}In -DOTA-MVK(EB-Folate)-OH in MDA-MB-231 tumor-bearing mouse ($n = 1$). The conjugate demonstrated long-term tumor retention out to 8 days, as well as a rapid reduction of radioactivity in the kidneys within 12 hours, leading to a favorable tumor-to-kidney ratio. White arrows indicate tumor. Yellow arrows indicate kidneys.

4.4.7 Radiotherapy of ^{177}Lu -DOTA-MVK(AB-Folate)-OH conjugates in KB tumor-bearing mice

Mice were implanted with KB tumors, which were grown to approximately 300 mm³ before initiation of the radiotherapy. Mice were intravenously injected with either PBS, or DOTA-MVK(EB-Folate)-OH or DOTA(IP-Folate)-OH radiolabeled with 18 MBq of lutetium-177 on day 0. The radiopurities are indicated in Supplementary Figure S4.5 Tumor sizes and body weights were measured every other day and are provided in Figure 4.7. The therapeutic effects of both conjugates are comparable, and show significant suppression of tumor growth relative to the controls. However, while the mice injected with the iodophenyl conjugate showed little weight loss and fast recovery, the mice injected with the Evans Blue conjugate showed significant weight loss and slow recovery.

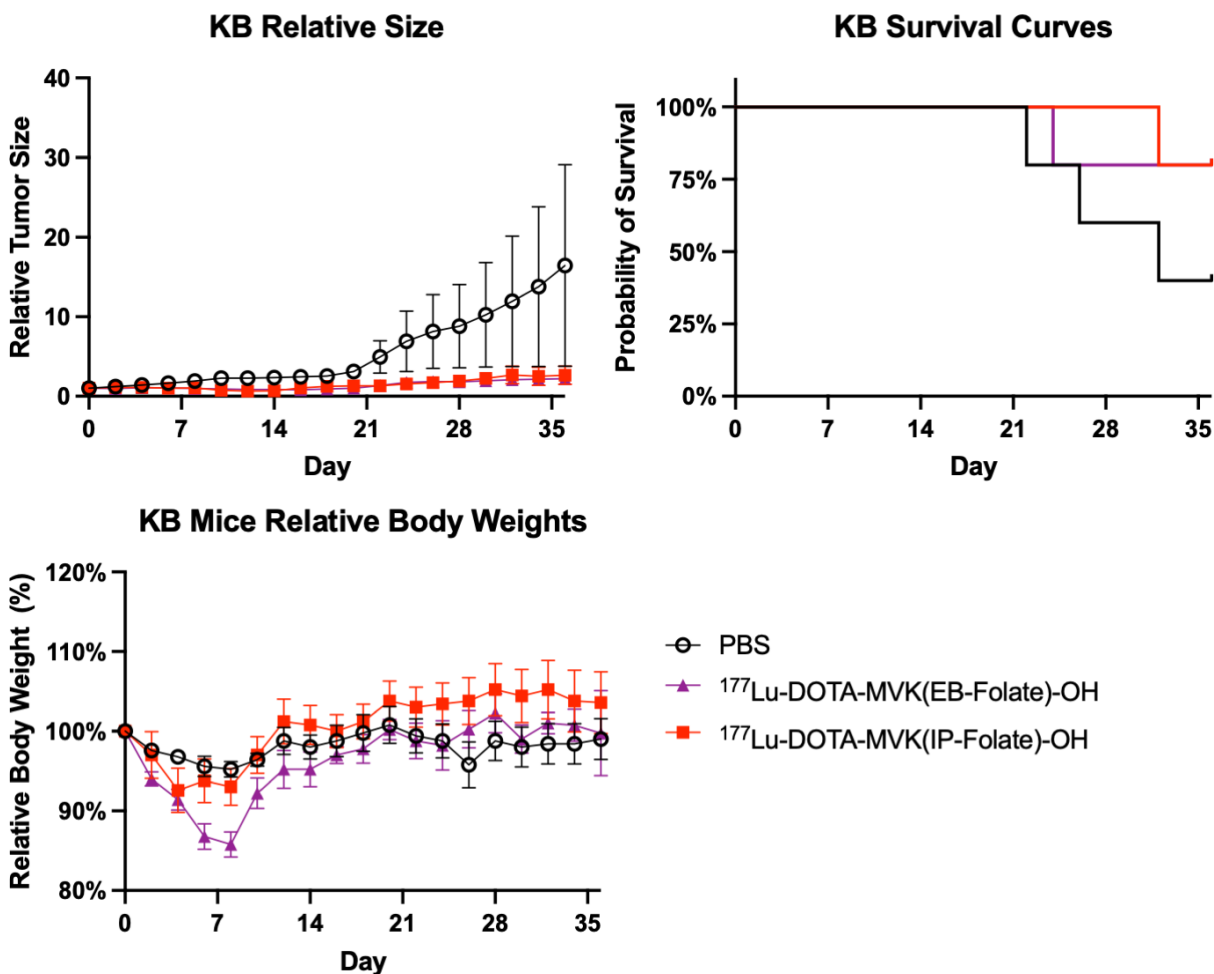
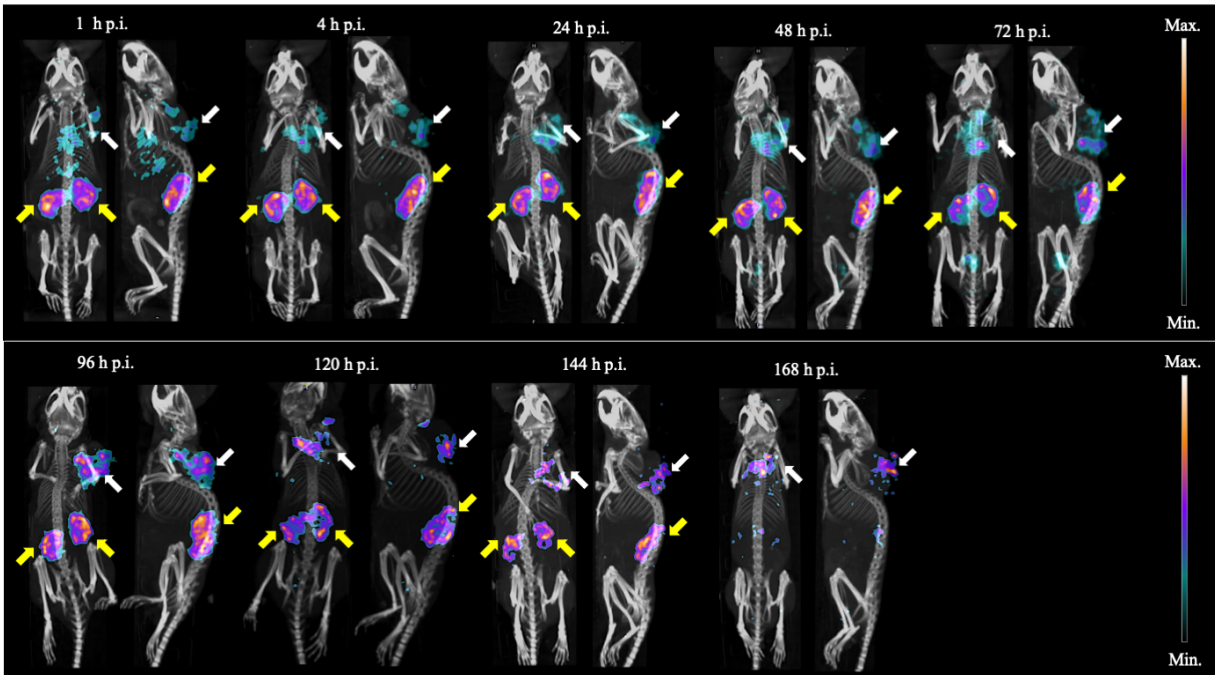


Figure 4.7. Radiotherapy of KB tumor with $^{177}\text{Lu-MVK(AB-Folate)-OH}$ conjugates. Mice ($n = 5$ per group) bearing KB tumors were injected with 5 nmol of $^{177}\text{Lu-MVK(EB-Folate)-OH}$ or $^{177}\text{Lu-MVK(IP-Folate)-OH}$ radiolabeled with 18 MBq of lutetium-177 on day 0.

SPECT/CT scans were also taken of one mouse from each radioactive group daily during the first week to evaluate relative tumor-to-kidney ratios, which are provided in Figure 4.8. The iodophenyl conjugate shows a favorable tumor-to-kidney ratio by 72 hours post injection. The Evans Blue conjugate shows a comparable amount of radioactivity in the tumor and kidneys only by 120 hours post injection and does not show a favorable tumor-to-kidney ratio until 168 hours post injection. Pictures of the tumors were also taken on a weekly basis for the first 3 weeks, which are provided in Supplementary Figure S4.6.

^{177}Lu -DOTA-MVK(EB-Folate)-OH



^{177}Lu -DOTA-MVK(IP-Folate)-OH

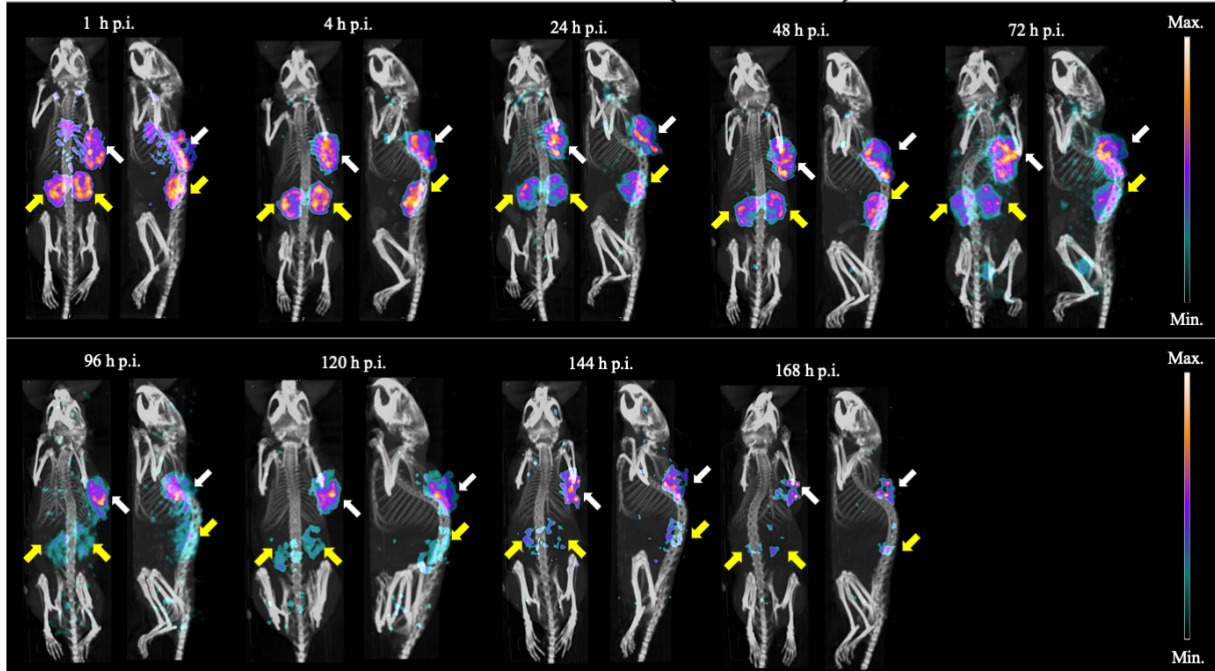


Figure 4.8. SPECT/CT scans of ^{177}Lu -DOTA-MVK(AB-Folate)-OH conjugates in KB tumor-bearing mice at therapeutic doses ($n = 1$). White arrows indicate tumors. Yellow arrows indicate kidneys.

4.5 Discussion

Due to the high uptake and sustained retention of folate conjugates, we thought it prudent to select a BBM sequence that would be cleaved as rapidly as possible. When comparing the kinetics of different BBM sequences published in the literature, the methionine-valine-lysine (MVK) sequence demonstrated the fastest kidney clearance.²⁵⁻³¹ This is likely because the MVK sequence is preferentially cleaved by multiple BBM enzymes, specifically by neutral endopeptidase (NEP) at the C-terminal lysine and by Carboxypeptidase M (CPM) at the methionine-valine amide bond. Furthermore, the effectiveness of the MVK sequence is well-elucidated, having been reported to improve the tumor-to-kidney ratio for small molecules by other labs.^{32, 34}

We first determined to investigate the hypothesis of BBM-cleavable linker facilitated renal clearance in the context of folate conjugates with a fluorescence reporter. We assembled a folate-S0456 conjugate with the MVK sequence using solid-phase synthesis (SPPS) first, then finishing with solution phase chemistry. Our fluorescence whole-body and biodistribution studies in healthy mice served as a useful proof-of-concept before proceeding to more expensive and time-intensive radioactive studies (see Fig. 4.2). Similar studies in tumor-bearing mice further demonstrated that the tumor-to-kidney ratio was improved relative to a folate-dye conjugate lacking a BBM cleavable linker, indicating that folate-targeting of tumor cells was relatively unaffected (see Fig. 4.3). We briefly explored a longer linker with a combination of BBM-cleavable sequences from different papers (see Supplemental Figure S4.7). While the kidney clearance was not significantly accelerated compared to the MVK sequence used throughout these studies, it should be noted that this longer sequence lacked a C-terminal lysine, which likely eliminated one key cleavage site in the linker.

We selected Evans Blue and iodophenyl as two albumin-binder candidates for our folate-targeted radiotherapeutic studies because they have two of the longest reported half-lives in radiotheranostics.^{20, 37, 42-44} While the Evans Blue albumin-binder has shown to be the best at improving tumor internalization, retention, and ultimately radiotherapy, it has also shown to significantly increase renal uptake and retention compared to the iodophenyl albumin-binder.³⁵ Whether the BBM-cleavable linker could counteract the effects of Evans Blue albumin-binder was uncertain and could only be determined experimentally.

The DOTA-MVK(IP-Folate)-OH conjugate showed significant clearance from the kidneys by 48–72 hours in healthy mice, which is a marked improvement over the reported renal retention

of similar radiofolates.^{20, 21} While the DOTA-MVK(EB-Folate)-OH conjugate appeared to be retained in the kidneys for at least 96 hours with minimal reduction in a healthy mouse, the tumor-to-kidney ratio in an MDA-MB-231 tumor-bearing mouse appeared significantly improved in as little as 12 hours. Based on these results, we moved forward to radiotherapy with both conjugates. Both treatment groups showed a similar repression of tumor growth compared to the control group, suggesting the tumor uptake and retention was similar regardless of the albumin-binder (see Fig. 4.7). However, the ¹⁷⁷Lu-DOTA-MVK(IP-Folate)-OH treated group showed minor body weight loss relative to the control, while the ¹⁷⁷Lu-DOTA-MVK(EB-Folate)-OH treated group showed significant and prolonged weight loss. This suggests that the kidney clearance was largely impeded by the Evans Blue albumin-binder despite the incorporation of a BBM-cleavable linker. The SPECT/CT scans of radiotherapy mice (see Fig. 4.8) showed a significant improvement in the expected tumor-to-kidney ratio of the iodophenyl conjugate by 72 hours, which is reflected in the recovery of the body weight after day 4. Meanwhile, the SPECT/CT scans of the Evans Blue conjugate did not show improvement in the expected tumor-to-kidney ratio until 168 hours, which is also reflected in the recovery of the body weight after only day 8. The discrepancy between the SPECT/CT scans for the Evans Blue conjugate in the MDA-MB-231 tumor versus the KB tumor is unclear. It is possible that the KB tumor, intended for therapy and thus was small, could not absorb as much of the injected conjugate as the MDA-MB-231 tumor, which was much larger as it was intended strictly for imaging.

Wilde et. al reported that albumin-Evans Blue complexes are absorbed from the glomerular filtrate by pinocytosis into the cells of the renal proximal tubes.⁴⁵ Because BBM enzymes are found on the surface of renal cells, the internalization of albumin-Evans Blue complexes likely denies access to the BBM conjugate and subsequent cleavage of the radioactive payload from the targeting ligand. It is possible that the administration of an amino acid solution could help mitigate the internalization of Evans Blue conjugates into renal cells.⁴⁶⁻⁴⁹ Ultimately however, the iodophenyl conjugate appears to be the superior conjugate due to the comparable tumor retention and radiotherapeutic efficacy as the Evans Blue conjugate, but without the prolonged kidney retention or toxic effects.

4.6 Conclusion

In this study, we demonstrated the first proof-of-concept that BBM enzymes could be exploited to facilitate rapid renal clearance of payloads from folate conjugates. The synthetic inclusion of such linkers is readily adaptable to standard folate synthesis protocols. Furthermore, we synthesized the first quadri-functional radioligand, comprised of a folate targeting ligand, a bifunctional chelator for radioactive payloads, an albumin-binder for increased tumor uptake, and a BBM cleavable linker for rapid renal clearance. We then evaluated the radioimaging and radiotherapy results with this quadri-functional radiofolate using either the Evans Blue or iodophenyl albumin-binder. The results of this study could promise the possibility of fluorescence-guided surgical resection of renal carcinomas, improved radioimaging of tumors near the kidneys, and the potential for folate-targeted radiotherapeutics.

4.7 References

1. Weitman, S. D.; Lark, R. H.; Coney, L. R.; Fort, D. W.; Frasca, V.; Zurawski, V. R.; Kamen, B. A., Distribution of the Folate Receptor GP38 in Normal and Malignant Cell Lines and Tissues. *Cancer research* **1992**, *52* (12), 3396.
2. Coney, L. R.; Tomassetti, A.; Carayannopoulos, L.; Frasca, V.; Kamen, B. A.; Colnaghi, M. I.; Zurawski, V. R., Cloning of a Tumor-associated Antigen: MOv18 and MOv19 Antibodies Recognize a Folate-binding Protein. *Cancer research* **1991**, *51* (22), 6125.
3. Garin-Chesa, P.; Campbell, I.; Saigo, P. E.; Lewis, J. L., Jr.; Old, L. J.; Rettig, W. J., Trophoblast and ovarian cancer antigen LK26. Sensitivity and specificity in immunopathology and molecular identification as a folate-binding protein. *The American journal of pathology* **1993**, *142* (2), 557-567.
4. Low, P. S.; Henne, W. A.; Doorneweerd, D. D., Discovery and Development of Folic-Acid-Based Receptor Targeting for Imaging and Therapy of Cancer and Inflammatory Diseases. *Accounts of Chemical Research* **2008**, *41* (1), 120-129.
5. Low, P. S.; Kularatne, S. A., Folate-targeted therapeutic and imaging agents for cancer. *Current Opinion in Chemical Biology* **2009**, *13* (3), 256-262.
6. Parker, N.; Turk, M. J.; Westrick, E.; Lewis, J. D.; Low, P. S.; Leamon, C. P., Folate receptor expression in carcinomas and normal tissues determined by a quantitative radioligand binding assay. *Analytical Biochemistry* **2005**, *338* (2), 284-293.
7. Shen, J.; Hu, Y.; Putt, K. S.; Singhal, S.; Han, H.; Visscher, D. W.; Murphy, L. M.; Low, P. S., Assessment of folate receptor alpha and beta expression in selection of lung and pancreatic cancer patients for receptor targeted therapies. *Oncotarget* **2017**, *9* (4), 4485-4495.

8. Shen, J.; Putt, K. S.; Visscher, D. W.; Murphy, L.; Cohen, C.; Singhal, S.; Sandusky, G.; Feng, Y.; Dimitrov, D. S.; Low, P. S., Assessment of folate receptor- β expression in human neoplastic tissues. *Oncotarget* **2015**, *6* (16), 14700-14709.
9. Saul, J. M.; Annapragada, A.; Natarajan, J. V.; Bellamkonda, R. V., Controlled targeting of liposomal doxorubicin via the folate receptor in vitro. *Journal of Controlled Release* **2003**, *92* (1), 49-67.
10. Crane, L. M. A.; Arts, H. J. G.; van Oosten, M.; Low, P. S.; van der Zee, A. G. J.; van Dam, G. M.; Bart, J., The effect of chemotherapy on expression of folate receptor-alpha in ovarian cancer. *Cellular Oncology* **2012**, *35* (1), 9-18.
11. Srinivasarao, M.; Galliford, C. V.; Low, P. S., Principles in the design of ligand-targeted cancer therapeutics and imaging agents. *Nat Rev Drug Discov* **2015**, *14* (3), 203-19.
12. Holm, J.; Hansen, S. I.; Høier-Madsen, M.; Bostad, L., A high-affinity folate binding protein in proximal tubule cells of human kidney. *Kidney International* **1992**, *41* (1), 50-55.
13. Birn, H.; Spiegelstein, O.; Christensen, E. I.; Finnell, R. H., Renal Tubular Reabsorption of Folate Mediated by Folate Binding Protein 1. *Journal of the American Society of Nephrology* **2005**, *16* (3), 608.
14. Sandoval, R. M.; Kennedy, M. D.; Low, P. S.; Molitoris, B. A., Uptake and trafficking of fluorescent conjugates of folic acid in intact kidney determined using intravital two-photon microscopy. *American Journal of Physiology-Cell Physiology* **2004**, *287* (2), C517-C526.
15. Müller, C.; Vlahov, I. R.; Santhapuram, H. K. R.; Leamon, C. P.; Schibli, R., Tumor targeting using ^{67}Ga -DOTA-Bz-folate — investigations of methods to improve the tissue distribution of radiofolates. *Nuclear Medicine and Biology* **2011**, *38* (5), 715-723.
16. Müller, C.; Mindt, T. L.; de Jong, M.; Schibli, R., Evaluation of a novel radiofolate in tumour-bearing mice: promising prospects for folate-based radionuclide therapy. *European Journal of Nuclear Medicine and Molecular Imaging* **2009**, *36* (6), 938-946.
17. Müller, C.; Brühlmeier, M.; Schubiger, P. A.; Schibli, R., Effects of Antifolate Drugs on the Cellular Uptake of Radiofolates In Vitro and In Vivo. *Journal of Nuclear Medicine* **2006**, *47* (12), 2057-2064.
18. Müller, C.; Schibli, R.; Forrer, F.; Krenning, E. P.; de Jong, M., Dose-dependent effects of (anti)folate preinjection on $^{99\text{m}}\text{Tc}$ -radiofolate uptake in tumors and kidneys. *Nuclear Medicine and Biology* **2007**, *34* (6), 603-608.
19. Müller, C.; Schibli, R.; Krenning, E. P.; de Jong, M., Pemetrexed Improves Tumor Selectivity of ^{111}In -DTPA-Folate in Mice with Folate Receptor-Positive Ovarian Cancer. *Journal of Nuclear Medicine* **2008**, *49* (4), 623-629.

20. Müller, C.; Struthers, H.; Winiger, C.; Zhernosekov, K.; Schibli, R., DOTA Conjugate with an Albumin-Binding Entity Enables the First Folic Acid–Targeted ^{177}Lu -Radionuclide Tumor Therapy in Mice. *Journal of Nuclear Medicine* **2013**, *54* (1), 124-131.
21. Farkas, R.; Siwowska, K.; Ametamey, S. M.; Schibli, R.; van der Meulen, N. P.; Müller, C., ^{64}Cu - and ^{68}Ga -Based PET Imaging of Folate Receptor-Positive Tumors: Development and Evaluation of an Albumin-Binding NODAGA–Folate. *Molecular Pharmaceutics* **2016**, *13* (6), 1979-1987.
22. Radford, L. L.; Fernandez, S.; Beacham, R.; El Sayed, R.; Farkas, R.; Benešová, M.; Müller, C.; Lapi, S. E., New ^{55}Co -labeled Albumin-Binding Folate Derivatives as Potential PET Agents for Folate Receptor Imaging. *Pharmaceutics* **2019**, *12* (4).
23. Guzik, P.; Benešová, M.; Ratz, M.; Monné Rodríguez, J. M.; Deberle, L. M.; Schibli, R.; Müller, C., Preclinical evaluation of 5-methyltetrahydrofolate-based radioconjugates—new perspectives for folate receptor–targeted radionuclide therapy. *European Journal of Nuclear Medicine and Molecular Imaging* **2021**, *48* (4), 972-983.
24. Kenny, A. J.; Maroux, S., Topology of microvillar membrane hydrolases of kidney and intestine. *Physiological Reviews* **1982**, *62* (1), 91-128.
25. Arano, Y.; Fujioka, Y.; Akizawa, H.; Ono, M.; Uehara, T.; Wakisaka, K.; Nakayama, M.; Sakahara, H.; Konishi, J.; Saji, H., Chemical Design of Radiolabeled Antibody Fragments for Low Renal Radioactivity Levels. *Cancer research* **1999**, *59* (1), 128-134.
26. Uehara, T.; Koike, M.; Nakata, H.; Hanaoka, H.; Iida, Y.; Hashimoto, K.; Akizawa, H.; Endo, K.; Arano, Y., Design, Synthesis, and Evaluation of [^{188}Re]Organorhenium-Labeled Antibody Fragments with Renal Enzyme-Cleavable Linkage for Low Renal Radioactivity Levels. *Bioconjugate Chemistry* **2007**, *18* (1), 190-198.
27. Akizawa, H.; Uehara, T.; Arano, Y., Renal uptake and metabolism of radiopharmaceuticals derived from peptides and proteins. *Advanced Drug Delivery Reviews* **2008**, *60* (12), 1319-1328.
28. Akizawa, H.; Imajima, M.; Hanaoka, H.; Uehara, T.; Satake, S.; Arano, Y., Renal Brush Border Enzyme-Cleavable Linkages for Low Renal Radioactivity Levels of Radiolabeled Antibody Fragments. *Bioconjugate Chemistry* **2013**, *24* (2), 291-299.
29. Suzuki, C.; Uehara, T.; Kanazawa, N.; Wada, S.; Suzuki, H.; Arano, Y., Preferential Cleavage of a Tripeptide Linkage by Enzymes on Renal Brush Border Membrane To Reduce Renal Radioactivity Levels of Radiolabeled Antibody Fragments. *Journal of Medicinal Chemistry* **2018**, *61* (12), 5257-5268.
30. Uehara, T.; Yokoyama, M.; Suzuki, H.; Hanaoka, H.; Arano, Y., A Gallium-67/68–Labeled Antibody Fragment for Immuno-SPECT/PET Shows Low Renal Radioactivity Without Loss of Tumor Uptake. *Clinical Cancer Research* **2018**, *24* (14), 3309-3316.

31. Uehara, T.; Kanazawa, N.; Suzuki, C.; Mizuno, Y.; Suzuki, H.; Hanaoka, H.; Arano, Y., Renal Handling of ^{99m}Tc-Labeled Antibody Fab Fragments with a Linkage Cleavable by Enzymes on Brush Border Membrane. *Bioconjugate Chemistry* **2020**, *31* (11), 2618-2627.
32. Vaidyanathan, G.; Kang, C. M.; McDougald, D.; Minn, I.; Brummet, M.; Pomper, M. G.; Zalutsky, M. R., Brush border enzyme-cleavable linkers: Evaluation for reducing renal uptake of radiolabeled prostate-specific membrane antigen inhibitors. *Nuclear Medicine and Biology* **2018**, *62-63*, 18-30.
33. Bendre, S.; Zhang, Z.; Kuo, H.-T.; Rousseau, J.; Zhang, C.; Merkens, H.; Roxin, Á.; Bénard, F.; Lin, K.-S., Evaluation of Met-Val-Lys as a Renal Brush Border Enzyme-Cleavable Linker to Reduce Kidney Uptake of ⁶⁸Ga-Labeled DOTA-Conjugated Peptides and Peptidomimetics. *Molecules* **2020**, *25* (17), 3854.
34. Zhang, M.; Jacobson, O.; Kiesewetter, D. O.; Ma, Y.; Wang, Z.; Lang, L.; Tang, L.; Kang, F.; Deng, H.; Yang, W.; Niu, G.; Wang, J.; Chen, X., Improving the Theranostic Potential of Exendin 4 by Reducing the Renal Radioactivity through Brush Border Membrane Enzyme-Mediated Degradation. *Bioconjugate Chemistry* **2019**, *30* (6), 1745-1753.
35. Wang, Z.; Tian, R.; Niu, G.; Ma, Y.; Lang, L.; Szajek, L. P.; Kiesewetter, D. O.; Jacobson, O.; Chen, X., Single Low-Dose Injection of Evans Blue Modified PSMA-617 Radioligand Therapy Eliminates Prostate-Specific Membrane Antigen Positive Tumors. *Bioconjugate Chemistry* **2018**, *29* (9), 3213-3221.
36. Chen, X.; Weiss, O. J. Chemical Conjugates of Evans Blue Derivatives and their use as Radiotherapy and Imaging Agents for Targeting Prostate Cancer. 2019.
37. Chen, H.; Jacobson, O.; Niu, G.; Weiss, I. D.; Kiesewetter, D. O.; Liu, Y.; Ma, Y.; Wu, H.; Chen, X., Novel “Add-On” Molecule Based on Evans Blue Confers Superior Pharmacokinetics and Transforms Drugs to Theranostic Agents. *Journal of Nuclear Medicine* **2017**, *58* (4), 590-597.
38. Leamon, C. P.; Parker, M. A.; Vlahov, I. R.; Xu, L.-C.; Reddy, J. A.; Vetzal, M.; Douglas, N., Synthesis and Biological Evaluation of EC20: A New Folate-Derived, ^{99m}Tc-Based Radiopharmaceutical. *Bioconjugate Chemistry* **2002**, *13* (6), 1200-1210.
39. Bendre, S.; Zhang, Z.; Kuo, H.-T.; Rousseau, J.; Zhang, C.; Merkens, H.; Roxin, Á.; Bénard, F.; Lin, K.-S., Evaluation of Met-Val-Lys as a Renal Brush Border Enzyme-Cleavable Linker to Reduce Kidney Uptake of ⁶⁸Ga-Labeled DOTA-Conjugated Peptides and Peptidomimetics. *Molecules* **2020**, *25* (17).
40. Roy, J.; Hettiarachchi, S. U.; Kaake, M.; Mukkamala, R.; Low, P. S., Design and validation of fibroblast activation protein alpha targeted imaging and therapeutic agents. *Theranostics* **2020**, *10* (13), 5778-5789.
41. Lv, P.-C.; Roy, J.; Putt, K. S.; Low, P. S., Evaluation of a Carbonic Anhydrase IX-Targeted Near-Infrared Dye for Fluorescence-Guided Surgery of Hypoxic Tumors. *Molecular Pharmaceutics* **2016**, *13* (5), 1618-1625.

42. Lau, J.; Jacobson, O.; Niu, G.; Lin, K.-S.; Bénard, F.; Chen, X., Bench to Bedside: Albumin Binders for Improved Cancer Radioligand Therapies. *Bioconjugate Chemistry* **2019**, *30* (3), 487-502.
43. Zorzi, A.; Linciano, S.; Angelini, A., Non-covalent albumin-binding ligands for extending the circulating half-life of small biotherapeutics. *MedChemComm* **2019**, *10* (7), 1068-1081.
44. Tian, R.; Jacobson, O.; Niu, G.; Kiesewetter, D. O.; Wang, Z.; Zhu, G.; Ma, Y.; Liu, G.; Chen, X., Evans Blue Attachment Enhances Somatostatin Receptor Subtype-2 Imaging and Radiotherapy. *Theranostics* **2018**, *8* (3), 735-745.
45. Wilde, W. S.; Legan, S. J.; Southwick, A. K., Reabsorption of Albumin-Evans Blue Via Membrane Vesicles of Proximal Kidney Tubule Cells. *Proceedings of the Society for Experimental Biology and Medicine* **1968**, *127* (3), 776-781.
46. Kobayashi, H.; Yoo, T. M.; Kim, I. S.; Kim, M.-K.; Le, N.; Webber, K. O.; Pastan, I.; Paik, C. H.; Eckelman, W. C.; Carrasquillo, J. A., L-Lysine Effectively Blocks Renal Uptake of ¹²⁵I- or ^{99m}Tc-labeled Anti-Tac Disulfide-stabilized Fv Fragment. *Cancer research* **1996**, *56* (16), 3788-3795.
47. Rolleman, E. J.; Valkema, R.; de Jong, M.; Kooij, P. P.; Krenning, E. P., Safe and effective inhibition of renal uptake of radiolabelled octreotide by a combination of lysine and arginine. *European Journal of Nuclear Medicine and Molecular Imaging* **2003**, *30* (1), 9-15.
48. Verwijnen, S. M.; Krenning, E. P.; Valkema, R.; Huijmans, J. G. M.; de Jong, M., Oral Versus Intravenous Administration of Lysine: Equal Effectiveness in Reduction of Renal Uptake of [¹¹¹In-DTPA] Octreotide. *Journal of Nuclear Medicine* **2005**, *46* (12), 2057.
49. Lin, Y.-C.; Hung, G.-U.; Luo, T.-Y.; Tsai, S.-C.; Sun, S.-S.; Hsia, C.-C.; Chen, S.-L.; Lin, W.-Y., Reducing renal uptake of ¹¹¹In-DOTATOC: A comparison among various basic amino acids. *Annals of Nuclear Medicine* **2007**, *21* (1), 79.

4.8 Appendix C. Supplemental Information

Additional data further validating our findings are provided below.

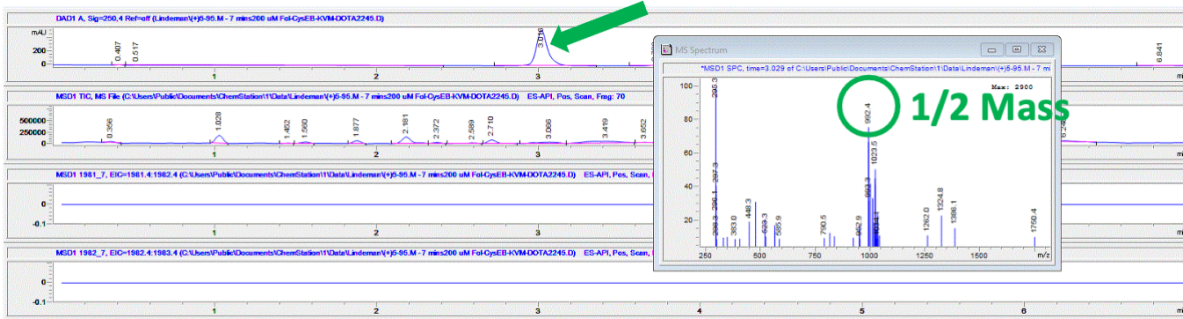
S0456-MVK(Folate)-OH

LC-MS: $[MH]^+ = 1013.8; 676.4$ (m/z), calc. = 2026.7



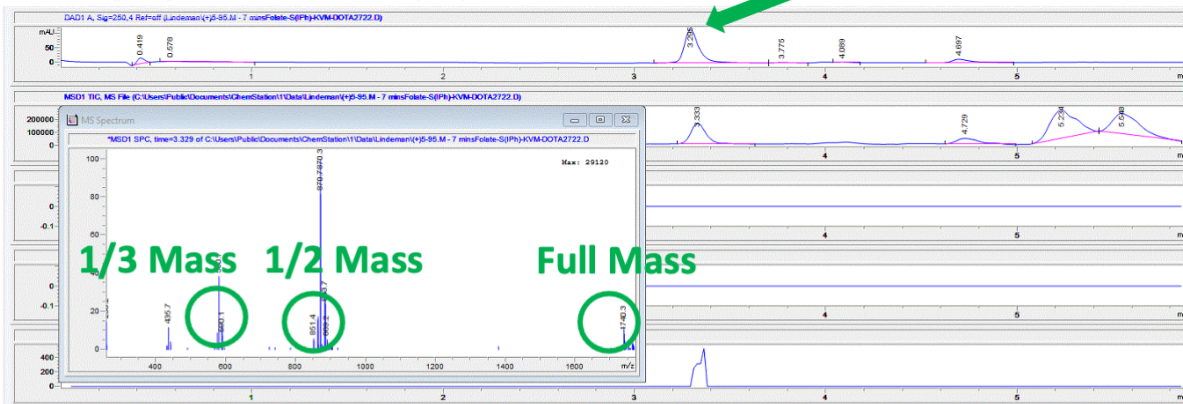
DOTA-MVK(EB-Folate)-OH

LC-MS: $[MH]^+ = 992.4$ (m/z), calc. = 1983.2

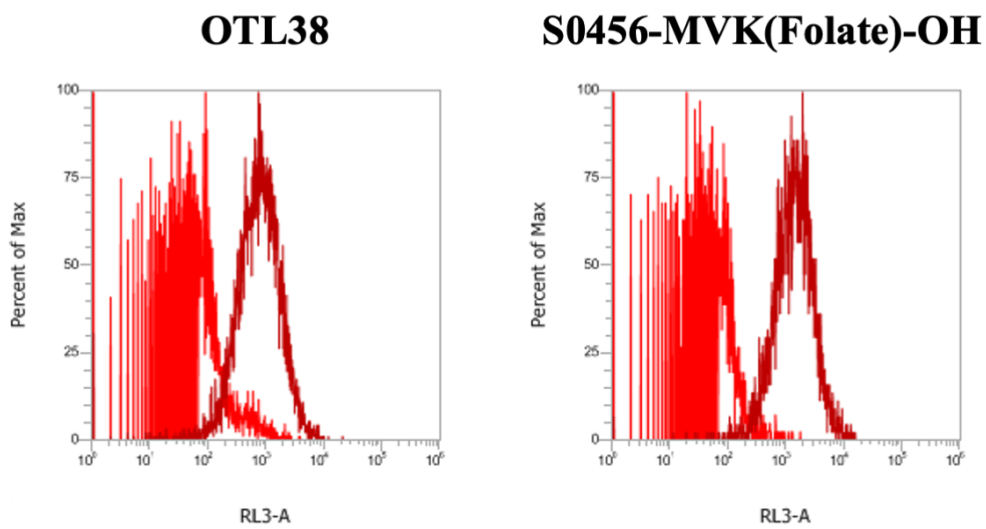


DOTA-MVK(IP-Folate)-OH

LC-MS: $[MH]^+ = 1702; 851.4; 567$ (m/z), calc. = 1701.7



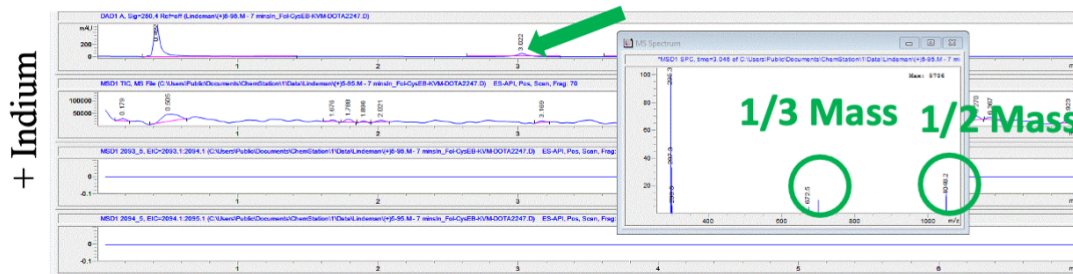
Supplementary Figure S4.1 LC/MS Analyses of Payload-MVK(Folate)-OH Conjugates.



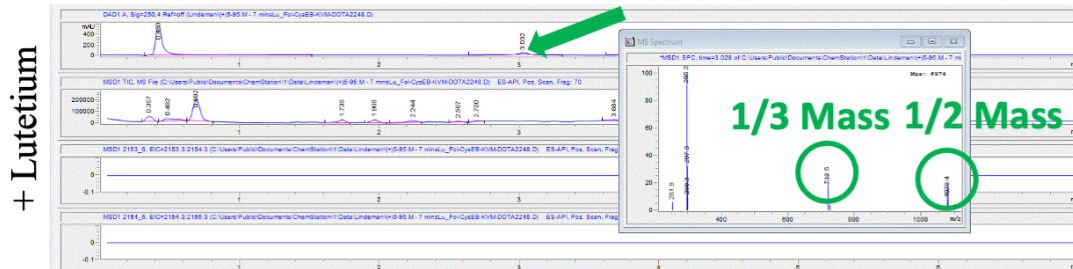
Supplementary Figure S4.2. Competition of Folate-S0456 conjugates on flow cytometry. 50 nM of either OTL38 or S0456-MVK(Folate)-OH was incubated with KB cells in the absence (dark red histogram) or presence of 100x of folate-glucosamine (bright red histogram).

DOTA-MVK(EB-Folate)-OH

$^{nat}\text{In-DOTA-MVK(EB-Fol)-OH}$. LC-MS: $[\text{MH}]^+ = 1047.2; 697 \text{ (m/z), calc.} = 1981.7 - 3 + 114.8 = 2093.5$

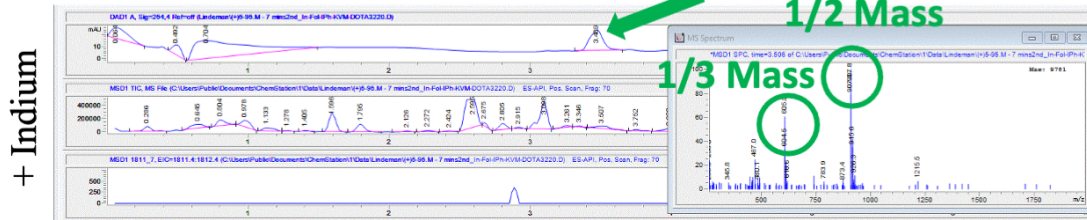


$^{nat}\text{Lu-DOTA-MVK(EB-Fol)-OH}$. LC-MS: $[\text{MH}]^+ = 1078.4; 719.5 \text{ (m/z), calc.} = 1981.7 - 3 + 175.0 = 2153.7$

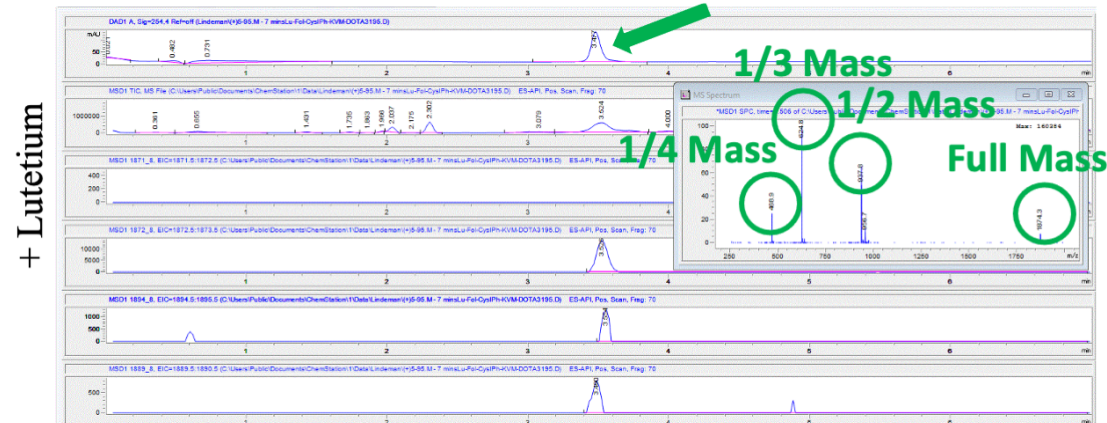


DOTA-MVK(IP-Folate)-OH

$^{nat}\text{In-DOTA-MVK(IP-Fol)-OH}$. LC-MS: $[\text{MH}]^+ = 907.8; 604.5 \text{ (m/z), calc.} = 1701.7 - 3 + 114.8 = 1813.5$

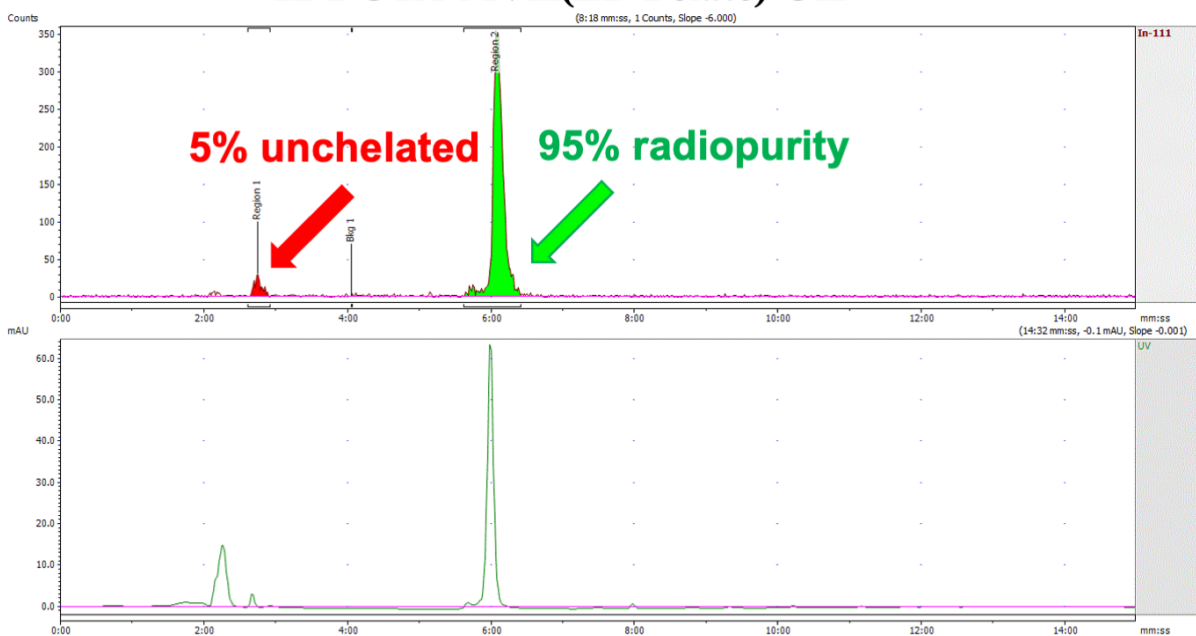


$^{nat}\text{Lu-DOTA-MVK(IP-Fol)-OH}$. LC-MS: $[\text{MH}]^+ = 1874.3; 937.8; 624.8; 468.9 \text{ (m/z), calc.} = 1701.7 - 3 + 175.0 = 1873.7$

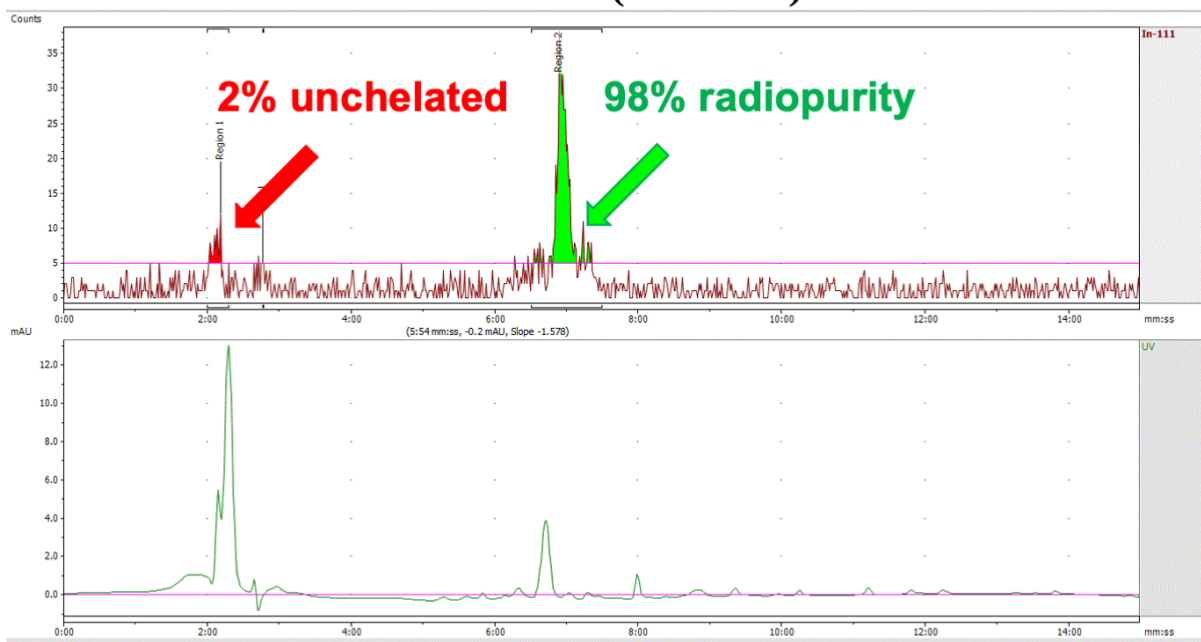


Supplementary Figure S4.3. LC/MS Analyses of DOTA-MVK(AB-Folate)OH Conjugate Cold Chelations.

¹¹¹In-DOTA-MVK(EB-Folate)-OH

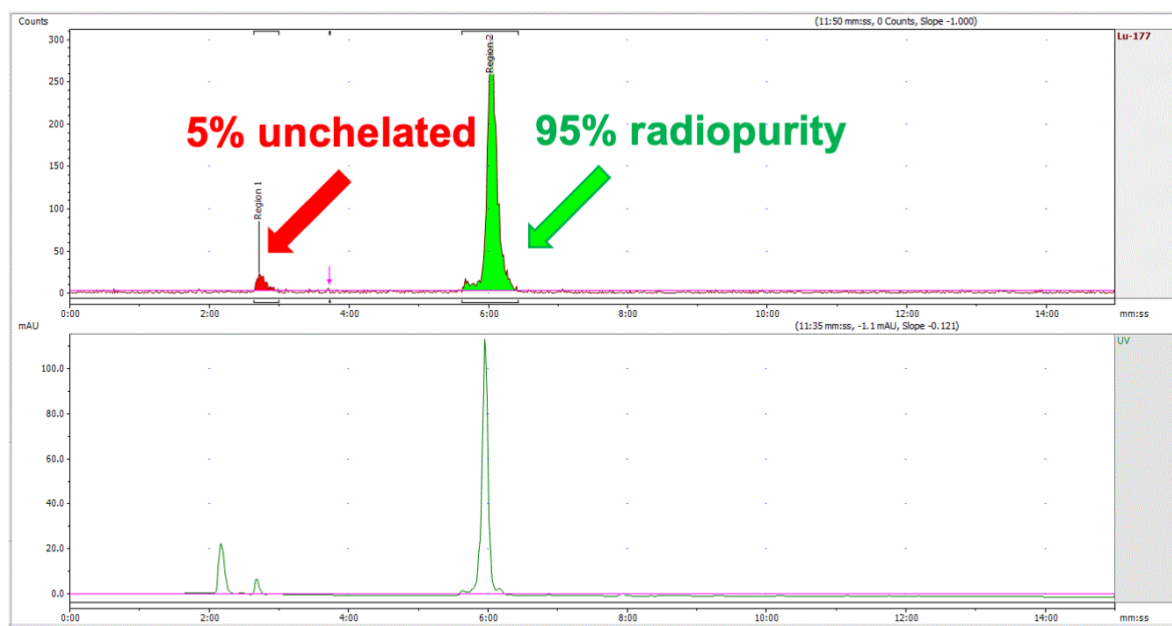


¹¹¹In-DOTA-MVK(IP-Folate)-OH

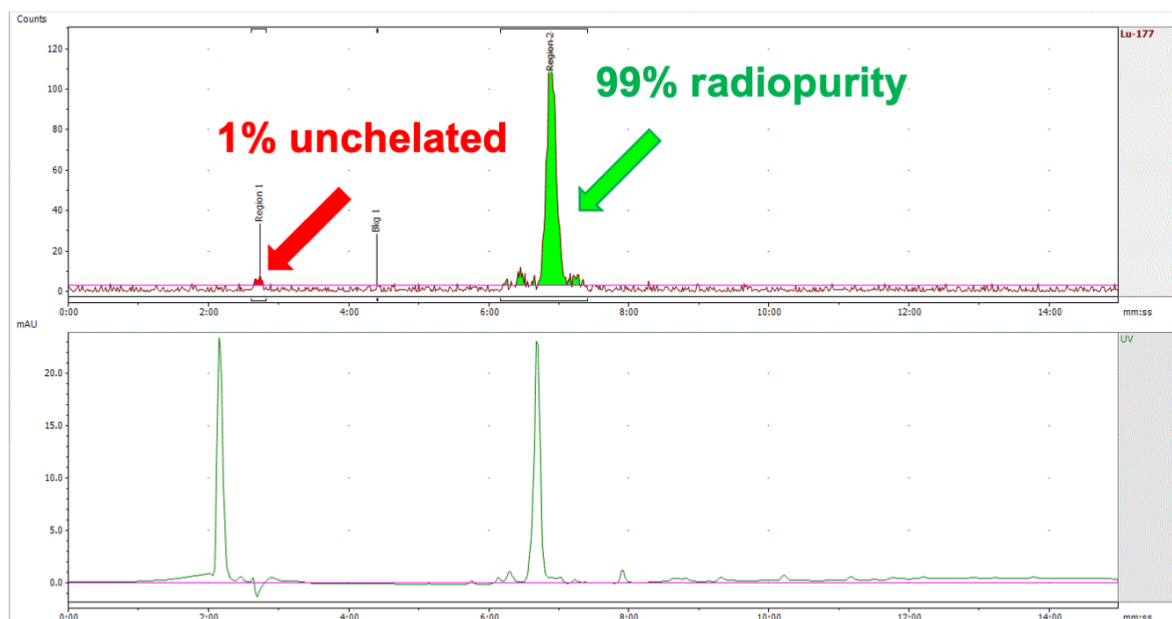


Supplementary Figure S4.4. Representative radiochromatograms of DOTA-MVK(Folate)-OH radiolabeled with indium-111.

^{177}Lu -DOTA-MVK(EB-Folate)-OH

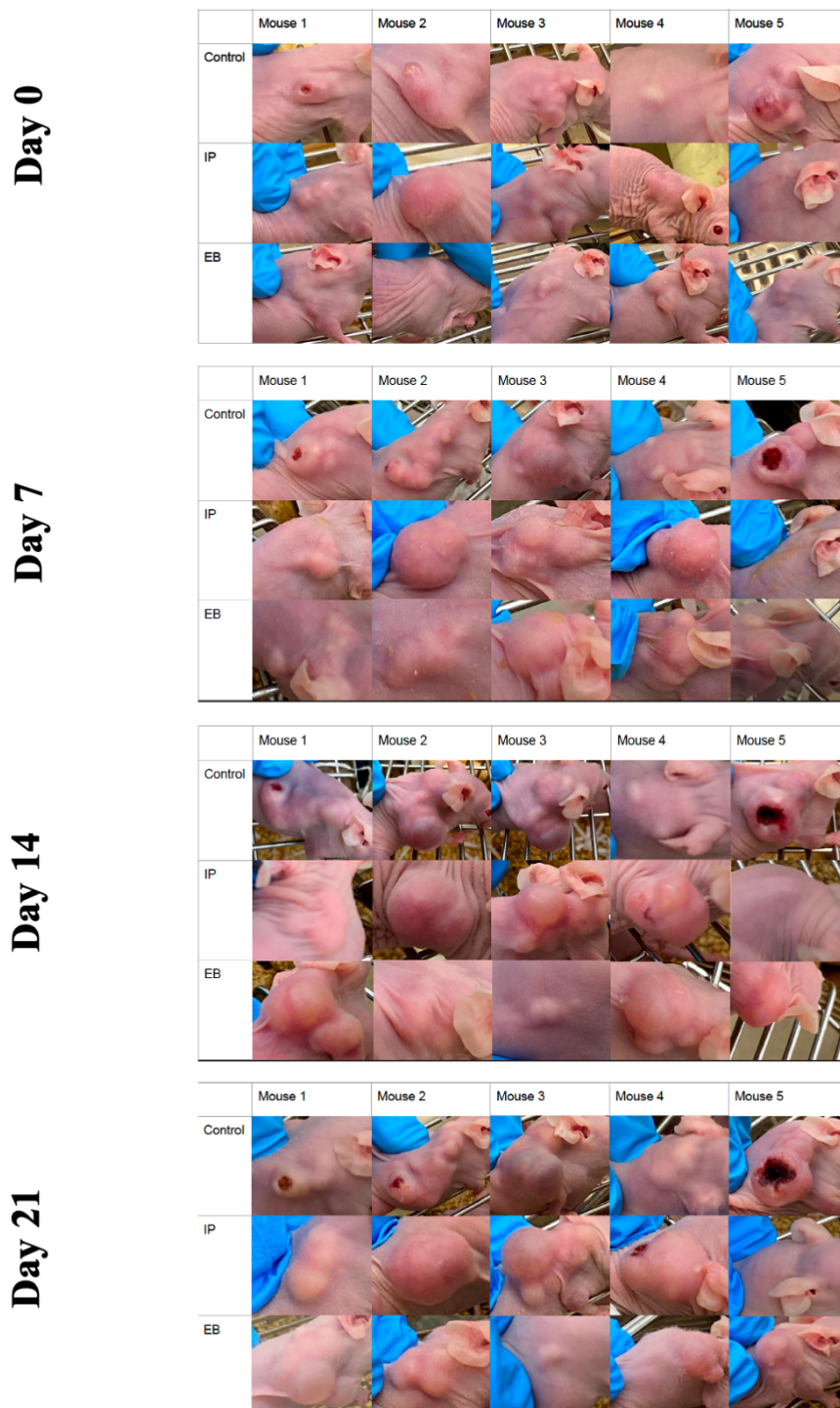


^{177}Lu -DOTA-MVK(IP-Folate)-OH



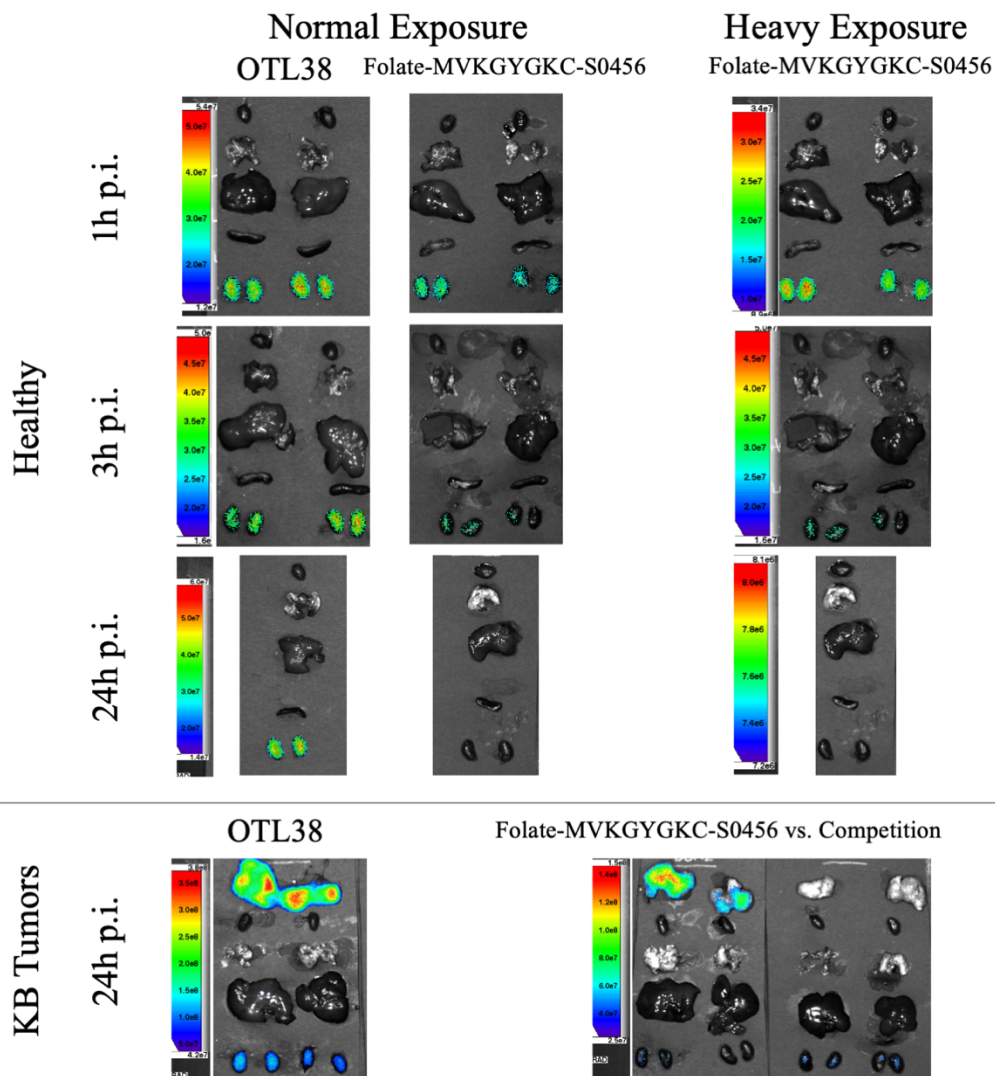
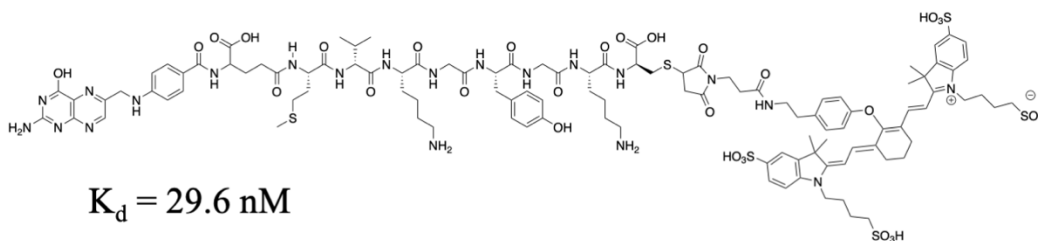
Supplementary Figure S4.5. Representative radiochromatograms of DOTA-MVK(Folate)-OH radiolabeled with lutetium-177.

Pictures of KB Tumors from Folate-DOTA Conjugate Radiotherapy



Supplementary Figure S4.6. Pictures of KB tumors throughout radiotherapy study with ^{177}Lu -MVK(IP-Folate)-OH or ^{177}Lu -MVK(EB-Folate)-OH.

Folate-MVK-GY-GK-C-S0456



Supplementary Figure S4.7. Parallel studies done with a combination of BBM-enzyme cleavable sequences within the linker. Organs in biodistribution shown from top to bottom: (Tumor) heart, lungs, liver, spleen, kidneys.

CURRICULUM VITA

CONTACT INFORMATION

- **Professional Address:** 720 Clinic Drive, West Lafayette, Indiana 47906, USA
- **LinkedIn Profile:** [linkedin.com/in/spencer-lindeman/](https://www.linkedin.com/in/spencer-lindeman/)
- **ORCID:** <https://orcid.org/0000-0001-5260-9270>

EDUCATION

Purdue University, Department of Chemistry *West Lafayette, IN*
Ph.D. in Chemistry, Supervisor: Dr. Philip S. Low *Graduation: 08/2021*

Brigham Young University, Department of Chemistry and Biochemistry *Provo, UT*
B.S. in Biochemistry, Minor in Mathematics *Graduated: 08/2014*

ACADEMIA EXPERIENCE

Purdue University, Department of Chemistry *10/2015 - present*
Research Assistant, Supervisor: Dr. Philip S. Low

Project 1: Ligand-targeted delivery of radioimaging and radiotherapeutic agents to cancer

- Designed and synthesized targeting ligands that bind to tumor and tumor stromal cells (e.g. FAP, folate)
- Purified synthetic products by flash chromatography or reverse-phase chromatography
- Characterized synthetic products on LC/MS and NMR
- Evaluated the performance of synthesized ligands *in vitro* using whole cell-based assays (e.g. binding curves, displacement assays)
- Cultured and implanted tumor xenografts in mice for *in vivo* imaging and therapy studies
- Conducted SPECT/ or PET/CT scans of tumor-bearing mice, then reconstructed and processed the data
- Conducted radioactive biodistribution studies
- Conducted radiotherapy studies in tumor-bearing mice

Project 2: Ligand-targeted delivery of inhibitors and imaging agents to IPF

- Designed, synthesized, purified, and characterized targeting ligands that bind to pathogenic fibroblasts in fibrotic lung
- Generated stably transfected cell lines that express FAP α receptor for *in vitro* evaluation of targeting ligands
- Surgically induced pulmonary fibrosis in mice for the *in vivo* evaluation of targeting ligands
- Conducted optimal imaging studies with the targeting ligands conjugated to NIR dyes
- Collaborated with a team of researchers to develop a FAP ligand-PI3K inhibitor and a folate-TLR7 agonist as novel therapeutics to reduce the fibrotic burden in pulmonary fibrosis

Other Duties

Lab Safety Officer, oversaw safety compliance and documentation of all lab personnel

Undergraduate Coordinator, oversaw placement and documentation of undergraduate researchers

BYU, Department of Chemistry and Biochemistry *06/2012 – 06/2014*
Research Assistant, Supervisor: Dr. Jaron C. Hansen

Project: Pretreatment of biomass to facilitate maximum anaerobic conversion to biofuel

- Pretreated biomass with bacteria or photocatalyzed UV radiation for anaerobic digestion
- Analytically measured biogas production via isothermal microcalorimetry and data analysis

Research Assistant, Supervisor: Dr. Richard K. Watt *02/2013 – 06/2014*

Project: Generation of hydrogen gas from biomolecules using solar energy

- Measured hydrogen gas evolution by UV radiation of methyl viologen via gas chromatography

PUBLICATIONS & PATENTS

- Low, P.S.; Srinivasarao, M.; Lindeman, S.D.; Gardeen, S.S. Folate targeted imaging and therapy agent with albumin-binders and brush border membrane enzyme cleavable linkers. Provisional Patent. 63/188,910.
- Low, P.S.; Srinivasarao, M.; Lindeman, S.D.; Mukkamala, R. Novel radiometal binding compounds for theranostics of fibroblast-activation protein-positive (FAP+) cancers. Provisional Patent. 62/200,593.
- Hettiarachchi, S.U.; Li, Y.H.; Roy, J.; Zhang, F.; Puchulu-Campanella, E.; Lindeman, S.D.; Srinivasarao, M.; Tsoyi, K.; Xiaoliang, L.; Ayaub, E.; Nickerson-Nutter, C.; Rosas, I.O.; Low, P.S. Targeted inhibition of PI3 kinase/mTOR specifically in fibrotic lung fibroblasts suppresses pulmonary fibrosis in experimental models. *Science translational medicine* 2020. <https://doi.org/10.1126/scitranslmed.aay3724>
- Zhang, F.; Wang, B.; Puchulu-Campanella, E.; Li Y.H.; Hettiarachchi, S.U.; Lindeman, S.D.; Rout, S.; Srinivasarao, M.; Cox, A.; Ayaub, E.; Tsoyi, K.; Nickerson-Nutter, C.; Rosas, I.O.; Low, P.S. Reprogramming of profibrotic macrophages for treatment of bleomycin-induced pulmonary fibrosis. *EMBO molecular medicine* 2020. <https://doi.org/10.15252/emmm.202012034>
- Low, P.S.; Lindeman, S.D.; Mukkamala, R. Fibroblast Activation Protein (FAP)-Targeted Antifibrotic Therapy. WO/PCT/US21/15907.

PRESENTATIONS

- F. Zhang, B. Wang, E. Puchulu-Campanella, Y.H. Li, S.U. Hettiarachchi, S. Lindeman, S. Rout, M. Srinivasarao, A. Cox, E. A. Ayaub, K. Tsoyi, C. Nickerson-Nutter, I.O. Rosas, P.S. Low. Selective Reprogramming of Pulmonary Macrophages for Treatment of Pulmonary Fibrosis. ATS 2020 International Conference. *American Journal of Respiratory and Critical Care Medicine*; 201:A7872. https://doi.org/10.1164/ajrcm-conference.2020.201.1_MeetingAbstracts.A7872
- S.U. Hettiarachchi, Y.H. Li, F.H. Zhang, E. Puchulu-Campanella, J. Roy, S. Lindeman, K. Tsoyi, M. Srinivasarao, B. Athenson, C. Nickerson-Nutter, I.O. Rosas, P.S. Low. Targeting Myofibroblasts for Novel Imaging and Therapeutic Applications in Idiopathic Pulmonary Fibrosis. ATS 2019 International Conference. *American Journal of Respiratory and Critical Care Medicine*; 199:A4087. https://doi.org/10.1164/ajrcm-conference.2019.199.1_MeetingAbstracts.A4087
- S.D. Lindeman and D.J. Robichaud. Mass Spectrometry & Infrared Spectra of the Unimolecular Thermal Decomposition Intermediates of Lignin Monomers to Elucidate Decomposition Mechanisms of Benzyl Radical. Poster presented at the NREL intern poster session, 2015.
- C.L. Hansen, S. Lindeman, J.C. Hansen, L.D. Hansen, 2014. Breakdown of lignocellulose with extreme thermophilic anaerobic bacteria. Presentation presented at the ASABE 2014 Annual International Meeting, Montreal, Canada July 13 – July 16, 2014. Abstract #2042904, ASABE 2950 Niles Road, St. Joseph, MI 49085-9659
- S. Lindeman, L.D. Hansen, J.C. Hansen. Bacterial Degradation of Biomass to Facilitate Biogas Production by Anaerobic Digestion. Presented at BYU College of Physical and Mathematical Sciences Annual Spring Research Conference 2014.

AWARDS

<i>Arthur Kelly Teaching Award</i> , Purdue Chemistry departmental award	2016
<i>Undergraduate Research Award</i> , BYU Chemistry departmental fellowship (6x recipient)	2012
<i>Heritage Scholarship</i> , BYU 4 year full-tuition scholarship	2008
<i>Eagle Scout</i> , Boy Scouts of America highest rank	2007

PROFESSIONAL EXPERIENCE

Purdue University , <i>Teaching Assistant</i>	08/2015 – 12/2018
--	-------------------

- General chemistry instruction of classes of 24 students and biochemistry lectures (CHM115, CHM 116, CHM333)

IBC Advanced Technologies

08/2014 – 06/2014

Lab Technician, Supervisor: Dr. Ronald Bruening

- Used ICP spectroscopy to investigate various ligands conjugated to resins for metal ion chromatography of raw materials (e.g. ocean water purification, catalyst recovery, etc.)

National Renewable Energy Laboratory

06/2014 – 08/2014

Summer Intern, Supervisor: Dr. David J. Robichaud

- Researched thermal decomposition of lignin monomers via photo-ionization time-of-flight mass spectrometry
- Identified decomposition intermediates of lignin monomers from pyrolytic reactions by using polarized matrix FTIR spectra unimolecular to elucidate thermal decomposition mechanisms

BYU Central Chemistry Stockroom, Staff Assistant

06/2012 – 09/2013

- Received, accounted for, and maintained an inventory of thousands of routine chemicals and lab equipment

SERVICE*Volunteer, Phi Lambda Upsilon (Nu chapter)*

06/2016 - present

- Performed fun chemistry demonstrations for children at a local elementary school to increase interest in STEM
- Participated in fund-raising activities every semester

Volunteer, Boy Scouts of America

2001-2008, 2017-2018

- As a leader, coordinated activities for Cub Scouts, training adult leaders, ceremony planning, and documentation
- As a participant, spent hundreds of hours contributing to various public service projects

PUBLICATIONS

- Lindeman, S.D.; Mukkamala, R.; Horner, A.; Hovstadius, A.; Tudi, P.; Martone, P.; Huff, R.; Kragness, K.; Srinivasarao, M.; Cox, A.; Low, P.S. Albumin-binding Motif Enhances Theranostic Targeting of Fibroblast Activation Protein Radioligand: Preclinical evaluation in multiple tumors. *Manuscript in preparation*.
- Mukkamala, R.; Lindeman, S.D.; Kragness, K. Shahriar, I.; Low, P.S. Design and Characterization of Fibroblast Activation Protein Targeted Pan-Cancer Imaging Agent for Fluorescence-Guided Surgery of Solid Tumors. *Manuscript in preparation*.
- Hettiarachchi, S.U.; Li, Y.H.; Roy, J.; Zhang, F.; Puchulu-Campanella, E.; Lindeman, S.D.; Srinivasarao, M.; Tsoyi, K.; Xiaoliang, L.; Ayaub, E.; Nickerson-Nutter, C.; Rosas, I.O.; Low, P.S. Targeted inhibition of PI3 kinase/mTOR specifically in fibrotic lung fibroblasts suppresses pulmonary fibrosis in experimental models. *Science translational medicine* 2020.
<https://doi.org/10.1126/scitranslmed.aay3724>
- Zhang, F.; Wang, B.; Puchulu-Campanella, E.; Li Y.H.; Hettiarachchi, S.U.; Lindeman, S.D.; Rout, S.; Srinivasarao, M.; Cox, A.; Ayaub, E.; Tsoyi, K.; Nickerson-Nutter, C.; Rosas, I.O.; Low, P.S. Reprogramming of profibrotic macrophages for treatment of bleomycin-induced pulmonary fibrosis. *EMBO molecular medicine* 2020.
<https://doi.org/10.15252/emmm.202012034>